DIPLOMARBEIT / DIPLOMA THESIS

Titel der Diplomarbeit / Title of the Diploma Thesis

"Establishment of a microfluidic chip to investigate the influence of shear stress on brain endothelial cells"

verfasst von / submitted by

Palle Steen Helmke

angestrebter akademischer Grad / in partial fulfilment of the requirements for the degree of

Magister der Pharmazie (Mag.pharm.)

Wien, 2021 / Vienna, 2021

Danksagung

Kurzzusammenfassung

Die Blut-Hirn-Schranke (BHS) ist eine lebensnotwendige Barriere, um das zentrale Nervensystem (ZNS) vor dem Einfluss schädlicher Substanzen aus dem menschlichen Körper zu schützen. Dabei wird das ZNS vor allem von Mikroorganismen und pathogenen Substanzen abgeschirmt, die potenziell Schäden und neurale Defekte auslösen können.

Somit kommt der BHS eine protektive Rolle zu. Allerdings bringt diese auch einen wesentlichen Nachteil mit sich. So schränkt die BHS die ZNS-Gängigkeit potenzieller Wirkstoffe in der Therapie verschiedener Erkrankungen wie Morbus Parkinson und Demenz (z.B. Morbus Alzheimer) ein. Um den Weg von Wirkstoffen durch die BHS ins ZNS verstehen zu können, ist es unerlässlich die Eigenschaften und Funktionen der BHS vollständig aufzuklären. Dabei scheint besonders der Blutfluss und der resultierende Scherstress einen Einfluss auf die Permeabilität der BHS zu haben.

In dieser Arbeit wurde ein geeignetes Protokoll für die Kultivierung einer humanen Endothelzelllinie (hCMEC/D3) unter Flussbedingungen entwickelt. Dazu wurde ein mikrofluidischer Chip konstruiert, auf dem die hCMEC/D3-Zellen kultiviert wurden. Für die Etablierung des Protokolls wurden die optimalen Kulturbedingungen festgelegt. So konnte festgestellt werden, dass die hCMEC/D3 über einen Versuchszeitraum von drei Tagen bei einer maximalen Scherbelastung von 7.5 dyne/cm² über sechs Stunden kultiviert werden können.

Das etablierte Protokoll wurde dazu genutzt bei definierten Scherungsraten und Zeitpunkten, Zell-Lysate zu generieren. Als Resultat konnten zeit- sowie scherungsabhängige Regulierungen in den mRNA-Expressionsmustern relevanter Zielgene der BHS festgestellt werden.

Besonders erwähnenswert war im Vergleich zu statischen Kontrollversuchen ein Trend zur Hochregulierung bei dem Transporter des „cationic aminoacid transporter 1" (CAT1), sowie dem Wachstumsfaktor „vascular endothelial growth factor" (VEGF). Im Gegensatz dazu konnte eine Tendenz zur Herabregulierung bei Genen der Junktionsmoleküle „VE-Cadherin" und „Zonula occludens" (ZO) sowie dem Transportmolekül „von Willebrand Faktor" (vWF) ermittelt werden.

Abstract in englisch

The blood-brain barrier (BBB) protects the central nervous system (CNS) against harmful substances. The CNS is predominantly secured against microorganisms and other pathogenic substances, which could potentially cause damage.

Hence, the BBB is the guardian of the CNS. Nonetheless, this role also entails a major disadvantage. The BBB inhibits potentially active substances, for the therapy of different diseases such as Morbus Parkinson or dementia (e.g. Morbus Alzheimer), from entering the brain. To understand the routes of transport of active substances across the BBB into the CNS, it is inevitable to fully elucidate the properties and functions of the BBB. In this regard, the blood flow and the resulting shear stress seem to influence the permeability of the BBB.

The aim of the current study was to establish a suitable protocol for the cultivation of a human endothelial cell line (hCMEC/D3) under flow conditions. For this purpose, a microfluidic chip was developed and the optimum culture conditions for hCMEC/D3 were determined. It was observed that the hCMEC/D3 cells could be cultured over a period of 3 days at a maximum shear stress of 7.5 dyne/cm² for 6 consecutive hours.

This protocol was applied in the second part of the current study to obtain cell-lysates at defined shear stresses and time points. As result, time- and shear dependent alterations in the mRNA expression patterns of relevant target genes of the BBB were detected.

Worth mentioning were time- and shear dependent upregulations, in comparison to the corresponding static controls, within the transporter "cationic aminoacid transporter 1" (CAT1) and the growth factor "vascular endothelial growth factor" (VEGF). On the contrary, downregulations were detected in genes of the junction molecules "VE-Cadherin" and "zonula occludens" (ZO) as well as the transporter molecule "von Willebrand factor" (vWF).

Table of contents

1 Introduction

1.1 The Blood-brain barrier

The blood capillaries of the brain are essential for the supply of the CNS with oxygen, nutrients and energy metabolites, but also for the disposal of carbon dioxide and metabolic waste products. Thus, the blood capillaries of the brain hold important roles to supply and protect the brain. In order to fulfill these tasks, the brain capillaries are organised within the neurovascular unit (Daneman, 2012; Abbott *et al.*, 2010).

This element is framed of neural cells, vascular cells and extracellular matrix components (Figure 1). The brain capillary endothelial cells (BCECs) form the first layer and line the wall of the vessels, hence providing the lumen for the blood to pass. The abluminal site of the vasculature is inconsistently covered with pericytes (PCs) (Daneman, 2012; Abbott *et al.*, 2010).

Both, the BCECs and the PCs share the same basement membrane (BM). This basal lamina consists of extracellular matrix proteins like collagen, laminins and heparan sulphate proteoglycans (HSPGs) (Daneman, 2012; Sweeney, Sagare, and Zlokovic, 2018).

The next cell type associated with the basement membrane are the astrocytes (ACs). This is the main glia cell type in the CNS. Finally, perivascular macrophages, called microglia, are present in this neurovascular unit. These immune cells patrol and grant immunity to the abluminal site of the vessels (Daneman, 2012; Fischer, 2012).
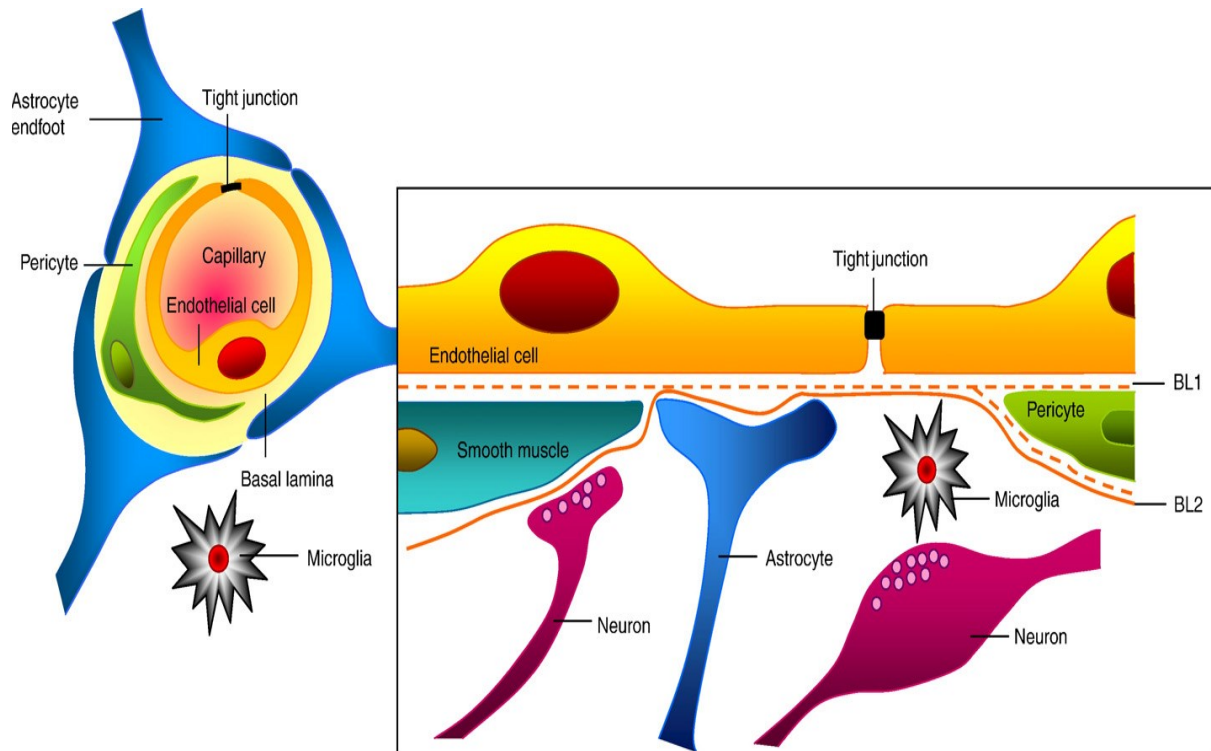
Figure 1: Cross section (left) and longitudinal section (right) of the cellular components of blood vessels. Image was taken from Abbott *et al.*, 2010.

1.1.1 Brain capillary endothelial cells

The BCECs line the lumen of the blood vessels and are vital to control the entry and exit of substances in the brain. For this purpose, the permeability of BCECs is strongly regulated and restricted for many molecules (Daneman, 2012).

Furthermore, the BCECs are responsible for the supply of nutrients to the CNS to enable proper function. On the other hand, the BBB prevents toxic substances from entering the brain due to its highly polarized nature, developing exclusive transport properties. In contrast to endothelial cells of the periphery, there are no fenestrations or intercellular gaps between BCECs and a minimum of pinocytosis is ongoing at the BBB. This important paracellular tightness is achieved by the tight junctions (TJs) (Daneman, 2012).

The majority of large and hydrophilic molecules are excluded from the brain due to the presence of TJs. In contrast, small and lipophilic molecules can potentially pass the BBB. Nonetheless, efflux transporters can greatly limit their diffusion (Abbott *et al.*, 2010; Cucullo *et al.*, 2011; Daneman, 2012; Fischer, 2012).

1.1.1.1 Tight junctions

TJs seal the gaps between the BCECs and thus grant the selective permeability of the BBB (Figure 2). Abbott *et al.* (2010) stated that cell-cell junctions at the BBB are differentiated into TJs and Adherens junctions (AJs). The latter consist of cadherins, including VE-Cadherin. The

AJs connect the endothelial cells to give them structural support and are the basis for the formation of the actual TJs (Abbott *et al.*, 2010; Daneman, 2012; Fischer, 2012; Daneman and Prat, 2015).

The most important TJ-constituents are junctional adhesion molecules (JAMs), occludins and more than 20 molecules of the claudin-family. Especially Claudin5 is important for the function of the TJs. The composition of the members of the claudin-family seems to influence the effectiveness of the tightness of the BBB (Daneman, 2012; Abbott *et al.*, 2010; Daneman and Prat, 2015).

These molecules bridge the intercellular space between adjacent ECs and strongly restrict the paracellular flux. Hence, the reduced paracellular permeability of ions results in high *in vivo* transendothelial electrical resistance (TEER) values of 1800 $\Omega*cm^2$ at the BBB. TEER of the BBB in rats can reach values of 5900 $\Omega*cm^2$. These values demonstrate the effectiveness of the TJs at the BBB (Daneman, 2012; Shuler and Hickman, 2016).

Consequently, the TJs restrict the paracellular transport to uncharged molecules below a size of 4 nm due to a pore of this scope. Moreover, the junctional proteins are connected to the cytoskeleton and actin by the cytoplasmic proteins zonula occludens1 (ZO1), ZO2 and ZO3. These are connected by Cingulin and control the TJs (Abbott *et al.*, 2010; Daneman, 2012; Fischer, 2012; Daneman and Prat, 2015).

The intracellular calcium-concentration also impacts the properties of the TJs, as this ion binds to the cytoskeleton (Abbott *et al.*, 2010).
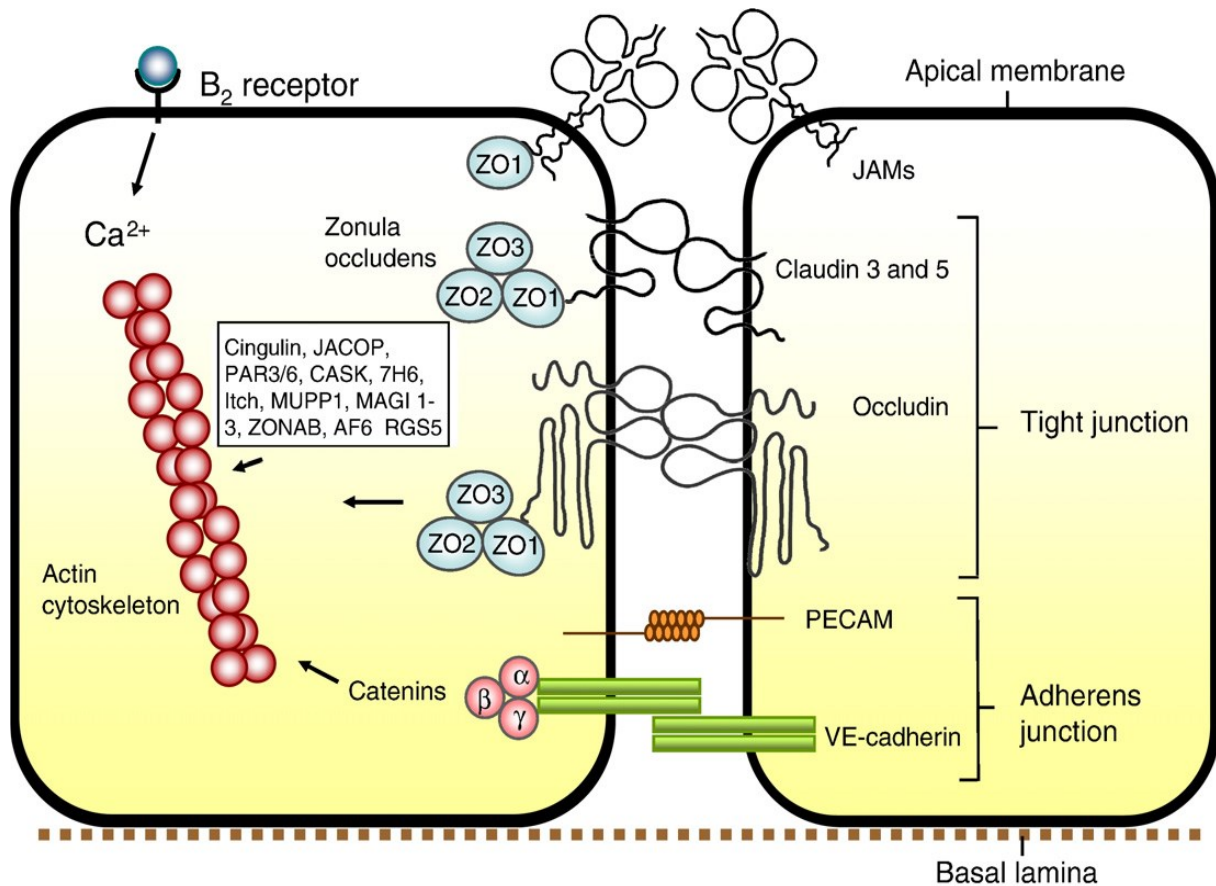
Figure 2: Structural overview of the tight junction structure between the BCECs at the BBB and the important proteins involved. Image was taken from Abbott *et al.*, 2010.

1.1.1.2 Transport across the BBB

BCECs are highly polarised, resulting in distinct luminal and abluminal sites. In combination with the TJs, the flux across the membrane towards the brain is greatly restricted. To regulate transcellular transport across the BBB, several transporters (Figure 3) were identified, which enable the supply with the required nutrients. On the other hand, there are transporters to prevent the entrance of xenobiotics into the brain and promote disposal of waste from the abluminal site of the barrier (Daneman, 2012; Abbott *et al.*, 2010).

Solutes can be transported by passive diffusion across the BBB. These include oxygen and carbon dioxide, which move along their concentration gradient. In addition, Sweeney *et al.* (2018) stated that lipophilic molecules with a molecular weight lower than 400 Da or 8 hydrogen bonds use the transcellular route to pass the BBB in contrast to hydrophilic molecules. Furthermore, it is assumed that higher lipid solubility and other factors including a low affinity to plasma proteins are an advantage to enter the brain via this route. However, most of the molecules trying to cross the BBB by passive diffusion are recognised and exported back into the blood by efflux transporters (Abbott *et al.*, 2010; Daneman, 2012; Sweeney *et al.*, 2018).

Many vital nutrients such as amino acids and glucose are polar. For the transport of these molecules, solute carriers (SLCs) are expressed in the BCECs membranes. The transport mediated by SLCs is called carrier-mediated transport (CMT). To control the entry and exit of these compounds into the brain, SLC transporters can be included in either the luminal or abluminal membrane or into both sides. This mediated transport occurs either bi-directional, in a single direction, hence being unidirectional, or involves the exchange of molecules. This is usually facilitated by a concentration or anion gradient. Examples include the glucose transporter 1 (GLUT1), which transports in a bi-directional way and the equilibrative nucleoside transporter 1 (ENT1), which carries nucleosides and nucleotides unidirectional from the blood into the CNS (Abbott *et al.*, 2010; Sweeney *et al.*, 2018).

ATP-binding cassette transporters (ABC transporters) are vital to restrict the entry of xenobiotics, such as several drugs, into the brain. P-glycoprotein (Pgp) and Breast Cancer Resistance Protein (BCRP) are present in the luminal membrane, whereas Multidrug Resistance-associated Proteins (MRPs) are localised in either the luminal or abluminal site. In certain types of epilepsy, Pgp is upregulated, which enhances drug resistance (Abbott *et al.*, 2010; Daneman, 2012).

Macromolecules, such as peptides and proteins, are commonly repressed from passing the BBB via the paracellular route by the presence of the TJs. Hence, vital macromolecules must be carried across the membrane via transcytosis. This process is either a receptor-mediated transcytosis (RMT) or adsorptive mediated transcytosis (AMT). For example, transferrin is transported via RMT and cationised albumin via AMT from the blood to the brain. Both processes involve vesicles transporting the intact macromolecules through the endothelium. Though, the lysosomal compartment is to be strictly avoided (Abbott *et al.*, 2010).

In addition, even cells can migrate across the BBB. These mostly include immune cells such as monocytes, macrophages or circulating neutrophils. The latter are important in neutrophil inflammation during ischemia of the BBB. However, their infiltration is significantly lower into brain than into other tissues. Mononuclear cells enter via transcytosis directly through the cytoplasm of the BCECs rather than via the paracellular route, leaving the TJs intact. Disturbance of the TJs for the paracellular entry of neutrophils occurs only during pathological conditions (Abbott *et al.*, 2010; Daneman, 2012).

(a) Passive **(b) ABC** **(c) Solute** **(d) Transcytosis** **(e) Mononuclear**
diffusion Transporter Carriers Receptor-mediated Cell
Efflux SLC Adsorptive-mediated Migration
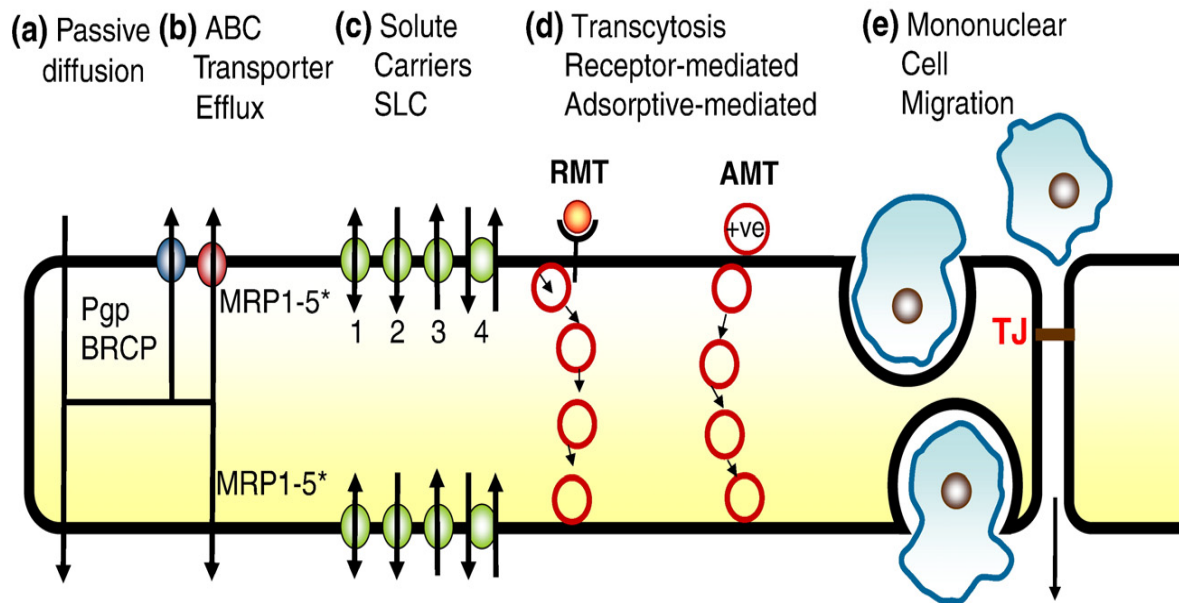
Figure 3: Overview of the paths of transport across the BBB. Image was taken from Abbott *et al.*, 2010.

1.1.2 Astrocytes

This glia cell type, also called star cells, can cover the BCECs almost entirely (60 to 95 %) from the CNS side and have to contact them via their perivascular end feet (Figure 1). Astrocytes (ACs) are important for the regulation of transport and junctional properties of the BBB. In addition, AC-activity is associated with synapse and blood vessel function. Thus, the regulation of blood flow by arterial contraction and dilatation in response to neuronal activity in certain areas appears to be one of their most important tasks according to Daneman (2012) (Abbott *et al.*, 2010; Saunders, Liddelow, and Dziegielewska, 2012; Fischer, 2012; Daneman, 2012).

Moreover, ACs influence the BCECs by regulating their phenotype and differentiation, in particular they control permeability, polarity and enzyme-equipment of BCECs. In addition, Fischer (2012) stated that ACs produce cholesterol and maintain extracellular ion concentration (Fischer, 2012).

However, AC-activation is also linked to BBB breakdown. An inflammatory response follows BBB collapse, which leads to the activation of ACs amongst others. As a consequence, ACs release cytokines and chemokines, which promote neuronal injury and synaptic dysfunction for instance. This ultimately can lead to neurodegeneration (Daneman, 2012; Daneman and Prat, 2015; Fischer, 2012; Sweeney *et al.*, 2018).

1.1.3 Pericytes

This cell type belongs to the mural cells together with vascular smooth muscle cells. Pericytes (PCs) are located on the abluminal surface of the capillary brain endothelium tube (Figure 1).

PCs are essential for the development and maintenance of the BBB. Consequently, the loss of PCs results in BBB breakdown (Daneman, 2012; Daneman and Prat, 2015; Siegenthaler *et al.*, 2013; Sweeney *et al.*, 2018).

The presence of PCs leads to the efficient establishment of tight junctions. Studies by Daneman (2015) demonstrated, that fully functioning PCs are vital for the formation of tight junctions and vesicle trafficking. Nonetheless, he also showed that PCs are rather involved in the inhibition of the expression of molecules that promote the permeability and the stabilisation of the peripheral vasculature than in the actual expression of genes specific to the BBB (Daneman, 2012; Saunders, Liddelow and Dziegielewska, 2012; Siegenthaler *et al.*, 2013).

Further debated tasks of PCs include their involvement as a contraction element for blood pressure regulation, macrophage-activity with a contribution to the preservation of immunity of the CNS and the regulation of mitosis of the BBB (Fischer, 2012).

1.1.4   Basement membrane

The BM is located on the outside of the BCECs, surrounding the cerebral capillaries, the BCECs and the PCs (Figure 1). The main constituents of this lamina are the proteins collagen IV from BCECs and collagen I from PCs according to Saunders *et al.* (2012). In addition, laminins and more glycoproteins, such as heparan sulphate as well as nidogen, are important for the function of the BM (Abbott *et al.*, 2010; Daneman, 2012; Saunders *et al.*, 2012).

According to Daneman (2012), one must differentiate between the endothelial vascular BM, which is secreted by BCECs and PCs and the parenchymal BM formed by ACs. The latter attaches AC-endfeet to the BM through protein-protein-interactions. Hence, the BM can be considered as a structural matrix, mediating the interaction of cells and secreted molecules with the vessels. Consequently, if molecules or cells seek to enter the brain, they must pass the EC-layer as well as both, the endothelial and the parenchymal BM. According to Abbott *et al.* (2010), the BM serves as a "second line of defence", forming an additional barrier (Abbott *et al.*, 2010; Daneman, 2012; Daneman and Prat, 2015; Saunders *et al.*, 2012).

1.2   Microfluidics

Modelling flow-like conditions and shear stress is one of the main challenges in cardiovascular research. The applicability of static *in vitro* models of the BBB is limited since shear stress alters RNA and protein expression levels of various tight junction proteins and transporters in their functions. Consequently, the use of flow-conditions is inevitable when trying to model the BBB in a more physiological manner (Cucullo *et al.*, 2011; McMillan, 2017).

The research discipline of microfluidics is about the behaviour of small quantities of fluids in a small space. Hence, microfluidic experiments are feasible in a short period and can be cost-effective. Therefore, this field offers the unique opportunity of cultivating cells in a small area, whilst exposing them to small volumes of fluids continuously. This technology enables laminar flow profiles similar to the ones seen in the microvasculature. Moreover, the monitoring of processes is possible by live microscopy. However, the creation of sterile cell culture conditions in microfluidic systems represents a main challenge (Cucullo *et al.*, 2011; Winckler, Fisch, Labonté, 2012; McMillan, 2017).

1.3   Shear stress

In the case of blood vessels, shear stress is defined as the tangential force of the flowing blood on the endothelial surface of the blood vessel as stated by Paszkowiak and Dardik (2003). Two different types of flow exist. First, there is general laminar flow accompanied with high wall shear stress in small blood vessels, which describes the forces applied in the current study. Shear stress applied by laminar flow is characterised by the mean fluid flow, the viscosity and the physical dimensions of the blood vessels or the geometry of the microfluidic device during *in vitro* studies. However, *in vitro* shear stress is Newtonian, as the viscosity does not vary due to the flow velocity according to Ballermann *et al.* (1998). In contrast, *in vivo* shear stress is not Newtonian, as the blood viscosity is decreasing with increasing velocity. Contributing to that, the microfluidic device has uniform dimensions, whereas the blood vessels are nonuniform. Second, there is low shear stress in branches and curvature, which describes a disturbing flow situation as specified by McMillan (2017) (Ballermann *et al.*, 1998; Cucullo *et al.*, 2011; Kiessling *et al.*, 2015; McMillan, 2017; Paszkowiak and Dardik, 2003).

Shear stress triggers several effects on BCECs in flow experiments in comparison to static conditions. Shear stress is vital to maintain the natural phenotype of the cells, which is typically lost when cultivating cell lines outside of the natural environment for a longer period. In addition, morphological changes, modifications in cellular signalling pathways and alterations in gene and protein expression levels occur due to shear. In this regard, Cucullo *et al.* (2011) also demonstrated the upregulation of RNA expression levels of multidrug resistance transporters, ion channels and CMT-systems for instance. In contrast, they detected decreasing RNA levels of modulatory enzymes of the glycolytic pathway. In their studies, they also showed an increase of cytoskeleton proteins compared to the total protein distribution. Furthermore, Cucullo *et al.* (2011) observed changes in junctional genes due to shear stress around 2.5 dyne/cm². Thus, barrier tightness seemed to increase under flow conditions. However,

Neuhaus (2020) assumed that shear stress in brain capillaries lies between 5 to 25 dyne/cm² (Ballermann *et al.*, 1998; Cucullo *et al.*, 2011; Kiessling *et al.*, 2015; Alex McMillan, 2017; Neuhaus, 2020).

2 Aim of the thesis

The aim of this work was to establish a protocol for the cultivation of hCMEC/D3 cells in a microfluidic device under flow conditions with subsequent cell lysis for the investigation of time- and shear stress dependent up- and downregulations of the relevant genes of the BBB. The chip design in terms of the favourable PDMS-height, the channel-width as well as the best surface for cell cultivation should be found. In addition, the maximum possible duration of hCMEC/D3 cultivation in the microfluidic device, the flow rate increase and the periods of final exposure to ultimate shear stress should be determined. Afterwards the mRNA expression of relevant genes of the BBB should be examined with respect to time- and shear stress dependency. All these experiments should be carried out to verify the hypothesis that hCMEC/D3 cells can be cultured under flow conditions in a microfluidic device and relevant genes of the BBB are regulated in their mRNA levels in a shear stress dependent manner.

3 Materials and Methods

3.1 Material list

Table 1: List of materials including chemicals, growth media, cell culture plastics ad pipettes.

Material	Company	Product number
24-well plates	Falcon	Ref 353504
2-Mercapto-Ethanol	Sigma Aldrich	M6250-500ML
Aptes	Sigma Aldrich	440140-100ML
Ascorbic acid	Sigma Aldrich	A92902-500G
Collagen IV	Sigma Aldrich	C5533
Coverslips	Paul Marienfeld	0111530
DAPI	Sigma-Aldrich	D9542
DMSO sterile filtered	R&D systems	3176/100ML
DPBS 1X -MgCl2 -CaCl2	Gibco	Ref 14190-094
EBM-2 endothelial basal medium	Lonza	Cat. #00190860
Epoxy adhesive	Loctite	458-7983
Ethanol 70 %	VWR	83.801.360
FBS	Life Technologies	10270-106
Fibronectin	Sigma Aldrich	F1141-5MG
FluoPrep	bioMerieux	75521
FrameStar 96 well semi-skirted PCR plate roche style	4titude	4ti-0951
Gelatine	SERVA	22151.02
Glass slides	Superior Marienfeld	1000000
Glycine for molecular biology	AppliChem	A1067,1000

hbFGF	Sigma-Aldrich	F0291
Helmanex Cleaning solution	Hellma	9-307-011-4-50
High-Capacity cDNA Reverse Transcription Kit with Rnase Inhibitor	Applied biosystems	Ref 4374966
Hypodermic needle, 18G x 1''	Terumo	NN1825R
Hypodermic needle, 20G x 1''	Terumo	NN2025R
Hypodermic needle, 21G x 1''	Terumo	NN2125R
Hypodermic needle, 23G x 1''	Terumo	NN2325R
Innoculation loop	Thermo Fisher scientific	QL10
Isopropanol	Carl Roth	771713
Nuclease free water	Ambion	AM9937
PBS, sterile	Gibco	14190-094
PCR tubes 0,2 mL	Biozyme	Art-Nr:711080X
PDMS foil 250 μm	MVQ Silicones GmbH	HT 6240 series
PDMS foil 500 μm	MVQ Silicones GmbH	HT 6240 series
PEEK tubing	VICI Jour	JR-T-5993-M10
Penicillin/Streptomycin 10000 U/ml / 10000μg/ml	Biochrom GmbH	A2213
Pipette boy	Sartorius	midi plus
Pipettes	Sartorius	proline plus
Pipettes (10 μL – 1000 μL)	Eppendorf	research plus
PVDF sterile filter 0.2 μm	Rotilab	P6661
Red food colour	Dr.Oetker Nahrungsmittel KG	1-01-525300
RNase AWAY™ Decontamination Reagent	Thermo Fisher scientific	10328011
Serological pipettes 10 mL	Sarstedt	861254001
Serological pipettes 25 mL	Sarstedt	861255001

Serological pipettes 5 mL	Sarstedt	861253001
Syringe 1 mL	Terumo	SS-01T
Syringe 30 mL	Terumo	SS-30L
Syringe 5 mL	Terumo	SS-05L
Syringe 60 mL	Terumo	SS-60L
Syringe insulin needle	Braun	Omnican 40
Tissue culture flask (T-25)	GreinerBioOne	690175
Tissue culture flask (T-75)	GreinerBioOne	658175
Triton X-100	Sigma-Aldrich	X100-500ML
Trypsin/EDTA solution 0.05 %/0.02 % (w/v) in PBS w/o Ca^{2+}	Biochrom GmbH	L2143
tubes 1,5 mL	Eppendorf	30120086
tubes 15 mL	GreinerBioOne	541070
tubes 50 mL	GreinerBioOne	210270
Tygon LMT – 55 tubing	IDEX Health and Science GmbH	07053405Ll – ND SC0029T

Table 2: List of primary and secondary antibodies used for immunostainings.

Primary antibodies			
Target	Hostspecies	Company	Product Number
Human VE-Cadherin Antibody Monoclonal Mouse IgG2B Clone# 123413	Mouse	Fisher scientific	FAB9381P025
Secondary antibodies			
Secondary anti-mouse	Alexa 488 conjugated (Goat antimouse)	Invitrogen	A-21141

Table 3: List of software.

Software	Company
AutoCAD	Autodesk
Autodesk CFD 2019	Autodesk
CellSens Dimension software	Olympus
Image J	NIH Image
Roland Cut Studio	Roland DG

Table 4: List of devices.

Device	Company	Product number
Air Blow Gun	BAHCO	BP218
Centrifuge	Eppendorf	5424 R
Cell counting chamber	Thoma "Neubauer improved" Marienfeld	00640010
-80°C ultra low temperature freezer	Panasonic	MDF-U700Vx-PE
fridge-freezer	Liebherr	CN 3915
Microscope heating plate	TOKAI HIT Thermo plate	
Flowmeter	Sensirion	SLI-0430
Fluorescence microscope	Olympus BX51 Fluorescence Microscope	
heating plate	Omega	CN1800
Incubator 5 % CO2	Binder Modell CB260	
Inculine Incubator	VWR-Inculine	390-0384P
Live cell microscope	Olympus IX83 Microscope	
Bench Drill machine TBM 220	Proxxon	NO 28128
Oven 120°C	Binder	9010-0333

Peristaltic pump	Watson Marlow	205S/CA
Plasma chamber	Harrick Plasma	PDC-002
KDS 250/250P Legacy Syringe Pump	KD scientific	780250
Ultrasound bath	Ultrasonic bath XUBA3	
Vinyl Cutter	Roland CAMM-1 GS-24	
Vortex shaker	VWR	44-2790
Waterbath	Grant Instruments JB2	

3.2   hCMEC/D3 cell line

hCMEC/D3 cells are immortalised brain endothelial cells derived from a female epileptic patient. According to Weksler, Romero and Couraud (2013), hCMEC/D3 show stable growth characteristics until passage 35, were used for over hundred scientific publications and represent a valid scientific BBB cell line (Weksler, Romero and Couraud, 2013).

3.2.1   Cell Culture

In a cell culture it is of vital importance to work under sterile conditions to protect the cells from contamination. Hence, all working steps with cells were carried out in a laminar air flow and all surfaces were wiped with 70 %-ethanol prior to the experiments.

3.2.1.1   Cultivation and sub-cultivation of cells

The hCMEC/D3 cells were cultivated in a 0.5 % gelatine coated T25-cell-culture-flask with an air filter for gas exchange. This cell line was cultivated in an incubator at 37 °C in a 95 % humified atmosphere with 5 % CO_2 and 95 % air. They were split with 0.05 % trypsin/EDTA in a 1:3 ratio after 7 days of cultivation once a week. The 0.5 % gelatine solution was applied to the surface of the flask for at least 30 minutes at room temperature (RT) before cell-seeding. Afterwards, the 0.5 % gelatine solution was discarded. Media exchange was accomplished every 2 to 3 days with fresh 5 mL endothelial cell growth basal medium-2 (EBM-2) three times a week. The cell number seeded in the flask was 80.000 cells/cm² and therefore $2x10^6$ cells per T25-flask. The supplements FBS, Pen/Strep, HEPES and ascorbic acid were added to the EBM-2 medium as well as the growth factor hbFGF, which was only supplemented shortly before usage.

For the preparation of the ascorbic acid solution, 20 mg ascorbic acid were dissolved in 20 mL EBM-2 basal medium. Afterwards, this solution was sterile filtered and stored as aliquots of 1mL at -20° in sterile Eppendorf tubes. For the hbFGF stock solution, 20 mg hbFGF were dissolved in 250µL 0.1 % BSA-solution. BSA was dissolved in PBS. Subsequently, 10µL of this stock was dissolved in another 5 mL of the 0.1 % BSA-solution. Finally, 1mL aliquots were stored in sterile Eppendorf tubes at -20°C.

Table 5: Composition of EBM-2 medium used for hCMEC/D3 cultivation.

Ingredients	Volume
EBM-2 basal medium	48 mL
FBS	2.65 mL
Pen/Strep 10000 U/mL/1000 µg/mL	531µL
Ascorbic acid 1mg/mL	265 µL
HEPES 1M	531 µL
hbFGF 200 ng/mL	265µL

3.3 Preparation workflow for cell culture experiments with microfluidic device or 24-well plates

Each experiment consisted of two parallel approaches. First, the microfluidic device, also called chip, had to be manufactured for the flow experiments. Second, a 24-well plate was prepared and served as a static control. After the fabrication of the chip, both were subjected to the same washing and coating procedure in order to work at similar conditions in each setup. Finally, the cells were seeded (Figure 4).
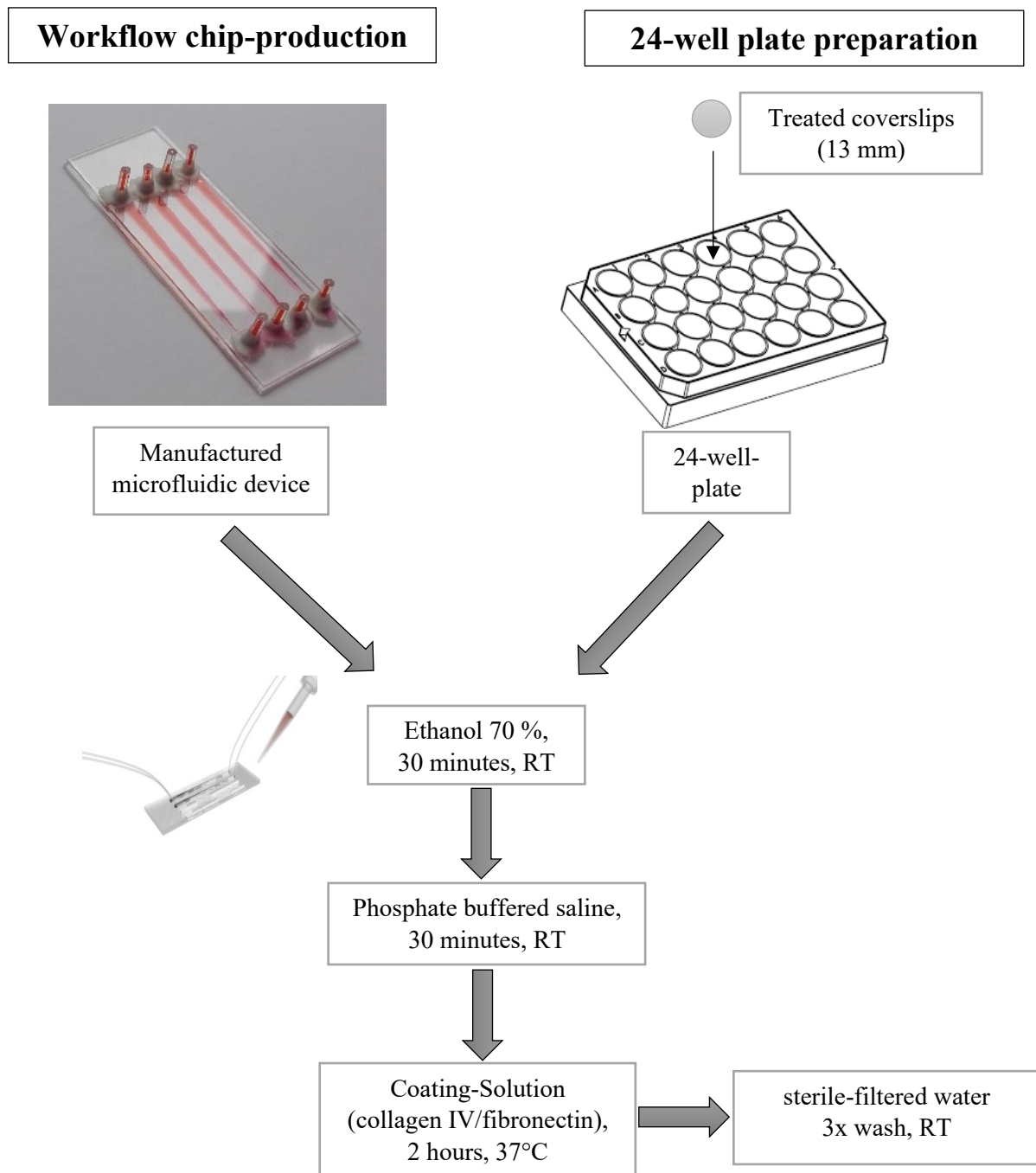
Figure 4: Workflow of Chip-manufacturing and 24-well plate preparation for cell culture experiments. Image of 24-well plate was taken from Ibidi, cells in focus, 2016.

3.4 Microfluidic devices

The chips used in the current study consisted of five main components. These were assembled to create a compact and tightly sealed microfluidic device. The upper and lower layer were formed by microscope glass slides. Holes were drilled into the upper slide for the following connection of the tubes, supplying the cells in the device with the medium. Polydimethylsiloxane foil (PDMS) built the middle layer and provided the template for the channels, in which hCMEC/D3 were seeded (Figure 5). Inlets and outlets also called ports, composed of 1 cm-long Tygon-tubing were placed on the designated and drilled holes. Finally, the bottom side of the channels of the chip had to be modified and prepared for subsequent cell seeding (3.4.1.8).
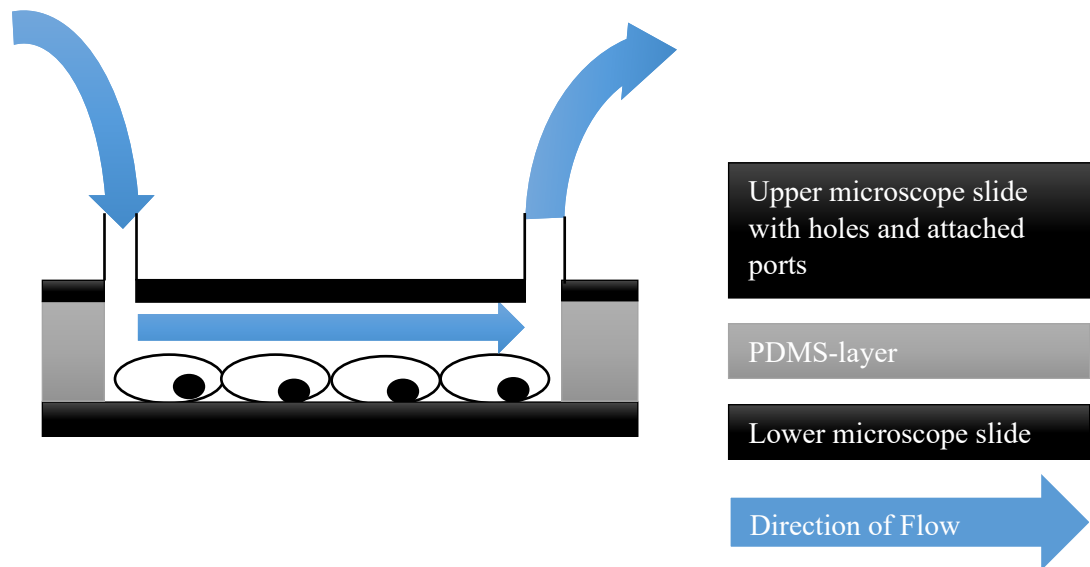
Figure 5: Basic scheme of a microfluidic device (layer-thicknesses for visualisation purposes, not according to real scale).

3.4.1 Chip-fabrication

Even though the process of chip-fabrication was complex, it was practicable within a time period of 5 hours and is described step by step in the following section (Figure 6).
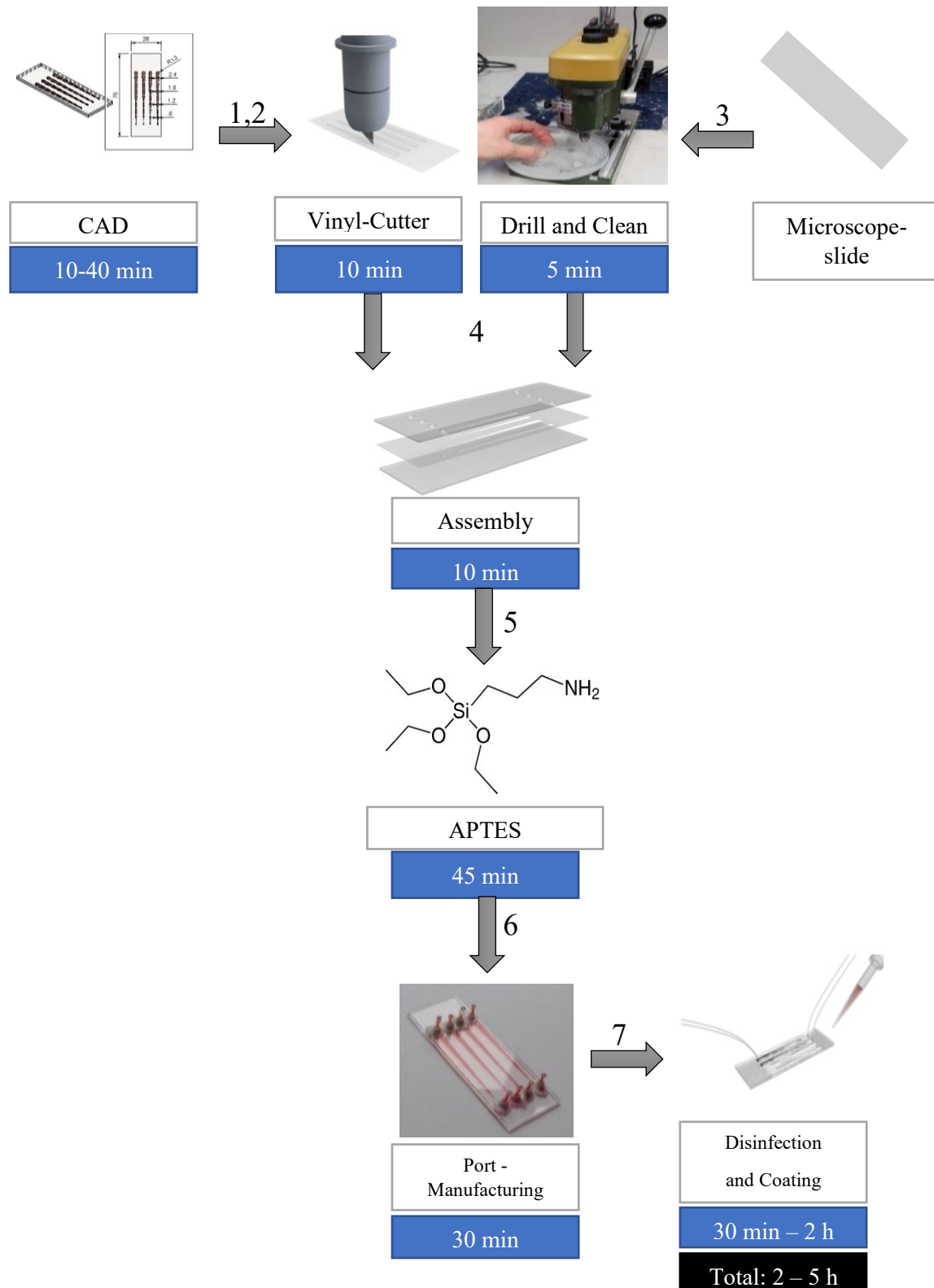
Figure 6: Workflow of chip-fabrication; Image of APTES was taken from https://www.carlroth.com/de/de/Life-Science/Histologie-Mikroskopie/Reagenzien/Standardreagenzien/3-Aminopropyltriethoxysilan-%28APTES%29/p/000000000001ade600030023_de, accessed September 27, 2019.

3.4.1.1 CAD (step 1)
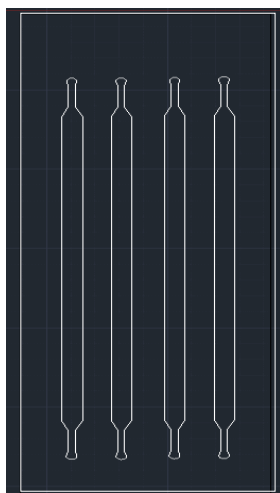
A template for the channels of the microfluidic device was constructed using AutoCAD (Figure 7). This software enables the user to draw and design 2-dimensional and 3-dimensional objects. This pattern featured microscope slide dimensions (76 mm x 26 mm) and the correctly measured channels. In the course of the experiments, two different chip designs were employed (3.5)

(AutoCAD software available at: https://www.autodesk.com/products/autocad/overview, accessed September 27, 2019).

Figure 7: Example of a template with microscopic slide dimensions designed with the software AutoCAD.

3.4.1.2 Vinyl Cutter (step 2)

Figure 8: Vinyl Cutter. Image was taken from https://www.rolanddg.de/produkte/software/roland-cutstudio, accessed September 25, 2019.

After the template for the PDMS foil was constructed, the design was copied and pasted into Roland CutStudio and the settings had to be adjusted (Settings: Setup: Piece, RolandCutStudio-software: use dimensions from piece, copy design into software, cut, slide dimensions: 26 x 76 mm, Cutting-force: 80 (for PDMS), after cutting: Menu, Unsetup, Enter). This software serves as a tool to adapt the drawing to the settings of the cutter and to select the right cutting-force for different materials, in this case PDMS. Thereafter, the upper protective film was removed from the PDMS per hand and the foil was inserted into the Vinyl Cutter (Figure 8). In our study, thicknesses of 250 µm and 500 µm were employed. Finally, the template with the channels was printed onto the PDMS foil with the correct blade and the inside of the channels was removed with tweezers (Roland CutStudio software and picture available at: https://www.rolanddg.de/produkte/software/roland-cutstudio, accessed September 25, 2019).

3.4.1.3 Preparation of microscope slides and micro-hole drilling (step 3)

The first step towards the assembly of the chip was the preparation of two microscope slides (76 mm x 26 mm). The holes for the inlets and outlets of the chip, separately for each channel,

were marked with a waterproof pen on one microscope slide. This had to occur in the same distance from the edges of the slide, as created in the template with AutoCad. This, later on, functioned as an upper layer and allowed the medium to enter the device and reach the cells (Figure 5). Afterwards the holes were drilled into the microscope slide at the marked spots. The next stage in the preparation involved four rinsing steps, in a Coplin staining jar, to create a clean surface for the assembly as described in the following:

1.) Helmanex-cleaning-solution 2 %: 50 mL, 5 minutes, Ultrasound
2.) Distilled-Water: 50 mL, 2-3x
3.) Isopropanol: 50 mL, 5 minutes, Ultrasound
4.) Distilled-Water: 50mL, 2-3x

This procedure was conducted with both, the drilled slide and the untreated slide for the bottom of the microfluidic chip (Figure 5). Subsequently, the slides were dried using a compressed air gun.

3.4.1.4   Assembly (step 4)

Figure 9: Plasma-cleaner.

The creation of a tight bond between the PDMS and the glass slides was essential in the process of chip fabrication. This was important to keep the fluids and cells inside the channels and to generate a closed chamber. For this purpose, a plasma-cleaner was employed (Figure 9). The procedure is known as plasma bonding, which creates silanol-groups on PDMS and hydroxyl-groups on glass slides, which then form a strong covalent bond in-between. Furthermore, plasma is also a strong disinfectant. This was important, as eucaryotic cells were used in the cell culture during our study up to 14 days of culture. The cells in the channels of the chip are easily contaminated with bacteria, yeast or fungi, which would cause significant changes to the cell properties during the experiments.

In two separate runs, the upper drilled glass slide was first attached to the PDMS foil, followed by the lower empty glass slide. The bonded sides were placed upwards inside the chamber at the highest radio-frequency-level (RF-level) of 30 W at vacuum for 2 minutes. Finally, the fully

assembled chip was baked for 10 minutes in the 70 °C-incubator (Place S. Plasma Bonding. Encycl Microfluid Nanofluidics. 2008; https://plasmatreatment.co.uk/henniker-plasma-technology/plasma-treatments/plasma-surface-activation-to-improve-adhesion/plasma-treatment-of-pdms/, accessed September 25, 2019; https://www.thierry-corp.com/plasma-cleaning/, accessed September 25, 2019).

3.4.1.5   APTES-treatment (step 5)

According to Kuddannaya *et al.* (2013)*,* the application of 3-Aminopropyltriethoxysilan (APTES) reduces the hydrophobicity of PDMS significantly. Besides, it supports the adhesion and viability of cells in combination with a coating solution, in our study collagen IV/fibronectin. Usually, the interaction between proteins and the material surface relies on weak forces like Van der Waals, electrostatic or hydrophobic bonds. To strengthen the assembly between proteins and the material surface, the linker APTES was introduced to form a strong covalent bond in-between (Kuddannaya *et al.*, 2013).

In the process, 25 µL of the amino silane were pipetted into each channel, incubated at RT for 30 minutes and each channel was afterwards rinsed with 25 µL of 96 % ethanol for three times. Finally, the chips were baked again for 1 hour at 70 °C to remove ethanol residues.

3.4.1.6   Inlet- and outlet tubes manufacturing with epoxy adhesive (step 6)
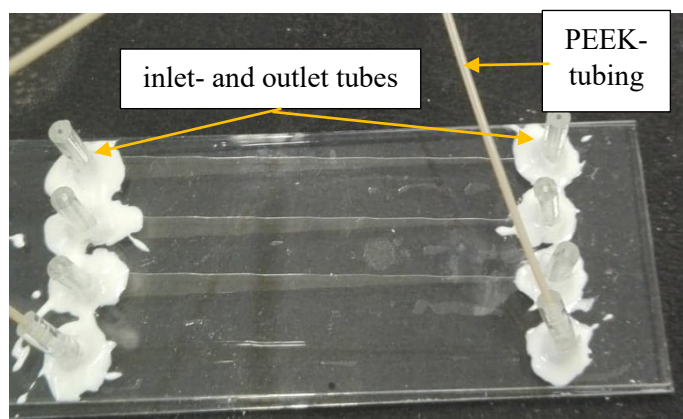
Figure 10: Inlet- and outlet tubes with connection to PEEK-tubing.

The next step in the process of chip-manufacturing was the attachment of inlet- and outlet tubes using Tygon tubing (1.58 mm = 1/16 inch). These were connected to Polyetherketone (PEEK) tubing (0.79 mm = 1/32 inches) and then to the medium syringes in the microfluidic pump or in the case of the outlets to the medium reservoir.

For this purpose, Tygon tubing was cut into 1 cm-pieces and sealed onto the drilled holes of the microfluidic device using epoxy adhesive. Drying the gum-like glue was done by placing the microfluidic device into the 70 °C-incubator. First, this was done for 15 minutes, after mounting a portion of the epoxy adhesive underneath the tubes, for a first attachment. Second, this was done, after placing the rest of the epoxy adhesive around the tubes, for 2 hours until completely hardened   (https://www.elveflow.com/microfluidic-tutorials/microfluidic-reviews-and-

tutorials/microfluidic-fittings-and-tubing-resources/the-basics-of-microfluidic-tubing-sleeves/, September 27, 2019).

3.4.1.7 Disinfection and coating (step 7)

The washing- and coating-steps were essential to achieve sterile devices and a suitable surface for the seeding of the cells within the channels of the microfluidic device. In the case of using the peristaltic pump, this was conducted for each solution for 30 minutes with 2 mL in circulation. For the syringe pump setups, 2 mL of each solution were manually flushed through the system.

First, for device disinfection, it was washed with 70 % ethanol. Second, phosphate-buffered saline (PBS) was used to remove ethanol residues, which would be toxic for the endothelial cells likewise. Third, the surface of wells and channels were coated with collagen IV (0.1 mg/mL)/fibronectin (1 mg/mL) in PBS. Therefore, 30 µL of this solution were manually pipetted into the channels and 250 µL into the wells and incubated for 2 hours at 37°C. These extracellular matrix components work as adhesion proteins and helped hCMEC/D3-cells to orientate and facilitate their attachment to the surface (Pankov and Yamada, 2002; Müller-Esterl, 2004).

Afterwards, both the wells and the channels of the microfluidic device were washed with sterile-filtered water for three consecutive times, because the coating solution was dissolved in acetic acid, which would be toxic for the endothelial cells. This step was conducted manually with 500 µL per well and 25 µL for each channel. Finally, the microfluidic system was rinsed with 2 mL EBM-2 to equilibrate the system and to provide the final environment for hCMEC/D3-cells (Pankov and Yamada, 2002; Müller-Esterl, 2004).

3.4.1.8 Cell-seeding (step 8)

After detaching the cells from the surface of the T25-flask with the enzyme trypsin (Trypsin/EDTA solution 0.05 %/0.02 %), they were pelleted in a centrifuge at 300 rcf for 5 minutes and resuspended in the volume of EBM-2 required to seed 80.000 cells/cm² in the wells and 240.000 cells/cm² in each channel. hCMEC/D3 detached latest after 3 days exposed to flow on the microfluidic device. Consequently, a higher cell number in comparison to the well plate experiments, was chosen to achieve a confluent cell monolayer overnight. For this purpose, 40 µL of the cell-suspension, equivalent to 240.000 cell/cm², were pipetted into a 200 µL pipette tip, which was placed in one of the ports. Afterwards, it was sucked into the channels with a 1 mL manual syringe when using the syringe pump. In the case of the peristaltic

pump, the cells were pipetted straight into the channels via the ports. This also provided a better distribution of the cells within the latter.

3.5 Chip-designs

3.5.1 Shear gradient chip

The first microfluidic chip design was drafted with the software AutoCAD and was provided by the Technical University Vienna (Figure 11B). This device featured four channels, in which hCMEC/D3 cells were cultivated in the following. Each of them had a height of 0.25 mm (material: PDMS 250 µm), an area of 0.58 cm² with a volume of 15 µL. Furthermore, each channel was composed of eight differing widths, ranging from 0.3 mm to 2.4 mm, resulting in a shear gradient (Figure 11A; corresponding shear stress: 3.8). This was valuable during the first set of experiments since eight different shear stress values could be tested at once and the widths preferred in the cultivation of hCMEC/D3 were selected. In addition, the "start flow rate" and the "maximum flow rate increase" on the chip were tested. With the aim of introducing a protocol for hCMEC/D3 cells on a microfluidic device, valuable conclusions could be drawn using the shear gradient chip combined with a syringe pump (AutoCAD software available at https://www.autodesk.com/products/autocad/overview, accessed September 27, 2019).
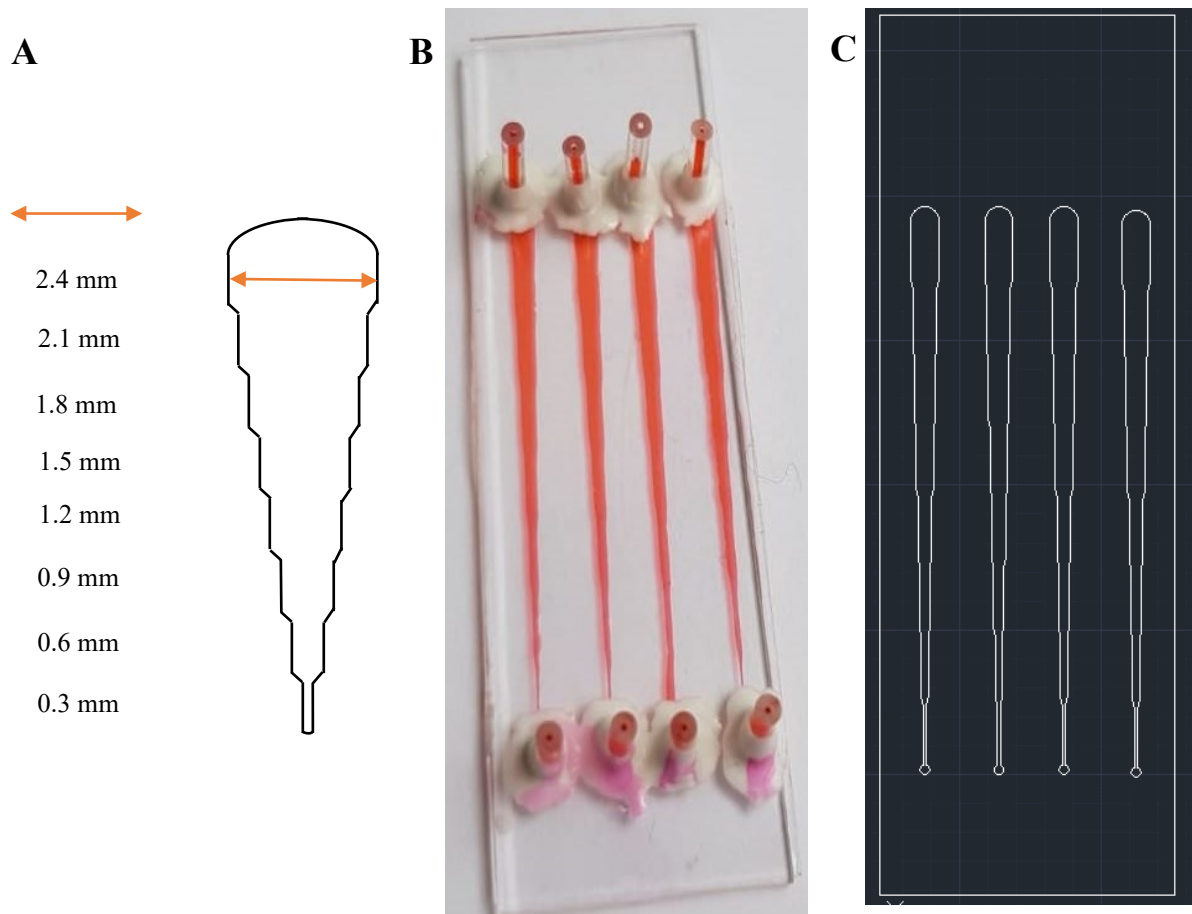
Figure 11: Properties of the shear gradient chip
(A) Basic properties of a channel of the microfluidic device. (B) Fully assembled microfluidic device with red Dr.Oetker food colour, diluted in water, to visualise the four channels. (C) AutoCAD-Plot of a microfluidic device with four channels.

3.5.2 Straight channel chip

The second microfluidic device employed during the current study was also designed using the software AutoCAD (Figure 12C). The hCMEC/D3 cells seemed to proliferate best to a confluent cell layer on the chip at areas with wider widths. Since a surface of 1 cm² was desired to obtain sufficient cell material for subsequent Real-Time qPCR analysis, 2.1 mm and 2.4 mm were the widths of interest for this chip format. In the following, these channels were compared with the conclusion that hCMEC/D3 were cultivated best at a width of 2.1 mm (Figure 12A; correspondent shear stress: 3.8). As the surface of the chip remained a critical factor, a modification with 2 % APTES was tested and the best coating medium was selected. Furthermore, the straight channel chip was combined with a peristaltic pump, which operated in a circulation. Relating to these alterations, the flow rate increase, the duration of the experiments and the duration of exposure to target shear stress values were adapted in comparison to the setups with the shear gradient chip and the syringe pump. In summary, the final design of this microfluidic device featured four channels with a consistent width of 2.1 mm, 0.25 mm height (PDMS 250 µm), a surface area of 1 cm² and a volume of 25 µL each. This chip format was developed for the cell lysis experiments with following Real-Time qPCR-analysis (AutoCAD software available at https://www.autodesk.com/products/autocad/overview, accessed September 27, 2019).
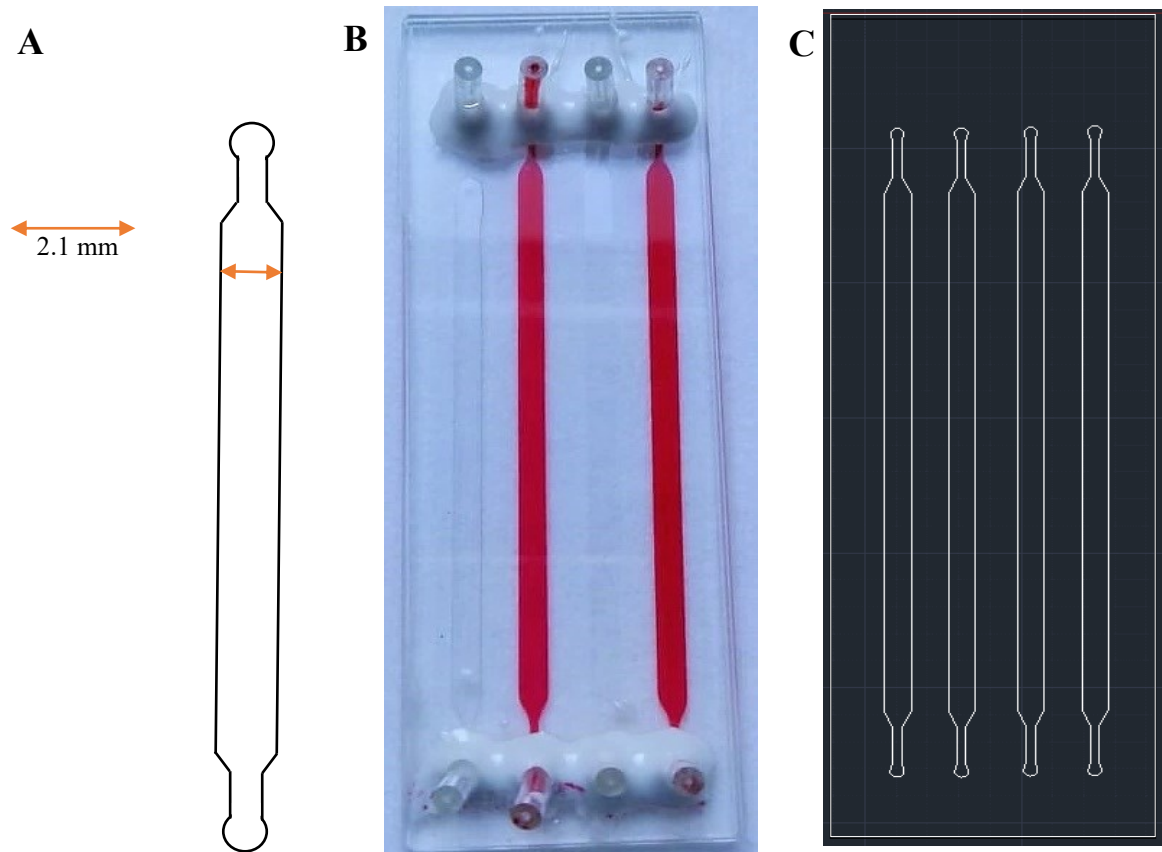
Figure 12: Properties of the straight channel chip
(A) Basic properties of a channel of the microfluidic device. (B) Fully assembled microfluidic device with
with red Dr.Oetker food colour, diluted in water to visualise the four channels. (C) AutoCAD-Plot of a
microfluidic device with four channels.

3.6 Microfluidic pumps: experimental designs

3.6.1 Syringe Pump
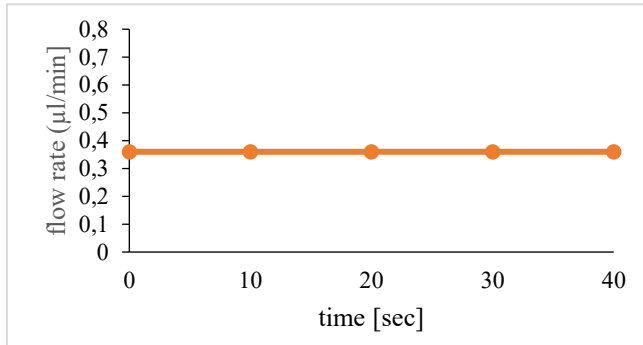
Figure 13: Constant flow profile of the syringe pump, e.g. 0.36 µL/sec.

The syringe pump transports the liquid, in this case EBM-2 medium, with a constant flow through the microfluidic device (Figure 13). A manual 5 mL-syringe was connected to remove air bubbles before the start of the experiment (Figure 14/5). The syringe pump was built up in a vertical position to cause the ascending of air bubbles in the medium-syringe and to prevent them from entering the system (Figure 14/1). After the tubes were connected to the initial medium syringe and a valve was passed (Figure 14/4), the EBM-2 medium entered the channels with the seeded cells. The shear gradient chip was only employed in combination with the syringe pump (3.5.1). The chip was placed on a heating plate and prewarmed to 37 °C to work at physiological temperature. Once the medium was pumped through the channel, it was collected in a 50 mL falcon tube. After the entire volume of one syringe was flushed through the system, the run was stopped. Subsequently, the medium was collected in the final falcon tube, sterile filtered and the process repeated. As the size of the syringes with a maximum of 50 mL greatly restricted the maximum flow rate and did not allow the application of high flow rates overnight, a peristaltic pump was more suitable and established later on.
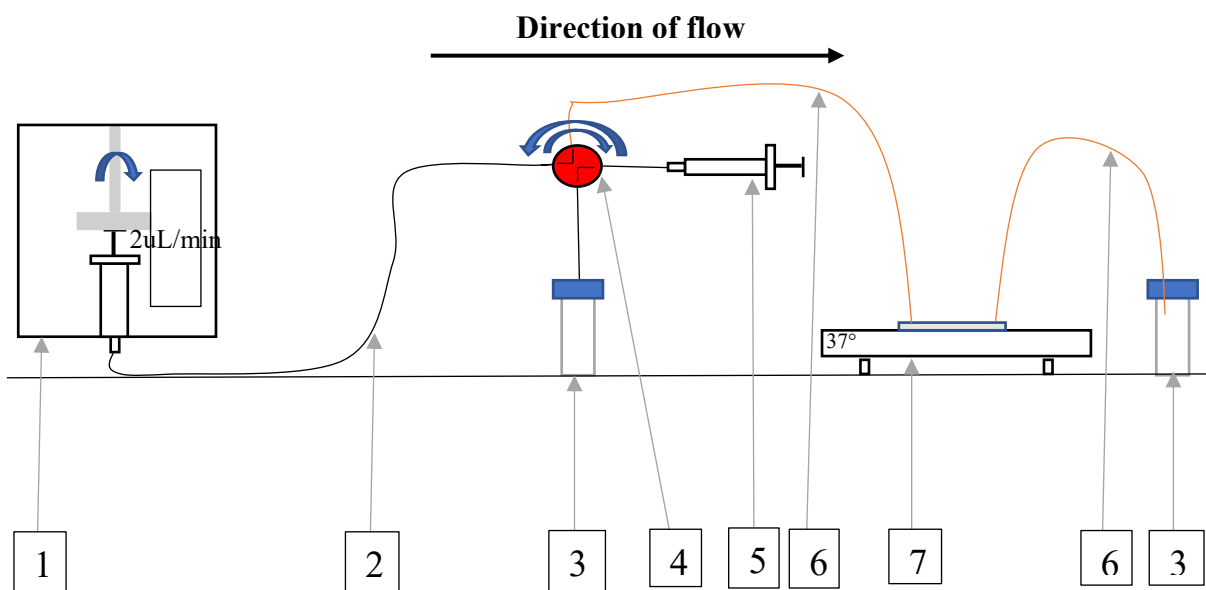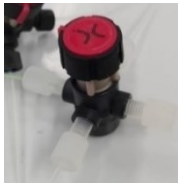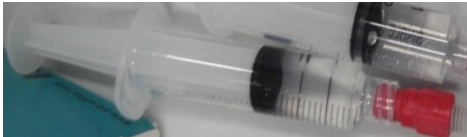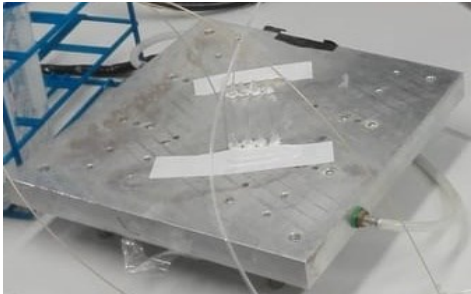
Figure 14: Syringe pump - experimental design. (1) Syringe pump. (2) Tygon-tubing. (3) Waste falcon tubes. (4) Valve. (5) Manual syringe. (6) PEEK tubing. (7) 37°C heating plate.

In Table 6, the materials required for the syringe pump setup are listed and illustrated.

Table 6: Properties of the syringe pump - experimental design.

Scheme-number	Material	Illustration
1	Syringe pump and plastic syringes (1-50 mL)	
2	Tygon-tubing	See Section 3.4.1.6, Inlet- and outlet tube manufacturing with epoxy adhesive
3	Falcon tubes collecting traversed EBM-2	
4	Valve	
5	5 mL-syringe (manual washing)	
6	PEEK tubing	Section 3.4.1.6, Inlet- and outlet tube manufacturing with epoxy adhesive
7	Heating plate (37°C) and microfluidic device (shear gradient chip)	

3.6.2 Peristaltic pump
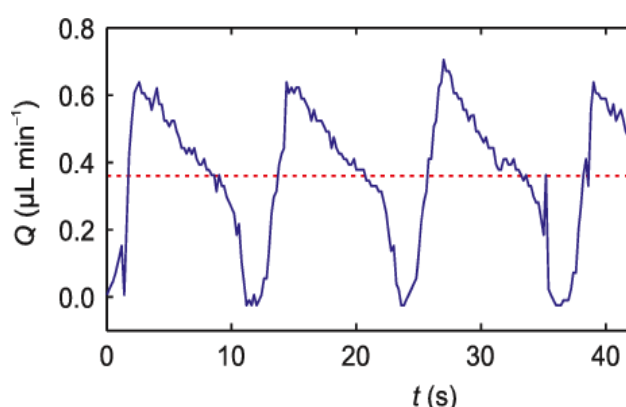
Figure 15: Peristaltic flow profile, e.g. 0.36 µL/sec. Image was taken from Skafte-Poedersen *et al.*, 2011.

To optimise the process and more importantly to apply higher shear stress values for a longer period, a peristaltic pump was installed. This device operates in circulation with a reservoir bottle. Hence, this circulation system saved medium in comparison to the syringe pump system. Besides and more significantly, it was not stopped to refill the syringes. This might have had an impact on the cells in the syringe pump setup. Most importantly, the peristaltic pump imitates a pulsatile flow profile as it is found in human blood vessels. Consequently, it performs a short backflow, whereas the syringe device produces a constant linear flow profile (Figure 13/Figure 15).

In this setup, two Marprene tubes with different diameters were sequenced in a row and connected with PEEK tubing. This was installed, as the range of flow rates needed was too wide for only one diameter of a tube. Hence, a minimum flow rate of 2 µL/min was reached by the 0.25 mm bore tube. This was set on day 0 to adapt the cells to the flow situation without immediately detaching them. However, this tube also had a maximum of 230 µL/min (1,75 dyne/cm²). To achieve shear stresses of 3 or 7.5 dyne/cm² for instance, higher flow rates had to be applied and were reached by the tube with a diameter of 0.5 mm. This had a minimum flow rate of 5.6 µL/min and a maximum of 1.01 mL/min. Consequently, a tube change was done when necessary to achieve the higher shear stress values. For this tube change, the system had to be stopped for about 30 minutes.

Figure 16 shows the arrangement of the peristaltic pump theoretically and as set up in the laboratory next to the fluorescent microscope (Figure 16, bottom, right).
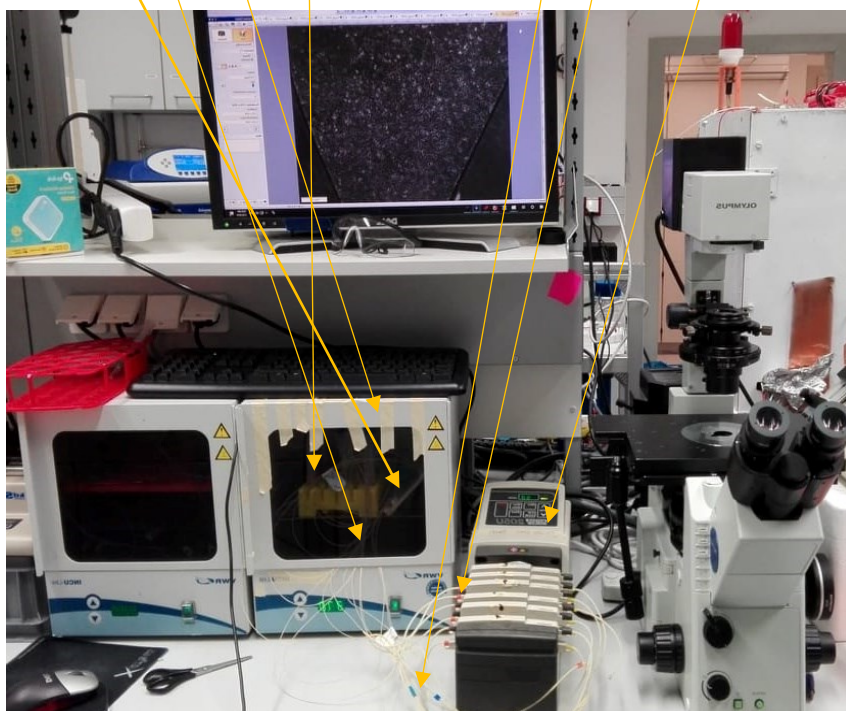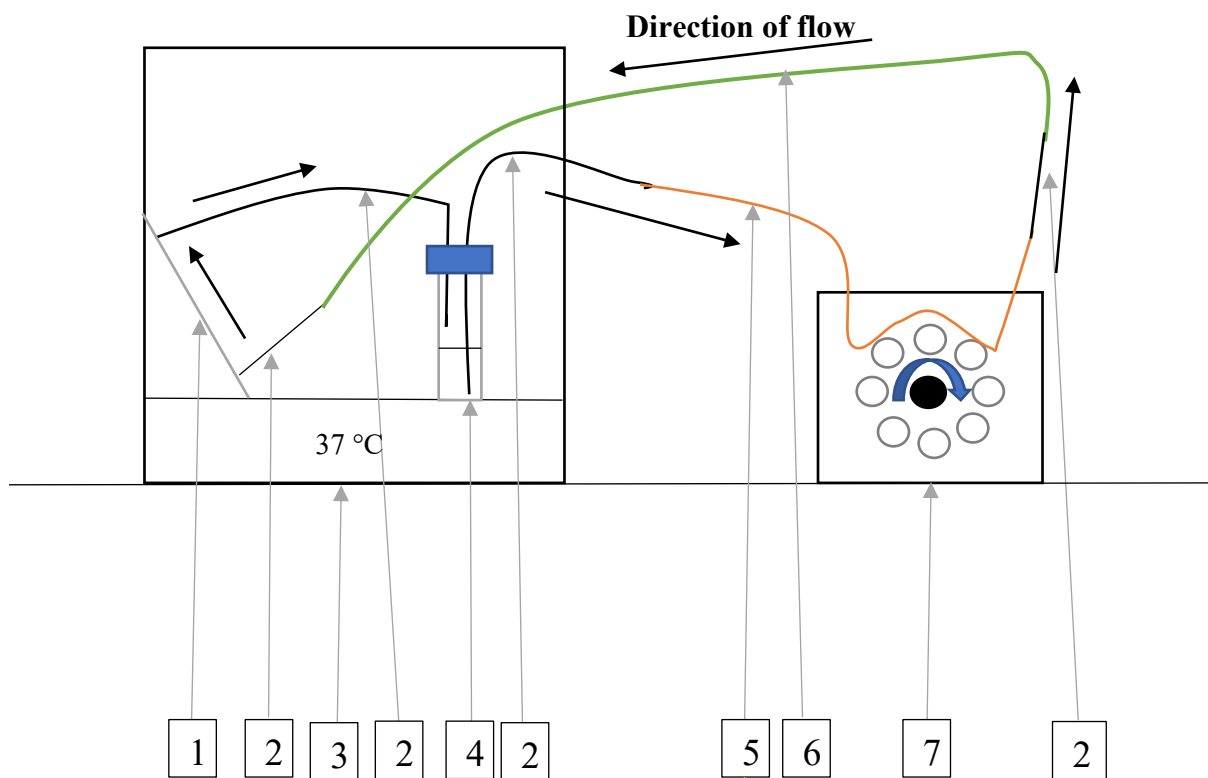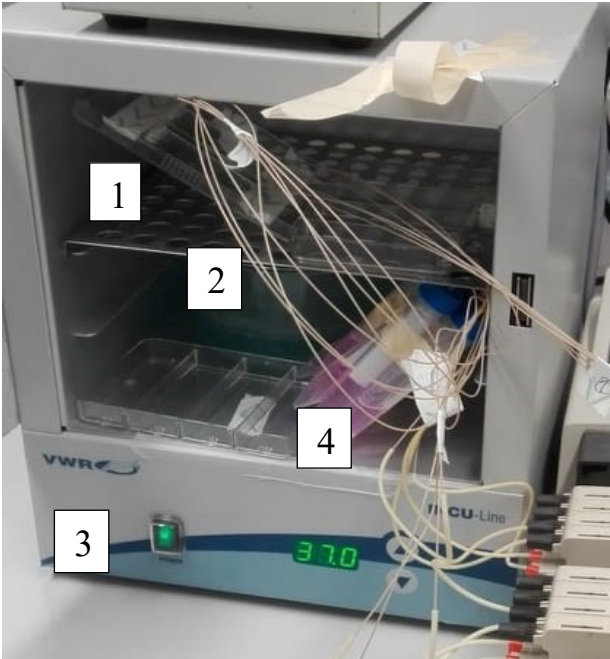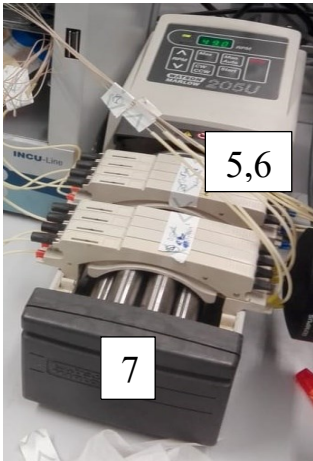
Figure 16: Peristaltic pump – experimental design. (1) Chip format. (2) PEEK-tubing. (3) Incu-Line 37 °C Incubator. (4) Falcon collecting tube. (5) 0.25 mm manifold peristaltic tube. (6) 0.5 mm manifold peristaltic tube. (7) Peristaltic pump.

In Table 7, the materials required for the peristaltic pump setup are listed and illustrated.

Table 7: Properties of the peristaltic pump - experimental design.

Scheme-number	Material	Illustration
1-4	Incu-Line 37 °C incubator (3) with microfluidic device (1), PEEK tubing (2) and Falcon collecting tube (4)	
5-7	Peristaltic pump (Watson Marlow 205 U) with Marprene tubes	

3.6.3 Flow-meter: Conversion from µL/min to rounds per minute (rpm)

Whereas the syringe pump is set to a constant flow rate, for instance in µL/min, the peristaltic pump is controlled in rounds per minute (rpm). Hence, to compare the results of the syringe pump with those of the peristaltic pump, the rpm values had to be converted in flow rates and shear stress values. This was done by using a table provided by Watson Marlow for the Marprene tubes with the bores of 0.25 mm and 0.50 mm (Figure 17) (Watson Marlow - Schlauchpumpen für Forschung und Labor).

Figure 17: Table provided by Watson Marlow for conversion from rpm to µL/min for tube bores 0.25 mm and 0.50 mm. Image was taken from https://www.omega.com/en-us/resources/flow-meters, accessed September 28, 2019.

Additionally, a flow meter was employed to verify if the peristaltic pump was equilibrated to the data provided by Watson Marlow. This instrument measures the linear flow rate of a liquid. The sensor used in the current study has a limit of 50 µL/min. Consequently, in the case of the tube bore of 0.25 mm, measurements were taken for 0.5, 5, 15 and 20 rpm. For the tube bore of 0.5 mm, measurements were taken for 0.5, 1, 2.5 and 5 rpm, consecutively. Afterwards, the mean values were calculated, extrapolated and a trendline was projected for the entire range of the peristaltic pump (https://www.omega.com/en-us/resources/flow-meters accessed September 28, 2019).
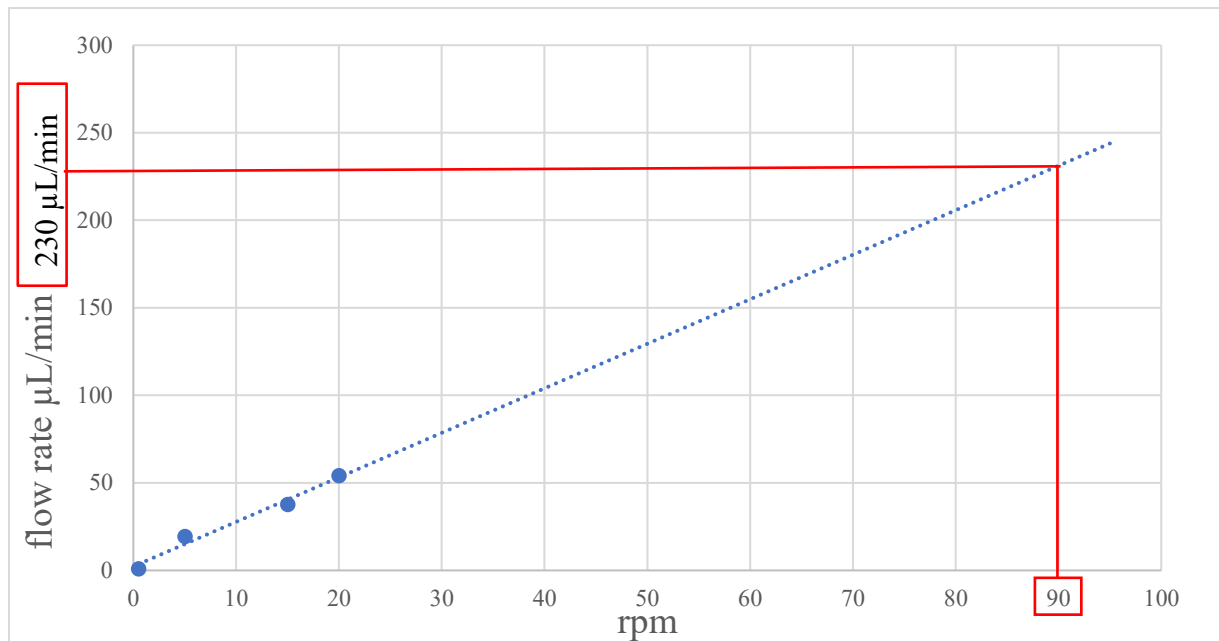
Figure 18: Conversion from rpm to µL/min for Marprene tube, bore: 0.25 mm.

The provided table of Watson Marlow for the tube bore of 0.25 mm stated a flow rate of 230 µL/min at 90 rpm. This was coherent with the flow rate for the peristaltic pump extrapolated from the measured data by the sensor (Figure 18). One experiment (n=1) was performed with 6903 measurements. Hence, the enclosed table by Watson Marlow was accurate enough to estimate shear stress values with the excel sheet in the next section (Figure 20).

The same was valid for the tube bore of 0.50 mm with 1.01 mL/min at 90 rpm, which was reproduced by the flow meter (Figure 19). Therefore, the peristaltic pump, employed in our study, was also equilibrated for the 0.50 mm tube according to the manufacturer's table. One experiment (n=1) was performed with 5691 measurements. Its data was then used to calculate shear stress values with the following excel sheet (Figure 20).
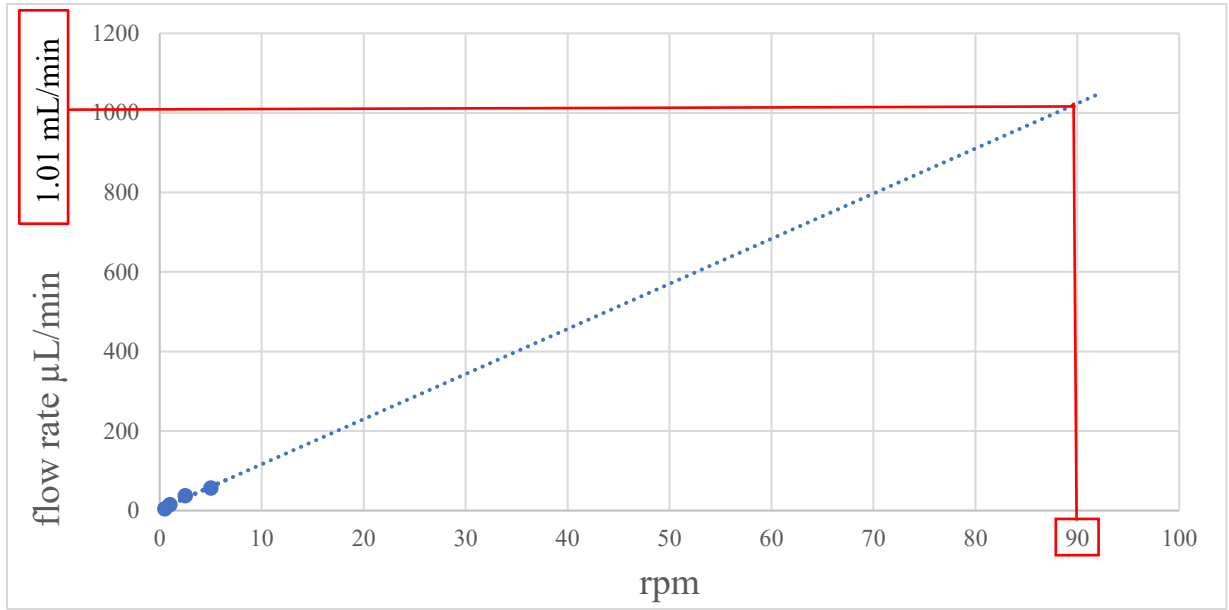
Figure 19: Conversion from rpm to µL/min for Marprene tube, bore: 0.50 mm.

3.7 Shear stress calculation

3.7.1 Excel Sheet

An excel sheet was used to calculate the shear stress values corresponding to the flow rates (Figure 20: Excel sheet for shear stress calculation provided by the Vienna University of Technology). It must be stated that the dynamic viscosity (µ) of the medium, used in our study, has a value above 1 (personal information from authors of Neuhaus *et al.*, 2006). However, in the current study, the model assumption was made that µ equals 1 and thus has the same dynamic viscosity as water. For a channel with a rectangular cross-section, the parameters inserted into the program were the width (w) and height (h) of the channel of the microfluidic device. In the case of the shear gradient chip (3.5.1), eight different values for each section were entered, resulting in eight different shear stress values. In addition, the volume flow rate (Q) in µL/min was considered. Finally, the shear stress in dyne/cm² was automatically calculated according to the formula:

$$\tau = \frac{6 * \mu * Q}{w * ht}$$

Figure 20: Excel sheet for shear stress calculation provided by the Vienna University of Technology.
τ: shear stress, µ: dynamic viscosity of water, Q: volumeflow, ht: height, w: width

3.7.2 Simulation of fluid flow within the channels

The simulation of fluid behaviour resulting in the shear stresses, applied in the shear gradient- and the rectangle channel – experiments, was conducted for the relevant flow rates by using the software Autodesk CFD. This program performs computational fluid dynamics simulations. These predict the flow of fluids in certain designs, in our study the channels within the microfluidic device (https://www.autodesk.com/products/cfd/overview, accessed April 11, 2020).

In the case of the shear gradient chip, a flow rate of 13 µL/min was applied for the simulation (4.2.1). For the straight channel chip with 2100 µm width, flow rates of 13, 130, 390 and 985 µL/min were entered into the program, respectively (4.2.2). This application was a valuable tool in the current study to verify, if the fluids behaved in the channels as calculated by the Excel sheet.

3.8 Experimental Setups

In the course of the current study, different experimental setups were applied. These were adapted towards the duration of the experiments, parameters in the design of the chip, the final flow rate, its increase and the FBS-concentration. The aim was to establish a flow-protocol for hCMEC/D3 in a microfluidic device and to obtain cell-lysates at different final shear stresses for subsequent Real-Time qPCR-analysis (3.13). Hence, the following tables describe the altered experimental parameters of the single experiments.

3.8.1 Experiment no. 1 to 4

The experiments no. 1 to 4 served as preliminary tests to study the basics of chip manufacturing and to develop a seeding procedure suitable for hCMEC/D3 on a microfluidic device in combination with a syringe pump. Three chips were built for each of these experiments.

3.8.2 Experiment no. 5

The maximum duration that hCMEC/D3 cells stay attached on the chip at low flow rates was evaluated using this setup. Cell's detachment and cluster formation were assessed. As the shear gradient chip was used, the response of the cells, located at different widths, was closely observed. The coating solution of this experiment was 0.5 % gelatine. The seeding number was 360.000 cells/cm². The flow rate of 0.063 µL/min was applied after initial 2 hours of cell seeding on day 0. PEEK and Tygon-tubing were used (tube diameters: 3.4.1.6). Two Chips were built for this experiment. The properties and the setup of experiment no. 5 are summarised in Table 8 and Table 9.

Table 8: Properties of experiment no. 5.

Parameter to be examined	Chip design	Pump device	Experiment no.
Maximum duration of the experiment	Shear gradient chip	Syringe pump	5

Table 9: Setup of experiment no. 5.

Day	Width Gradient Chip [mm]								Flow rate [µL/min]	Duration [h]	FBS [%]
	0.3	0.6	0.9	1.2	1.5	1.8	2.1	2.4			
	Shear stress [dyne/cm²]										
0	0.0034	0.0017	0.0011	0.00084	0.00067	0.00056	0,00048	0.00042	0.063	24	5
1	0.0034	0.0017	0.0011	0.00084	0.00067	0.00056	0,00048	0.00042	0.063	24	5
2	0.0034	0.0017	0.0011	0.00084	0.00067	0.00056	0,00048	0.00042	0.063	24	5
3	0.0067	0.0034	0.0022	0.0017	0.0013	0.0011	0.00096	0.00084	0.125	24	5
4	0.013	0.0067	0.0044	0.0033	0.0026	0.0022	0.0019	0.0017	0.25	24	5
5	0.027	0.013	0.009	0,0067	0.0053	0.0044	0.0038	0.0033	0.5	24	5
6	0.053	0.027	0.018	0.013	0.011	0.0088	0.0076	0.0067	1	24	5
7	0.11	0.054	0.036	0.026	0.021	0.018	0.015	0.013	2	24	5
8	0.21	0.11	0.072	0.53	0.043	0.036	0.031	0.027	4	24	5
9	0.53	0.27	0.18	0.13	0.11	0.089	0.076	0.067	10	24	0.25
10	0.7	0.36	0.24	0.18	0.14	0.12	0.1	0.08	13	24	0.25
11	1.3	0.67	0.44	0.33	0.27	0.22	0.19	0.17	25	24	0.25
12	2.1	1.06	0.71	0.53	0.43	0.36	0.31	0.27	40	10	0.25
13	3.2	1.6	1.1	0.8	0.64	0.53	0.46	0.4	60	4	0.25
13	0.011	0.54	0.036	0.026	0.021	0.018	0.015	0.013	2	24	0.25
14	4.8	2.4	1.6	1.2	0.96	0.8	0.69	0.6	90	4	0.25
14	End of the experiment										

3.8.3 Experiment no. 6

The channel width was an important parameter to be examined before the establishment of the straight channel chip. The assumption was that the broader the channel width, the lower the shear stress and hence the higher the aggregation of cells. In contrast, the smaller the channel width, the higher the shear stress and thus the more cells were likely to detach. Consequently, these parameters had to be taken into consideration. In addition, the start flow rate was investigated and chosen to be 0.125 µL/min. This flow rate was applied after initial 2 hours of cell seeding on day 0. PEEK and Tygon-tubing were used. Two chips were built for this experiment. The properties and the setup of experiment no. 6 are summarised in Table 10 and Table 11.

Table 10: Properties of experiment no. 6.

Parameter to be examined	Chip design	Pump device	Experiment no.
Channel-width Start flow rate	Straight channel chip	Syringe pump	6

Table 11: Setup of experiment no. 6.

Day	Width straight channels [mm]		Flow Rate [µL/min]	Duration [h]	FBS [%]
	2.1	2.4			
	Shear stress [dyne/cm²]				
0	0.00095	0.00084	0.125	24	5
1	0.0019	0.0017	0.250	24	5
2	0.0038	0.0033	0.5	24	5
3	0.0076	0.0067	1	24	5
4	0.015	0.013	2	24	0.25
5	0.031	0.027	4	24	0.25
6	0.061	0.053	8	24	0.25
6	0.11	0.1	15	24	0.25
7	0.23	0.2	30	24	0.25
8	0.46	0.4	60	4	0.25
8	0.015	0.013	2	24	0.25
9	0.92	0.8	120	4	0.25
9	0.015	0.013	2	24	0.25
10	3.66	3.2	480	1	0.25
10	End of the experiment				

3.8.4 Experiment no. 7

The optimum height for the channel should be selected with this setup. PDMS material of 250 µm and 500 µm height was available. When the height is doubled, the shear stress is quartered and the same difficulties as previously described in section 3.8.3 emerge. Furthermore, the start flow rate was tested again and set to be 1 µL/min, as this higher initial flow rate seemed to support the confluency of the cells and repress the overgrowing of cells. This flow rate was applied after initial 2 hours of cell seeding on day 0. PEEK and Tygon-tubing were used. Two chips were built for this experiment. From this experiment onwards, collagen IV (0.1 mg/mL)/fibronectin (1 mg/mL) was applied as a coating solution. The properties and the setup of experiment no. 7 are summarised in Table 12 and Table 13.

Table 12: Properties of experiment no. 7.

Parameter to be examined	Chip design	Pump device	Experiment no.
Channel-height	Straight channel chip	Syringe pump	7
Start flow rate			

Table 13: Setup of experiment no. 7.

Day	Height straight channels [mm]		Flow rate [µl/min]	Duration [h]	FBS [%]
	0.25	0.5			
	Shear stress [dyne/cm²]				
0	0.0076	0.0019	1	24	5
1	0.015	0.0038	2	24	5
2	0.031	0.0037	4	24	5
3	0.061	0.015	8	24	0.25
4	0.11	0.029	15	24	0.25
5	0.23	0.057	30	24	0.25
6	0.46	0.11	60	4	0.25
6	End of the experiment				

3.8.5 Experiment no. 8

The chips were baked in the incubator for 2 hours instead of overnight and 2 % APTES was applied for surface modification and better cell adhesion. Furthermore, the start flow rate was once again altered to 4 µL/min as cells withstood an initial high flow rate in experiment no. 7 (3.8.4). This flow rate was applied after initial 2 hours of cell seeding on day 0. PEEK and Tygon-tubing were applied during this experiment. Three chips were built for this experiment. The properties and the setup of experiment no. 8 are summarised in Table 14 and Table 15.

Table 14: Properties of experiment no. 8.

Parameter to be examined	Chip design	Pump device	Experiment no.
Duration of chips baked in the oven after assembly	Straight channel chip	Syringe pump	8
Modification of chip-surface			
Start flow rate			

Table 15: Setup of experiment no. 8.

Day	Shear stress [dyne/cm²]	Flow rate [µL/min]	Duration [h]	FBS [%]
0	0.03	4	24	5
1	0.09	12	24	0.25
2	0.27	36	4	0.25
2	0.015	2	24	0.25
3	0.82	108	3	0.25
3	0.015	2	24	0.25
4	2.5	324	1	0.25
4	0.015	2	24	0.25
5	7.6	1000	0.33	0.25
5	End of the experiment			

3.8.6 Experiment no. 9 to 11

The peristaltic pump was used for the first time in the current study. Moreover, the manufactured microfluidic devices were leaky before the start of the experiments no. 9 to 11. This was most likely due to the reason, that the plasma-cleaner did not function properly. Consequently, the binding of the glass to the PDMS did not work with medium leaking out of the channels before the start of the experiment. Three chips were built for each experiment. These experiments were used to circulate medium in the peristaltic pump without a microfluidic device, whilst the plasma-cleaner got repaired.

3.8.7 Experiment no. 12

To obtain comparable cell-lysates for Real-Time qPCR-analysis, a consistent protocol had to be applied. The cells were thought to express stable gene patterns only when subjected to target shear stress values for 3 consecutive days. Thus, to reach these values without detaching the cells, a protocol with a duration of at least 7 days was chosen. As a start flow rate of 4 µL/min seemed to detach cells previously, 2 µL/min were chosen. This flow rate was applied after initial 2 hours of cell seeding on day 0. The target shear stress was selected relatively low at 0.1 dyne/cm² to examine if the cells generally do not detach for the specified duration on the chip. Furthermore, a 24-well plate approach was set up in parallel to the flow experiments as a static control with a seeding number of 80.000 cells/cm². Besides, the seeding number of the flow experiments was altered to 240.000 cells/cm². Three chips were built for this experiment. The properties and the setup of experiment no. 12 are summarised in Table 16 and Table 17.

Table 16: Properties of experiment no. 12.

Parameter to be examined	Chip design	Pump device	Experiment no.
Final shear stress: 0.1 dyne/cm²			
Duration of the experiment	Straight channel chip	Peristaltic pump	12
Exposure to final shear stress			
Start flow rate			

Table 17: Setup of experiment no. 12.

Day	Shear stress [dyne/cm²]	Flow rate [µL/min]	Duration [h]	rpm	Tube-bore [mm]	FBS [%]
0	0.015	2	24	0.8	0.25	5
1	0.015	2	2	0.8	0.25	0.25
1	0.026	3.4	2	1.3	0.25	0.25
1	0.040	5.2	2	2	0.25	0.25
1	0.055	7.3	24	2.8	0.25	0.25
2	0.07	9.1	2	3.5	0.25	0.25
2	0,085	11.2	2	4.3	0.25	0.25
2	0.1	13	24	5	0.25	0.25
3	0.1	13	24	5	0.25	0.25
4	0.1	13	24	5	0.25	0.25
5	0.1	13	24	5	0.25	0.25
6	End of the experiment					

3.8.8   Experiment no. 13

Since hCMEC/D3 remained on the chip at a final shear stress of 0.1 dyne/cm², afterwards 5 dyne/cm² were investigated. Additionally, an intermediate target shear stress of 1 dyne/cm² was reached on day 2 towards further standardisation of the protocol. The start flow rate of 2 µL/min was applied after initial 2 hours of cell seeding on day 0. Three chips were built for this experiment. The properties and the setup of experiment no. 13 are summarised in Table 18 and Table 19.

Table 18: Properties of experiment no. 13.

Parameter to be examined	Chip design	Pump device	Experiment no.
Final shear stress: 5 dyne/cm²	Straight channel chip	Peristaltic pump	13
Intermediate shear stress on day 2			

Table 19: Setup of experiment no. 13.

Day	Shear stress [dyne/cm²]	Flow rate [µl/min]	Duration [h]	rpm	Tube-bore [mm]	FBS [%]
0	0.015	2	20	0.8	0.25	5
1	0.015	2	2	0.8	0.25	0.25
1	0.026	3.4	2	1.3	0.25	0.25
1	0.040	5.2	2	2	0.25	0.25
1	0.055	7.3	24	2.8	0.25	0.25
2	0.1	13	2	5.6	0.25	0.25
2	0.20	26	2	10	0.25	0.25
2	0.40	52	2	20	0.25	0.25
2	0.70	91	2	35	0.25	0.25
2	1	130	24	50	0.25	0.25
3	0.30	39	2	3.5	0.5	0.25
3	0.60	78	2	7	0.5	0.25
3	1.30	168	2	15	0.5	0.25
3	2.60	336	2	30	0.5	0.25
3	5	650	24	58.9	0.5	0.25
4	5	650	24	58.9	0.5	0.25
5	5	650	24	58.9	0.5	0.25
6	End of the experiment					

3.8.9 Experiment no. 14

Prior to the seeding of hCMEC/D3, the channels of the microfluidic device were leaky at the connection between the microscopic slides and the ports. This could have been due to a product change of the epoxy adhesive. Consequently, the EBM-2 medium did not remain inside the channels. Three chips were built for this experiment.

3.8.10 Experiment no. 15

The cells seemed to detach in a 6-day-setup and could not endure a final shear stress exposure of 3 days. Consequently, a 4-day-setup was designed and the final shear stress exposure was shortened to 24 hours. The target shear stress was kept at 5 dyne/cm². In addition, 1 dyne/cm² was reached on day 2. The start flow rate of 2 µL/min was applied after initial 2 hours of cell

seeding on day 0. Three chips were built for this experiment. The properties and the setup of experiment no. 15 are summarised in Table 20 and Table 21.

Table 20: Properties of experiment no. 15.

Parameter to be examined	Chip design	Pump device	Experiment no.
Final shear stress: 5 dyne/cm²			
Duration of the experiment	Straight channel chip	Peristaltic pump	15
Exposure to final shear stress			

Table 21: Setup of experiment no. 15.

Day	Shear stress [dyne/cm²]	Flow rate [µL/Min]	Duration [h]	rpm	Tube-bore [mm]	FBS [%]
0	0.015	2	24	0.8	0.25	5
1	0.015	2	2	0.8	0.25	0.25
1	0.034	4.5	2	1.7	0.25	0.25
1	0.09	12	2	4.6	0.25	0.25
1	0.27	36	24	13.8	0.25	0.25
2	0.30	39	2	3.5	0.5	0.25
2	0.60	78	2	7	0.5	0.25
2	1	130	24	11.6	0.5	0.25
3	1.30	168	2	15	0.5	0.25
3	2.5	330	2	30	0.5	0.25
3	5	650	24	58.9	0.5	0.25
4	End of the experiment					

3.8.11 Experiment no. 16

The chips built in advance of experiment no. 16 were leaky at the connection between the microscopic slides and the ports. This could have been due to a change of the needle of the drilling machine. This resulted in a too large diameter of the drilled holes, which exceeded the diameter of the ports. Consequently, the EBM-2 medium did not remain inside the channels. Three chips were built for this experiment.

3.8.12 Experiment no. 17

2.5 dyne/cm² were tested in this experiment in a 4-day-setup and 1 dyne/cm² was reached on day 1. The cells got exposed to the final shear stress only for 24 hours. The start flow rate of 2 µL/min was applied after initial 2 hours of cell seeding on day 0. Three chips were built for

this experiment. The properties and the setup of experiment no. 17 are summarised in Table 22 and Table 23.

Table 22: Properties of experiment no. 17.

Parameter to be examined	Chip design	Pump device	Experiment no.
Final shear stress: 2.5 dyne/cm²	Straight channel chip	Peristaltic pump	17
Exposure to final shear stress			

Table 23: Setup of experiment no. 17.

Day	Shear stress [dyne/cm²]	Flow rate [µL/min]	Duration [h]	rpm	Tube-bore [mm]	FBS [%]
0	0.015	2	24	0.8	0.25	5
1	0.015	2	2	0.8	0.25	0.25
1	0.034	4.5	2	1.7	0.25	0.25
1	0.09	12	2	4.6	0.25	0.25
1	0.27	36	24	13.8	0.25	0.25
1	0.60	78	2	30	0.25	0.25
1	1	130	24	50	0.25	0.25
2	1.1	145.6	2	13	0.50	0.25
2	1.7	224	2	20	0.50	0.25
2	2.5	330	24	29.5	0.50	0.25
3	2.5	330	24	29.5	0.50	0.25
4	End of the experiment					

3.8.13 Experiment no. 18 and 19

In the coating procedure of experiment no. 18 and 19, the collagen IV/fibronectin coating solution was used more often than four times. Consequently, hCMEC/D3 did not adhere to the surface of the microfluidic device (Figure 103).

3.8.14 Experiments no. 20 to 23

For the last set of experiments, a 3-day-setup was chosen. In addition, an extra time point for cell lysis was introduced on day 2 after 6 hours of exposure to the target shear stress, followed by a cell lysis on day 3 after 24 hours at the target shear stress. The start flow rate of 2 µL/min was applied after initial 2 hours of cell seeding on day 0 for the last set of experiments. The intermediate flow increase-steps, before the 6-hour cell lysis, were shortened to 0.5 hours. Moreover, 0.1 dyne/cm² were chosen as the intermediate shear stress to be reached on day 1 for the standardisation of the protocol. Besides, the FBS-concentration was reduced from 5 % to

1 % instead of 0.25 %. This was due to the reason, that cells seemed to thin out throughout the experiments at an FBS-concentration of 0.25 %. Hence, 1 % was chosen to enable the endothelial cells to steadily proliferate. Finally, the last set of experiments served the main purpose of obtaining cell-lysates in a comparable setup for shear stresses of 0, 0.1, 1, 3, and 7.5 dyne/cm². Three chips were built for the last set of experiments. The properties and setups of the last set of experiments no. 20 to 23 are summarised in Table 24 to Table 32.

Table 24: Properties of experiment no. 20 to 23.

Parameter to be examined	Chip design	Pump device	Experiment no.
Point of cell lysis	Straight channel chip	Peristaltic pump	20 - 23
Reach intermediate shear stress of 0.1 dyne/cm² on day 1			
FBS-concentration			
Duration of the experiment			

3.8.14.1 Experiment no. 20

Table 25: Properties of experiment no. 20.

Final shear stress: 1 dyne/cm²	Straight channel chip	Peristaltic pump	20

Table 26: Setup of experiment no. 20.

Day	Shear stress [dyne/cm²]	Flow rate [µL/min]	Duration [h]	rpm	Tube-bore [mm]	FBS [%]
0	0.015	2	24	0.8	0.25	5
1	0.015	2	2	0.8	0.25	1
1	0.05	6.5	2	0.6	0.5	1
1	0.1	13	24	1.2	0.5	1
2	0.3	40	0.5	3.6	0.5	1
2	0.6	80	0.5	7.2	0.5	1
2	1	130	6	11.6	0.5	1
2	1	130	24	11.6	0.5	1
3	End of the experiment					

3.8.14.2 Experiment no. 21

Table 27: Properties of experiment no. 21.

Final shear stress: 3 dyne/cm²	Straight channel chip	Peristaltic pump	21

Table 28: Setup of experiment no. 21.

Day	Shear stress [dyne/cm²]	Flow rate [µL/min]	Duration [h]	rpm	Tube-bore [mm]	FBS [%]
0	0.015	2	24	0.8	0.25	5
1	0.015	2	2	0.8	0.25	1
1	0.05	6.5	2	0.6	0.5	1
1	0.1	13	24	1.2	0.5	1
2	0.3	40	0.5	3.6	0.5	1
2	0.6	80	0.5	7.2	0.5	1
2	1	130	0.5	11.6	0.5	1
2	1.7	224	0.5	20	0.5	1
2	3	390	6	34.8	0.5	1
2	3	390	24	34.8	0.5	1
3	End of the experiment					

3.8.14.3 Experiment no. 22

Table 29: Properties of experiment no. 22.

Final shear stress: 7.5 dyne/cm²	Straight channel chip	Peristaltic pump	22

Table 30: Setup of experiment no. 22.

Day	Shear stress [dyne/cm²]	Flow rate [µL/min]	Duration [h]	rpm	Tube-bore [mm]	FBS [%]
0	0.015	2	24	0.8	0.25	5
1	0.015	2	2	0.8	0.25	1
1	0.05	6.5	2	0.6	0.5	1
1	0.1	13	24	1.2	0.5	1
2	0.3	40	0.5	3.6	0.5	1
2	0.6	80	0.5	7.2	0.5	1
2	1	130	0.5	11.6	0.5	1
2	1.7	224	0.5	20	0.5	1
2	3	390	0.5	34.8	0.5	1
2	4.6	600	0.5	53.6	0.5	1
2	6.1	800	0.5	71.4	0.5	1
2	7.5	985	6	87.9	0.5	1
2	7.5	985	24	87.9	0.5	1
3	End of the experiment					

3.8.14.4 Experiment no. 23

Table 31: Properties of experiment no. 23.

Final shear stress: 0.1 dyne/cm²	Straight channel chip	Peristaltic pump	23

Table 32: Setup of experiment no. 23.

Day	Shear stress [dyne/cm²]	Flow rate [µL/min]	Duration [h]	rpm	Tube-bore [mm]	FBS [%]
0	0.015	2	24	0.8	0.25	5
1	0.015	2	2	0.8	0.25	1
1	0.05	6.5	2	0.6	0.5	1
1	0.1	13	24	1.2	0.5	1
2	0.1	13	6	1.2	0.5	1
2	0.1	13	24	1.2	0.5	1
3	End of the experiment					

3.9 Static control (24-well plate)

The aim of the current study was to investigate the influence of shear stress on BBB markers of hCMEC/D3 cells. However, for the Real-Time qPCR-method, a static control equivalent to 0 dyne/cm² was required for comparing reasons. To account for this, a parallel setup based on a 24-well plate was established for each chip experiment.

3.9.1 Material

The material for the well-preparation is listed in Table 33.

Table 33: Material for the well-preparation.

Material	Step in Figure 21	Company	Product number
Coverslips (glass, 13 mm diameter)	1-9	Paul Marienfeld	0111530
Plasma-cleaner	2	Harrick-Plasma	PDC-002
24-well plate	3/7	Falcon	Ref353504
APTES 2 % (in ethanol)	5	Sigma Aldrich	440140-100ML
70 % ethanol	4-6	VWR	83.801.360
PBS, sterile	4,8	Gibco	14190-094
Oven 120 °C	6	Binder	9010-0333
Collagen IV Fibronectin	8	Sigma Aldrich	C5533 F1141-5MG
EBM-2	9	Lonza	Cat.#00190860

3.9.2 Workflow of 24-well plate preparation

The workflow of the preparation of the 24-well plate static control is illustrated in Figure 21.
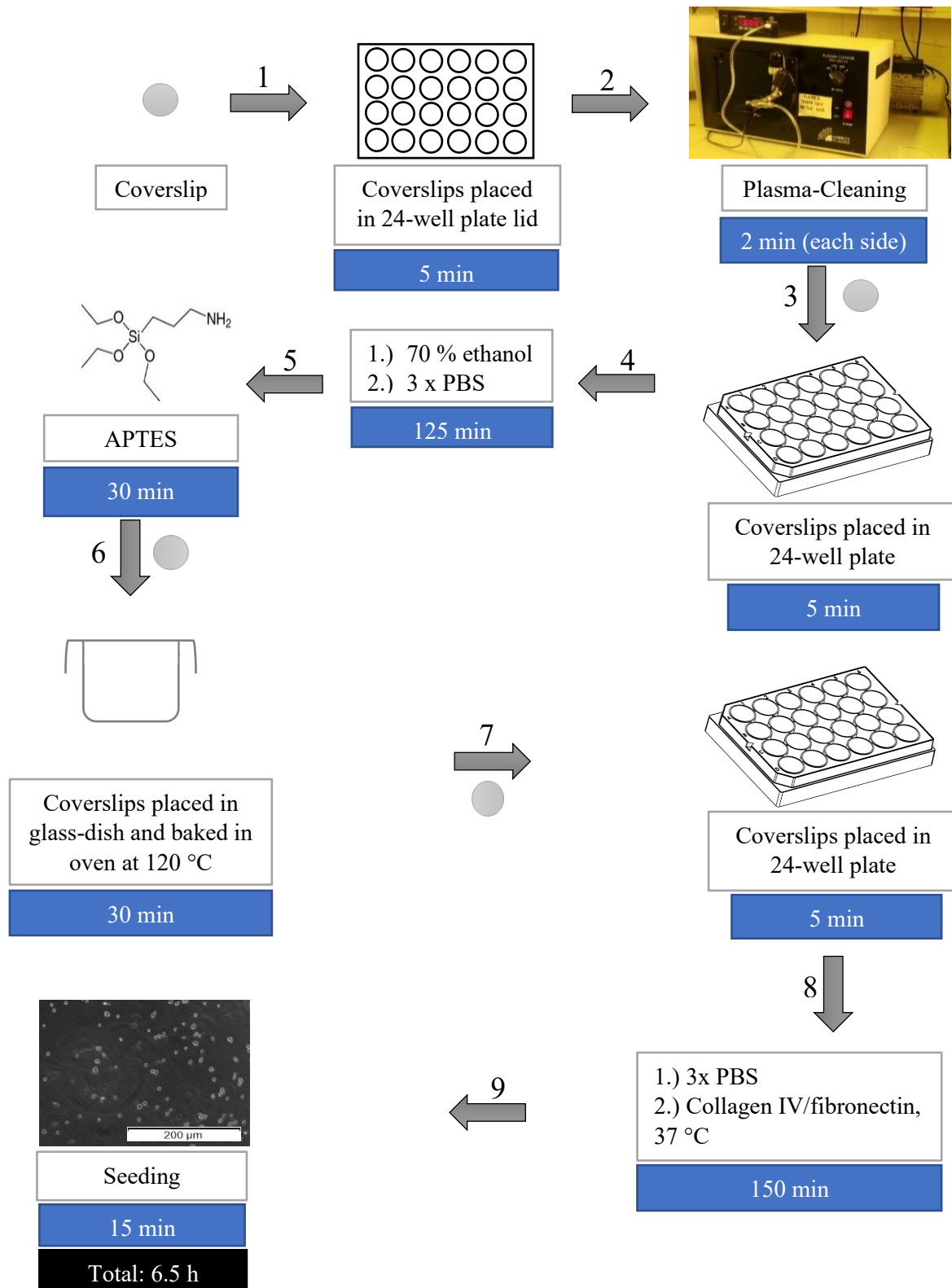
Figure 21: Scheme, illustrating the preparation of a 24-well plate. Image of APTES taken from https://www.carlroth.com/de/de/Life-Science/Histologie-Mikroskopie/Reagenzien/Standardreagenzien/3-Aminopropyltriethoxysilan-%28APTES%29/p/000000000001ade600030023_de, accessed September 27, 2019. Image of 24-well plate taken from Ibidi, cells in focus, 2016.

In the first steps of the preparation of the wells, their surface was treated in the same way as the chip. This was essentially a glass-bottom side combined with 2 % APTES and a coating

solution of collagen IV/fibronectin (Figure 5). Therefore, coverslips with a diameter of 13 mm were used in a 24-well plate.

The basic issue in the process of the well-preparation was the adequate disinfection of the coverslips. Hence, both sides of each coverslip were treated in the plasma-chamber for 2 minutes, as conducted with the chips (3.4.1.4). Next, 70 % ethanol was sterile filtered and 1 mL was pipetted into each well with a following incubation for 60 minutes at RT. It was important to add 70 % ethanol, since it offers an adequate concentration to pass the bacterial cell wall and denature the proteins (https://www.mpibpc.mpg.de/151749/Desinfizierende_Wirkung_von_Alkohol, accessed September 30, 2019).

In contrast, 96 % ethanol evaporates too quickly from surfaces and therefore cannot enter the bacteria. The next step in the well-preparation were three PBS-rinses with 1 mL to remove ethanol-residues. Afterwards, 1 mL of a 2 % APTES solution was added for 30 minutes (Figure 21). APTES-remnants were removed by washing three times with 1 mL absolute ethanol and the coverslips were placed in a glass-lab-dish with a cover. This jar was placed in the incubator and baked at 120 °C for 3 hours.

On the following day, the coverslips were positioned back into the 24-well plate, washed with 1 mL PBS twice and coated with 250 µL collagen IV/fibronectin per well at 37 °C for 3 hours. Subsequently, each well was rinsed with sterile H_2O for three times to remove the acetic acid of the coating solution. Finally, 675 µL cell-solution, to achieve 80.000 cells/cm², was added to each well and incubated at 37 °C (Figure 21). hCMEC/D3 in static conditions were cultivated for the same period as the corresponding flow experiments. At confluency, the FBS in the EBM-2 was reduced to 0.25 % and later 1 %, both according to the setup-tables in section 3.8 (https://www.mpibpc.mpg.de/151749/Desinfizierende_Wirkung_von_Alkohol, accessed September 30, 2019).

3.10 Fluorescence Staining-methods

3.10.1 Live dead staining

The live dead staining was performed in both, the channels and the wells. This was done to determine the cell-vitality at different flow rates in comparison to static conditions. For this purpose, a staining solution of 1 mL EBM-2 with 2 µL calcein-AM (50 µM) and 4 µL ethidium homodimer (2 mM) was prepared and pipetted directly into the destined channel (25 µL) or well (250 µL). Afterwards, these were incubated for 30 minutes at 37 °C. Subsequently, rinsing with EBM-2 (50 µL) was performed manually to eliminate the non-bound dye and reduce

background fluorescence. This step had to occur very carefully, not to accidentally flush away the cells. In principle, the polyanionic dye calcein-AM is non-fluorescent. However, due to intracellular esterase activity, it is converted to fluorescent calcein. This process is only possible in living cells, which then produce green fluorescence detected at excitation/emission (ex/em) 495-515 nanometres (nm). In contrast, ethidium homodimer is excluded by intact cell membranes and only passes those with a damaged cell membrane (Figure 22). The live/dead-ratio was calculated by dividing the live and dead-images in nine sections. The live and dead cells out of three sections were separately and automatically counted with the program ImageJ (https://tools.thermofisher.com/content/sfs/manuals/mp03224.pdf, accessed January 29, 2021; https://slideplayer.com/slide/4088630/, accessed October 2, 2019).
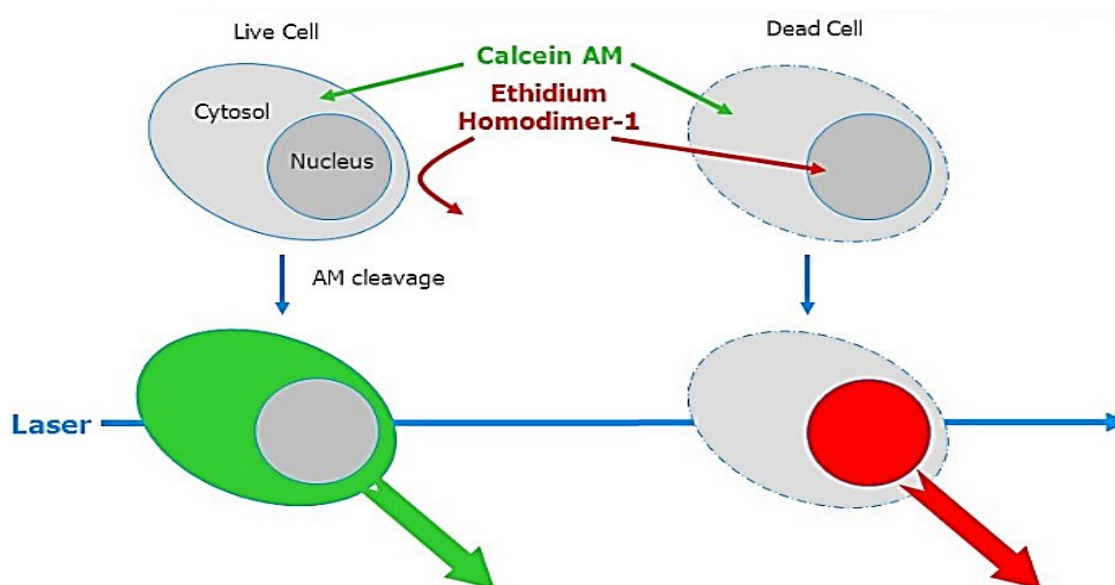
Figure 22: Principle of Live dead Stain. Image was taken from https://slideplayer.com/slide/4088630/, accessed October 2, 2019.

3.10.2 F-Actin staining
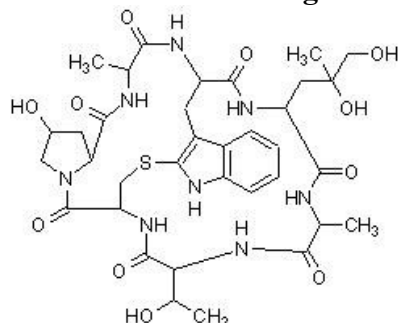
Figure 23: Structure of Phalloidin. Image was taken from https://www.abcam.com/phalloidin-f-actin-depolymerization-inhibitor-ab143533.html, accessed October 2, 2019.

F-actin is a protein of the cytoskeleton. The cytoskeleton has important tasks in the organisation of a cell and forms a network through the whole cytoplasm. Therefore, it plays an important part in the formation of a cell, organises its organelles, but is also involved in cytoplasmic streaming for instance, which transports nutrients and cell organelles across the cytosol (https://biologydictionary.net/cytoskeleton/, accessed October 2, 2019).

In the current study, phalloidin conjugated to rhodamine was selected to stain f-actin (Figure 24). Phalloidin is a fungal

toxin and produced by the mushroom Amanita phalloides. It binds with high affinity and predominantly to filamentous f-actin. As seen in Figure 23, phalloidine is a bicyclic peptide. This dye is a significant marker for the status of a cell (https://biologydictionary.net/cytoskeleton/, accessed October 2, 2019; Phalloidin structure available at https://www.abcam.com/phalloidin-f-actin-depolymerization-inhibitor-ab143533.html, accessed October 2, 2019; https://www.sciencedirect.com/topics/agricultural-and-biological-sciences/phalloidin, accessed October 2, 2019).
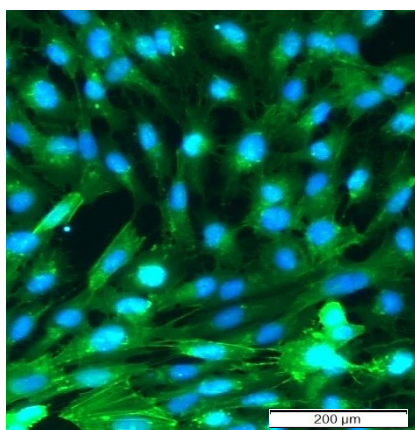
Figure 24: Fluorescent microscopic image of F-Actin (greens) and DAPI (blue) stained on 24-well plate.

In the first step of the process, cells had to be fixed and permeabilized for the conjugated phalloidin to pass the plasma membrane. This was done by preheating an in advance prepared fixing solution (4 % paraformaldehyde (PFA), 0.2 % Triton-X-100) for 20 minutes at 37 °C. Afterwards, the cells were rinsed with 1 mL PBS per well and 500 µL of the fixative were pipetted manually into the channels and the wells. This step had to occur very carefully, especially in the microfluidic device, not to detach the cells from the surface. The cells were incubated with the fixative for 15 minutes at 37 °C and subsequently washed with 1 mL PBS twice. The phalloidine conjugate (stock-concentration: 33µM) was diluted 1:100 in EBM-2 and 250 µL were carefully pipetted into the channel or well and incubated for 60 minutes at 37 °C. Prior to the fluorescent microscope evaluation, cells were rinsed with 1 mL PBS for three times (https://www.abcam.com/protocols/phalloidin-staining-protocol, accessed October 2, 2019).

3.10.3 Immunofluorescent staining: VE-Cadherin

VE-Cadherin is an adhesion molecule that is located between endothelial cells to form a tight connection between adjacent cells (Location of VE-Cadherin: Figure 2). Consequently, staining VE-Cadherin visualises this seal (Vestweber, 2008; https://www.ncbi.nlm.nih.gov/pubmed/26621373, accessed October 2, 2019). The first steps in the staining of VE-Cadherin were the fixation of the cells and the incubation with 250 µL of a primary antibody. The fixation was already done during the staining with phalloidin (3.10.2). Hence, after staining f-actin the medium was aspired and the cells were washed three times with PBS. Afterwards, the cells were incubated with 250 µL of the primary antibody (Human VE-Cadherin Antibody, Monoclonal Mouse IgG2B Clone # 123413; stock concentration: 0.5 mg/mL) diluted 1:200 in 1 % bovine serum albumin (BSA)-V/PBS to block unspecific
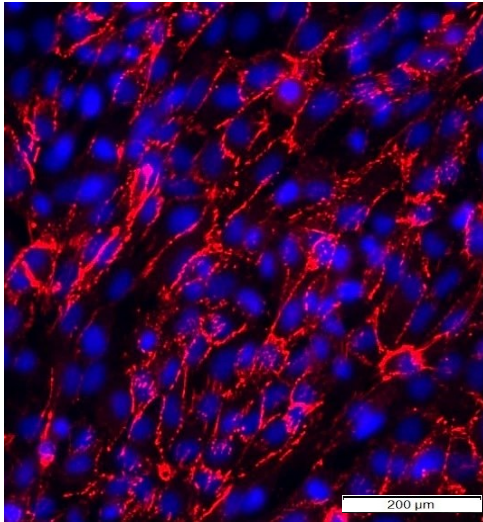
Figure 25: Fluorescent microscopic image of VE-Cadherin (red) and DAPI (blue) stained on 24-well plate.

regions. Moreover, the well or microfluidic device was sealed with parafilm and put in a 4 °C-fridge overnight. After rinsing another three times with 1 mL PBS, 250 µL of the secondary antibody (anti-mouse Alexa 488, goat anti-mouse), diluted 1:200 in 1 % BSA-V/PBS was added, incubated for 1 hour at 37 °C and washed with PBS for three times. Finally, 250 µL of 4′,6-diamidino-2-phenylindole (DAPI) (1:5000 diluted in PBS, 5mg/mL) were added, incubated for 10 minutes at RT and washed another three times with 1 mL PBS, before the coverslips were embedded in mounting medium (FluoPrep). Finally, the fluorescent microscope imaging was started (Figure 25).

3.11 Cell lysis

For RNA/DNA/Protein-isolation and the following Real-Time qPCR, the cells had to be detached from the surface of the channels and the wells. This process was performed under sterile conditions in the laminar airflow to prevent contamination with other genomic nucleic acids or nucleases and hence, the pollution of the samples. At the end of each experiment, the remaining medium had to be removed from the channel or well with a pipette. This was carried out once again very carefully, not to cause early detachment of the cells. Afterwards, 350 µL of Qiagen RLT lysis buffer, containing 1 % β-mercaptoethanol, were applied. In the case of the wells, the buffer was added with a 1 mL-serological pipette directly onto the cells, resuspended ten times to detach them from one another and transferred into a sterile Eppendorf-tube. This tube was immediately stored on dry ice and finally in a - 80 °C-freezer.

When the cells were lysed from the channels, this step was more complex as each of the channels only contained a volume of 25 µL and manual pipetting was impossible. Consequently, a 200 µL pipette tip was placed in one of the ports and a 1 mL syringe connected to PEEK tubing via an adapter, constructed of a cut needle with Tygon-tubing, was placed at the other port (Figure 26). Thereafter, 350 µL of Qiagen RLT lysis buffer were pipetted into the 200 µL open tip, sucked into the channel with the 1 mL syringe and were resuspended for ten times. Finally, the whole volume was pulled into the syringe and transferred into an Eppendorf-tube, which was stored as described above.
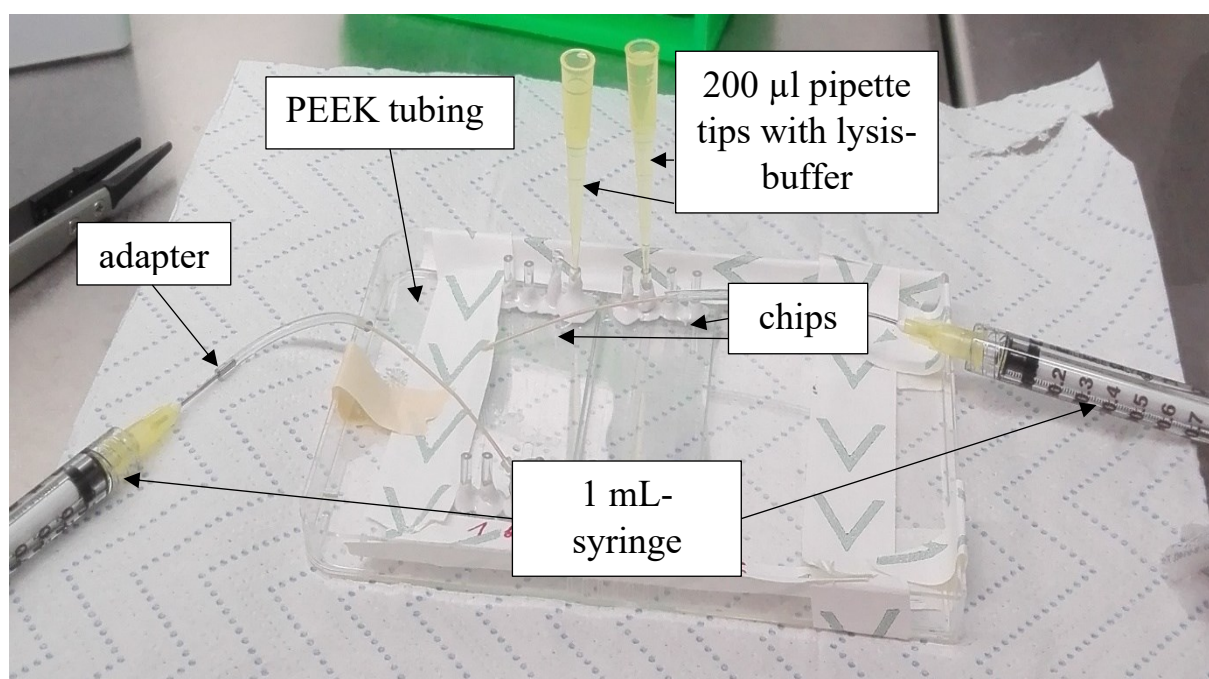
Figure 26: Scheme showing the lysis of hCMEC/D3 cells performed on the channels of a chip.

3.12 RNA/DNA-Protein-Mini-Prep

After successful cell lysis a Qiagen AllPrep DNA/RNA/Protein Kit was used to isolate the latter. The protocol was provided by Qiagen and the isolation steps for RNA, subsequently used in qPCR, included the following steps (Qiagen, 2005):

1.) Cell lysis: 350 µL lysis buffer used (RLT with added beta-Mercapto-EtOH, 1 µL/100 µL)

2.) Lysate homogenised by using an omnican insuline syringe, lysate passed through the needle for ten times

3.) Lysate transferred to ALLPrep DNA spin column (purple), placed in a collection tube and centrifuged for 30 seconds at 8000 g (10000 rpm) (no liquid remaining on the column)

4.) DNA column placed in a new 2 mL collection tube and stored at 4 °C, while RNA was isolated

5.) 250 µL 96 % ethanol added to flow-through from step 3 and pipetted up and until liquid got clear

6.) Liquid transferred to RNAeasy spin column (pink) placed in a 2 mL collection tube and centrifuged for 15 seconds at 8000 g (10000 rpm)

7.) Flow-through transferred to a 1,5 mL Eppendorf tube and stored as well at 4 °C for protein isolation

8.) 700 µL RW1 buffer added to RNeasy spin column (placed in the same collection tube as step 7), for 15 seconds at 8000 g (10000 rpm) centrifuged, flow-through discarded and collection tube used for step 7

9.) 350 µL of RPE buffer added and centrifuged for 15 seconds at 8000 g

10.) Flow-through discarded and column placed in the same collection tube

11.) 350 µL of RPE buffer added and centrifuged for 2 minutes at 8000 g

12.) RNeasy column placed in a new collection tube and centrifuged at 10000 g for 1 minute (drying of the membrane)

13.) RNeasy column placed in a properly labelled 1,5 mL Eppendorf tube and add 30-50 µL RNase free water directly to the membrane

14.) Centrifuged for 1 minute at 8000 g

15.) RNA re-eluted with eluate from step 14 and centrifuged for 1 minute at 8000 g

16.) RNA content measured with nanodrop and samples stored at – 80 °C.(Qiagen, 2005)

3.13 Barrier high-throughput qPCR chip

The high-throughput qPCR-method was carried out at the AIT. This process included the following steps (Ramme *et al.*, 2019):

1.) 250 ng per sample transcribed to cDNA using High-Capacity cDNA Reverse Transcription Kit (Applied Biosystems, Cat. No. 4368814), according to manufacturer's protocol

2.) 96 targets were investigated

3.) Targets were preamplified using tenfold concentrated primer pools mixing with Qiagen Mastermix applying following program: 15 minutes at 95°C for HotStar Plus Taq Polymerase (Qiagen, Cat. No. 203603), 18 cycles (with 40 seconds at 95 °C, 40 seconds at 60 °C, 80 seconds at 72 °C) and 7 minutes at 72 °C

4.) High-throughput qPCR was accomplished with a BiomarkTM-System containing IFC Controller HX and 96.96 Dynamic ArraysTM IFC, according to manufacturer's instructions

5.) 96 sample wells were loaded with DNA-Mix including Tagman GeneExpression Mastermix, DNA binding dye sample loading reagent, EVAGreen binding dye and 1:8 diluted preamplified cDNA

6.) 96 target wells were filled with Assay-Mix containing Assay loading reagent and according primers

7.) qPCR and data allocation

3.14 Analysis of Real-Time-qPCR

The analysis of the qPCR data was conducted by using the threshold cycle, commonly referred to as Ct-value. The lower the Ct-value the higher the initial amount of mRNA. Mean Ct-values for each sample were calculated (Spreyer, 2008).

In the next step of the analysis, the ΔCt-values were calculated (ΔCt = target gene – reference gene). The reference gene (PPIA), also called housekeeping gene, is a member of a set of genes, that serve a basic function within the cell and is required for its maintenance and expressed regardless of normal or pathophysiological conditions (https://www.genomics-online.com/resources/16/5049/housekeeping-genes/, April 04, 2020; Spreyer, 2008).

These genes serve as internal, also called endogenous control, as they form stable expression patterns and thus minimise deviations in qPCR efficiency and faults in sample quantification (https://www.genomics-online.com/resources/16/5049/housekeeping-genes/, April 04, 2020). For this purpose, Peptidylpropyl isomerase A (PPIA) was chosen in the current study. This

enzyme catalyses the cis-trans isomerisation of proline imidic peptide bonds in oligopeptides and thus promotes the folding of proteins (https://www.uniprot.org/uniprot/P62937, accessed April 4, 2020.)

A ΔCt value below zero indicates, that the threshold was reached earlier by the target gene and therefore had an initial higher amount of mRNA. In contrast, ΔCt values above zero suggest the opposite case.

Following this, the potency of the ΔCt-values was calculated to express how many times more the target gene got expressed in comparison to the refence gene. Consequently, any number above one indicates, that the expression of the target gene was higher than the one of PPIA. *Vice versa*, a number smaller than one shows that the reference gene had a higher expression rate. Hence, this relationship was portrayed as x-fold on the y-axis in the following bar graphs. In the next step of the qPCR-analysis the correspondent values of the static controls (well experiments) were also set as one (x-fold mRNA expression) and portrayed as a dotted line in the diagrams (4.5.1 to 4.5.5). If the bar graph of a target is below the dotted line, it reveals that its quantity was lower than the one of the corresponding static control. Hence, if the bar graph of a target is above this line, its quantity was higher than the amount of the associated well experiment. However, following this dependence, supposed up- and downregulations in the mRNA expression-levels could also be due to variations in the parallel static controls, which have been cultured for different durations dependent on the single experimental setups (https://www.genomics-online.com/resources/16/5049/housekeeping-genes/, accessed April 4, 2020; https://www.uniprot.org/uniprot/P62937 , accessed April, 4, 2020, Spreyer, 2008).

4 Results

4.1 Establishment of a flow-protocol for hCMEC/D3 cells in a microfluidic device with subsequent cell lysis and qPCR

The aim of establishing a general flow-protocol for hCMEC/D3 cells in a peristaltic pump setup required several different parameters to be considered and ultimately adapted. The objective was to create a procedure, where the cells survive in the channels of the microfluidic device without detachment, but also to apply the target shear stress values for an adequate period. A specific minimum of treatment time was vital to develop stable RNA expression patterns, subsequently being analysed by qPCR. However, during the experiments, it was found that the cells did not attach longer than 3 days exposed to flow in the microfluidic device in a reproducible manner. Therefore, a compromise between treatment duration and shear stress had to be established. The relevant parameters, which were modified for the aimed protocol for hCMEC/D3 cells with subsequent cell lysis and qPCR, are summarised in Table 34.

Table 34: Modified parameters in the course of the study.

Parameter	Alteration	Reason for alteration	Date of alteration
Preliminary tests to study the basics of chip manufacturing and develop a seeding procedure for hCMEC/D3 on a microfluidic device in combination with a syringe pump.			01.05.2018 – 04.07.2018 Experiment no. 1 - 4
Heat source	From heating plate to 37 °C Incu-Line incubator	The heating plate only supplied heat from below the surface of the chip, the incubator created a surrounding with 37 °C and decreased the air-bubble formation.	11.07.2018 Experiment no. 5
Fetal bovine serum	0.25 % FBS at confluency	The proliferation of attached cells decreased.	
Chip design	Channels with a consistent diameter of 2.1 mm replaced channels with a shear-gradient (2.4 mm vs. 2.1 mm width were tested)	Channels with small widths showed detachment of cells and channels with larger widths showed aggregation. 1 cm² channel-surface needed for subsequent lysis of cells.	18.07.2018 Experiment no. 6

	Height of channels (250 μm vs. 500 μm tested)	The height of the PDMS foil preferred by the cells was examined.	23.07.2018 Experiment no. 7
Coating	Gelatine coating changed to collagen IV/ fibronectin	Created more efficient adhesion of the cells to decrease their detachment.	
Chip-Assembly	Chips baked in 120 °C oven for 2 hours instead of overnight	The channel surface lost its hydrophilic properties through extensive baking, hence the coating efficiency and attachment of cells decreased.	01.08.2018 Experiment no. 8
Chip-surface	Chip-surface treated with 2 % APTES	Functionalised the surface to enable more effective coating and attachment of the cells.	
The microfluidic devices were leaky before the start of the experiments, as the plasma-cleaner did not function properly and the binding of the glass to the PDMS did not work with medium leaking out of the channels. Moreover, the peristaltic pump was utilised for the first time in the current study and was tested without a chip.			10.08.2018 – 25.09.2018 Experiment no. 9 - 11
Cell seeding number	240.000 cells/cm² instead of 360.000 cell/cm² seeded	Reduced overgrowing and the formation of aggregates at low shear stress.	
Experimental setup	6-day-setup	hCMEC/D3 were cultivated for 6 days on the chip with a final shear stress exposure of 72 hours to obtain comparable cell-lysates in a standardised setup.	03.10.2018 Experiment no. 12
	24-well plate experiments as a static control	Well experiments with 0 dyne/cm² established as a static control for the flow experiments.	

Final shear stress and intermediate target shear stress	5 dyne/cm² as final shear stress and 1 dyne/cm² as intermediate target shear stress on day 2.	Cells did remain on the surface of the microfluidic device in experiment no. 12. Therefore, a higher target shear stress was tested and the intermediate target shear stress of 1 dyne/cm² was introduced on day 2 to standardise the protocol.	10.10.2018 Experiment no. 13
The channels of the microfluidic device were leaky at the connection between the microscopic slides and the ports due to a product change of the epoxy adhesive.			18.10.2018 Experiment no. 14
Experimental setup	4-day-setup	hCMEC/D3 were cultivated for 4 instead of 6 days on the microfluidic device, since detachment occurred and the cells did not withstand flow-conditions for 6 days.	14.11.2018 Experiment no. 15
Exposure to final shear stress and preparation of cell-lysates	24-hour final shear stress exposure instead of 72 hours	As the cells were only cultured for 4 consecutive days instead of 6, a 24-hour final shear stress exposure seemed sufficient for hCMEC/D3 to be cultured on the microfluidic device without detachment and still express stable gene-expression-patterns.	
The channels of the microfluidic devices were leaky at the connection between the microscopic slides and the ports due to a change in the needle of the drilling machine, which resulted in a too large diameter of the drilled holes exceeding the diameter of the ports.			21.11.2018 Experiment no. 16
Final shear stress	2.5 dyne/cm² instead of 5 dyne/cm²	As the 4-day-setup could not be applied for the aimed physiological shear stress of 5 dyne/cm², 2.5 dyne/cm² were tested in a 4-day-setup.	28.11.2018 Experiment no. 17

The collagen IV/fibronectin coating solution was used more often than four times. Consequently, hCMEC/D3 did not adhere to the surface of the microfluidic device.		16.01.2019, 23.01.2019 Experiment no. 18, 19	
Experimental setup	3-day-setup	hCMEC/D3 were cultivated for 3 instead of 4 days, as they detached and did not withstand flow-conditions over 4 days on the microfluidic device.	30.1.2019 Experiment no. 20
Time point of cell lysis	Lysates obtained on day 2 after 6 hours and day 3 after 24 hours at a final shear stress of 1 dyne/cm²	In the case of a detachment of hCMEC/D3 in the last 24 hours exposed to the final shear stress, a comparable result after a 6-hour shear stress exposure was taken.	
Fetal-bovine-serum	1 % instead of 0.25 % FBS at confluency	The cells were not able to regrow sufficiently at 0.25 % FBS.	
Final shear stress	3 dyne/cm² instead of 1 dyne/cm² with cell-lysates obtained on day 2 after 6 hours and day 3 after 24 hours	Different final shear stresses were applied to obtain cell-lysates for subsequent qPCR.	06.02.2019 Experiment no. 21
Final shear stress	7.5 dyne/cm² instead of 3 dyne/cm² with cell-lysates obtained on day 2 after 6 hours and day 3 after 24 hours		12.02.2019 Experiment no. 22
Final shear stress	0.1 dyne/cm² instead of 7.5 dyne/cm² with cell-lysates obtained on day 2 after 6 hours and day 3 after 24 hours		19.02.2019 Experiment no. 23

Flow rate	Adaptation	Continuous adaptation of the flow rates according to the microfluidic pump in operation and the duration of the experiments.	01.05.2018 – 19.02.2019 Experiment no. 1 - 23

4.2 Simulation of the fluid flow within the channels

For the following analysis, the software Autodesk CFD 2019 was employed (3.7.2) to examine if the simulations of the microfluidic models resulted in shear stresses equal to the corresponding calculations (3.7.1).

4.2.1 Shear gradient chip

The simulation of shear stress within the gradient chip demonstrated the range of shear stress values, which were exposable onto the cells with this channel at one single flow rate. The flow rate of 13 µL/min was chosen, as it corresponded to 0.1 dyne/cm² in the 2100 µm-part, which was utilised as a straight channel later on.

Generally, this simulation matched with the calculations (3.7.1). The smaller sections of the channel (900 µm–300 µm) displayed that the shear stress increased towards its centre at the same flow rate (Figure 27B). Therefore, in the case of the 600 µm-section, a green colour is visible at the sides of the channel, which represents a lower shear stress. In contrast, an orange-red colour is observable at the centre and shows a higher shear stress. The yellow colour displays the actual calculated shear stress and is only evident in between. This observation of greater shear stress variations is more present in the smaller sections of the channel (Figure 27B, C). This supported considerations of using a wider section, 2400 µm or 2100 µm, of the channel for the later on constructed straight channel chip, as these parts revealed fewer variations in the shear stress.
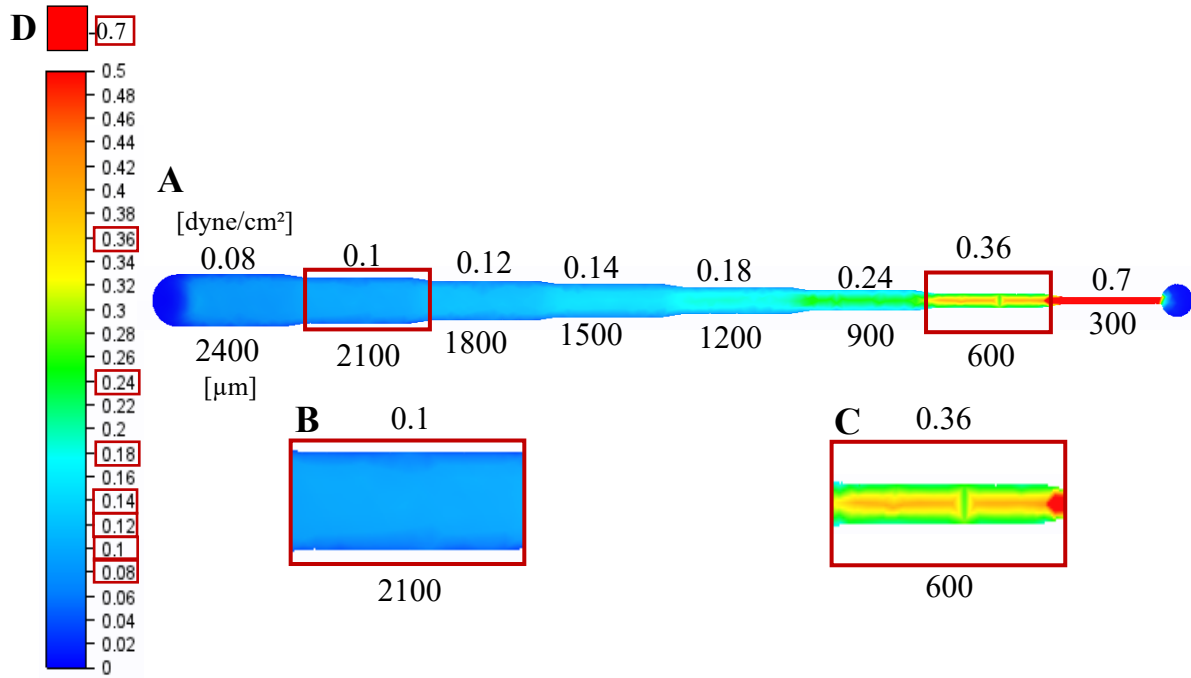
Figure 27: Simulation of fluid flow within the shear gradient chip
(A) Flow rate: 3 µL/min. (B) 2100 µm-section (C) 600 µm-section. (D) Caption [dyne/cm²].

4.2.2 Straight channel chip

For this simulation, the flow rates of the final set of experiments (3.8.14) were applied to validate the corresponding calculated shear stress (3.7.1) for the straight channel chip- design with 2100 µm of width. Hence, the flow rates 13, 130, 390 and 985 µL/min were utilised for 0.1, 1, 3 and 7.5 dyne/cm² in this simulation, respectively.

Considering the caption (Figure 28E), the shear stress calculations fit with the simulations of this model. However, it has to be noted, that the shear stress values appeared to be higher at the channels' entry and exit (Figure 28A, red Boxes). Due to this reason, images of hCMEC/D3 in the very centre of each channel (Figure 28A, green Box) were examined by microscopic evaluation, since this area represented the actual desired shear stress (4.3.1 - 4.3.12).
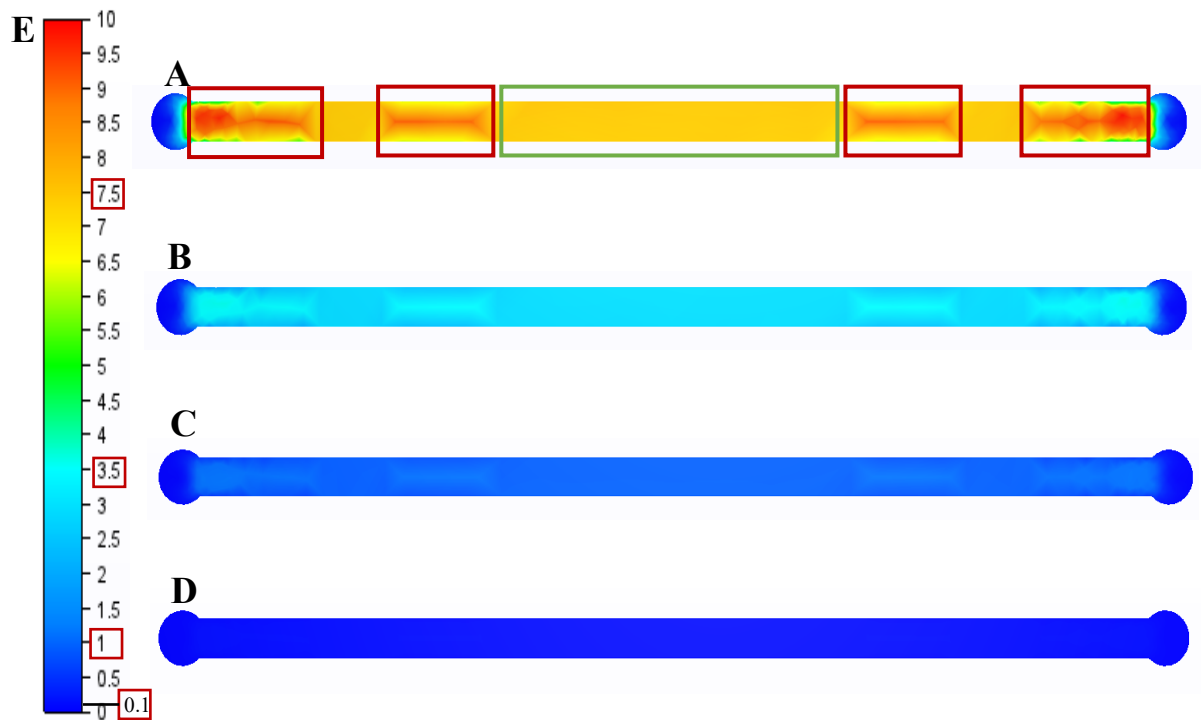
Figure 28: Simulation of fluid flow within the straight channel chip
(A) Flow rate: 985 µL/min, 7.5 dyne/cm². (B) 390 µL/min, 3 dyne/cm². (C) 130 µL/min, 1 dyne/cm².
(D) 13 µL/min, 0.1 dyne/cm². (E) Caption [dyne/cm²].
(Red Boxes) Areas showing shear stress variations. (Green Box) Area without shear stress variation.

4.3 Microscopic evaluation

The microscopic documentation and evaluation of the experiments guided the development of the optimised protocol, which enabled the lysis of cells for subsequent qPCR and analysis. In this process, effects of the flow rates on the proliferation, cluster formation and detachment of hCMEC/D3 over a certain period were analysed in comparison to the static control. In the following sections 4.3.1-4.3.12., the development of the protocol is described.

4.3.1 Experiment no. 5

This experiment analysed the development of hCMEC/D3 cells over 14 days with shear stresses ranging from 0.00042 dyne/cm² (0.063 µL/min) in the 2400 µm width section on day 0, up until 4.8 dyne/cm² (90 µL/min) in the gradient chip in the 300 µm-part of the channel on day 14. hCMEC/D3 proliferated towards a dense layer of cells until day 7 (Figure 29A-C). However, on day 10, some cluster formation occurred at the side of the channels (Figure 29D). This undesirable effect increased until day 12, even at higher shear stresses of 0.17 dyne/cm² to 1.3 dyne/cm² (25µL/min). In this case, the clusters formed in the middle of the channel. This became yet more apparent on the last day of the experiment at 0.6 dyne/cm² to 4.8 dyne/cm² (90 µL/min), with the cells moving closer together in the centre of the channel (Figure 29F, G). Additionally, there were also aggregates observable at the side of the channels again.

The drawn conclusions of this experiment were to shorten the experimental duration and to achieve the final shear stress faster in order to avoid the formation of aggregates. Thus, this experiment indicated, that hCMEC/D3 cells could not be cultivated in a microfluidic device for 14 consecutive days without cluster formation under the chosen conditions.
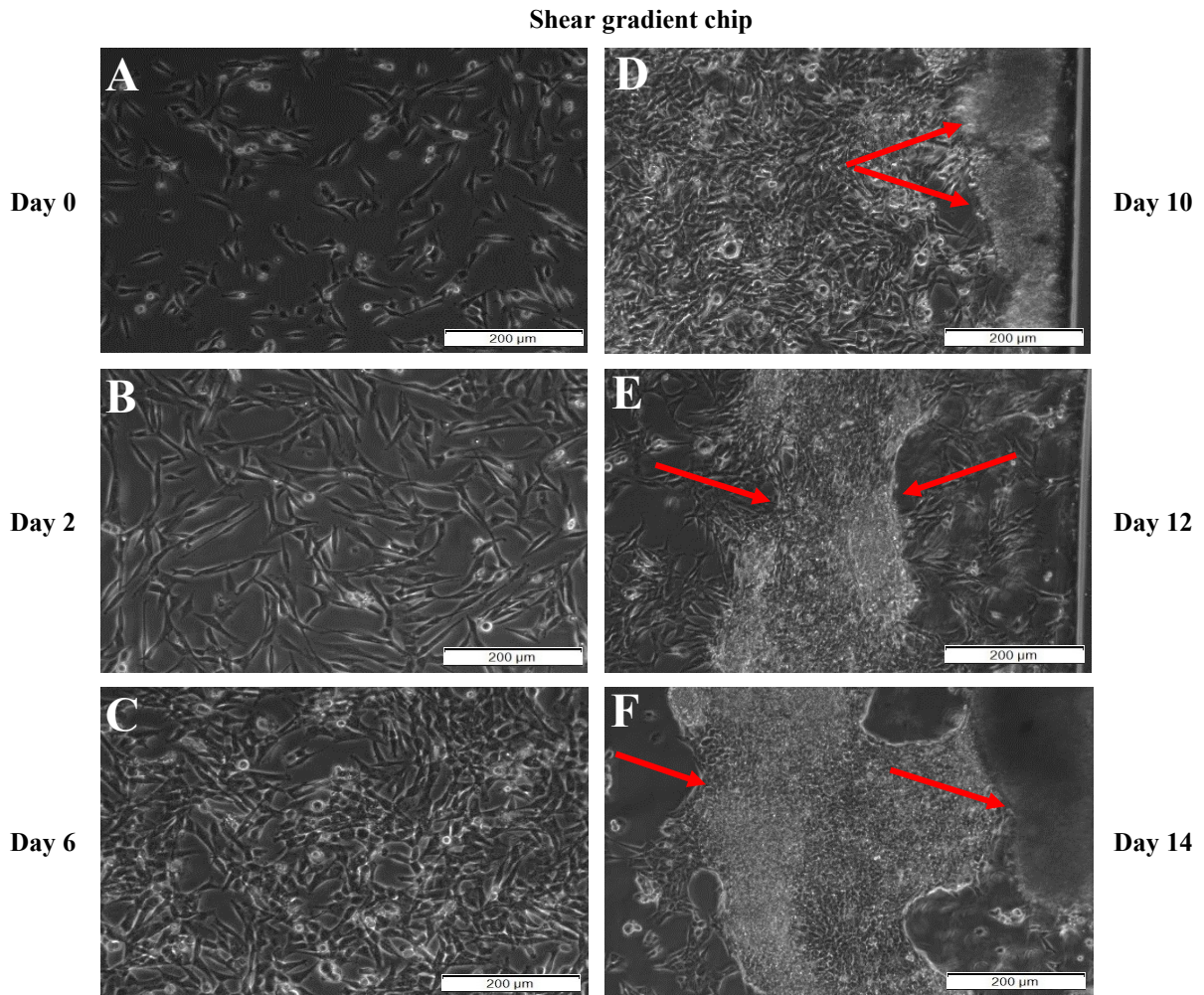
Figure 29: Brightfield microscopic images of experiment no. 5
(A-F) Shear gradient chip.
(A) Day 0: 2 hours after seeding. (B) Day 2 (3.8µL/h), 24 hours. (C) Day 6: 0.5 µL/min, 24 hours.
(D) Day 10: 10 µL/min, 24 hours. (E) Day 12: 25 µL/min, 24 hours. (F) Day 14: 90 µL/min, 4 hours.
(Red Arrows) Cluster-formation. Images were taken with a 10x objective.

4.3.2 Experiment no. 6

This experiment was accomplished to compare the effects of hCMEC/D3 cells' proliferation in two different widths, 2100 µm and 2400 µm of the straight channel chips. The same flow rate was applied for both widths, which resulted in lower shear stress in the 2400 µm channel, 0.00084 dyne/cm² to 3.2 dyne/cm² (0.125 µL/min to 480 µL/min) and higher shear stress for the 2100 µm channel, 0.00095 dyne/cm² to 3.66 dyne/cm² (0.125 µL/min to 480 µL/min) (3.8.3). In the wider channel, it was observed that the cells immediately started clustering without forming a cell layer already on day 1 at 0.00084 dyne/cm² (0.125 µL/min, Figure 30F). This indicated that the lower the shear stress, the higher the risk of aggregation under these conditions.

It was noted that the cells formed a complete layer in the 2100 µm channel at a shear stress of 0.00095 dyne/cm² (0.125 µL/min, Figure 30B). However, the first aggregates of cells also

already appeared on day 2 at a shear stress of 0.0019 dyne/cm² (0.25 µL/min, Figure 30C). Consequently, for the remaining experiments a start flow rate higher than 0.125 µL/min had to be selected to avoid clustering and still achieve a continuous cell layer.

Experiment no. 6 was progressed with the 2100 µm channel for 10 days overall. The last image (Figure 30D) displayed a very dense cell layer, indicating that the cells have overgrown each other. Hence, higher flow rates should be selected to prevent this effect. Alternatively, the duration of the experiments must be shortened.

Overall, this experiment showed that a width of 2100 µm was favourable for hCMEC/D3 cells to develop a continuous cell layer, however, higher flow rates were to be chosen to avoid the clustering and overgrowing of cells over time.
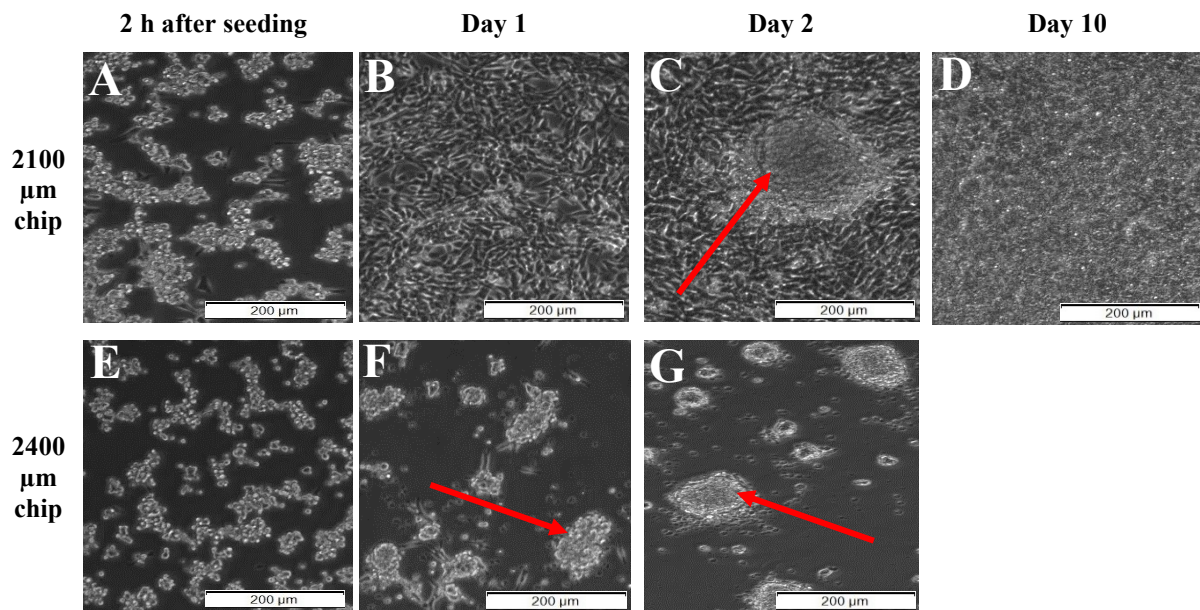
Figure 30: Brightfield microscopic images of experiment no. 6
(A-D) Channel with 2100 µm width. (E-G) Channel with 2400 µm width.
(A,E) Day 0: 2 hours after seeding. (B,F) Day 1: 0.00095 dyne/cm², 0.00084 (0.125 µL/min) , 24 hours.
(C,G) Day 2: 0.0019 dyne/cm², 0.0017 dyne/cm² (0.25µL/min), 24 hours.
(D) Day 10: 0.015 dyne/cm², 0.013 dyne/cm² (2 µL/min), 24 hours.
(Red Arrows) Cluster-formation. Images were taken with a 10x objective.

4.3.3   Experiment no. 7

The height of the PDMS foil was another important parameter to be investigated. In the course of this experiment heights of 500 µm and 250 µm were tested. For the channels of both heights, the same flow rates were applied. It must be noted that the cells in the 250 µm high channel steadily proliferated towards a continuous layer without aggregation. The avoidance of cluster formation was also due to the selected higher initial shear stress of 0.0019 dyne/cm² (500 µm) and 0.0076 dyne/cm² (250 µm; 1 µL/min) in comparison to experiment no. 6 (4.3.2).

The cells in the channel of 500 µm PDMS foil started aggregating until day 4 (Figure 31E), on which shear stresses of 0.015 dyne/cm² and 0.061 dyne/cm² (8 µL/min) were reached. This

effect was due to the quartered shear stress in the 500 µm channel in comparison to the 250 µm channel. Therefore, the results of the 500 µm channel confirmed that too low shear stress promoted cell aggregation as described before. Regarding the microscopic overview of the whole channel, the cluster formation culminated on day 6 with the cells forming one entire cluster with gaps in between at a shear stress of 0.11 dyne/cm² (60 µL/min, Figure 31F).

On the contrary, the cells of the PDMS foil with 250 µm height showed a continuous cell layer at this point at a shear stress of 0.46 dyne/cm² (60 µL/min, Figure 31C). Thus, the PDMS foil featuring this height was selected for the remaining experiments of the current study. However, it must be mentioned that a cell number of 240.000 cells/cm² was seeded in the PDMS 250 µm channel and 480.000 cells/cm² in the PDMS 500 µm channel. Since this was twice the cell number, aggregation might also have been caused by the double seeding cell number.
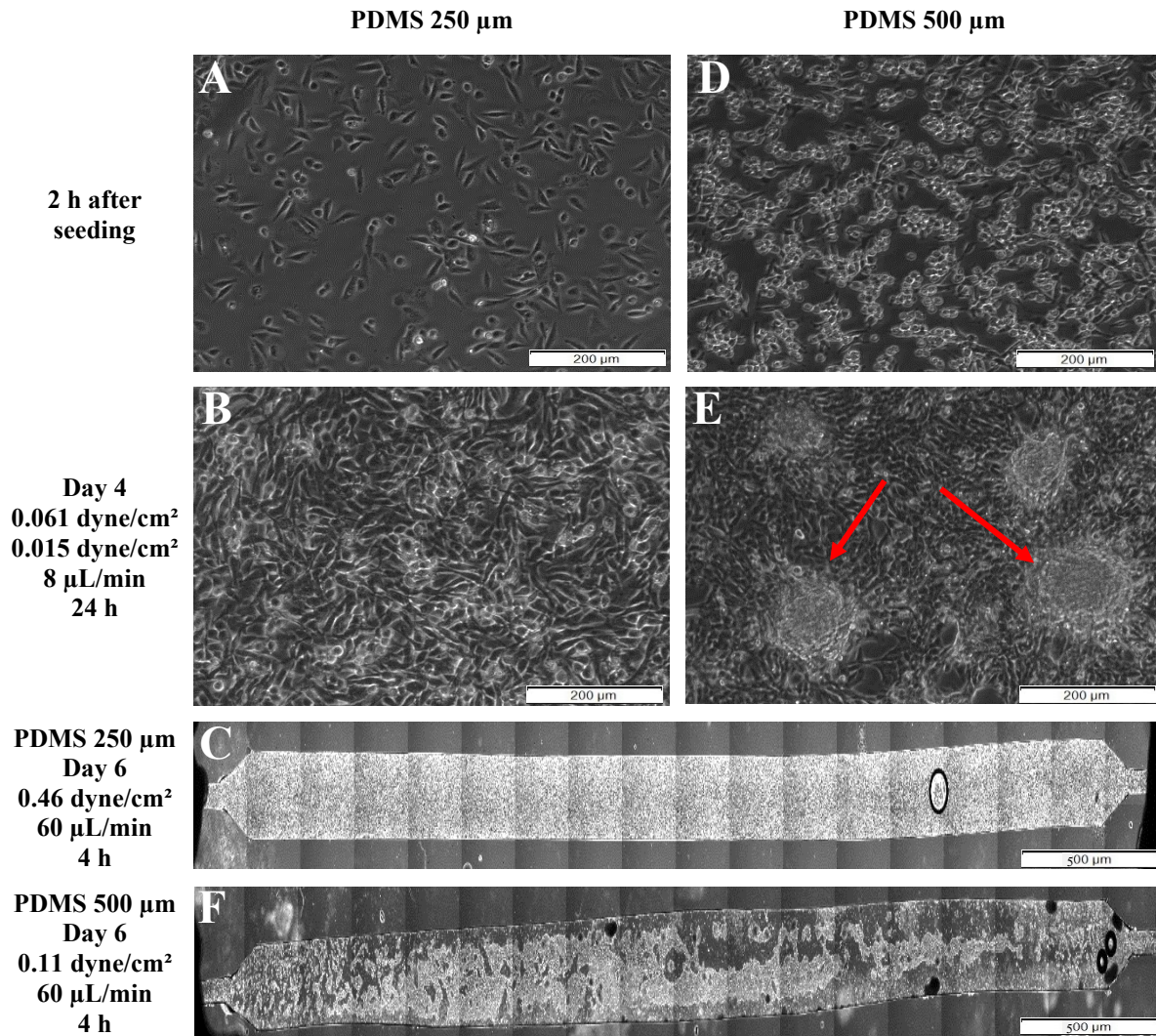
Figure 31: Brightfield microscopic images of experiment no. 7
(A-C) PDMS 250 µm. (D-F) PDMS 500 µm.
(A,D) Day 0: 2 hours after seeding. (B,E) Day 4: 0.061 dyne/cm², 0.015 dyne/cm² (8 µL/min), 24 hours.
(C,F) Day 6: 0.46 dyne/cm², 0.11 dyne/cm² (60 µL/min), 4 hours
(Red Arrows) Cluster-formation. Images were taken with a 10x objective (A, B, D, E) and a 4x objective (C, F).

4.3.4 Experiment no. 8

The coating with the aminosilane APTES was introduced to improve the adherence of hCMEC/D3 to the surface. This effect was improved by baking the microfluidic device for 2 hours instead of overnight. Additionally, an initial shear stress of 0.03 dyne/cm² (4µL/min) was tested. With these adjustments, the cells revealed a proliferation and a continuous cell sheet until the end of the experiment, at which a shear stress of 7.6 dyne/cm² was applied (1000 µL/min, Figure 32A-C). However, cells started to detach from the edges of the channels at this point on day 5 (Figure 32C). The live-dead staining displayed mostly living cells with few detached dead cells on top with a live/dead-ratio of 7.64:1 (Figure 32D).

2100 µm chip
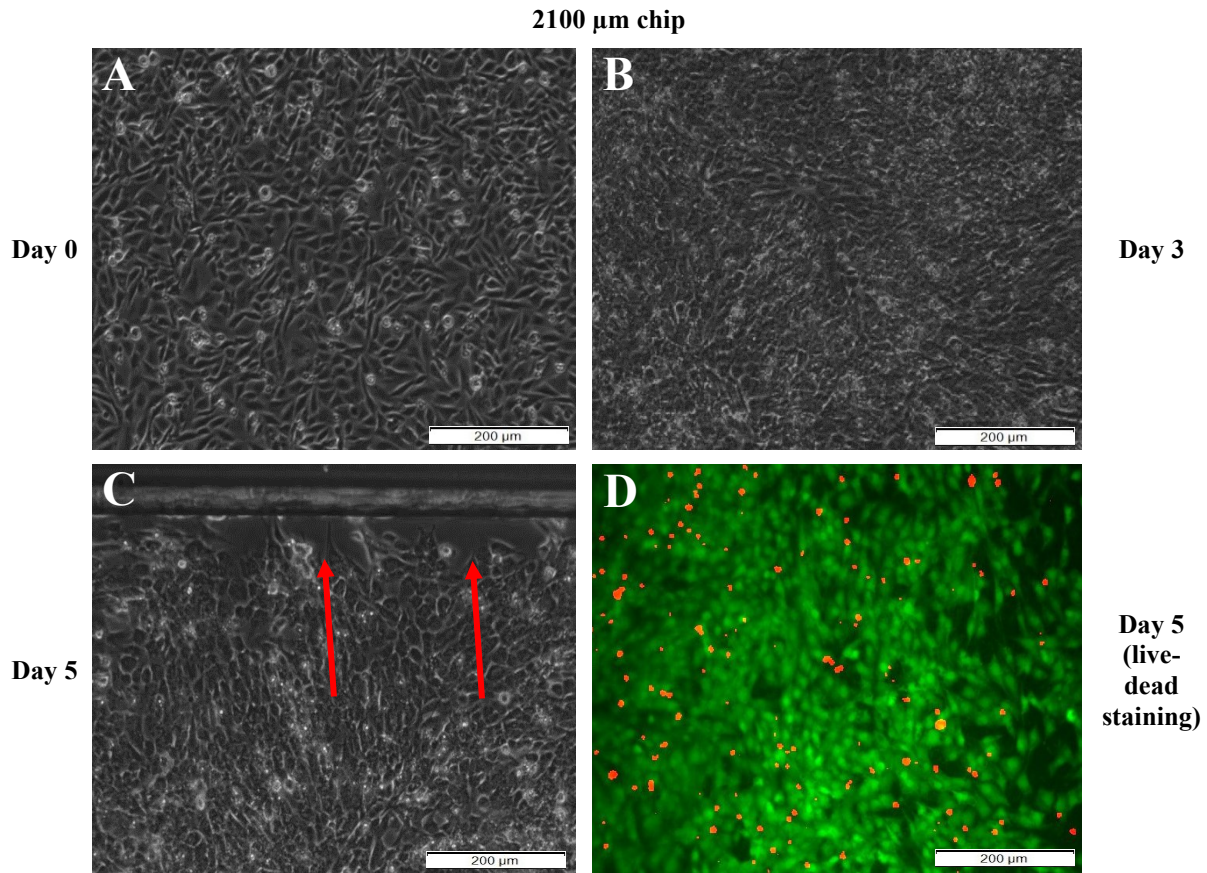
Figure 32: Brightfield and fluorescent microscopic images of experiment no. 8
(A-D) Channel with 2100 µm width.
(A) Day 0: 2 hours after seeding. (B) Day 3: 0.82 dyne/cm² (108 µL/min), 3 hours.
(C) Day 5: 7.6 dyne/cm² (1000 µL/min), 20 minutes. (D) Day 5: live-dead staining (live/dead-ratio: 7.64:1).
(Red Arrows) Gaps between the cells. Images taken with 10x objective.

4.3.5 Experiment no. 12

To obtain comparable cell-lysates, a 6-day-setup with a 72-hour final shear stress exposure, in this case 0.1 dyne/cm² (13 µL/min), was introduced. Since 0.1 dyne/cm² (13 µL/min) was also set as intermediate shear stress value to be reached on day 3, the actual final duration of shear stress exposure was 96 hours. Besides, well experiments were introduced as a static control.

The cells of the microfluidic device displayed a steady proliferation throughout this experiment towards a dense cell layer (Figure 33A-F). Considering the images after 24 hours at final shear stress of 0.1 dyne/cm² (13 µL/min) in the microfluidic and the control well experiments (Figure 33B, E), a confluent cell layer was visible in both cases. However, the image of the cells after 96 hours at 0.1 dyne/cm² (13 µL/min) showed an overgrowing of the cells with gaps in the cell layer (Figure 33C), which did not occur on part at the static control at the same point (Figure 33F).

Thus, 0.1 dyne/cm² (13µL/min) applied for this period almost induced clustering and should be applied for a shorter period to avoid this phenomenon. Additionally, higher shear stress should

be tested with the same setup to investigate if the cells would take a comparable development or do not form cluster. A start shear stress of 0.015 dyne/cm² (2 µL/min) was appropriate.
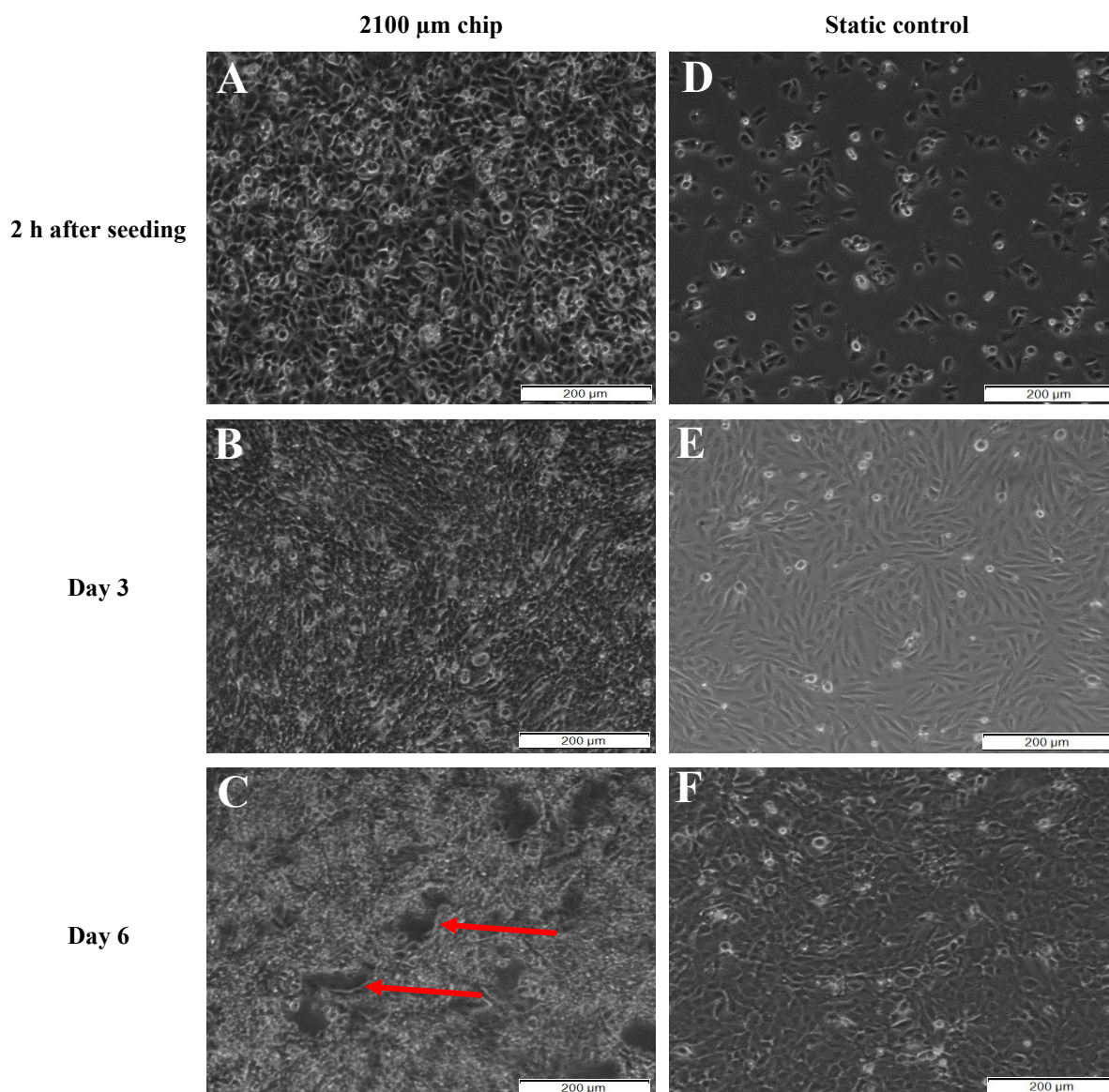
Figure 33: Brightfield microscopic images of experiment no. 12
(A-C) Channel with 2100 µm width. (D-F) Static control.
(A) 2100 µm width channel: day 0, 2 hours after seeding. (B) 2100 µm width channel: day 3, 0.1 dyne/cm² (13 µL/min), 24 hours. (C) 2100 µm width channel: day 6, 0,1 dyne/cm² (13 µL/min), 96 hours.
(D) Static control: day 0, 2 hours after seeding. (E) Static control: day 3. (F) Static control: day 6.
(Red Arrows) Gaps between the cells. Images were taken with a 10x objective.

4.3.6 Experiment no. 13

The implementation of a second intermediate shear stress value of 1 dyne/cm² (130 µL/min) on day 2 was important to achieve further comparability between the experiments. Both, the cells on the microfluidic device and the control-well displayed continuous cell layers after 24 hours at 1 dyne/cm² (Figure 34B, F).

Moreover, the final shear stress was set to 5 dyne/cm² (650 µL/min) and was planned to be applied for 72 consecutive hours. After 24 hours of exposure to 5 dyne/cm² (650 µL/min), the cells already revealed gaps in the cell layer in comparison to the static control (Figure 34C, G). After 48 hours at 5 dyne/cm² (650 µL/min) the gaps became even more apparent with only cell remnants left (Figure 34D, H). Consequently, the experiment was stopped after 48 hours at 5 dyne/cm² (650 µL/min).

In summary, on the one hand, a low final shear stress of 0.1 dyne/cm² (13 µL/min) displayed overgrown layers of cells after 96 hours of final exposure (4.3.5). A final shear stress of 5 dyne/cm² (650 µL/min) caused the cell layer gaps. Following these findings, the final shear stress exposure and the overall duration of the experiment must be shortened to avoid both effects.
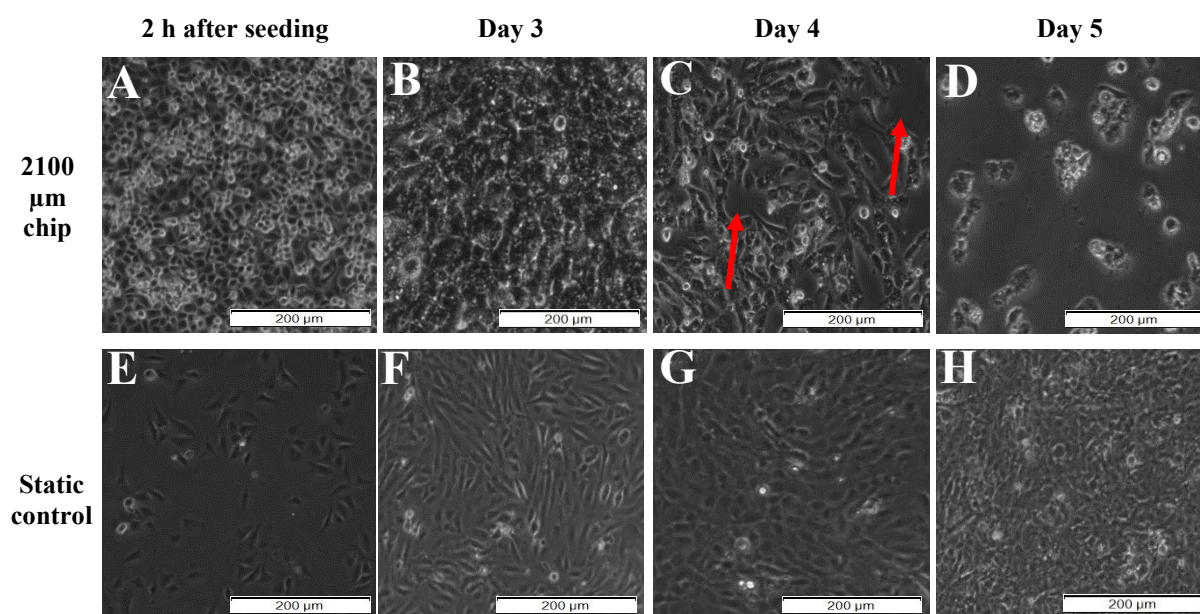
Figure 34: Brightfield microscopic images of experiment no. 13
(A-D) Channel with 2100 µm width. (E-H) Static control.
(A) 2100 µm width channel: day 0, 2 hours after seeding. (B) 2100 µm width channel: day 3, 1 dyne/cm² (130 µL/min), 24 hours. (C) 2100 µm width channel: day 4, 5 dyne/cm² (650 µL/min), 24 hours. (D) 2100 µm width channel: day 5, 5 dyne/cm² (650 µL/min), 48 hours.
(E) Static control: day 0, 2 hours after seeding. (F) Static control: day 3. (G) Static control: day 4. (H) Static control: day 5.
(Red Arrows) Gaps between the cells. Images were taken with a 10x objective.

4.3.7 Experiment no. 15

The final exposure at targeted maximum shear stress was shortened to 24 hours in this experiment. The final shear stress was, again, set at 5 dyne/cm² (650 µL/min). The cell layer was again intact after reaching the intermediate shear stress of 1 dyne/cm² (130 µL/min, Figure 35B, F), but interrupted after the final exposure to 5 dyne/cm² (650 µL/min) in comparison to the static control (Figure 35C, G). Besides, there were also more detached and dead cells visible

in the microfluidic chip, which was supported by the calculated live/dead ratios of 11.73:1 for the chip and 16.78:1 for the static control (Figure 35D, H). These observations lead to the conclusion, that this setup was presumably only applicable for lower shear stresses beneath 5 dyne/cm² for hCMEC/D3 or that the overall duration of the experiment needed to be reduced further.
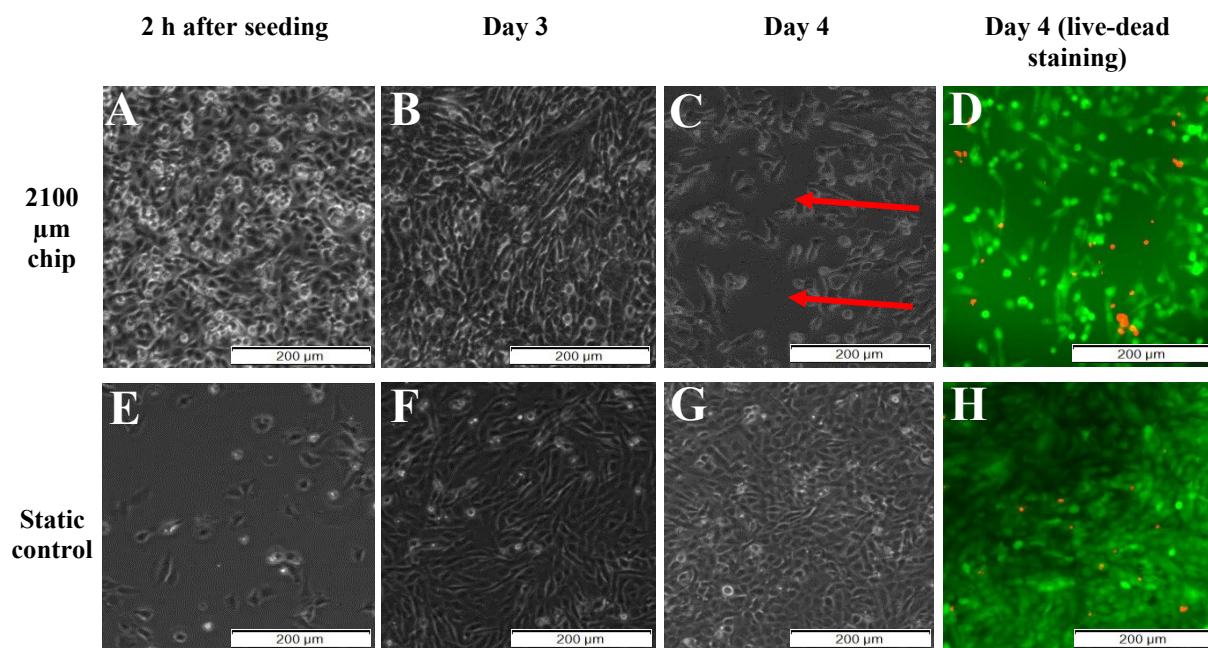
Figure 35: Brightfield and fluorescent microscopic images of experiment no. 15
(A-D) Channel with 2100 µm width. (E-H) Static-control.
(A) 2100 µm width channel: day 0, 2 hours after seeding. (B) 2100 µm width channel: day 3, 1 dyne/cm² (130 µL/min), 24 hours. (C) 2100 µm width channel: day 4, 5 dyne/cm² (650 µL/min), 24 hours. (D) 2100 µm width channel: day 4, 5 dyne/cm² (650 µL/min), 24 hours, live-dead staining (live/dead-ratio: 11.73:1).
(E) Static control: day 0, 2 hours after seeding. (F) Static control: day 3. (G) Static control: day 4. (H) Static control: day 4, live-dead staining (live/dead-ratio: 16.78:1).
(Red Arrows) Gaps between the cells. Images were taken with a 10x objective.

4.3.8 Experiment no. 17

As the 4-day-setup could not be applied for aimed physiological shear stresses as 5 dyne/cm² (650 µL/min, 4.3.7), 2.5 dyne/cm² (330 µL/min) were tested with a 24-hour final shear stress exposure to verify, if the setup is applicable for lower shear stresses. Since 2.5 dyne/cm² (330 µL/min) was also set as shear stress to be reached on day 3 towards reaching 5 dyne/cm² (650 µL/min) in experiment no. 15, the actual final duration of shear stress exposure was 48 hours.

After an exposure of 24 hours with 2.5 dyne/cm² (330 µL/min) a dense cell layer was observed (Figure 37A). However, after an exposure of additional 24 hours at this shear stress the cells detached, leaving an interrupted layer. This revealed that the setup of 4 days could not be applied at lower shear stress as 2.5 dyne/cm² (330 µL/min) either. This finding was supported

by the live-dead staining, which presented more detached dead cells on the chip compared to the static control. The calculated live/dead-ratios were 3.88:1 for the microfluidic device and 6.92:1 for the static control (Figure 37C, F). As hCMEC/D3 still formed a continuous layer after a 24-hour exposure on day 3, the experiment duration was, again, reduced to 3 days. This was done in the last set of experiments (4.3.9 to 4.3.12).
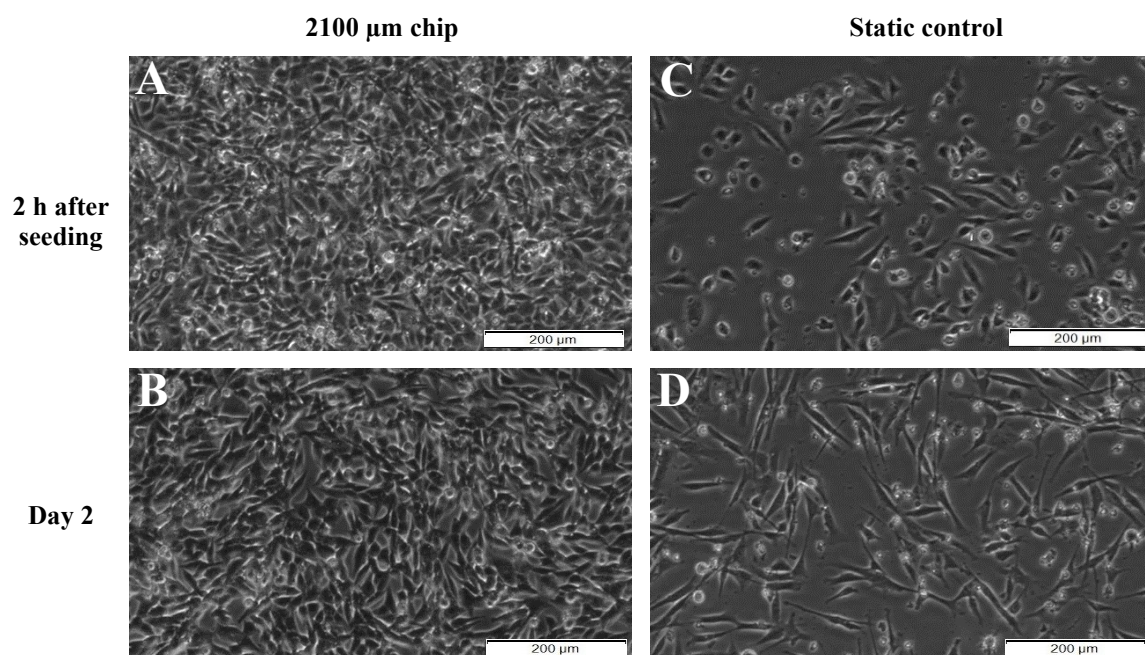
Figure 36: Brightfield microscopic images of experiment no. 17 (1)
(A, B) Channel with 2100 µm width. (C, D) Static control.
(A) 2100 µm width channel: day 0, 2 hours after seeding. (B) 2100 µm width channel: day 2, 1 dyne/cm² (130 µL/min), 24 hours.
(C) Static control: day 0, 2 hours after seeding. (D) Static control: day 2.
Images were taken with a 10x objective.
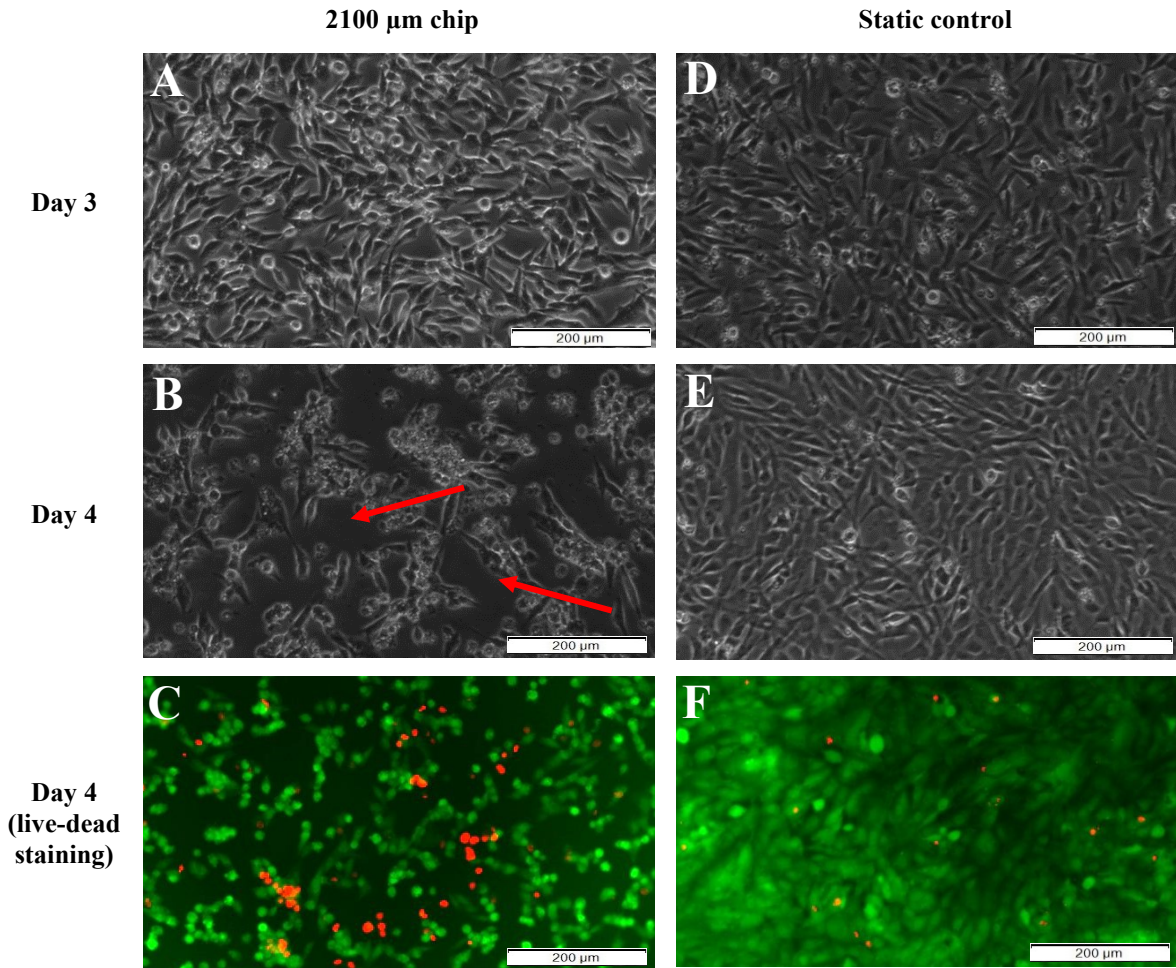
Figure 37: Brightfield and fluorescent microscopic images of experiment no. 17 (2)
(A-C) Channel with 2100 µm width. (D-F) Static control.
(A) 2100 µm width channel: day 3: 2.5 dyne/cm² (330 µL/min), 24 hours. (B) 2100 µm width channel, day 4, 2.5 dyne/cm² (330 µL/min), 48 hours. (C) 2100 µm width channel: day 4, 2.5 dyne/cm² (330 µL/min), 48 hours, live-dead staining (live/dead-ratio: 3.88:1).
(D) Static control: day 3. (E) Static control: day 4. (F) Static control: day 4, live-dead-staining (live/dead-ratio: 6.92:1).
(Red Arrows) Gaps between the cells. Images were taken with a 10x objective.

4.3.9 Experiment no. 20

The first tested shear stress in the final 3-day-setup experiments was 1 dyne/cm² (130 µL/min). The cells revealed a steady proliferation towards a confluent cell layer throughout the total experiment in the flow and the well setups. The cell lysates for subsequent molecular analysis were obtained after a 6-hour exposure at 1 dyne/cm² (130µL/min) on day 2 and a 24-hour exposure on day 3 (Figure 38C,F; Figure 39A,C).

The live-dead staining showed slightly more dead cells in the chip in comparison to the static control, which was supported by the estimated live/dead-ratios of 29.42:1 for the chip and 34:1 for the static control.

2100 μm chip   **Static control**
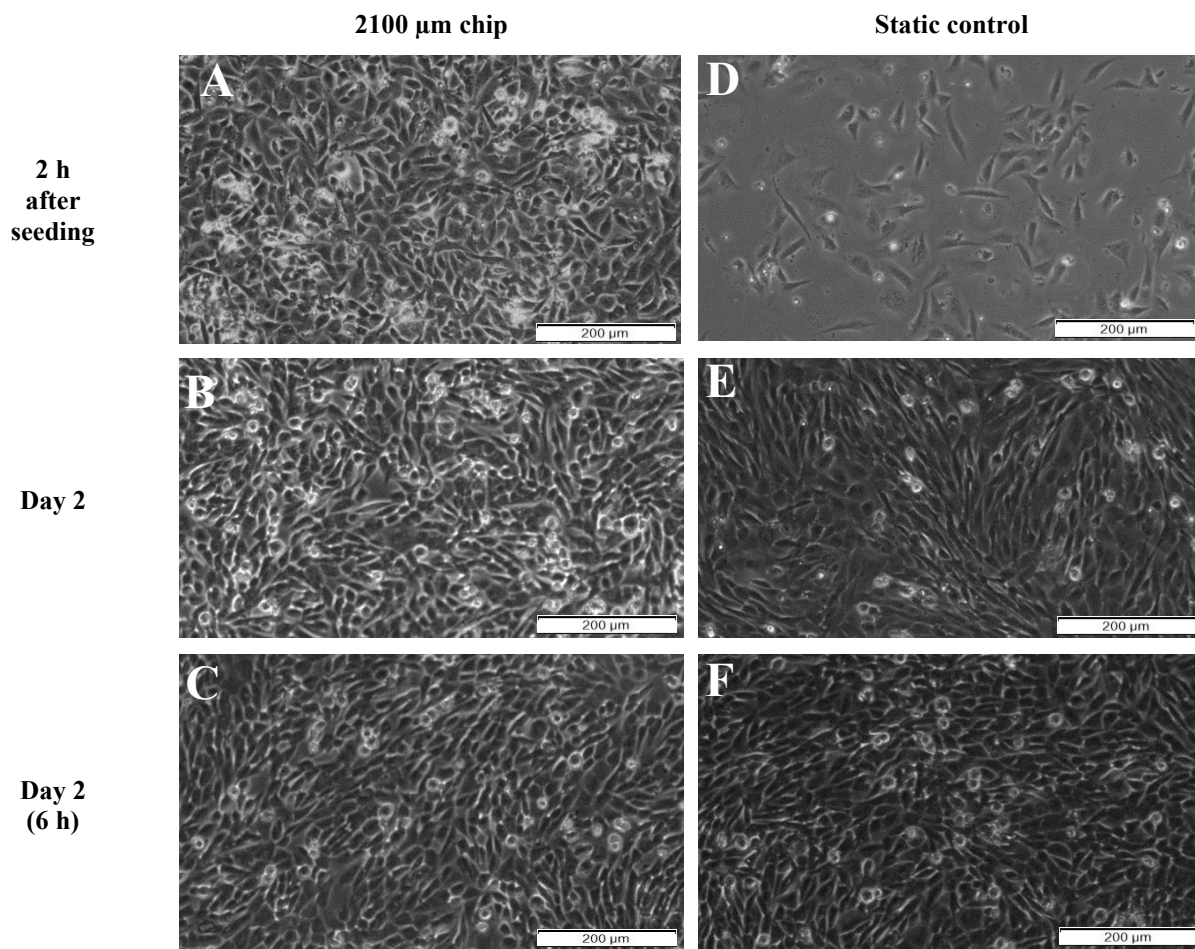
Figure 38: Brightfield microscopic images of experiment no. 20 (1)

(A-C) Channel with 2100 μm width. (D-F) Static control.

(A) 2100 μm width channel: day 0, 2 hours after seeding. (B) 2100 μm width channel: day 2: 0,1 dyne/cm² (13 μL/min), 24 hours. (C) 2100 μm width channel, day 2: 1 dyne/cm² (130 μL/min), 6 hours.

(D) Static control: day 0, 2 hours after seeding. (E) Static control: day 2. (F) Static control: day 2, corresponding to time point of 6 hours of final shear stress exposure.

Images were taken with a 10x objective.
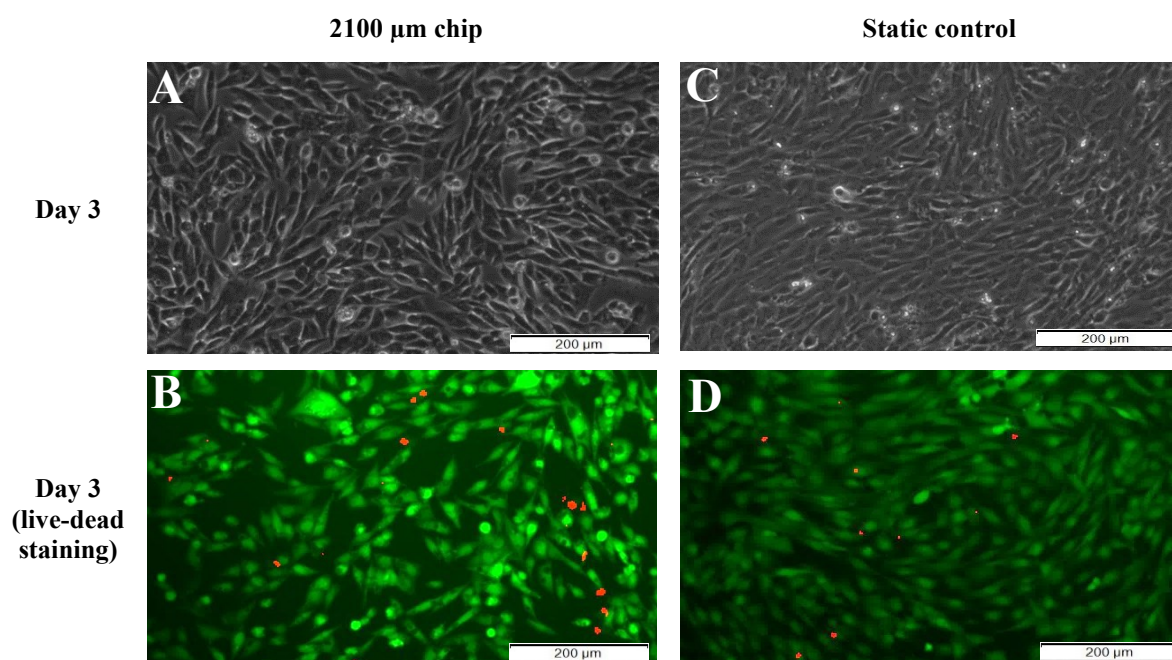
Figure 39: Brightfield and fluorescent microscopic images of experiment no. 20 (2)
(A, B) Channel with 2100 µm width. (C, D) Static control.
(A) 2100 µm width channel: day 3, 1 dyne/cm² (130 µL/min), 24 hours. (B) 2100 µm width channel: day 3, 1 dyne/cm² (130 µL/min), 24 hours, live-dead staining (live/dead-ratio: 29.42:1).
(C) Static control: day 3. (D) Static control: day 3, live-dead staining (live/dead-ratio: 34:1).
Images were taken with a 10x objective.

4.3.10 Experiment no. 21

The effects of a final shear stress of 3 dyne/cm² (390 µL/min) were evaluated in this experiment. After 6 hours at 3 dyne/cm² (390 µL/min) on day 2 at the first cell lysis, a dense cell layer was observed in the channels of the chip (Figure 40C). In contrast, after a 24-hour exposure at 3 dyne/cm² (390 µL/min) the cell layer was visibly thinned out with gaps between the cells (Figure 41A). However, the cell density was still adequate to obtain cell-lysates, judging from the microscopic images. The static control presented a continuous cell layer without gaps at this point (Figure 41C).

Moreover, the live-dead staining of the cells in the microfluidic device on day 3 at 3 dyne/cm² showed a greater extent of dead cells compared to the static control, which was supported by the estimated live/dead-ratios of 11.55:1 for the chip and 55.18:1 for the well (Figure 41B, D). As a result of this experiment, considering the arisen gaps in the cell layer after the 24-hour exposure, it can be assumed, that cell-lysates are not obtainable with the 3-day-setup above 3 dyne/cm² (390 µL/min).

2100 µm chip   **Static control**
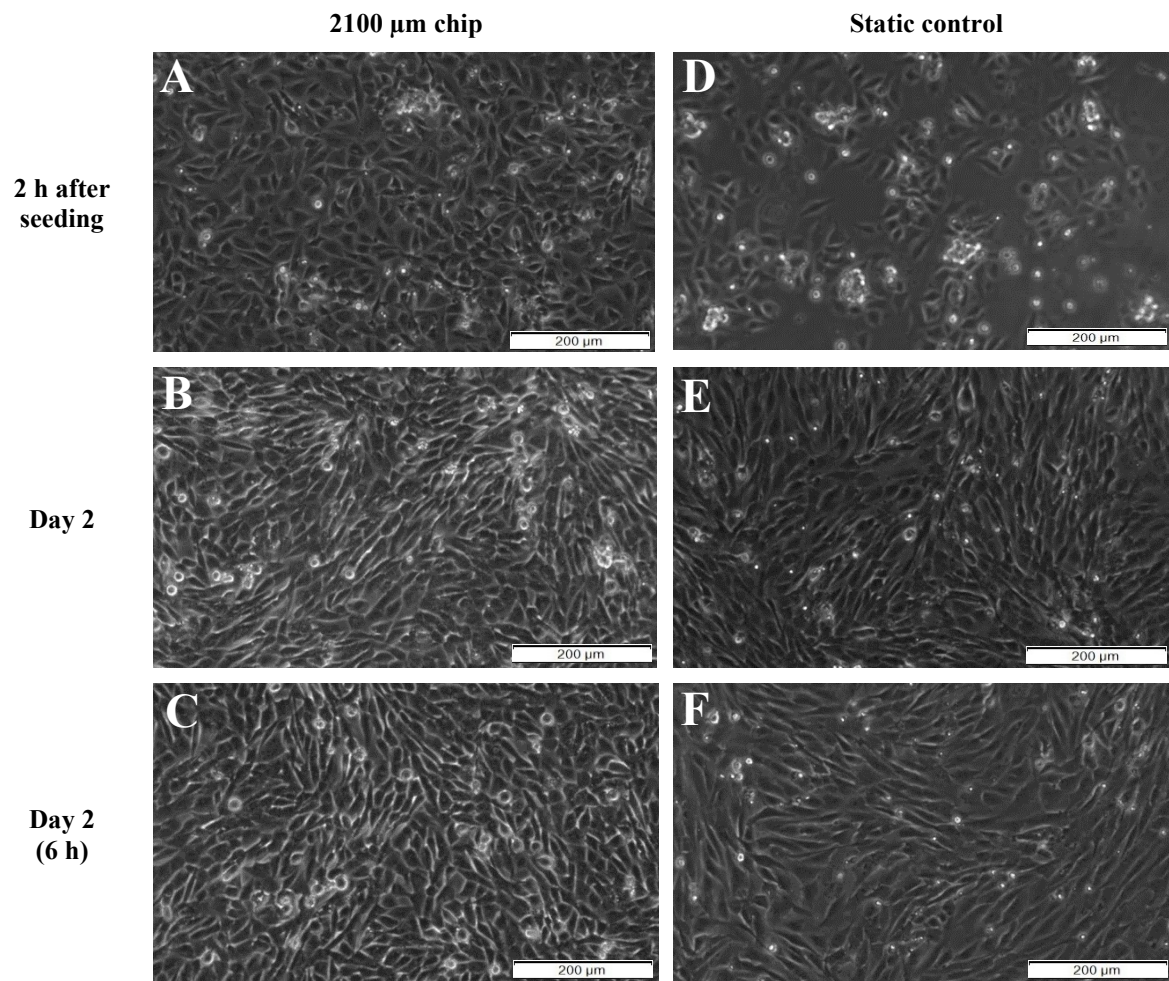
Figure 40: Brightfield microscopic images of experiment no. 21 (1)
(A-C) Channel with 2100 µm width. (D-F) Static control.
(A) 2100 µm width channel: day 0, 2 hours after seeding. (B) 2100 µm width channel: day 2: 0,1 dyne/cm²
(13 µL/min). (C) 2100 µm width channel: day 2: 3 dyne/cm² (390 µL/min), 6 hours.
(D) Static control: day 0, 2 hours after seeding. (E) Static control: day 2. (F) Static control: day 2, corresponding
to time point of 6 hours of final shear stress exposure. Images were taken with a 10x objective.

2100 µm chip **Static control**
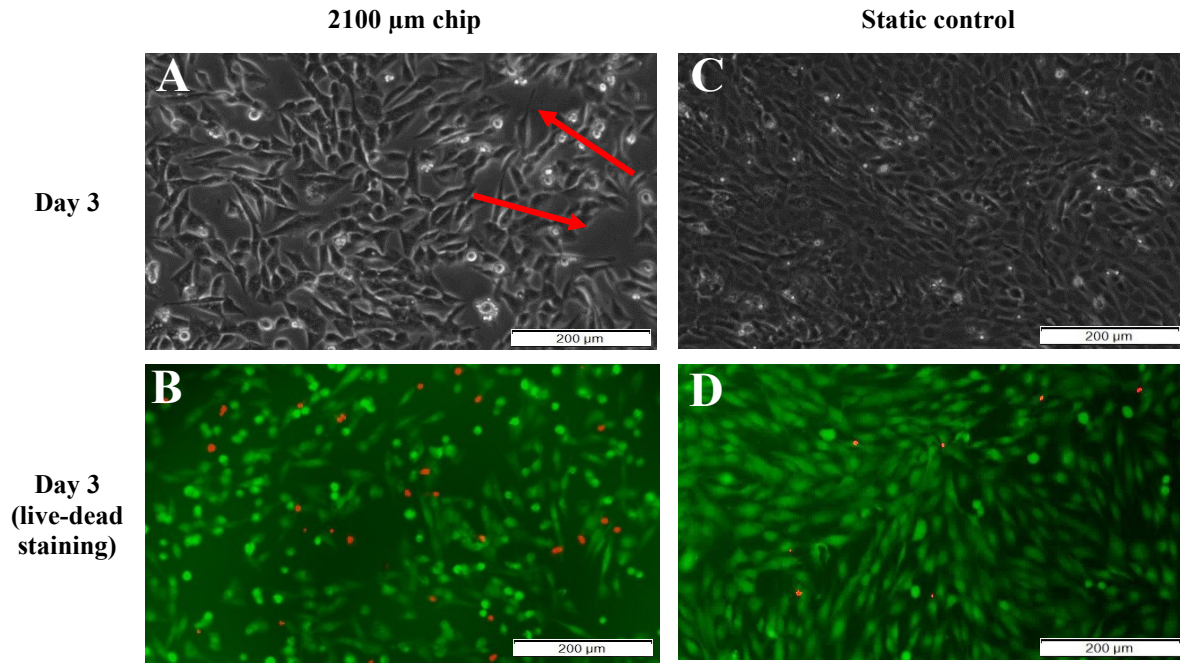
Figure 41: Brightfield and fluorescent microscopic images of experiment no. 21 (2)
(A, B) Channel with 2100 µm width. (C, D) Static control.
(A) 2100 µm width channel: day 3, 3 dyne/cm² (390 µL/min), 24 hours. (B) 2100 µm width channel: day 3, 3 dyne/cm² (390 µL/min), 24 hours, live-dead staining (live/dead-ratio: 11.55:1).
(C) Static control: day 3. (D) Static control: day 3, live-dead staining (live/dead-ratio: 55.18:1).
(Red Arrows) Gaps between the cells. Images taken with 10x objective.

4.3.11 Experiment no. 22

The assumption of experiment no. 21 (4.3.10) was verified with the application of a final shear stress of 7.5 dyne/cm² (985 µL/min). Thus, after the 6-hour exposure to 7.5 dyne/cm² (985 µL/min), hCMEC/D3 still appeared in a continuous cell layer at the first lysis time point (Figure 42C). This was not the case after a 24-hour contact to 7.5 dyne/cm² (985 µL/min) with only single cells remaining in the channels (Figure 43A). The estimated live/dead-ratios were 3.36:1 for the microfluidic device and 24.9:1 for the static control. Besides, the proportion of dead cells to visible cells was the highest at 7.5 dyne/cm² (985 µL/min) compared to experiments no. 20 and 21 (Figure 39B, Figure 41B).

2100 μm chip **Static control**
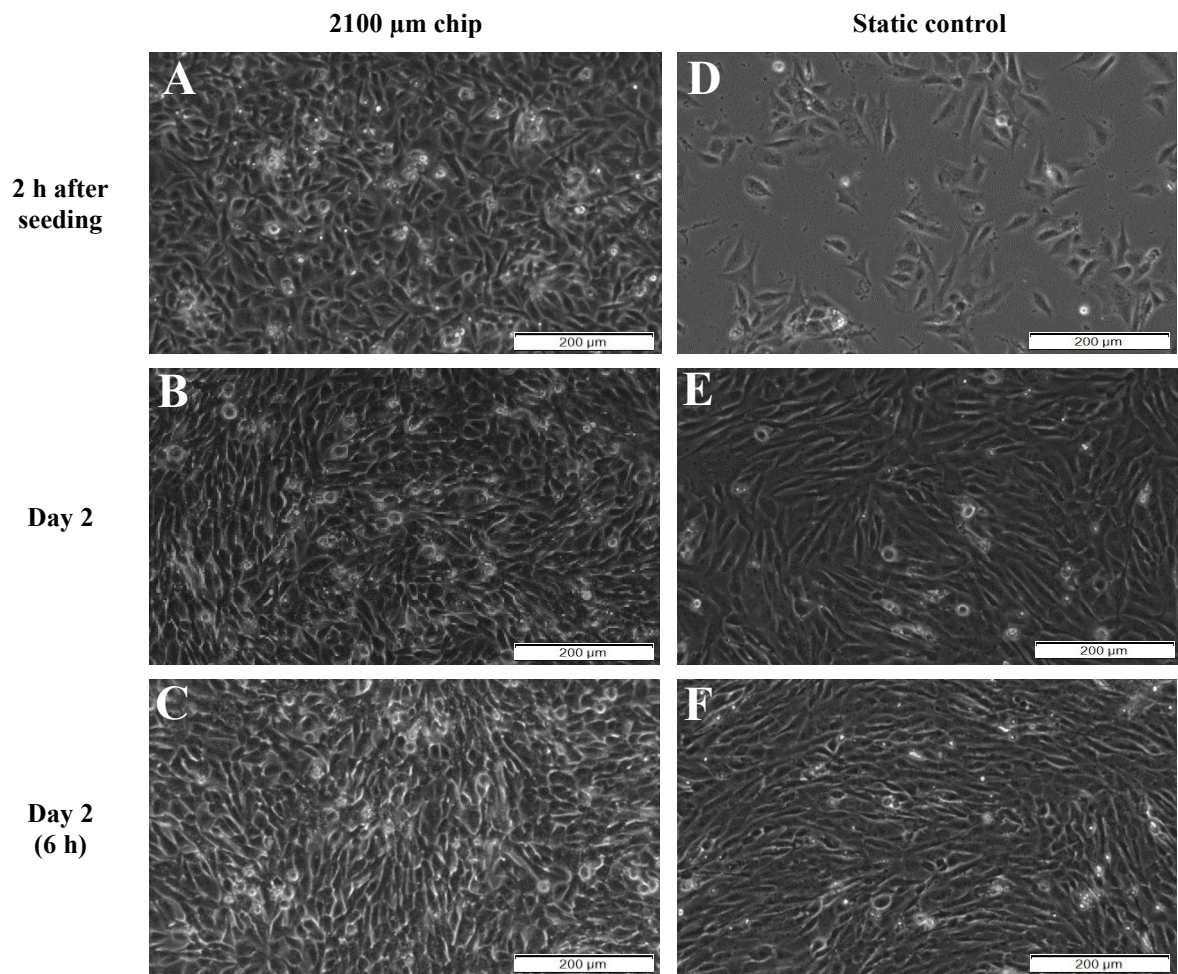
Figure 42: Brightfield microscopic images of experiment no. 22 (1)
(A-C) Channel with 2100 μm width. (D-F) Static control.
(A) 2100 μm width channel: day 0, 2 hours after seeding. (B) 2100 μm width channel: day 2: 0,1 dyne/cm²
(13 μL/min), 24 hours. (C) 2100 μm width channel: day 2, 7.5 dyne/cm² (985 μL/min), 6 hours.
(D) Static control: day 0, 2 hours after seeding. (E) Static control: day 2. (F) Static control: day 2, corresponding
to time point of 6 hours of final shear stress exposure.
Images taken with 10x objective.

	2100 μm chip	**Static control**
Day 3	A	C
Day 3 (live-dead staining)	B	D
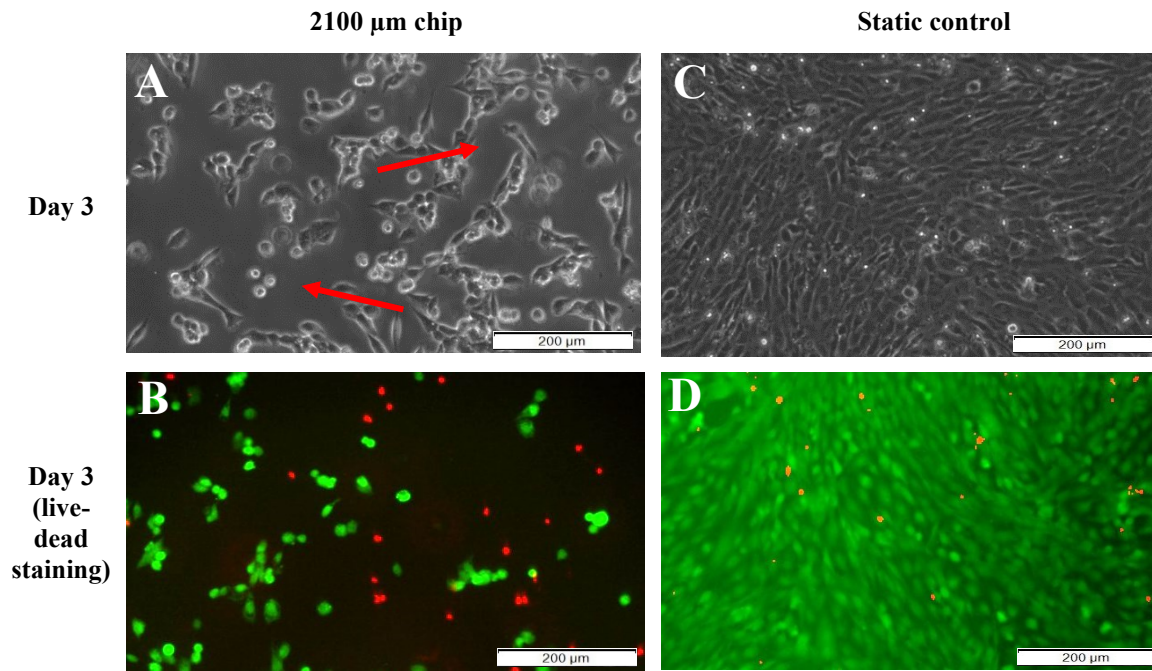
Figure 43: Brightfield and fluorescent microscopic images of experiment no. 22 (2)
(A, B) Channel with 2100 μm width. (C, D) Static control.
(A) 2100 μm width channel: day 3, 7.5 dyne/cm² (985 μL/min), 24 hours. (B) 2100 μm width channel: day 3, 7.5 dyne/cm² (985 μL/min), 24 hours, live-dead staining (live/dead-ratio: 3.36:1).
(C) Static control: day 3. (D) Static control: day 3, live-dead staining (live/dead-ratio: 24.9:1).
(Red Arrow) Gaps between the cells. Images taken with 10x objective.

4.3.12 Experiment no. 23

Finally, a shear stress of 0.1 dyne/cm² (13 μL/min) was applied to the cells for 24 hours. These still revealed a continuous cell layer on the last day of the experiment (Figure 44D). The live-dead staining demonstrated also a higher proportion of dead cells under these conditions compared to the static control with estimated live/dead-ratios of 3.7:1 for the chip and 18.42:1 for the static control (Figure 45A, D). This was presumably mostly due to the reason that the dead cells were not flushed away at the relatively low shear stress of 0.1 dyne/cm² (13 μL/min). Moreover, even at a low shear stress cell aggregates did not form in a 3-day-setup at 0.1 dyne/cm² (13 μL/min).

In addition, f-actin and VE-Cadherin were stained on day 3 after 24 hours at 0.1 dyne/cm². The f-actin, which builds stress fibres, was present in the flow and the static experiment. It seemed to be aligned in the direction of flow under the influence of 0.1 dyne/cm² (13 μL/min, Figure 45B, E). Moreover, VE-Cadherin was also visible in both cases, as distinct lines, at the cell-cell borders. However, it appeared to be more intensive in the cell layers of the chip (Figure 45C, F).
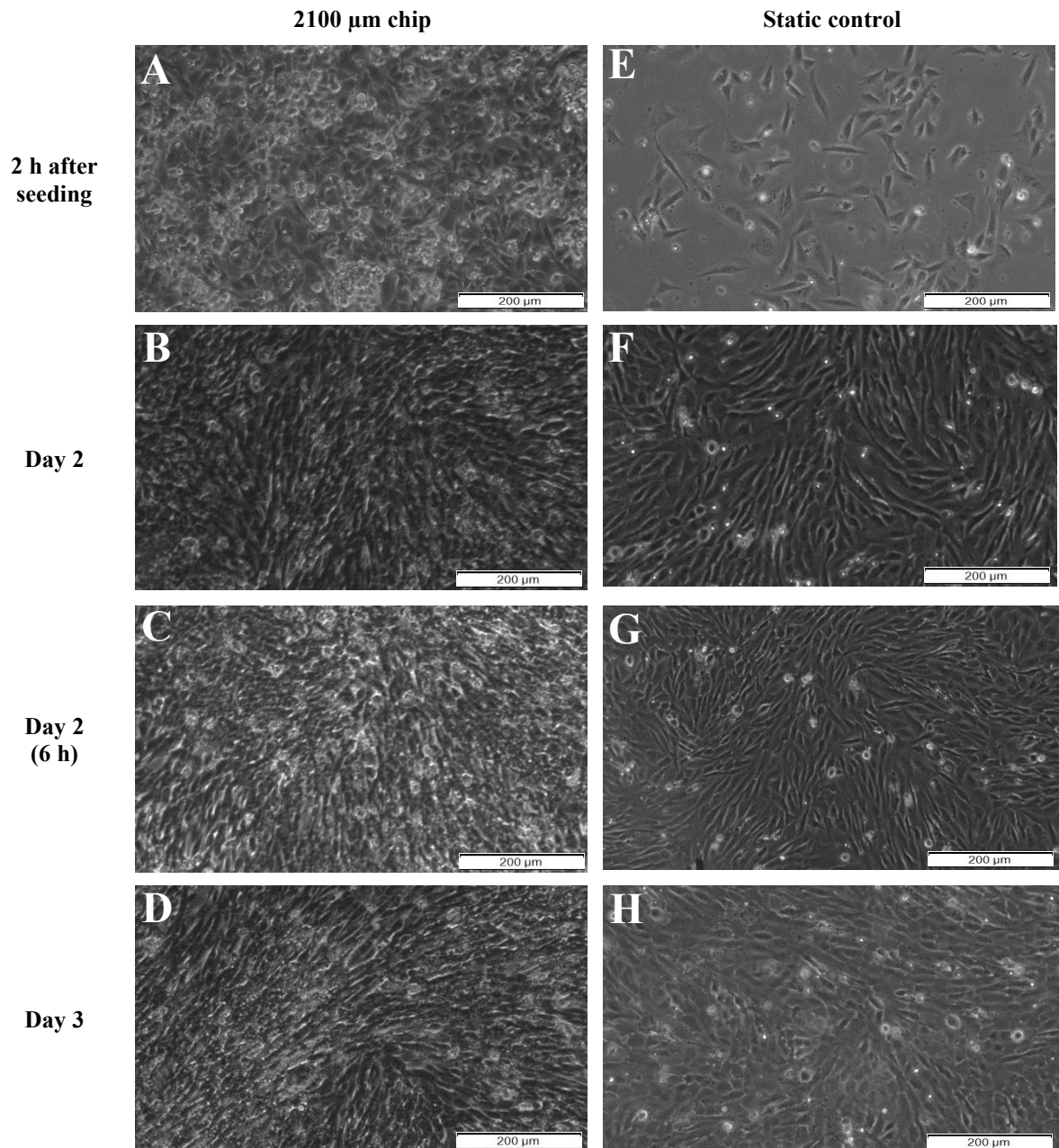
Figure 44: Brightfield microscopic images of experiment no. 23 (1)

(A-D) Channel with 2100 μm width. (E-H) Static control.

(A) 2100 μm width channel: day 0, 2 hours after seeding. (B) 2100 μm width channel: day 2: 0,1 dyne/cm² (13 μL/min), 24 hours. (C) 2100 μm width channel: day 2, 0.1 dyne/cm² (13 μL/min), 6 hours. (D) 2100 μm width channel: day 3, 0.1 dyne/cm² (13 μL/min), 24 hours.

(E) Static control: day 0, 2 hours after seeding. (F) Static control: day 2. (G) Static control: day 2, corresponding to time point of 6 hours of final shear stress exposure. (H) Static control: day 3.

Images were taken with a 10x objective.

2100 µm chip
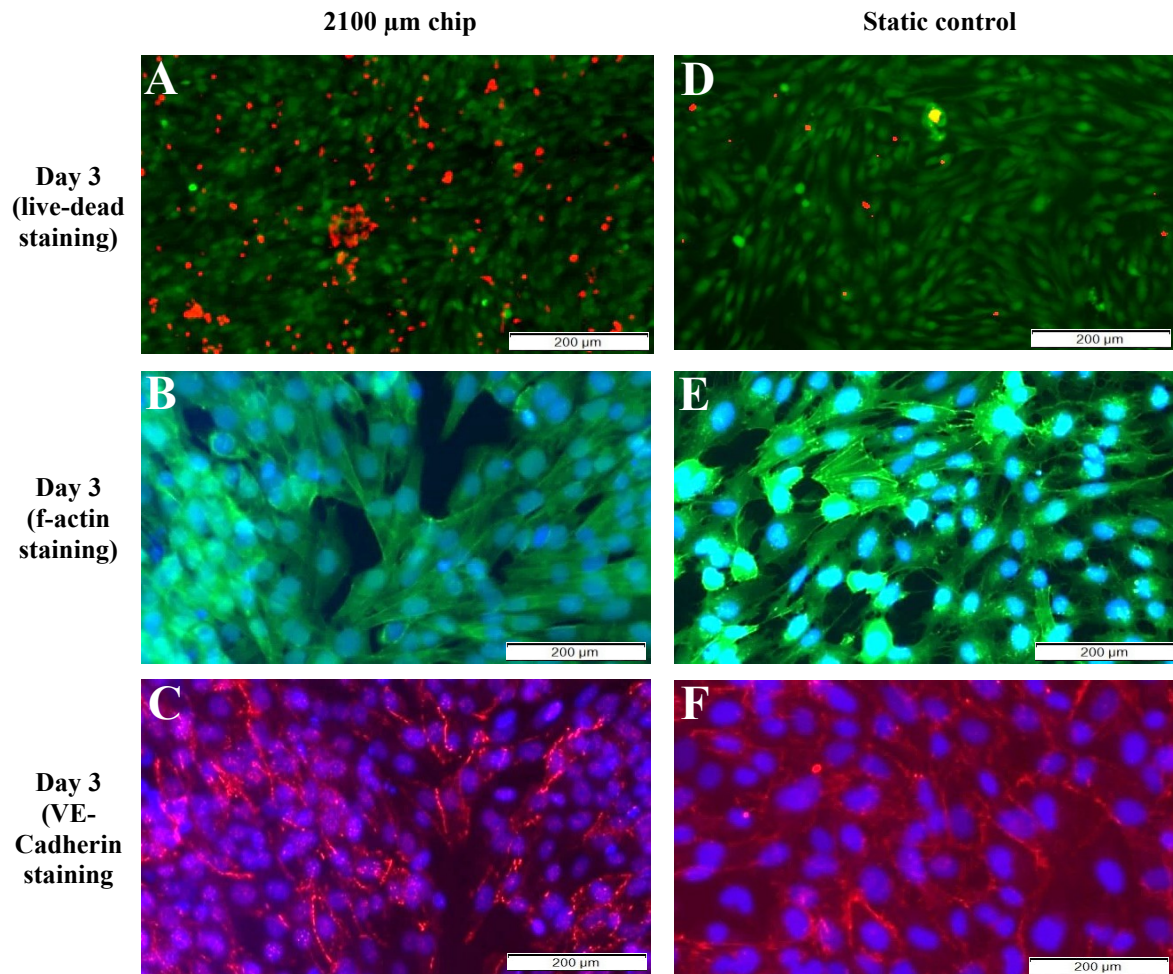
Static control

Figure 45: Fluorescent microscopic images of experiment no. 23 (2)
(A-C) Channel with 2100 µm width. (D-F) Static control.
(A) 2100 µm width channel: day 3: 0.1 dyne/cm² (13 µL/min), 24 hours, live-dead staining (live/dead-ratio: 3.7:1).
(B) 2100 µm width channel: day 3, 0,1 dyne/cm² (13 µL/min), 24 hours, f-actin staining. (C) 2100 µm width channel: day 3, 0,1 dyne/cm² (13 µL/min), 24 hours, VE-Cadherin staining.
(D) Static control: day 3, live-dead staining (live/dead-ratio: 18.42:1). (E) Static control: day 3, f-actin staining.
(F) Static control: day 3, VE-Cadherin-staining.
Images were taken with a 10x objective.

4.4 Evaluation of live/dead-ratio

The live and dead cells of the chip- and well experiments were counted in three view fields per condition with a 10x objective. The numbers were summarised in Figure 46.
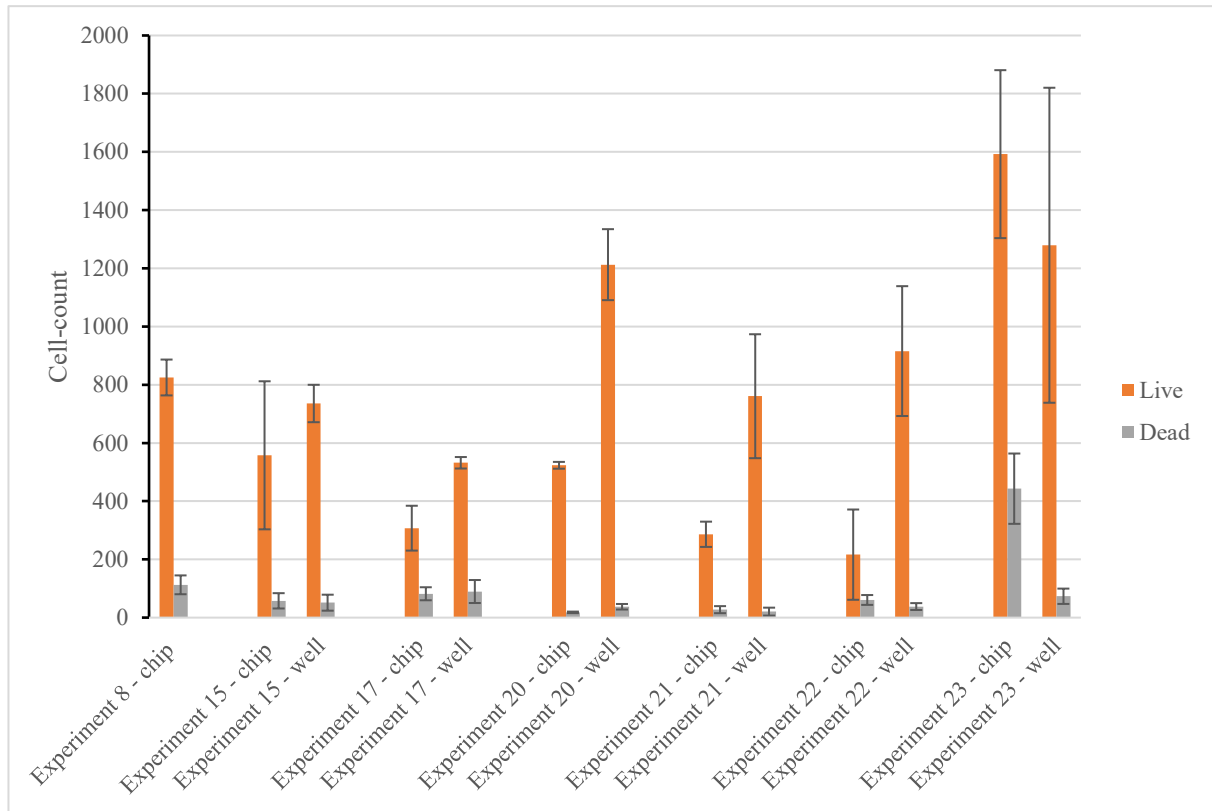
Figure 46: Cell-count of live and dead cells of the chip- and well experiments
n=3, data represents +/- standard deviation.
Experiment no. 8 (7.6 dyne/cm², 1000µL/min, 20 minutes). Experiment no. 15 (5 dyne/cm², 660µL/min, 24 hours). Experiment no. 17 (2.5 dyne/cm², 330 µL/min, 48 hours). Experiment no. 20 (1 dyne/cm², 130 µL/min, 24 hours). Experiment no. 21 (3 dyne/cm², 390 µL/min, 24 hours). Experiment no. 22 (7.5 dyne/cm², 985 µL/min, 24 hours). Experiment no. 23 (0.1 dyne/cm², 13 µL/min, 24 hours).

It must be noted that the live-cell-count is almost exclusively higher in the static well experiments than the corresponding chip experiments, apart from experiment no. 23. This experiment was done at the lowest shear stress and revealed a higher number of living cells in the microfluidic device. In Figure 47 the live/dead cell-ratios are depicted.
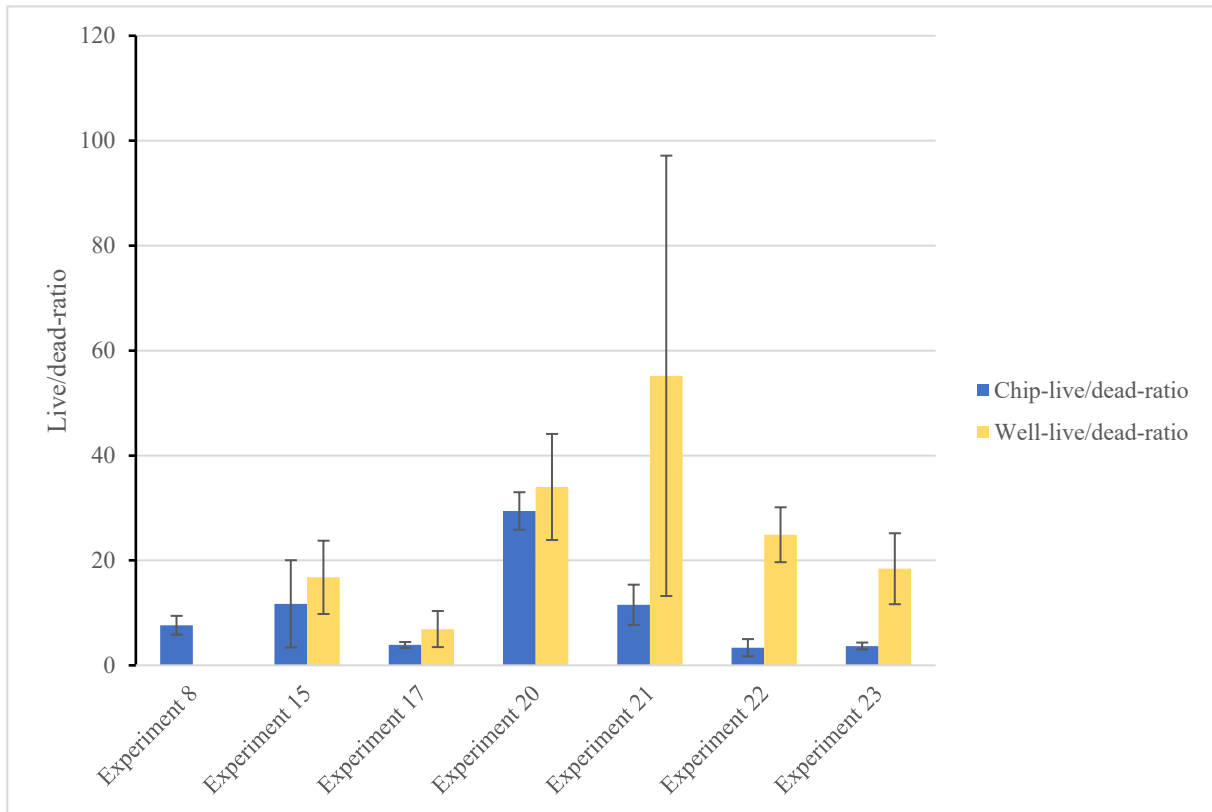
Figure 47: Live/dead-ratios of the chip- and well experiments
n=3, data represents +/- standard deviation.
Experiment no. 8 (Live/dead-ratio chip: 7.64:1, 7.6 dyne/cm², 1000µL/min, 20 minutes).
Experiment no.15 (L/D-ratio chip: 11.73:1, L/D-ratio well: 16.78:1, 5 dyne/cm², 660µL/min, 24 hours).
Experiment no. 17 (L/D-ratio chip: 3.88:1, L/D-ratio well: 6.92:1, 2.5 dyne/cm², 330 µL/min, 48 hours).
Experiment no. 20 (L/D-ratio chip: 29.42:1, L/D-ratio well: 34:1, 1 dyne/cm², 130 µL/min, 24 hours).
Experiment no. 21 (L/D-ratio chip: 11.55:1, L/D-ratio well: 55.18:1, 3 dyne/cm², 390 µL/min, 24 hours).
Experiment no. 22 (L/D-ratio chip: 3.36:1, L/D-ratio well: 24.89, 7.5 dyne/cm², 985 µL/min, 24 hours).
Experiment no. 23 (L/D-ratio chip: 3.69:1, L/D-ratio well: 18.42:1, 0.1 dyne/cm², 13 µL/min, 24 hours).

It must be noted that the live/dead-ratios of the well experiments are exclusively higher in the static well experiments than in the corresponding chip-experiments. Comparing the chip-experiments to each other, experiment no. 20 at a final shear stress of 1 dyne/cm² showed the highest live/dead-ratio and experiment no. 22 the lowest at a final shear stress of 7.5 dyne/cm². With further regard to the final set of experiments, which were carried out with the same setup (experiment no. 20 to experiment no. 23), experiment no. 22 at a final shear stress of 7.5 dyne/cm² and experiment no. 23 at a final shear stress of 0.1 dyne/cm², presented equally low live/dead-ratios.

4.5 Influence of shear stress on mRNA expression of barrier target genes

96 targets were analysed by high-throughput qPCR as described in section 3.14. Targets were split into different groups in the following analysis for visualisation purposes. For the following analysis, experimental settings with less than n = 3 repetitions were also presented to allow trend analysis. Considering this fact, it was decided to conduct no statistical analysis and to consider the obtained data as descriptive. The targets investigated during this qPCR-analysis are listed in Table 35.

Table 35: The qPCR-targets summarised according to target-groups

Target Group	Targets
Housekeeping genes	PPIA GAPDH B-ACTIN B2M
Junctions	Claudin1-20, 22, 23, 24, 25, 26, 27 JAM1-3 ZO1-3 Occludin CDH5 (= VE-Cadherin) MarvelD3 (=Tricellulin) WWC2
Receptors	LRP1, LRP8 TfR InR RAGE
Transporters	GLUT1 ABCB1 MRP1-5 BCRP CAT1, CAT3 ENT1 LAT1 MCT1, MCT8 MFSD2a
Cytokines	CK (8, 18, 19)
Carrier proteins	vWF E-cadherin (CDH1)
Calcium binding proteins	S100A4
Aquaporines	AQP 1-12
Cell-adhesion proteins	FIBRONECTIN SELE (E-Selectin)
Signaling molecules	VEGFA
Glykoproteins	MUC1A, 1B, 18, 20
Structure proteins	b catenin VIMENTIN

4.5.1 mRNA expression level changes after 6 hours at different shear stresses

In the following section the expression patterns of hCMEC/D3 cells were compared 6 hours after the exposure to the different final shear stress values to detect targets showing shear stress dependency. The applied shear stress values included 0.1, 1 and 3 dyne/cm² respectively. The corresponding timeline of the increase in shear stress with the points of cell lysis is shown in Figure 48. Moreover, the mRNA target-levels of the flow experiments in comparison to the static controls are shown in Figure 49 to Figure 56.

Figure 48: Experimental setup of mRNA-harvest after 6 hours on day 2
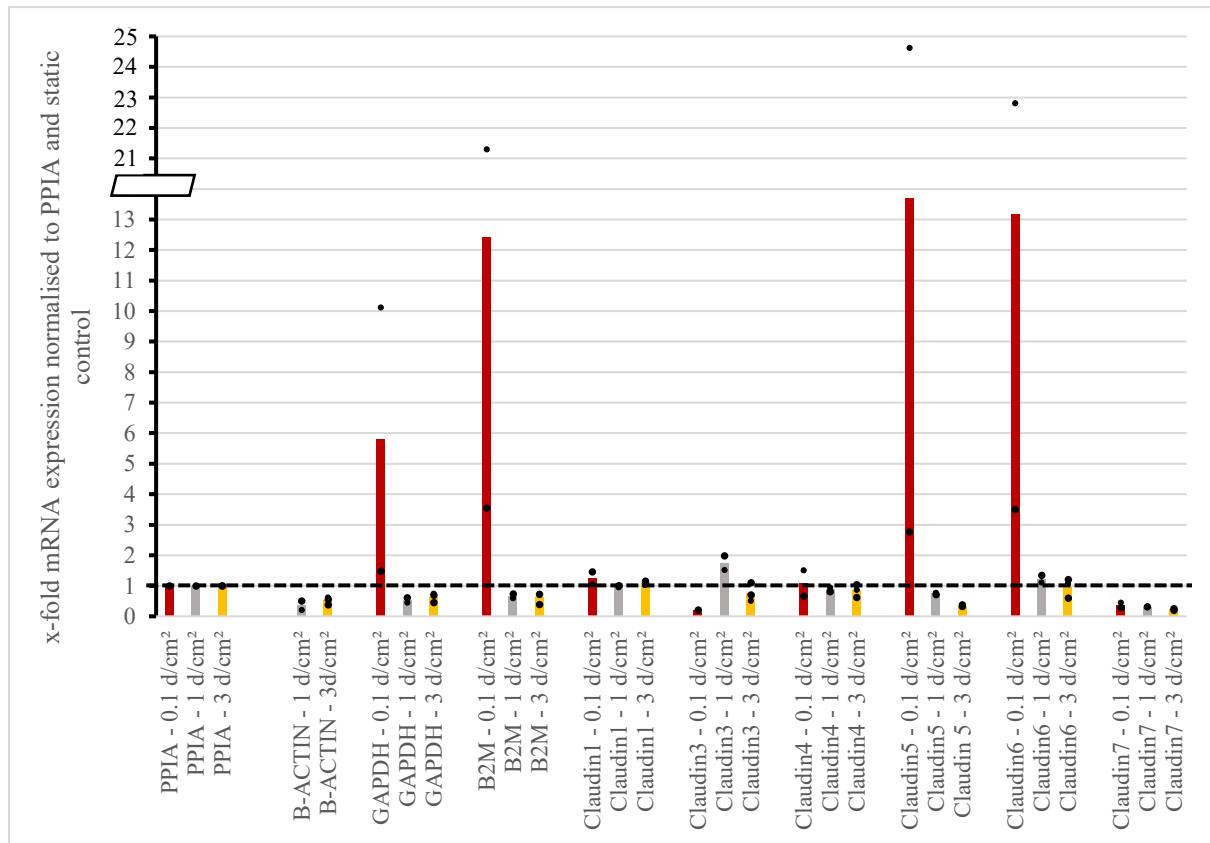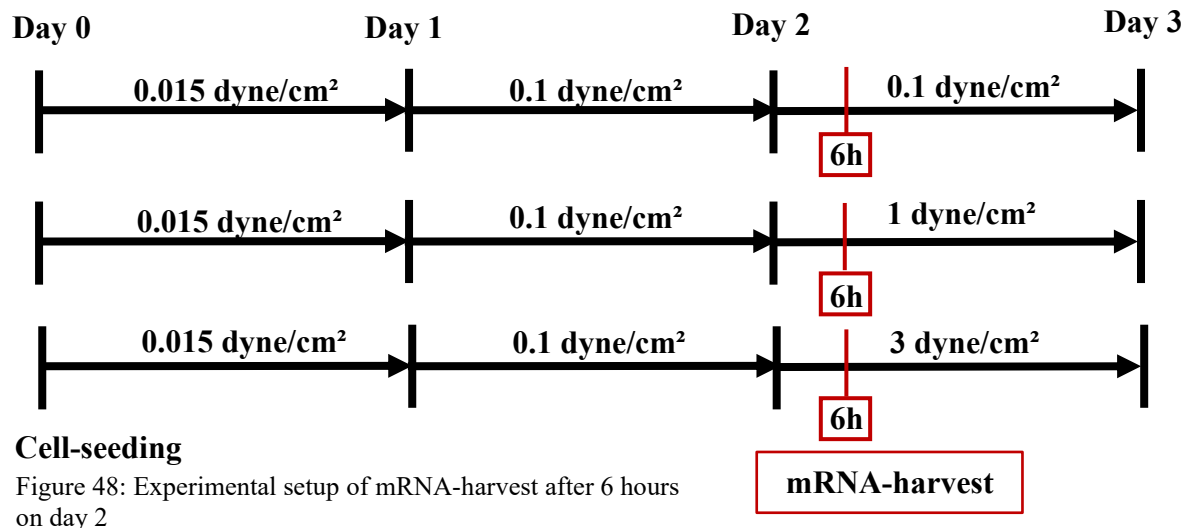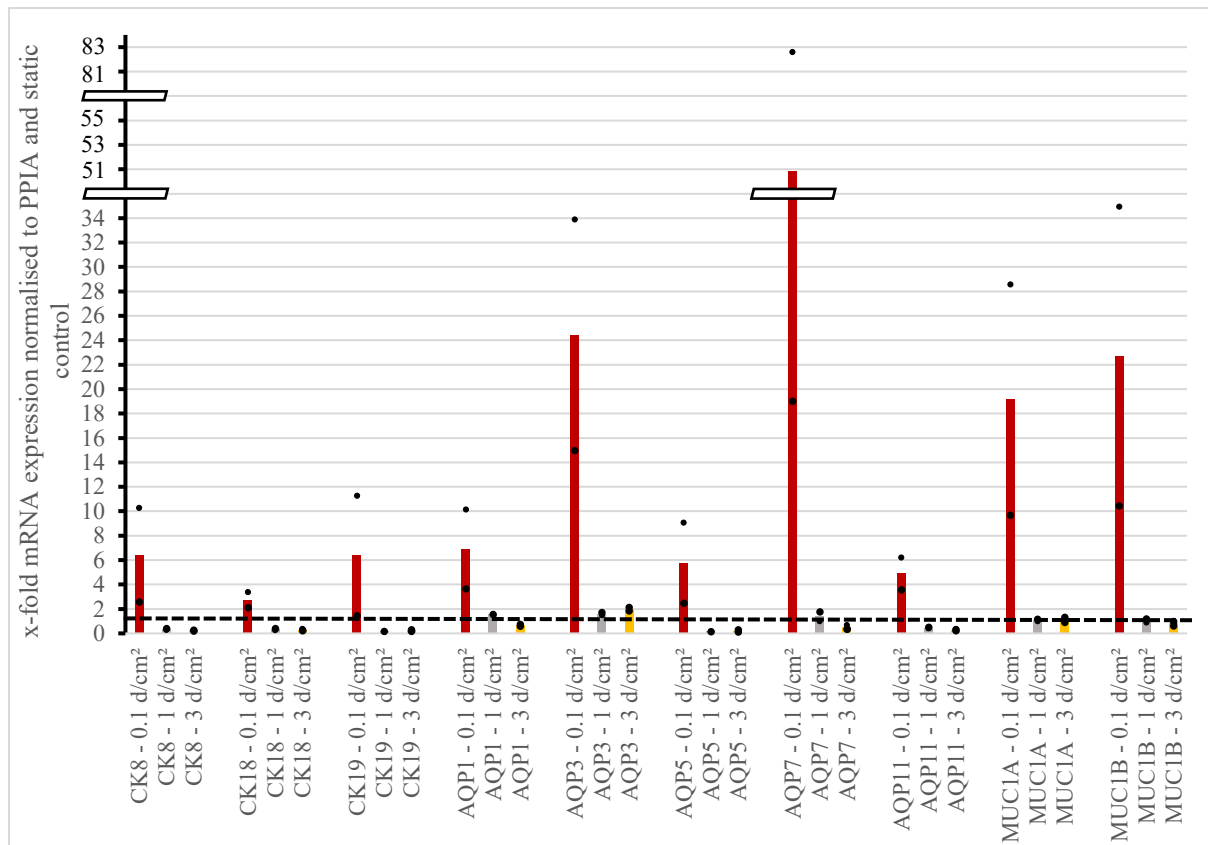

Figure 49: Bar graph 1 with trending mRNA expression level changes after 6 hours due to shear stress (Red) 0.1 dyne/cm². (Grey) 1 dyne/cm². (Yellow) 3 dyne/cm². n=3: PPIA, B-ACTIN, GAPDH, B2M, Claudin1, Claudin3, Claudin4, Claudin5, Claudin6, Claudin7 – 3 dyne/cm²; n=2: PPIA, B-ACTIN, GAPDH, B2M, Claudin1, Claudin4, Claudin5, Claudin6, Claudin7 – 0.1 and 1 dyne/cm²; Claudin3 – 1 dyne/cm²; n=1: Claudin3 - 0.1 dyne/cm².

B-ACTIN showed a 0.36-fold downregulation at 1 dyne/cm² and a 0.52-fold downregulation at

3 dyne/cm² in comparison to its static control and PPIA, however, B-ACTIN did not reveal a

significant change shear dependent. The analysis of the 0.1 dyne/cm²-value did not function for B-ACTIN.

GAPDH was 5.8-fold increased at 0.1 dyne/cm², 0.54-fold decreased at 1 dyne/cm² and 0.64-fold decreased at 3 dyne/cm² compared to the static control and PPIA. Thus, GAPDH was decreased from 0.1 to 1 dyne/cm² and did not show a significant difference between 1 and 3 dyne/cm².

B2M was 12.43-fold higher at 0.1 dyne/cm², 0.67-fold lower at 1 dyne/cm² and 0.61-fold lower at 3 dyne/cm² related to the static control and PPIA. Hence, there was a decrease in mRNA expression from 0.1 to 1 dyne/cm² and no significant change from 1 to 3 dyne/cm².

In comparison to the static control and PPIA, there was no noticeable trend for Claudin1-expression with mean x-fold values of 1.26, 0.98 and 1.1 for 0.1 dyne/cm², 1 dyne/cm² and 3 dyne/cm², respectively. The same accounted for the comparison between the shear stresses.

For Claudin3 a downregulation was detected for 0.1 dyne/cm² with a mean x-fold value of 0.22 in comparison to the static control. For 1 dyne/cm² an upregulation occurred with a mean x-fold value of 1.75. For 3 dyne/cm² a downregulation was found with a mean x-fold value of 0.77 compared to PPIA and the static control. In terms of the comparison between the shear stresses, first an upregulation occurred in Claudin3-expression from 0.1 dyne/cm² to 1 dyne/cm² and afterwards a downregulation was found from 1 dyne/cm² to 3 dyne/cm².

Claudin4 did not reveal a change in mean x-fold values in comparison to the static control and PPIA at all three final shear stresses. The same accounted for the shear stresses among each other.

Claudin5 indicated a 13.7-fold upregulation at 0.1 dyne/cm² in comparison to the static control and PPIA, whereas the mean x-fold values of 1 and 3 dyne/cm² displayed downregulations with 0.74 and 0.34, respectively. Overall, there was a trend towards downregulation in the mRNA expression of Claudin5 from 0.1 to 1 dyne/cm² and from 1 to 3 dyne/cm².

Claudin6 also showed an upregulation in the mean x-fold value of 0.1 dyne/cm² in comparison to the static control and PPIA with a value of 13.16. The mean x-fold values at the shear stresses of 1 and 3 dyne/cm² did not reveal significant differences in comparison to the static control and PPIA. Claudin6 displayed a downregulation from 0.1 to 1 dyne/cm² in the mean x-fold values, however, did not show a significant difference from 1 to 3 dyne/cm².

Claudin7 was 0.37-fold lower at 0.1 dyne/cm², 0.31-fold lower at 1 dyne/cm² and 0.23-fold lower at 3 dyne/cm² in relation to PPIA and the static control. Consequently, there was no significant trend in the mRNA expression of Claudin7 among the shear stresses.
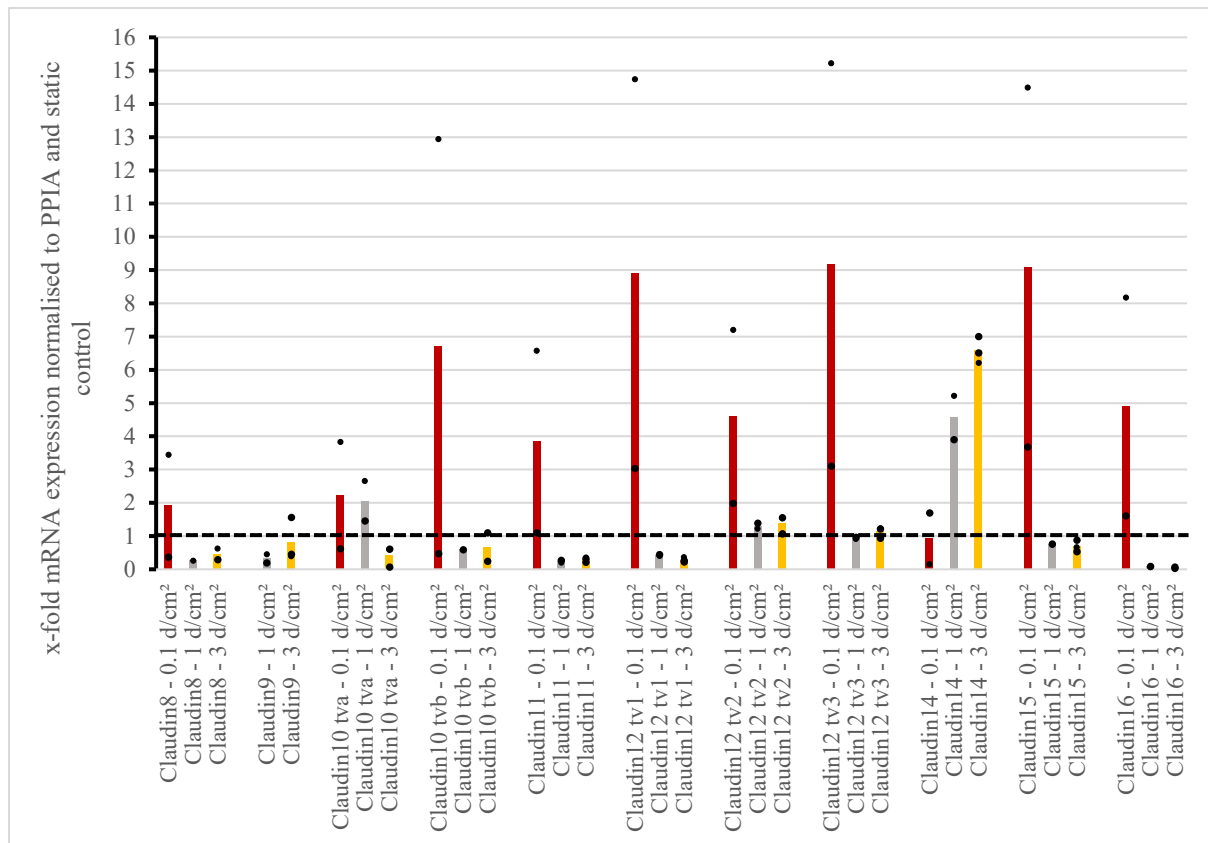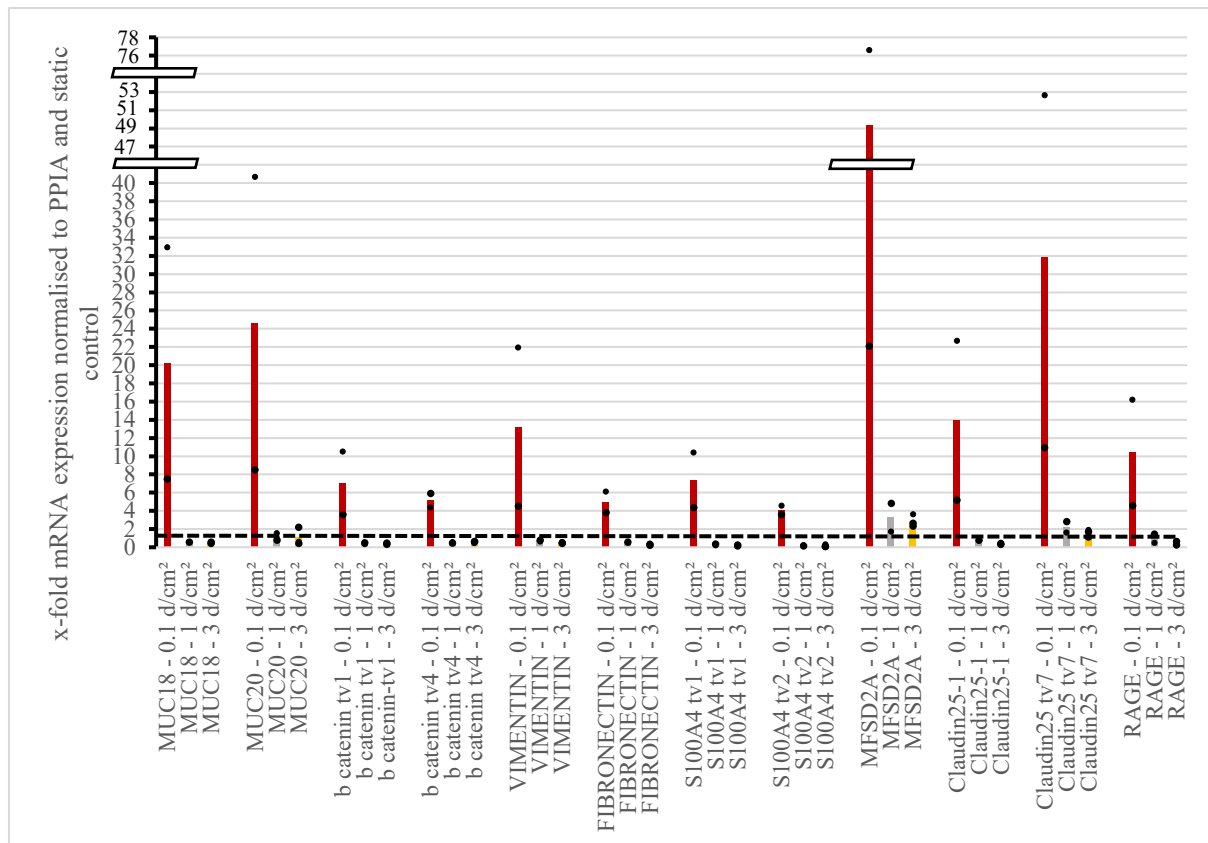
Figure 50: Bar graph 2 with trending mRNA expression level changes after 6 hours due to shear stress
(Red) 0.1 dyne/cm². (Grey) 1 dyne/cm². (Yellow) 3 dyne/cm². n=3: Claudin9, Claudin10 tva, Claudin11, Claudin12 tv1, Claudin12 tv2, Claudin12 tv3, Claudin14, Claudin15, Claudin16 – 3 dyne/cm²; n=2: Claudin8, Claudin10tva, Claudin10tvb, Claudin12 tv2, Claudin12 tv3, Claudin14, Claudin15, Claudin16 – 0.1 dyne/cm²; Claudin8 – 3 dyne/cm²; Claudin9, Claudin10 tva, Claudin11, Claudin12 tv1, Claudin12 tv2, Claudin14, Claudin15, Claudin16 – 1 dyne/cm²; n=1: Claudin8, Claudin10 tvb – 1 dyne/cm².

Claudin8 was 1.92-fold higher, Claudin10 tvb 6.71-fold higher, Claudin11 3.84-fold higher, Claudin12 tv1 8.89-fold higher, Claudin15 9.09-fold higher and Claudin16 4.89-fold higher at 0.1 dyne/cm² in mRNA expression compared to the static control and PPIA. These targets similarly presented downregulations in the mean x-fold values at 1 and 3 dyne/cm² in comparison to the static control and PPIA. Hence a downregulation in the mRNA expression resulted from 0.1 to 1 dyne/cm² and no further trend was detected from 1 to 3 dyne/cm².

Claudin9 was 0.33-fold lower at 1 dyne/cm² and 0.81-fold lower at 3 dyne/cm² related the static control and PPIA as well as with increasing shear stress from 1 to 3 dyne/cm². The qPCR did not work for 0.1 dyne/cm² for Claudin9.

Claudin10 tva was 2.22-fold higher at 0.1 dyne/cm², 2.06-fold higher at 1 dyne/cm² and 0.43-fold lower in comparison to the static control and PPIA. Hence, there was no significant difference in the mRNA expression from 0.1 to 1 dyne/cm², however, a downregulation occurred from 1 to 3 dyne/cm².

Claudin12 tv2 was 4.49-fold higher at 0.1 dyne/cm², 1.31-fold higher at 1 dyne/cm² and 1.4-fold higher at 3 dyne/cm² in comparison to the static control and PPIA. Therefore, a tendency

91

towards downregulation was detected from 0.1 to 1 dyne/cm² in Claudin12 tv2-expression, whereas there was no significant trend from 1 to 3 dyne/cm².

Claudin12 tv3 was 9.17-fold higher at 0.1 dyne/cm² and 1.13-fold higher at 3 dyne/cm² compared to the static control and PPIA. There was no significant change in the mRNA expression at 1 dyne/cm² in comparison to the static control and PPIA. Hence, there was a downregulation in Claudin12 tv3-expression from 0.1 to 1 dyne/cm², however, no significant trend from 1 to 3 dyne/cm².

Claudin14 was 4.57-fold upregulated at 1 dyne/cm² and 6.58-fold upregulated at 3 dyne/cm² in comparison to the static control and PPIA. There was no significant difference in the mRNA expression at 0.1 dyne/cm² in relation to the static control and PPIA. Consequently, there was an overall trend towards upregulation in Claudin14-expression from 0.1 to 1 dyne/cm² and from 1 to 3 dyne/cm².
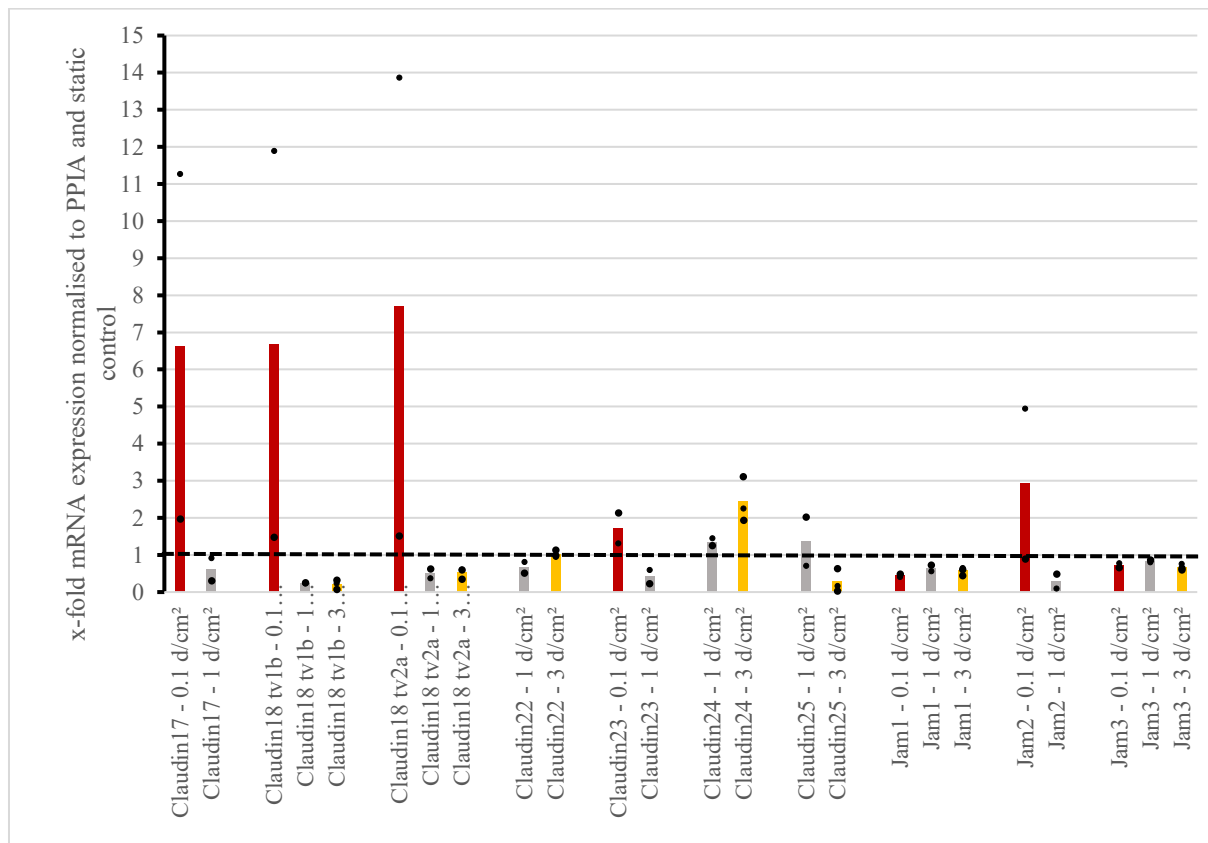
Figure 51: Bar graph 3 with trending mRNA expression level changes after 6 hours due to shear stress
(Red) 0.1 dyne/cm². (Grey) 1 dyne/cm². (Yellow) 3 dyne/cm². n=3: Claudin18 tv1b, Claudin18 tv2a, Claudin22, Claudin24, Claudin25, Jam1, Jam3 – 3 dyne/cm²; n=2: Claudin17, Claudin18 tv1b, Claudin18 tv2a, Claudin22, Claudin23, Claudin24, Claudin25, Jam1, Jam2, Jam3 – 1 dyne/cm²; Claudin17, Claudin18 tv1b, Claudin18 tv2a, Claudin23, Jam1, Jam2, Jam3 – 0.1 dyne/cm².

For Claudin17 the qPCR of the mRNA expression of 3 dyne/cm² could not be conducted. Claudin17 was 6.62-fold higher at 0.1 dyne/cm² compared to the static control and PPIA,

whereas a 0.61-fold downregulation was detected at 1 dyne/cm². Hence, there was a trend towards downregulation in Claudin17-expression from 0.1 to 1 dyne/cm².

Claudin18 tv1b was 6.69-fold upregulated at 0.1 dyne/cm² in relation to the static control and PPIA. In contrast, Claudin18 tv1b was 0.25-fold downregulated at 1 dyne/cm² and 0.21-fold decreased at 3 dyne/cm² in comparison to the static control and PPIA. Consequently, there was a trend towards downregulation in the mRNA expression from 0.1 to 1 dyne/cm² and no significant trend from 1 to 3 dyne/cm².

Claudin18 tv2a was 7.69-fold upregulated at 0.1 dyne/cm² compared to the static control and PPIA. In contrast, Claudin18 tv2a was found to be 0.5-fold lower at 1 dyne and 0.52-fold lower at 3 dyne/cm² compared to the static control and PPIA. Therefore, a trend towards downregulation in Claudin18 tv2a-expression was noted from 0.1 to 1 dyne/cm² and no significant trend was detected from 1 to 3 dyne/cm².

For Claudin22 the qPCR of the mRNA expression at 0.1 dyne/cm² did not function. Claudin22 was 0.66-fold downregulated at 1 dyne/cm² and there was no significant difference compared to the static control and PPIA at 3 dyne/cm². Hence, there was a slight upregulation from 1 to 3 dyne/cm².

For Claudin23 the qPCR of the mRNA expression at 3 dyne/cm² did not function. Claudin 23 was 1.73-fold higher at 0.1 dyne/cm² and 0.41-fold lower at 1 dyne/cm² in comparison to the static control and PPIA. Consequently, there was a downregulation from 0.1 to 1 dyne/cm² in Claudin23.

For Claudin24 the qPCR of the mRNA expression at 0.1 dyne/cm² did not function. Claudin24 was 1.35-fold higher at 1 dyne/cm² and 2.43-fold higher at 3 dyne/cm² compared to the static control and PPIA. Therefore, there was a trend towards upregulation from 1 to 3 dyne/cm² at Claudin 24.

Jam1 was 0.45-fold lower at 0.1 dyne/cm², 0.65-fold lower at 1 dyne/cm² and 0.57-fold lower at 3 dyne/cm² compared to the static control and PPIA. However, there was no significant trend in the mRNA expression of Jam1 among the shear stresses.

For Jam2 the qPCR of the mRNA expression of 3 dyne/cm² did not function. Jam2 was 2.92-fold upregulated at 0.1 dyne/cm² and 0.29-fold downregulated at 1 dyne/cm² in relation to the static control and PPIA. As a result, there was a trend towards downregulation in the mRNA expression from 0.1 to 1 dyne/cm².

Jam3 was found to be 0.72-fold lower at 0.1 dyne/cm², 0.84-fold downregulated at 1 dyne/cm² and 0.67-fold downregulated at 3 dyne/cm² compared to the static control and PPIA. Nonetheless, there was no significant trend in the mRNA expression among the shear stresses.
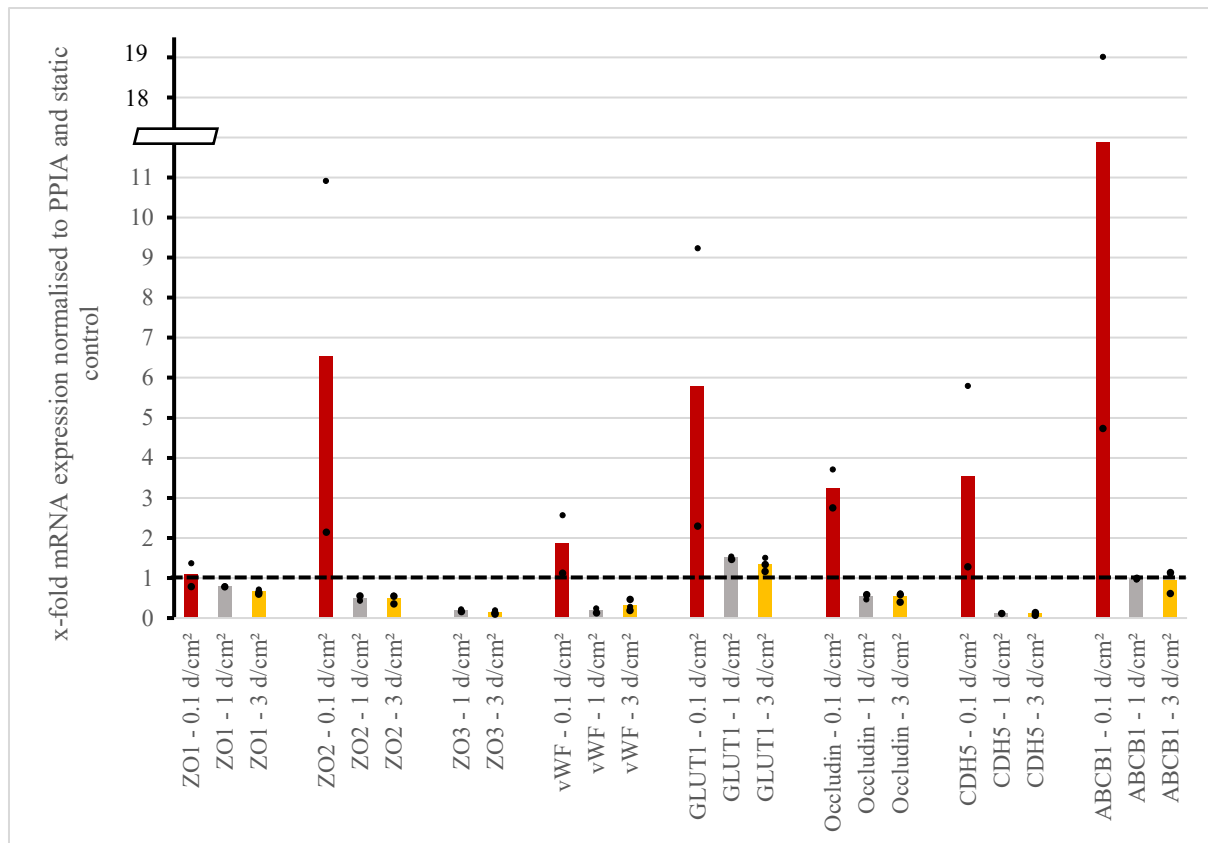
Figure 52: Bar graph 4 with trending mRNA expression level changes after 6 hours due to shear stress
(Red) 0.1 dyne/cm². (Gray) 1 dyne/cm². (Yellow) 3 dyne/cm². n=3: ZO1, ZO2, ZO3, vWF, GLUT1, Occludin, CDH5, ABCB1 – 3 dyne/cm²; n=2: ZO1, ZO2, ZO3, vWF, GLUT1, Occludin, CDH5, ABCB1 – 0.1 and 1 dyne/cm².

ZO1 was 0.78-fold downregulated at 1 dyne/cm² and 0.65-fold downregulated at 3 dyne/cm² in comparison to the static control and PPIA. However, ZO1 did not show a significant difference compared to the static control and PPIA at 0.1 dyne/cm². Overall, there was a slight downregulation from 0.1 to 1 dyne/cm² and no significant trend from 1 to 3 dyne/cm² in ZO1-expression.

ZO2 was 6.53-fold higher at 0.1 dyne/cm², 0.5-fold lower at 1 dyne/cm² and 0.49-fold lower at 3 dyne/cm² compared to the static control and PPIA. Hence, there was a downregulation from 0.1 to 1 dyne/cm² and no significant trend from 1 to 3 dyne/cm².

For ZO3 the qPCR of the mRNA expression at 0.1 dyne/cm² did not function. ZO3 was 0.19-fold downregulated at 1 dyne/cm² and 0.14-fold downregulated at 3 dyne/cm² related to the static control and PPIA, however, there was no significant trend among the shear stresses.

vWF was 1.85-fold higher at 0.1 dyne/cm², 0.19-fold lower at 1 dyne/cm² and 0.31-fold lower at 3 dyne/cm² compared to the static control and PPIA. Hence, there was a downregulation in vWF-expression from 0.1 to 1 dyne/cm² and no significant trend from 1 to 3 dyne/cm².

The same trends accounted for Occludin and CDH5. Occludin was 3.24-fold higher at 0.1 dyne/cm² and 0.53-fold lower at 1 and 3 dyne/cm² compared to the static control and PPIA.

94

CDH5 was 3.54-fold upregulated at 0.1 dyne/cm², 0.13-fold downregulated at 1 dyne/cm² and 0.10-fold downregulated at 3 dyne/cm² in comparison to the static control and PPIA. Consequently, the same trends among the shear stresses were noted as for vWF.

ABCB1 was 11.88-fold upregulated at 0.1 dyne/cm² in comparison to the static control and PPIA. For 1 and 3 dyne/cm², there was no significant change in the x-fold values related to the static control and PPIA. As a result, there was a downregulation in the mRNA expression from 0.1 to 1 dyne/cm², however, no significant change from 1 to 3 dyne/cm².
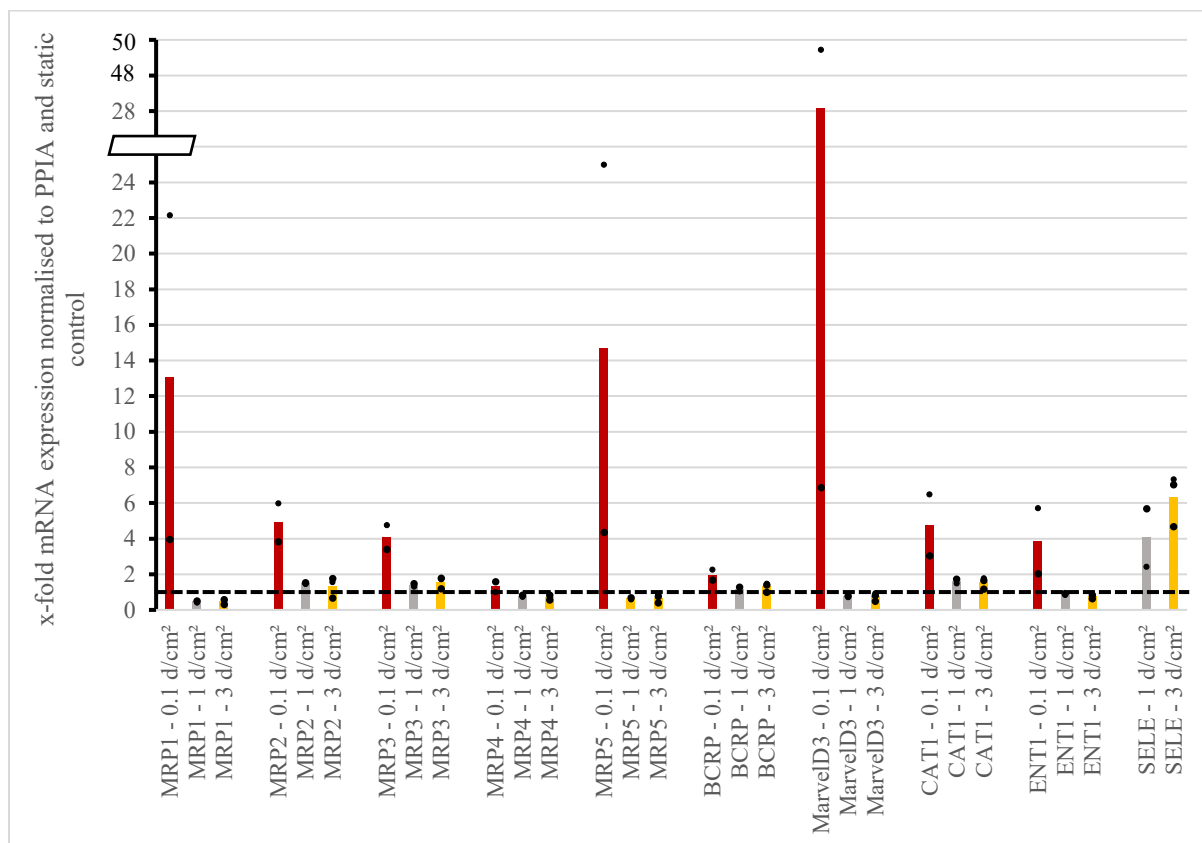
Figure 53: Bar graph 5 with trending mRNA expression level changes after 6 hours due to shear stress (Red) 0.1 dyne/cm². (Gray) 1 dyne/cm². (Yellow) 3 dyne/cm². n=3: MRP1, MRP2, MRP3, MRP4, MRP5, BCRP, MarvelD3, CAT1, ENT1, SELE – 3 dyne/cm²; n=2: MRP1, MRP2, MRP3, MRP4, MRP5, BCRP, MarvelD3, CAT1, ENT1 – 0.1 and 1 dyne/cm²; SELE – 1 dyne/cm².

MRP1 was 13.06-fold upregulated at 0.1 dyne/cm², 0.45-fold downregulated at 1 dyne/cm² and 0.49-fold downregulated at 3 dyne/cm² in comparison to the static control and PPIA. Thus, there was a significant downregulation from 0.1 to 1 dyne/cm² in MRP1-expression, however, no further trend could be detected from 1 to 3 dyne/cm².

MRP2 revealed upregulations compared to the static control for all three shear stresses. Hence, there was a 4.91-fold upregulation at 0.1 dyne/cm², a 1.49-fold upregulation at 1 dyne/cm² and a 1.33-fold upregulation for 3 dyne/cm² compared to the static control and PPIA. Consequently, there was a downregulation from 0.1 to 1 dyne/cm² and no significant further trend from 1 to 3 dyne/cm².

The same trends were noticed for MRP3-expression, which was 4.08-fold higher at 0.1 dyne/cm², 1.38-fold higher at 1 dyne/cm² and 1.56-fold higher at 3 dyne/cm² compared to the static control and PPIA. Thus, a downregulation was noticed from 0.1 to 1 dyne/cm² and no further significant trend was detected from 1 to 3 dyne/cm².

MRP4 displayed a 1.3-fold upregulation at 0.1 dyne/cm², a 0.78-fold downregulation at 1 dyne/cm² and a 0.71-fold downregulation at 3 dyne/cm² related to the static control and PPIA. Once again, a trend towards a downregulation in the mRNA expression was revealed from 0.1 to 1 dyne/cm² and no significant further trend was noticed from 1 to 3 dyne/cm².

MRP5 was 14.67-fold higher at 0.1 dyne/cm², 0.63-fold lower at 1 dyne/cm² and 0.67-fold lower at 3 dyne/cm² in comparison to the static control and PPIA. Hence, there was a downregulation from 0.1 to 1 dyne/cm², however, no significant change from 1 to 3 dyne/cm².

BCRP displayed upregulations at all three shear stresses. Hence BCRP was 1.96-fold higher at 0.1 dyne/cm², 1.16-fold higher at 1 dyne/cm² and 1.29-fold higher at 3 dyne/cm² compared to the static control and PPIA. Therefore, there was a downregulation from 0.1 to 1 dyne/cm² and no significant trend from 1 to 3 dyne/cm².

MarvelD3 was found to be 28.15-fold higher at 0.1 dyne/cm², 0.75-fold lower at 1 dyne/cm² and 0.74-fold lower at 3 dyne/cm² in relation to the static control and PPIA. Once again, a significant downregulation in the mRNA expression was detected from 0.1 to 1 dyne/cm² and no further trend was observed from 1 to 3 dyne/cm².

CAT1 showed upregulations at all three shear stresses. A 4.76-fold upregulation was detected at 0.1 dyne/cm², a 1.61-fold upregulation at 1 dyne/cm² and a 1.53-fold upregulation at 3 dyne/cm² compared to the static control and PPIA. Thus, there was a downregulation in CAT1-expression from 0.1 to 1 dyne/cm² and no significant trend from 1 to 3 dyne/cm².

ENT1 was 3.87-fold higher at 0.1 dyne/cm², 0.88-fold lower at 1 dyne/cm² and 0.79-fold lower at 3 dyne/cm² related to the static control and PPIA. As a result, a downregulation in ENT1-expression was found from 0.1 to 1 dyne/cm² and no significant trend from 1 to 3 dyne/cm² was noticed.

For SELE the qPCR of the mRNA expression at the shear stress of 0.1 dyne/cm² did not function. SELE was upregulated at 1 and 3 dyne/cm². Hence, it was 4.04-fold higher at 1 dyne/cm² and 6.34-fold higher at 3 dyne/cm² in comparison to the static control and PPIA. Consequently, there was an upregulation from 1 to 3 dyne/cm².
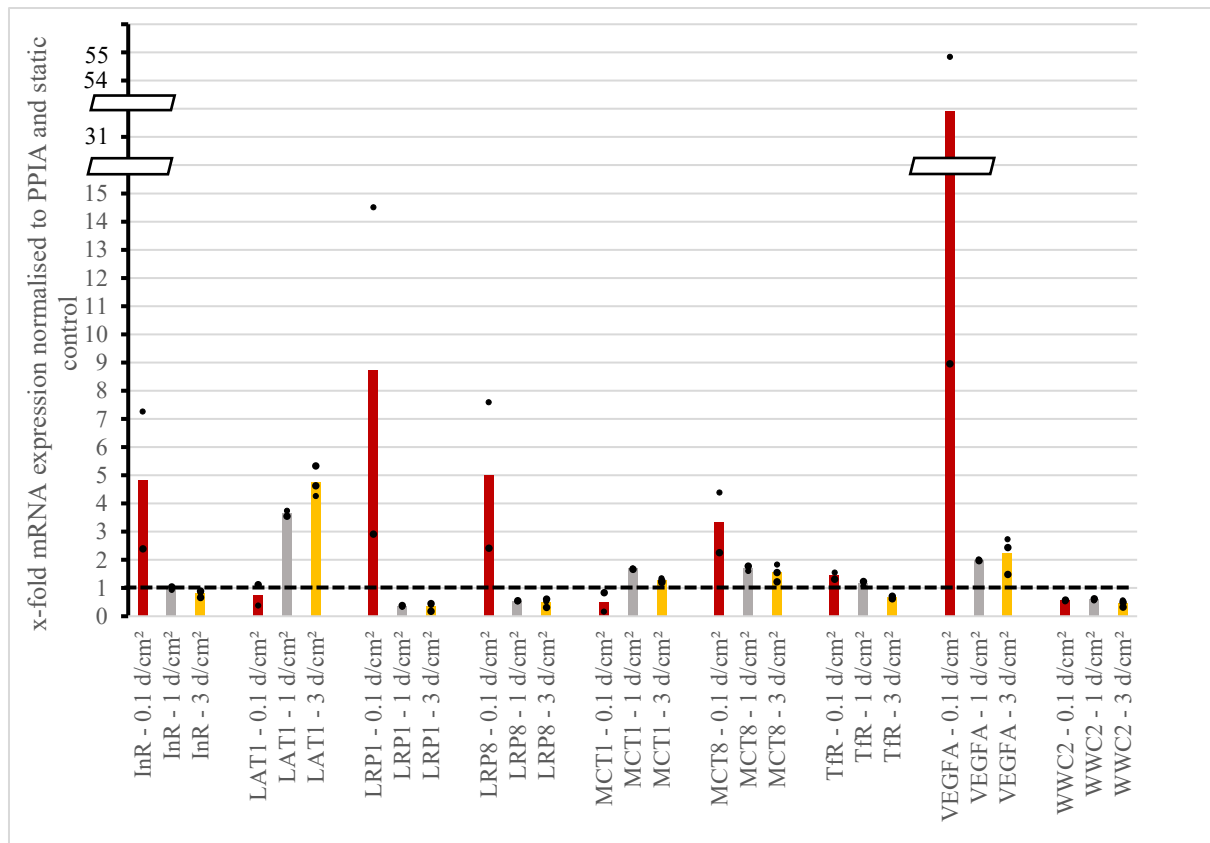
Figure 54: Bar graph 6 with trending mRNA expression level changes after 6 hours due to shear stress
(Red) 0.1 dyne/cm². (Gray) 1 dyne/cm². (Yellow) 3 dyne/cm². n=3: InR, LAT1, LRP1, LRP8, MCT1, MCT8, TfR, VEGFA, WWC2 – 3 dyne/cm²; n=2: InR, LAT1, LRP1, LRP8, MCT1, MCT8, TfR, VEGFA, WWC2 – 0.1 and 1 dyne/cm².

InR was 4.83-fold upregulated at 0.1 dyne/cm² and 0.81-fold downregulated at 3 dyne/cm² in relation to the static control and PPIA. InR did not show a significant difference in the mRNA expression compared to the static control and PPIA at 1 dyne/cm². Hence, a downregulation occurred from 0.1 to 1 dyne/cm² and no further trend was detected from 1 to 3 dyne/cm².

LAT1 was 0.76-fold lower at 0.1 dyne/cm², 3.65-fold higher at 1 dyne/cm² and 4.75-fold higher at 3 dyne/cm² compared to the static control and PPIA. Thus, there was an overall trend towards upregulation in the mRNA expression with increasing shear stress for LAT1.

LRP1 displayed an 8.72-fold upregulation at 0.1 dyne/cm², a 0.36-fold downregulation at 1 dyne/cm² and a 0.35-fold downregulation at 3 dyne/cm² related to the static control and PPIA. As a result, there was a trend towards downregulation from 0.1 to 1 dyne/cm² and no further significant trend in the mRNA expression from 1 to 3 dyne/cm².

The same observation accounted for LRP8, which was 5.01-fold higher at 0.1 dyne/cm², 0.55-fold lower at 1 dyne/cm² and 0.50-fold lower at 3 dyne/cm² in comparison to the static control and PPIA. Once again, a tendency towards downregulation was noticed from 0.1 to 1 dyne/cm² and no further trend was detected from 1 to 3 dyne/cm².

MCT1 was 0.51-fold lower at 0.1 dyne/cm², 1.69-fold higher at 1 dyne/cm² and 1.27-fold higher at 3 dyne/cm² in relation to the static control and PPIA. Therefore, an upregulation in MCT1-expression occurred from 0.1 to 1 dyne/cm² and a downregulation was detected from 1 to 3 dyne/cm².

MCT8 was upregulated at all three shear stresses in comparison to the static control and PPIA. Hence, MCT8 was 3.32-fold upregulated at 0.1 dyne/cm², 1.7-fold upregulated at 1 dyne/cm² and 1.55-fold upregulated at 3 dyne/cm². As a result, there was a downregulation from 0.1 to 1 dyne/cm² and no significant difference in the mRNA expression between 1 and 3 dyne/cm².

TfR showed a 1.44-fold upregulation at 0.1 dyne/cm² and a 1.16-fold upregulation at 1 dyne/cm² in comparison to the static control and PPIA. At 3 dyne/cm², TfR displayed a 0.66-fold downregulation related to the static control and PPIA. Overall, there was a trend towards downregulation in the mRNA expression with increasing shear stress.

VEGFA presented upregulations at all three shear stresses. Therefore, VEGFA was 31.91-fold higher at 0.1 dyne/cm², 2-fold higher at 1 dyne/cm² and 2.22-fold higher at 3 dyne/cm² in relation to the static control and PPIA. Consequently, there was a significant downregulation from 0.1 to 1 dyne/cm² and no further trend in the mRNA expression of VEGFA between 1 and 3 dyne/cm².

WWC2 was 0.56-fold downregulated at 0.1 dyne/cm², 0.60-fold downregulated at 1 dyne/cm² and 0.47-fold downregulated at 3 dyne/cm² compared to the static control and PPIA. Thus, there was no significant difference in the mRNA expression of WWC2 between the shear stresses.
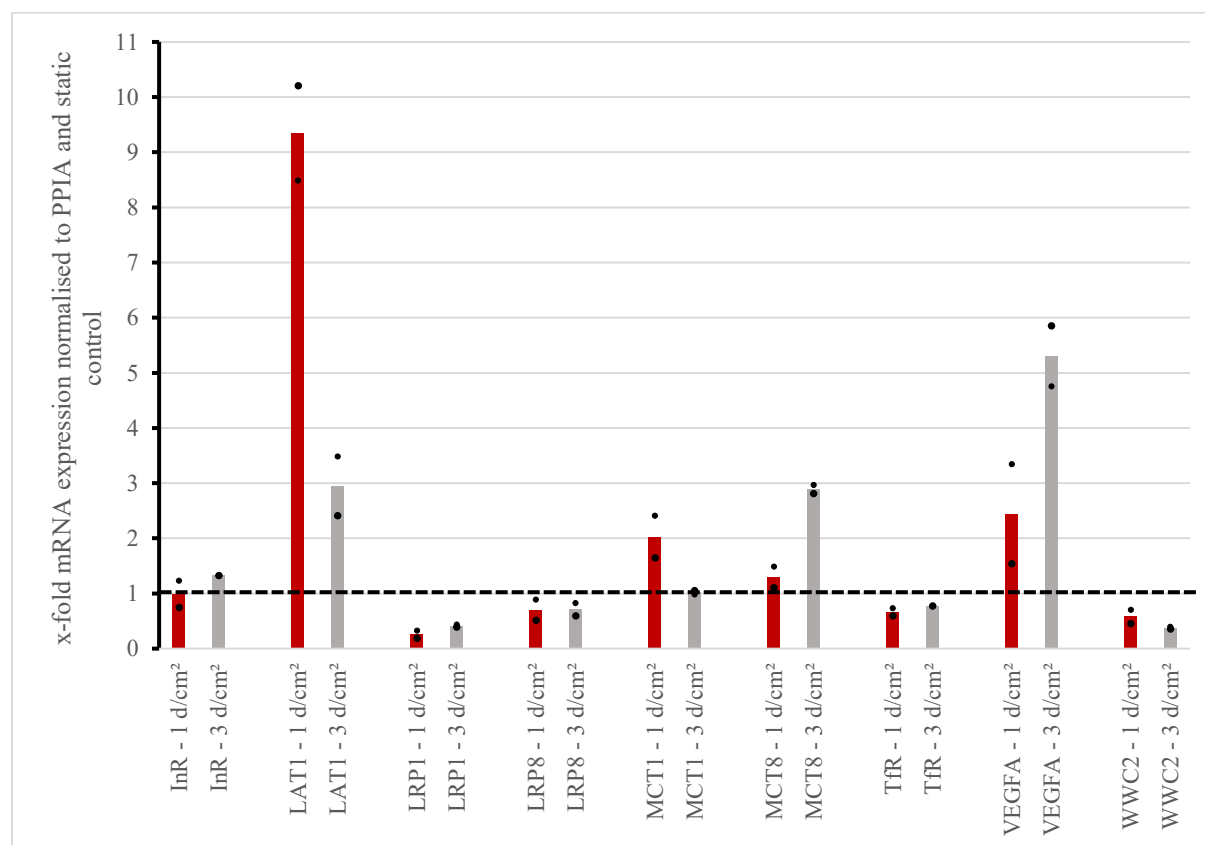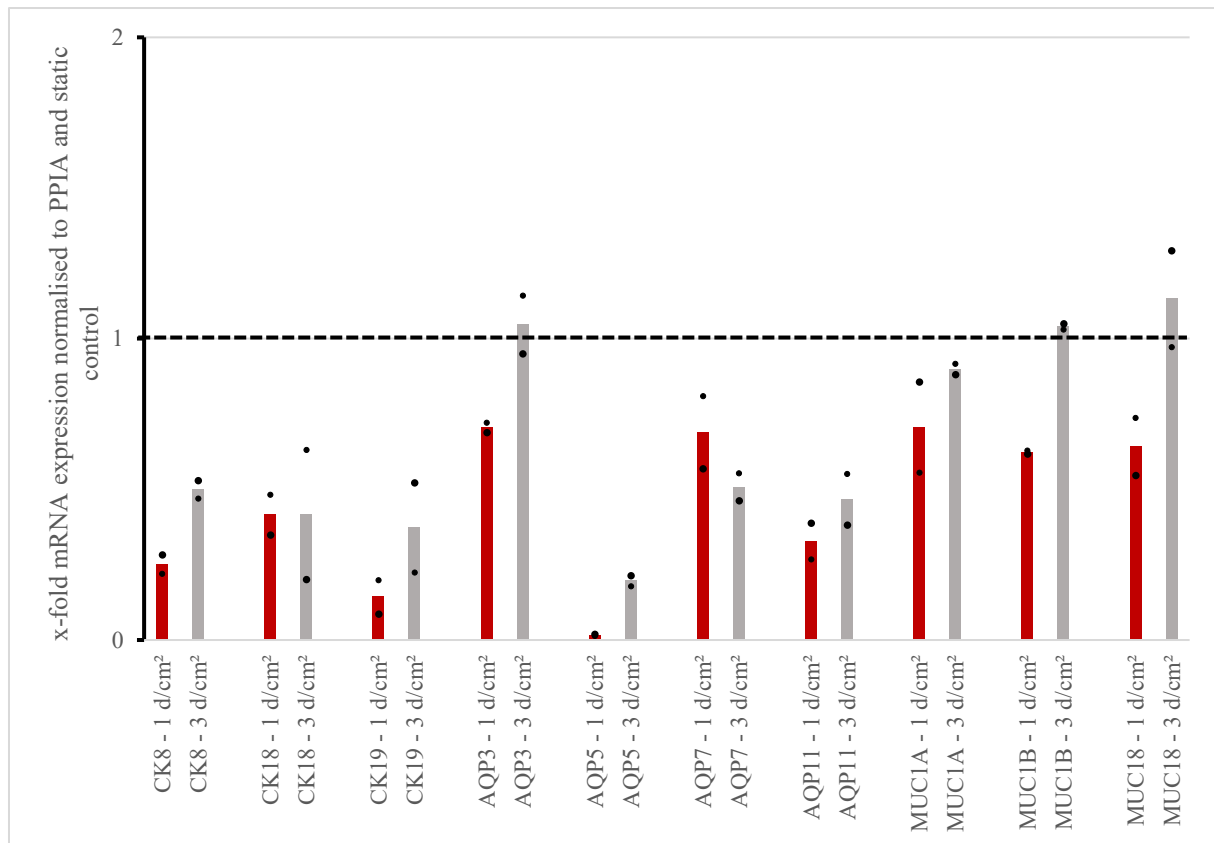
Figure 55: Bar graph 7 with trending mRNA expression level changes after 6 hours due to shear stress
(Red) 0.1 dyne/cm². (Gray) 1 dyne/cm². (Yellow) 3 dyne/cm². n=3: CK8, CK18, CK19, AQP1, AQP3, AQP7, AQP11, MUC1A, MUC1B – 3 dyne/cm²; n=2: CK8, CK18, CK19, AQP1, AQP3, AQP7, AQP11, MUC1A, MUC1B – 0.1 and 1 dyne/cm².

CK8 was 6.43-fold upregulated at 0.1 dyne/cm², 0.36-fold downregulated at 1 dyne/cm² and 0.26-fold downregulated at 3 dyne/cm² in comparison to the static control and PPIA. As a result, there was a downregulation from 0.1 to 1 dyne/cm² and no significant further variation in the mRNA expression of CK8 from 1 to 3 dyne/cm².

The same accounted for CK18, which displayed a 2.76-fold upregulation at 0.1 dyne/cm², a 0.35-fold downregulation at 1 dyne/cm² and a 0.3-fold downregulation at 3 dyne/cm² related to the static control and PPIA. Once again, there was a downregulation from 0.1 to 1 dyne/cm² and no further significant trend in the mRNA expression from 1 to 3 dyne/cm².

CK19 was 6.39-fold higher at 0.1 dyne/cm², 0.18-fold lower at 1 dyne/cm² and 0.27-fold lower at 3 dyne/cm² compared to the static control and PPIA. Hence, there was a downregulation from 0.1 to 1 dyne/cm² and no significant variation in the mRNA expression of CK19 from 1 to 3 dyne/cm².

AQP1 was 6.9-fold upregulated at 0.1 dyne/cm², 1.58-fold upregulated at 1 dyne/cm² and 0.68-fold downregulated at 3 dyne/cm² in relation to the static control and PPIA. As a result, there was an overall tendency towards downregulation from 0.1 to 1 dyne/cm² and from 1 to 3 dyne/cm².

99

AQP3 displayed upregulations at all three shear stresses in comparison to the static control and PPIA. Hence, AQP3 was 24.45-fold higher at 0.1 dyne/cm², 1.61-fold higher at 1 dyne/cm² and 1.95-fold higher at 3 dyne/cm². As a result, there was a downregulation from 0.1 to 1 dyne/cm² and a slight upregulation from 1 to 3 dyne/cm² in AQP3-expression.

AQP5 was 5.78-fold higher at 0.1 dyne/cm², 0.17-fold lower at 1 dyne/cm² and 0.22-fold lower at 3 dyne/cm² related to the static control and PPIA. Consequently, there was a downregulation from 0.1 to 1 dyne/cm² and no further significant change in AQP5-expression from 1 to 3 dyne/cm².

AQP7 displayed a 50.82-fold increase at 0.1 dyne/cm², a 1.39-fold increase at 1 dyne/cm² and a 0.48-fold decrease at 3 dyne/cm² in comparison to the static control and PPIA. Hence, there was an overall trend towards downregulation in AQP7-expression with increasing shear stress.

AQP11 was 4.9-fold higher at 0.1 dyne/cm², 0.47-fold lower at 1 dyne/cm² and 0.29-fold lower at 3 dyne/cm² compared to the static control and PPIA. Consequently, there was a downregulation from 0.1 to 1 dyne/cm² and no further significant trend in the mRNA expression of AQP11 from 1 to 3 dyne/cm².

MUC1A was 19.14-fold increased at 0.1 dyne/cm² and did not show significant differences in its mRNA expression at 1 and 3 dyne/cm² in relation to the static control and PPIA. Therefore, a downregulation could be noticed from 0.1 to 1 dyne/cm² and no further significant variation in MUC1A-expression was detected from 1 to 3 dyne/cm².

MUC1B was 22.70-fold higher at 0.1 dyne/cm² and 0.82-fold lower at 3 dyne/cm², however, MUC1B did not show a significant difference at 1 dyne/cm² compared to the static control and PPIA. As a result, there was a downregulation from 0.1 to 1 dyne/cm² and no significant tendency in the mRNA expression from 1 to 3 dyne/cm².

Figure 56: Bar graph 8 with trending mRNA expression level changes after 6 hours due to shear stress
(Red) 0.1 dyne/cm². (Gray) 1 dyne/cm². (Yellow) 3 dyne/cm². n=3: MUC18, MUC20, b catenin tv1, b catenin tv4, VIMENTIN, FIBRONECTIN, S100A4 tv1, S100A4 tv2, MFSD2A, Claudin25-1, Claudin25 tv7, RAGE – 3 dyne/cm²; n=2: MUC18, MUC20, b catenin tv1, b catenin tv4, VIMENTIN, FIBRONECTIN, S100A4 tv1, S100A4 tv2, MFSD2A, Claudin25-1, Claudin25 tv7, RAGE – 0.1 and 1 dyne/cm².

MUC18 was 20.24-fold higher at 0.1 dyne/cm², 0.59-fold lower at 1 dyne/cm² and 0.54-fold lower at 3 dyne/cm² in comparison to the static control and PPIA. Hence, there was a downregulation from 0.1 to 1 dyne/cm² and no significant change in the mRNA expression from 1 to 3 dyne/cm².

The same observation was made for MUC20. This target was 24.63-fold higher at 0.1 dyne/cm², 1.19-fold higher at 1 dyne/cm² and did not display a significant difference at 3 dyne/cm² related to the static control and PPIA. Thus, there was a downregulation from 0.1 to 1 dyne/cm² and no significant variation in the mRNA expression from 1 to 3 dyne/cm².

B catenin tv1 was 7.08-fold higher at 0.1 dyne/cm², 0.46-fold lower at 1 dyne/cm² and 0.45-fold lower at 3 dyne/cm² compared to the static control and PPIA. As a result, there was a downregulation from 0.1 to 1 dyne/cm² and no significant change in the mRNA expression from 1 to 3 dyne/cm².

B catenin tv4 revealed the same tendencies. Hence, b catenin tv4 was 5.15-fold increased at 0.1 dyne/cm², 0.53-fold decreased at 1 dyne/cm² and 0.58-fold decreased at 3 dyne/cm² in

comparison to the static control and PPIA. Once again, a downregulation from 0.1 to 1 dyne/cm² was noticed and no significant further trend in the mRNA expression from 1 to 3 dyne/cm² was detected.

VIMENTIN was 13.24-fold higher at 0.1 dyne/cm², 0.73-fold lower at 1 dyne/cm² and 0.52-fold lower at 3 dyne/cm² related to the static control and PPIA. Consequently, there was a downregulation from 0.1 to 1 dyne/cm² and no significant change from 1 to 3 dyne/cm².

FIBRONECTIN was 4.98-fold increased at 0.1 dyne/cm², 0.57-fold decreased at 1 dyne/cm² and 0.33-fold decreased at 3 dyne/cm² compared to the static control and PPIA. Therefore, a downregulation could be noted from 0.1 to 1 dyne/cm² and no significant further change in the mRNA expression of FIBRONECTIN was detected from 1 to 3 dyne/cm².

S100A4 tv1 was 7.41-fold higher at 0.1 dyne/cm², 0.32-fold lower at 1 dyne/cm² and 0.24-fold lower at 3 dyne/cm² related to the static control and PPIA. Hence, there was a downregulation from 0.1 to 1 dyne/cm² and no significant change in the mRNA expression of S100A4 tv1 from 1 to 3 dyne/cm².

S100A4 tv2 showed a 4.1-fold upregulation at 0.1 dyne/cm², a 0.21-fold downregulation at 1 dyne/cm² and a 0.19-fold downregulation at 3 dyne/cm² in comparison to the static control and PPIA. Consequently, there was, again, a downregulation from 0.1 to 1 dyne/cm² and no significant trend in S100A4 tv2-expression from 1 to 3 dyne/cm².

MFSD2A revealed upregulations at all three shear stresses in comparison to the static control and PPIA. Hence, MFSD2A was 49.36-fold higher at 0.1 dyne/cm², 3.3-fold higher at 1 dyne/cm² and 2.9-fold higher at 3 dyne/cm². As a result, there was an overall downregulation with increasing shear stress in the mRNA expression of MFSD2A.

Claudin25-1 was 13.95-fold increased at 0.1 dyne/cm², 0.78-fold decreased at 1 dyne/cm² and 0.44-fold decreased at 3 dyne/cm² compared to the static control and PPIA. Thus, there was a significant downregulation from 0.1 to 1 dyne/cm² and a slight downregulation in the mRNA expression of Claudin25-1 from 1 to 3 dyne/cm².

Claudin25 tv7 displayed upregulations at all three shear stresses related to the static control and PPIA. Hence, Claudin25 tv7 was 31.82-fold increased at 0.1 dyne/cm², 2.25-fold increased at 1 dyne/cm² and 1.6-fold increased at 3 dyne/cm². Consequently, there was an overall tendency towards downregulation in the mRNA expression of Claudin25 tv7 with increasing shear stress.

RAGE presented a 10.41-fold increase at 0.1 dyne/cm², a 0.52-fold decrease at 3 dyne/cm² and no significant change at 1 dyne/cm² related to the static control and PPIA. As a result, there was an overall downregulation in RAGE-expression with increasing shear stress.

Overall, most targets presented an increase in the mRNA expression at 0.1 dyne/cm² after 6 hours of final shear stress exposure in comparison to the static control and PPIA. Among the shear stresses, there were predominantly downregulations in the mRNA expressions from 0.1 to 1 dyne/cm² and no significant further changes from 1 to 3 dyne/cm².

4.5.2   mRNA expression level changes after 24 hours at different shear stresses

In the following section the mRNA expression patterns of the target genes at the final shear stresses of 1 and 3 dyne/cm² were examined. In particular possible up- and downregulations in comparison to the static control were considered and shear dependency was evaluated again (Figure 58 to Figure 65). This time, the mRNA-harvests were conducted after 24 hours with ultimate shear stress exposure. The experimental setup is shown in Figure 57.
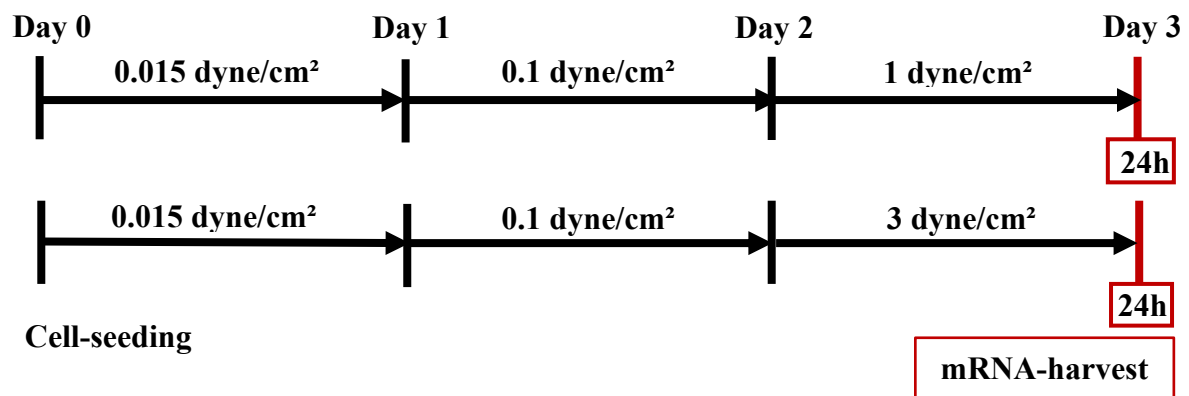
Figure 57: Experimental setup of mRNA-harvest after 24 hours
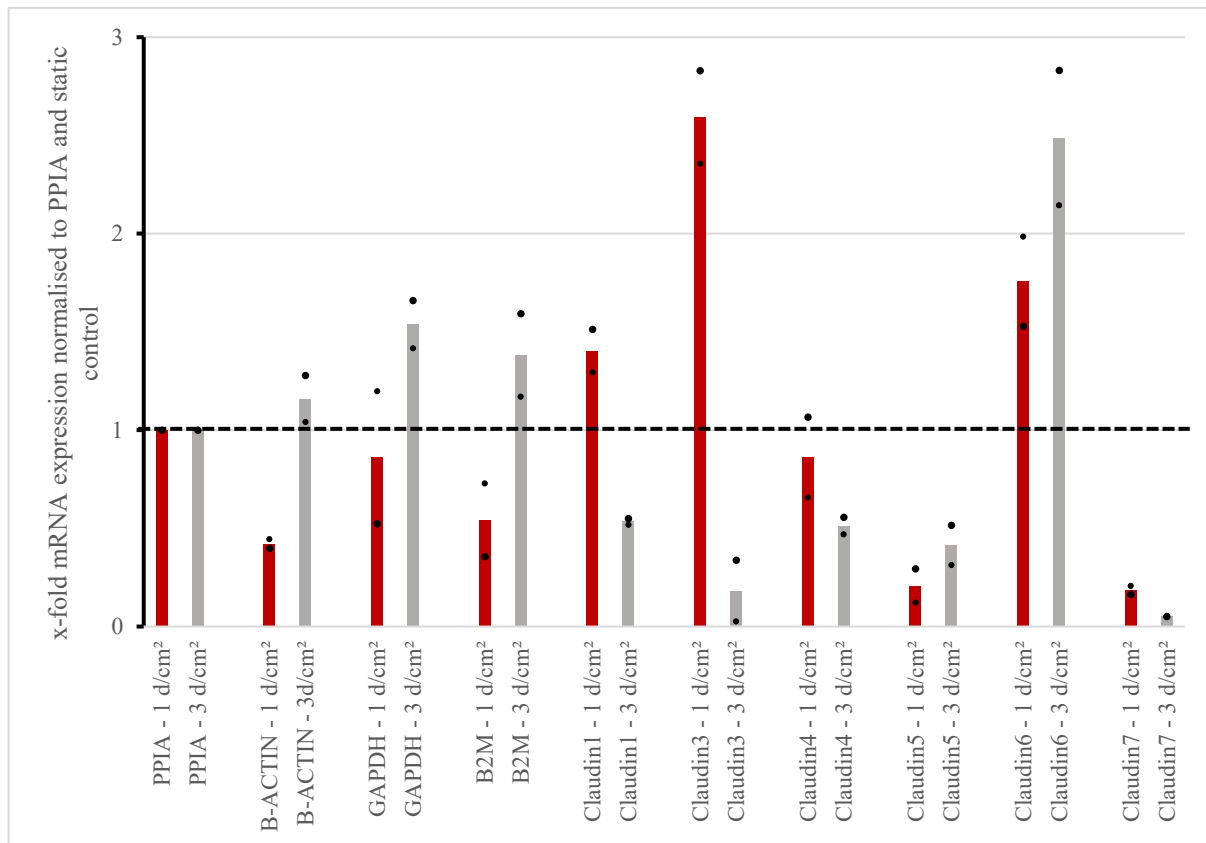
Figure 58: Bar graph 1 with trending mRNA expression level changes after 24 hours
(Red) 1 dyne/cm². (Gray) 3 dyne/cm². n=2: PPIA, B-ACTIN, GAPDH, B2M, Claudin1, Claudin3, Claudin4, Claudin5, Claudin6, Claudin7 – 1 and 3 dyne/cm².

B-ACTIN was 0.42-fold lower at 1 dyne/cm² and 1.16-fold higher at 3 dyne/cm² in comparison to the static control and PPIA. Therefore, B-ACTIN was upregulated from 1 to 3 dyne/cm².

GAPDH displayed a 0.86-fold downregulation at 1 dyne/cm² and a 1.54-fold upregulation at 3 dyne/cm² related to the static control and PPIA. Hence, there was a trend towards upregulation in the mRNA expression of GAPDH from 1 to 3 dyne/cm².

B2M was 0.54-fold decreased at 1 dyne/cm² and 1.38-fold increased at 3 dyne/cm² compared to the static control and PPIA. Once again, there was an upregulation in the mRNA expression with increasing shear stress.

Claudin1 was 1.4-fold higher at 1 dyne/cm² and 0.53-fold lower at 3 dyne/cm² in comparison to the static control and PPIA. Consequently, Claudin1 was downregulated with increasing shear stress.

Claudin3 showed a 2.6-fold upregulation at 1 dyne/cm² and a 0.18-fold downregulation at 3 dyne/cm² compared to the static control and PPIA. As a result, again, there was a downregulation in the mRNA expression from 1 to 3 dyne/cm².

Claudin4 was 0.86-fold decreased at 1 dyne/cm² and 0.51-fold decreased at 3 dyne/cm² in comparison to the static control and PPIA. Hence, there was a slight downregulation in the mRNA expression with increasing shear stress.

Claudin5 was 0.21-fold lower at 1 dyne/cm² and 0.41-fold lower at 3 dyne/cm² related to the static control and PPIA. Therefore, Claudin5 did not show a significant change in the mRNA expression among the shear stresses.

Claudin6 was 1.76-fold increased at 1 dyne/cm² and 2.49-fold increased at 3 dyne/cm² in relation to the static control and PPIA. Consequently, Claudin6 was upregulated from 1 to 3 dyne/cm².

Claudin7 revealed a 0.19-fold downregulation at 1 dyne/cm² and a 0.05-fold downregulation at 3 dyne/cm² compared to the static control and PPIA. Therefore, Claudin7 was downregulated with increasing shear stress.
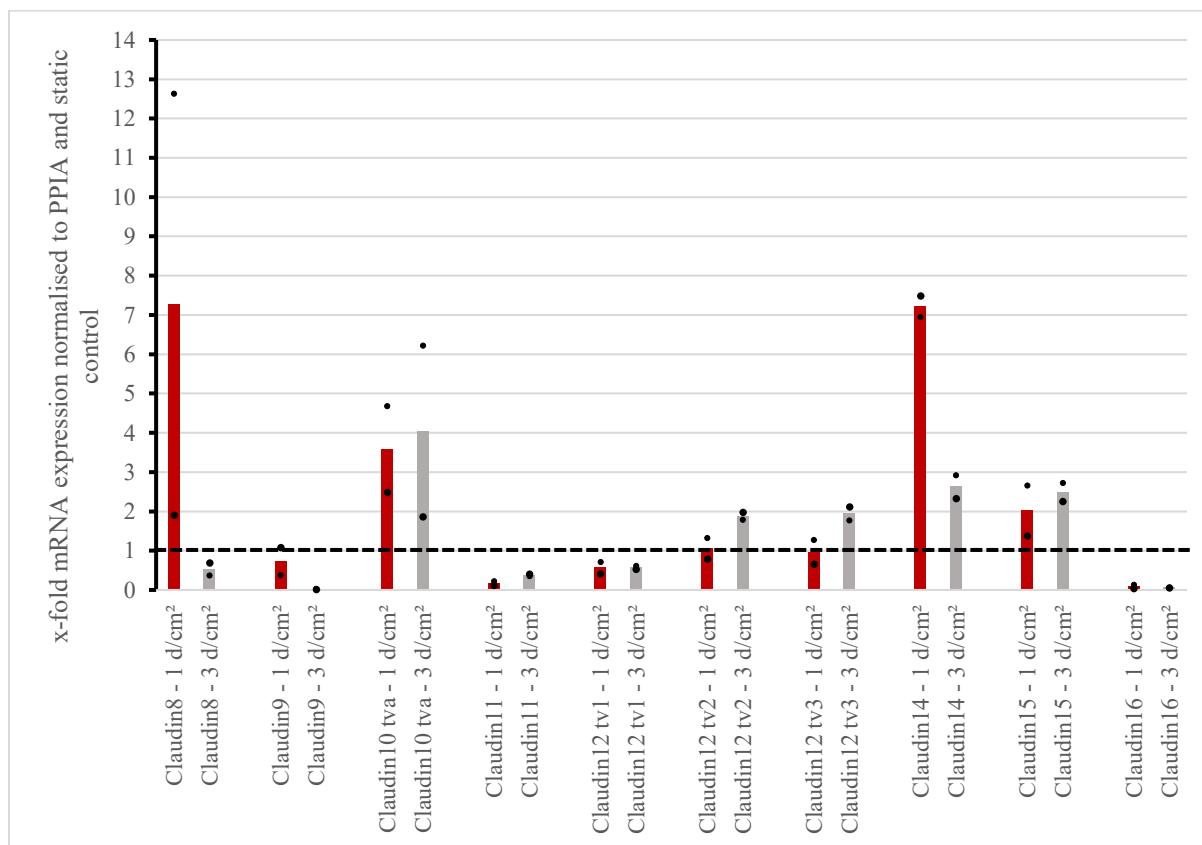
Figure 59: Bar graph 2 with trending mRNA expression level changes after 24 hours
(Red) 1 dyne/cm². (Gray) 3 dyne/cm². n=2: Claudin8, Claudin9, Claudin10 tva, Claudin11, Claudin12 tv1, Claudin12 tv2, Claudin12 tv3, Claudin14, Claudin15, Claudin16 – 1 and 3 dyne/cm².

Claudin8 was 7.27-fold increased at 1 dyne/cm² and 0.53-fold decreased at 3 dyne/cm² in relation to the static control and PPIA. Therefore, Claudin8 showed a significant downregulation in the mRNA expression with increasing shear stress.

Claudin9 was 0.73-fold decreased at 1 dyne/cm² and 0.023-fold decreased at 3 dyne/cm² in comparison to the static control and PPIA. Hence, there was a downregulation in the mRNA expression among the shear stresses from 1 to 3 dyne/cm².

Claudin10 tva was 3.59-fold higher at 1 dyne/cm² and 4.04-fold higher at 3 dyne/cm² related to the static control and PPIA. As a result, Claudin10 tva displayed a slight upregulation in its mRNA expression from 1 to 3 dyne/cm².

Claudin11 was 0.17-fold decreased at 1 dyne/cm² and 0.39-fold decreased at 3 dyne/cm² compared to the static control and PPIA. Claudin11 showed no significant difference in the mRNA expression among the shear stress values.

Claudin12 tv1 showed a 0.56-fold decrease at 1 dyne/cm² and a 0.57-fold decrease at 3 dyne/cm² in comparison to the static control and PPIA and therefore did not display a significant variation in its mRNA expression with increasing shear stress.

Claudin12 tv2 displayed no change at 1 dyne/cm² and was 1.88-fold higher at 3 dyne/cm² in relation to the static control and PPIA. Hence, there was an upregulation in the mRNA expression of Claudin12 tv2 from 1 to 3 dyne/cm².

Claudin12 tv3 also did not indicate a significant variation at 1 dyne/cm², however, showed a 1.95-fold upregulation at 3 dyne/cm² in comparison to the static control and PPIA. Consequently, there was an upregulation in the mRNA expression of Claudin12 tv3 from 1 to 3 dyne/cm².

Claudin14 was 7.22-fold higher at 1 dyne/cm² and 2.63-fold higher at 3 dyne/cm² compared to the static control and PPIA. Consequently, Claudin14 displayed a downregulation in the mRNA expression from 1 to 3 dyne/cm².

Claudin15 showed a 2.02-fold increase at 1 dyne/cm² and a 2.5-fold increase at 3 dyne/cm² related to the static control and PPIA. Therefore, Claudin15 was upregulated from 1 to 3 dyne/cm².

Claudin16 was 0.087-fold lower at 1 dyne/cm² and 0.056-fold lower at 3 dyne/cm² in comparison to the static control and PPIA. As a result, Claudin16 did not show a significant difference in the mRNA expression among the shear stress values.
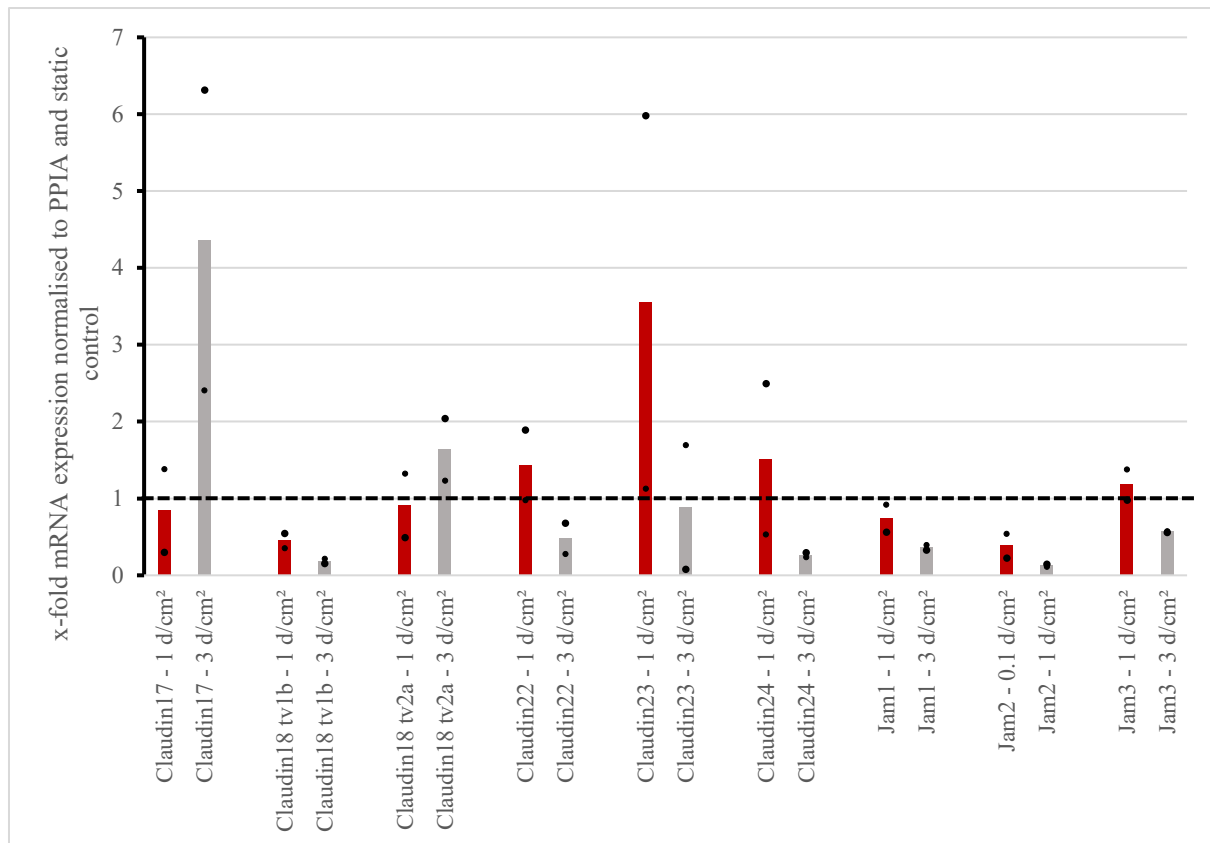
Figure 60: Bar graph 3 with trending mRNA expression level changes after 24 hours
(Red) 1 dyne/cm². (Gray) 3 dyne/cm². n=2: Claudin17, Claudin18 tv1b, Claudin18 tv2a, Claudin22, Claudin23, Claudin24, Jam1, Jam2, Jam3 – 1 and 3 dyne/cm².

Claudin17 was 0.84-fold downregulated at 1 dyne/cm² and 4.36-fold upregulated at 3 dyne/cm² in comparison to the static control and PPIA. Hence, there was a significant upregulation in the mRNA expression of Claudin17 from 1 to 3 dyne/cm².

Claudin18 tv1b was 0.45-fold lower at 1 dyne/cm² and 0.19-fold lower at 3 dyne/cm² related to the static control and PPIA. Therefore, Claudin18 tv1b did not show a significant difference in the mRNA expression among the shear stress values.

Claudin18 tv2a did not reveal a significant variation at 1 dyne/cm², however, displayed a 1.63-fold increase at 3 dyne/cm² compared to the static control and PPIA. Consequently, there was an upregulation in Claudin18 tv2a-expression from 1 to 3 dyne/cm².

Claudin22 indicated a 1.44-fold upregulation at 1 dyne/cm² and a 0.48-fold downregulation at 3 dyne/cm² related to the static control and PPIA. As a result, there was a significant downregulation in the mRNA expression of Claudin22 from 1 to 3 dyne/cm².

Claudin23 displayed a 3.56-fold increase at 1 dyne/cm² and a 0.89-fold decrease at 3 dyne/cm² in comparison to the static control and PPIA. Consequently, there was, again, a significant downregulation in the mRNA expression with increasing shear stress.

Claudin24 was 1.51-fold higher at 1 dyne/cm² and 0.27-fold lower at 3 dyne/cm² compared to the static control and PPIA. Hence, Claudin24 revealed a significant downregulation in its mRNA expression from 1 to 3 dyne/cm².

Jam1 presented downregulations at 1 and 3 dyne/cm² compared to the static control and PPIA with a 0.74-fold decrease and a 0.36-fold decrease, respectively. Therefore, Jam1 was slightly downregulated from 1 to 3 dyne/cm².

Jam2 was also downregulated at 1 and 3 dyne/cm² related to the static control and PPIA with a 0.39-fold downregulation and a 0.13-fold downregulation, respectively. As a result, Jam2 was also slightly decreased with increasing shear stress.

Jam3 was 1.18-fold higher at 1 dyne/cm² and 0.57-fold lower at 3 dyne/cm² in relation to the static control and PPIA. Hence, Jam3 showed a downregulation in its mRNA expression from 1 to 3 dyne/cm².
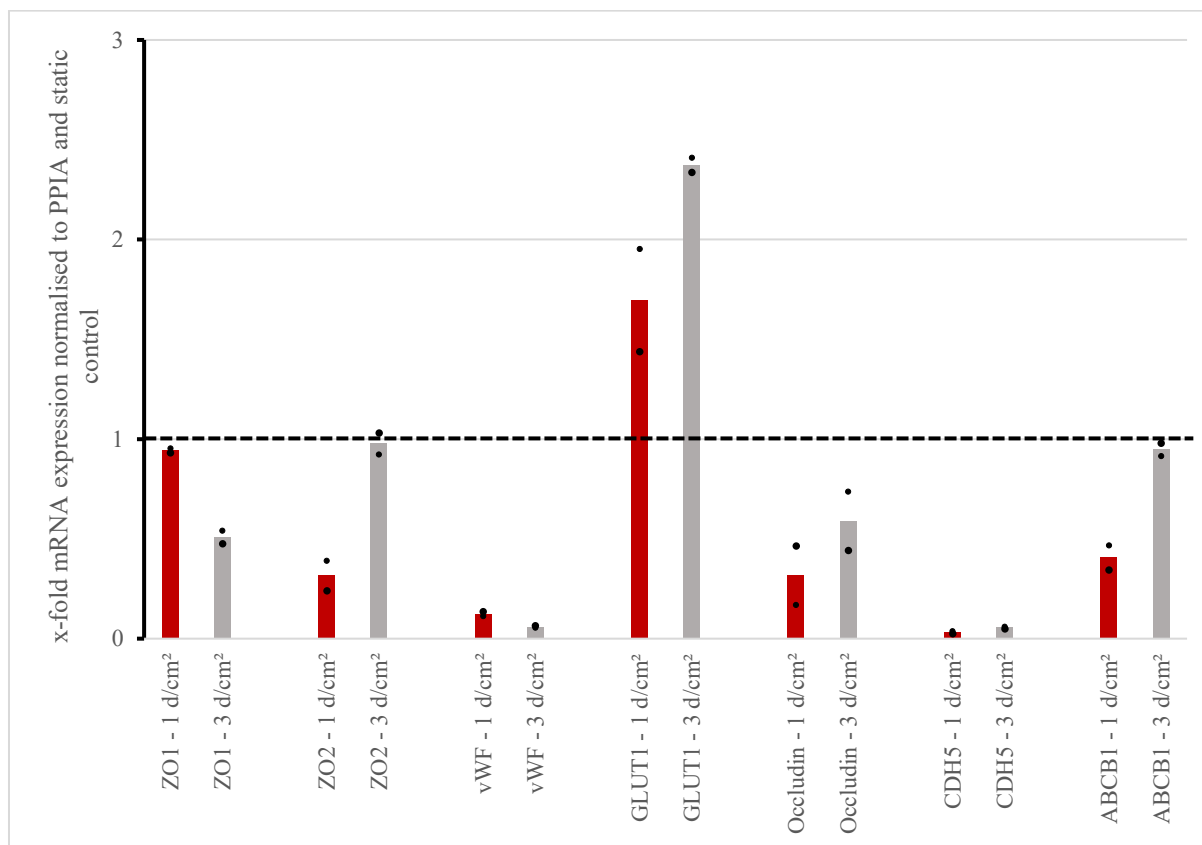
Figure 61: Bar graph 4 with trending mRNA expression level changes after 24 hours
(Red) 1 dyne/cm². (Gray) 3 dyne/cm². n=2: ZO1, ZO2, vWF, GLUT1, Occludin, CDH5, ABCB1 – 1 and 3 dyne/cm².

ZO1 did not show a significant difference at 1 dyne/cm², however, presented a 0.51-fold decrease at 3 dyne/cm² in comparison to the static control and PPIA. Therefore, a downregulation in the mRNA expression was noted for ZO1 with increasing shear stress.

ZO2 was 0.32-fold lower at 1 dyne/cm² and did not reveal a significant variation at 3 dyne/cm² related to the static control and PPIA. Consequently, there was an upregulation in the mRNA expression of ZO2 from 1 to 3 dyne/cm².

vWF was 0.12-fold lower and 0.06-fold lower in comparison to the static control and PPIA at 1 and 3 dyne/cm², respectively. Hence, vWF did not show a significant difference in the mRNA expression among the shear stress values.

GLUT1 was 1.69-fold higher and 2.37-fold higher related to the static control and PPIA at 1 and 3 dyne/cm², respectively. As a result, an upregulation in GLUT1-expression was noted with increasing shear stress.

Occludin was 0.32-fold lower at 1 dyne/cm² and 0.59-fold lower at 3 dyne/cm² compared to the static control and PPIA. Therefore, Occludin was slightly downregulated in its mRNA expression from 1 to 3 dyne/cm².

CDH5 was 0.032-fold downregulated at 1 dyne/cm² and 0.055-fold downregulated at 3 dyne/cm² in comparison to the static control and PPIA. Thus, CDH5 did not show a significant difference in its mRNA expression among the shear stress values.

ABCB1 revealed a 0.41-fold downregulation at 1 dyne/cm², however, did not show a significant difference to the static control and PPIA at 3 dyne/cm². Hence, ABCB1 was slightly upregulated from 1 to 3 dyne/cm².
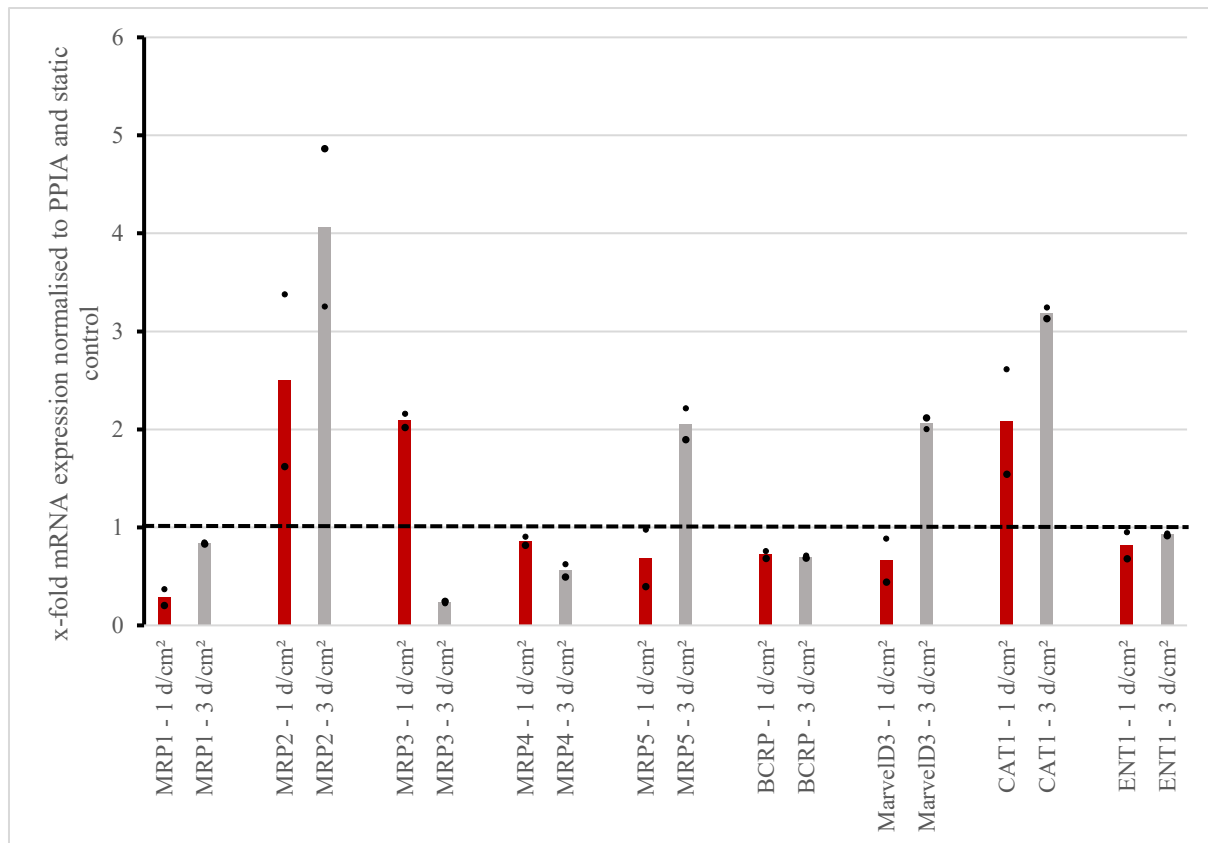
Figure 62: Bar graph 5 with trending mRNA expression level changes after 24 hours
(Red) 1 dyne/cm². (Gray) 3 dyne/cm². n=2: MRP1, MRP2, MRP3, MRP4, MRP5, BCRP, MarvelD3, CAT1, ENT1 – 1 and 3 dyne/cm².

MRP1 was 0.29-fold lower at 1 dyne/cm² and 0.84-fold lower at 3 dyne/cm² in comparison to the static control and PPIA. Hence, MRP1 was slightly upregulated in the mRNA expression from 1 to 3 dyne/cm².

MRP2 was 2.5-fold increased at 1 dyne/cm² and 4.06-fold increased at 3 dyne/cm² related to the static control and PPIA. Therefore, MRP2 also showed an upregulation in the mRNA expression from 1 to 3 dyne/cm².

MRP3 was 2.09-fold higher at 1 dyne/cm² and 0.24-fold lower at 3 dyne/cm² compared to the static control and PPIA. Consequently, MRP3-expression was increased with rising shear stress.

MRP4 showed a 0.86-fold decrease at 1 dyne/cm² and a 0.56-fold decrease at 3 dyne/cm² in relation to the static control and PPIA. Therefore, MRP4 was slightly downregulated in its mRNA expression from 1 to 3 dyne/cm².

MRP5 was 0.69-fold lower at 1 dyne/cm² and 2.05-fold higher at 3 dyne/cm² in comparison to the static control and PPIA. Hence, MRP5 was significantly upregulated in the mRNA expression from 1 to 3 dyne/cm².

BCRP was equally downregulated at 1 and 3 dyne/cm² compared to the static control and PPIA with 0.72 and 0.70 as x-fold values, respectively. Nonetheless, BCRP did not display a significant variation in its mRNA expression among the shear stress values.

MarvelD3 was 0.66-fold lower at 1 dyne/cm² and 2.06-fold higher at 3 dyne/cm² in comparison to the static control and PPIA. Therefore, MarvelD3 was upregulated in the mRNA expression from 1 to 3 dyne/cm².

CAT1 was 2.08-fold increased at 1 dyne/cm² and 3.19-fold increased at 3 dyne/cm² in comparison to the static control and PPIA. Therefore, CAT1 was upregulated with rising shear stress.

ENT1 was 0.82-fold lower at 1 dyne/cm² and did not present a significant difference at 3 dyne/cm² compared to the static control and PPIA. Hence, there was no significant change in the mRNA expression of ENT1 among the shear stresses.

Figure 63: Bar graph 6 with trending mRNA expression level changes after 24 hours
(Red) 1 dyne/cm². (Gray) 3 dyne/cm². n=2: InR, LAT1, LRP1, LRP8, MCT1, MCT8, TfR, VEGFA, WWC2 – 1 and 3 dyne/cm².

InR did not reveal a significant difference at 1 dyne/cm², however, was 1.32-fold upregulated at 3 dyne/cm² compared to the static control and PPIA. Consequently, InR was slightly upregulated in its mRNA expression from 1 to 3 dyne/cm².

LAT1 was 9.34-fold higher at 1 dyne/cm² and 2.95-fold higher at 3 dyne/cm² related to the static control and PPIA. Therefore, LAT1 was significantly downregulated from 1 to 3 dyne/cm².

LRP1 presented a 0.26-fold decrease at 1 dyne/cm² and a 0.41-fold decrease at 3 dyne/cm² in comparison to the static control and PPIA. Hence, LRP1 did not show a significant trend in its mRNA expression among the shear stress values.

LRP8 was equally downregulated at 1 and 3 dyne/cm² in comparison to the static control and PPIA with x-fold values of 0.70 and 0.71, respectively. As a result, there was no significant difference in LRP8-expression among the shear stress values.

MCT1 was 2.03-fold higher at 1 dyne/cm² and did not show a significant difference at 3 dyne/cm² in comparison to the static control and PPIA. Consequently, there was a downregulation in the mRNA expression of MCT1 from 1 to 3 dyne/cm².

MCT8 was 1.30-fold increased at 1 dyne/cm² and 2.89-fold increased at 3 dyne/cm² related to the static control and PPIA. Therefore, MCT8 was upregulated in its mRNA expression from 1 to 3 dyne/cm².

TfR was equally downregulated at 1 and 3 dyne/cm² in comparison to the static control and PPIA with x-fold values of 0.67 and 0.77, respectively. Hence, TfR did not display a significant change in its mRNA expression with increasing shear stress.

VEGFA was equally upregulated at 1 and 3 dyne/cm² related to the static control and PPIA with x-fold values of 2.45 and 5.31, respectively. Consequently, VEGFA was upregulated in its mRNA expression from 1 to 3 dyne/cm².

WWC2 was 0.58-fold lower at 1 dyne/cm² and 0.38-fold lower at 3 dyne/cm² in comparison to the static control and PPIA. However, there was no significant trend in the mRNA expression of WWC2 among the shear stress values.

Figure 64: Bar graph 7 with trending mRNA expression level changes after 24 hours
(Red) 1 dyne/cm². (Gray) 3 dyne/cm². n=2: CK8; CK18, CK19, AQP3, AQP5, AQP7, AQP11, MUC1A, MUC1B, MUC18 – 1 and 3 dyne/cm².

CK8 was 0.25-fold lower at 1 dyne/cm² and 0.50-fold lower at 3 dyne/cm² in comparison to the static control and PPIA. Hence, there was no significant change in the mRNA expression of CK8 among the shear stress values.

CK18 was 0.42-fold lower for both, 1 and 3 dyne/cm² in comparison to the static control and PPIA. Therefore, CK18 did not show a significant trend from 1 to 3 dyne/cm².

CK19 was 0.14-fold lower at 1 dyne/cm² and 0.37-fold lower at 3 dyne/cm² related to the static control and PPIA. Consequently, there was no significant change in the mRNA expression of CK19 from 1 to 3 dyne/cm².

AQP3 presented a 0.71-fold decrease and no significant variation at 3 dyne/cm² in comparison to the static control and PPIA. As a result, there was a slight upregulation in the mRNA expression of AQP3 from 1 to 3 dyne/cm².

AQP5 was 0.017-fold lower at 1 dyne/cm² and 0.20-fold lower at 3 dyne/cm² compared to the static control and PPIA. Hence, AQP5 was upregulated from 1 to 3 dyne/cm².

AQP7 showed a 0.69-fold decrease at 1 dyne/cm² and a 0.51-fold decrease at 3 dyne/cm² in relation to the static control and PPIA. Therefore, AQP7 did not show a significant trend in its mRNA expression among the shear stress values.

MUC1A was 0.71-fold lower at 1 dyne/cm² and 0.90-fold lower at 3 dyne/cm² related to the static control and PPIA. However, there was no significant difference in the mRNA expression of MUC1A among the shear stress values.

MUC1B was 0.62-fold decreased at 1 dyne/cm² and did not show a significant variation at 3 dyne/cm² compared to the static control and PPIA. Hence, there was a slight upregulation in the mRNA expression of MUC1B from 1 to 3 dyne/cm².

MUC18 showed a 0.64-fold downregulation at 1 dyne/cm² and a 1.13-fold upregulation at 3 dyne/cm² in comparison to the static control and PPIA. Thus, MUC18 was slightly upregulated from 1 to 3 dyne/cm².
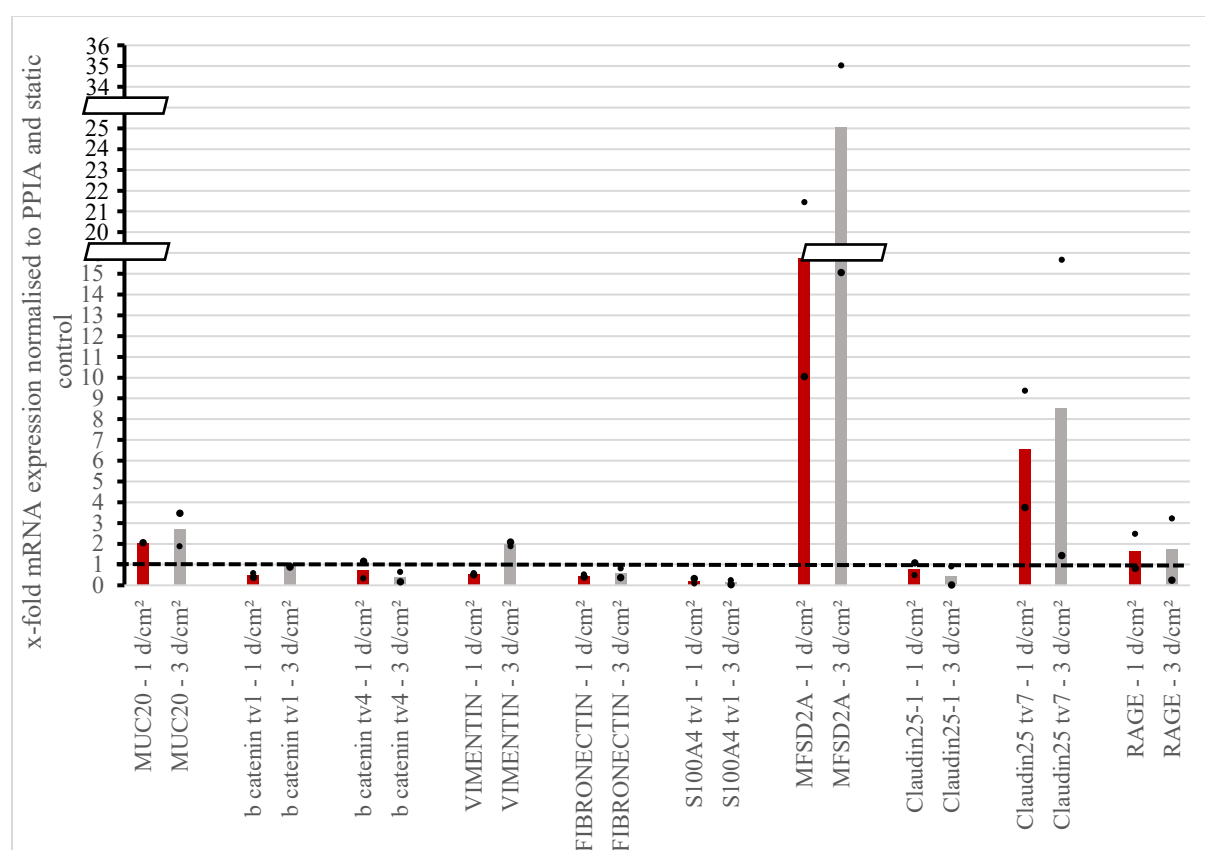
Figure 65: Bar graph 8 with trending mRNA expression level changes after 24 hours
(Red) 1 dyne/cm². (Gray) 3 dyne/cm². n=2: MUC20, b-catenin-tv1, b-catenin-tv2, VIMENTIN, FIBRONECTIN, S100A4 tv1, MFSD2A, Claudin25-1, Claudin25 tv7, RAGE – 1 and 3 dyne/cm².

MUC20 was 2.05-fold higher at 1 dyne/cm² and 2.68-fold higher at 3 dyne/cm² compared to the static control and PPIA. Hence, there was an upregulation in the mRNA expression of MUC20 from 1 to 3 dyne/cm².

B catenin tv1 presented a 0.48-fold decrease at 1 dyne/cm² and no significant difference at 3 dyne/cm² in comparison to the static control and PPIA. Therefore, b catenin tv1 was slightly upregulated in its mRNA expression from 1 to 3 dyne/cm².

B catenin tv4 was 0.74-fold lower at 1 dyne/cm² and 0.41-fold lower at 3 dyne/cm² related to the static control and PPIA. As a result, there was a slight downregulation in the mRNA expression of b catenin tv4 from 1 to 3 dyne/cm².

VIMENTIN was 0.55-fold decreased at 1 dyne/cm² and 1.98-fold increased at 3 dyne/cm² in relation to the static control and PPIA. Hence, VIMENTIN was upregulated from 1 to 3 dyne/cm².

FIBRONECTIN was 0.46-fold lower at 1 dyne/cm² and 0.59-fold lower at 3 dyne/cm² in comparison to the static control and PPIA. Consequently, there was no significant difference in the mRNA expression of FIBRONECTIN from 1 to 3 dyne/cm².

S100A4 tv1 showed a 0.21-fold decrease at 1 dyne/cm² and a 0.14-fold decrease at 3 dyne/cm² compared to the static control and PPIA. Therefore, S100A4 tv1 also did not show a significant variation in its mRNA expression with increasing shear stress.

MFSD2A was 15.75-fold higher at 1 dyne/cm² and 25.05-fold higher at 3 dyne/cm² compared to the static control and PPIA. As a result, there was a significant upregulation in the MFSD2A-expression from 1 to 3 dyne/cm².

Claudin25-1 was 0.79-fold downregulated at 1 dyne/cm² and 0.46-fold downregulated at 3 dyne/cm² compared to the static control and PPIA. Hence, Claudin25-1 presented a slight downregulation in its mRNA expression from 1 to 3 dyne/cm².

Claudin25 tv7 was upregulated at 1 and 3 dyne/cm² related to the static control and PPIA with x-fold values of 6.56 and 8.55, respectively. Consequently, Claudin25 tv7 was upregulated from 1 to 3 dyne/cm².

RAGE was 1.65-fold higher at 1 dyne/cm² and 1.73-fold higher at 3 dyne/cm² in relation to the static control and PPIA. Thus, RAGE did not show a significant difference in its mRNA expression between 1 and 3 dyne/cm².

4.5.3 mRNA expression level changes at 0.1 dyne/cm² at different points in time

The final shear stress of 0.1 dyne/cm² was firstly measured in a 3-day-setup, 6 hours after final shear stress exposure on day 2. Secondly, its effects were detected in a 6-day-setup after a 96-hour-exposure (Figure 66). Thus, up- and downregulations were examined with time dependency. The corresponding bar-charts are displayed in Figure 67 to Figure 73.
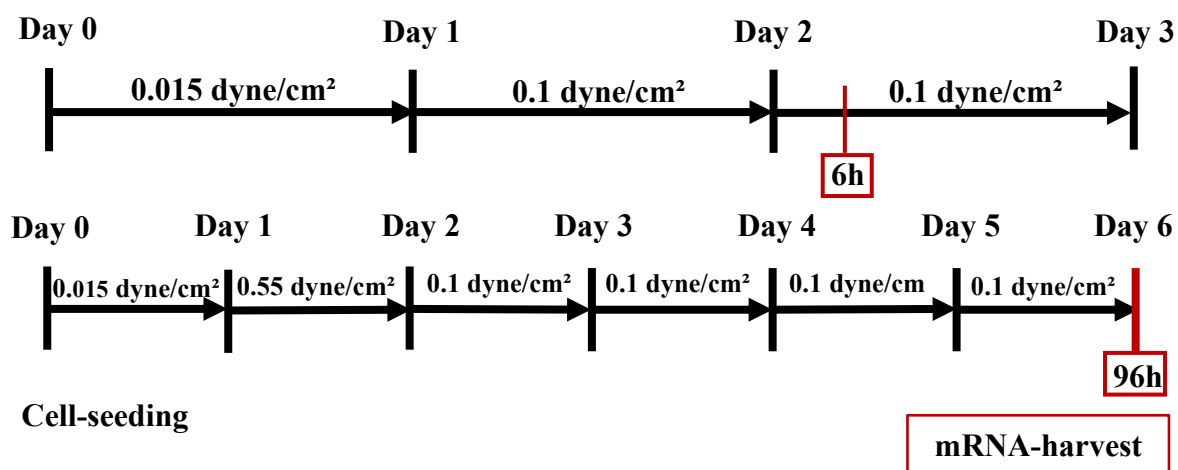
Figure 66: Experimental setup of mRNA-harvest for 0.1 dyne/cm² after 6 and 96 hours
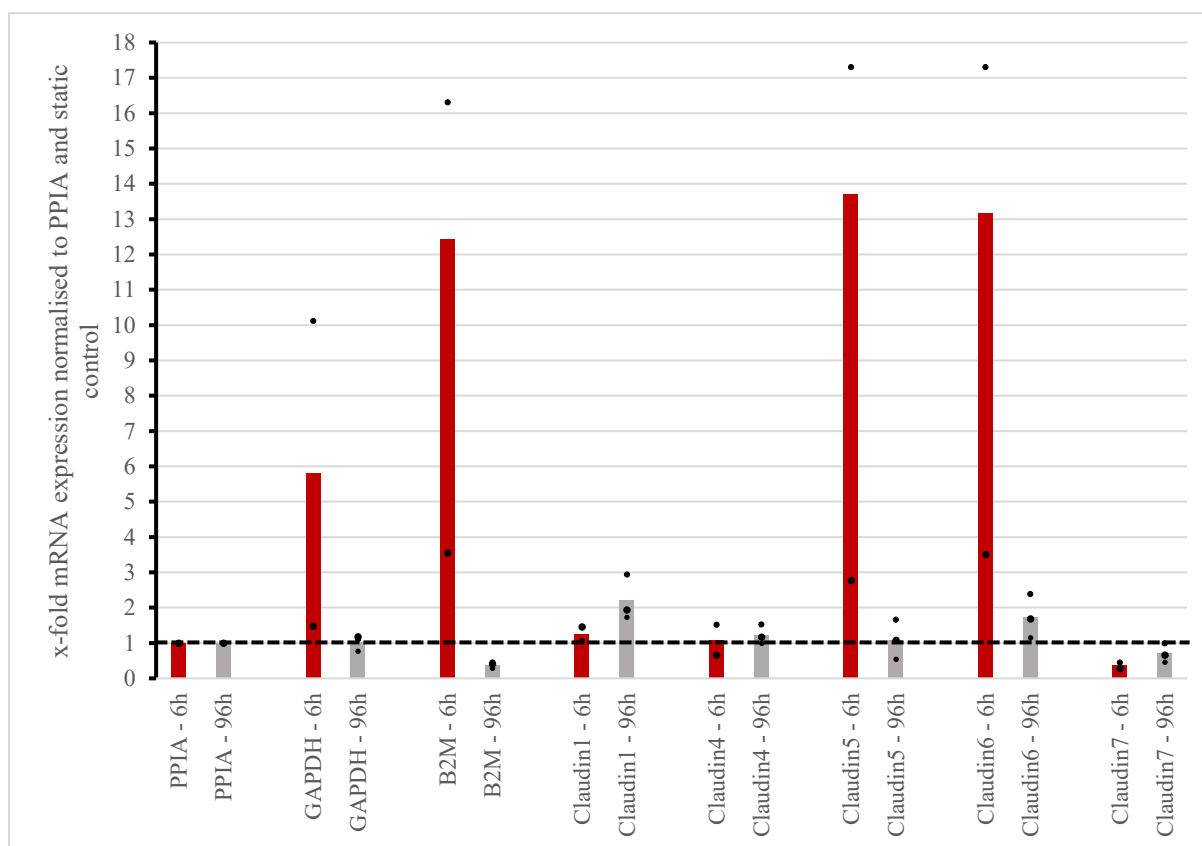
Figure 67: Bar graph 1 with trending mRNA expression level changes for 0.1 dyne/cm² after 96 hours
(Red) 6 hours. (Gray) 96 hours. n=3: PPIA, GAPDH, B2M, Claudin1, Claudin4, Claudin5, Claudin6, Claudin7 – 96 hours; n=2: PPIA, GAPDH, B2M, Claudin1, Claudin4, Claudin5, Claudin6, Claudin7 - 6 hours.

GAPDH was 5.8-fold higher after a 6-hour-exposure and did not show a significant difference after a 96-hour-exposure to 0.1 dyne/cm² in comparison to the static control and PPIA. Hence, GAPDH was significantly downregulated in its mRNA expression from 6 to 96 hours of exposure to the final shear stress.

B2M presented a 12.43-fold upregulation after a 6-hour-exposure and a 0.38-fold downregulation after a 96-hour-exposure to 0.1 dyne/cm² in comparison to the static control and PPIA. Therefore, B2M was significantly downregulated from 6 to 96 hours of exposure to the final shear stress.

Claudin1 was 1.26-fold higher after a 6-hour-exposure and 2.21-fold higher after a 96-hour-exposure to 0.1 dyne/cm² in comparison to the static control and PPIA. As a result, Claudin1 was upregulated with an increased duration of exposure to the final shear stress.

Claudin4 did not show a significant difference after a 6-hour-exposure and a 1.23-fold upregulation after a 96-hour-exposure to 0.1 dyne/cm² in comparison to the static control and PPIA. Consequently, there was no significant difference in the mRNA expression of Claudin4 from 6 to 96 hours of exposure to the final shear stress.

Claudin5 was 13.7-fold higher after a 6-hour-exposure and did not display a significant change after a 96-hour-exposure to 0.1 dyne/cm² in comparison to the static control and PPIA. Therefore, Claudin5 was significantly downregulated from a 6- to a 96-hour-exposure to the final shear stress.

Claudin6 was 13.16-fold upregulated after a 6-hour-exposure and 1.74-fold upregulated after a 96-hour-exposure to 0.1 dyne/cm² in comparison to the static control and PPIA. Thus, Claudin6 was significantly downregulated from a 6- to a 96-hour-exposure to the final shear stress.

Claudin7 was 0.37-fold downregulated after a 6-hour-exposure and 0.71-fold downregulated after a 96-hour-exposure to 0.1 dyne/cm² in comparison to the static control and PPIA. Therefore, Claudin7 was slightly upregulated with an increased final shear stress duration.
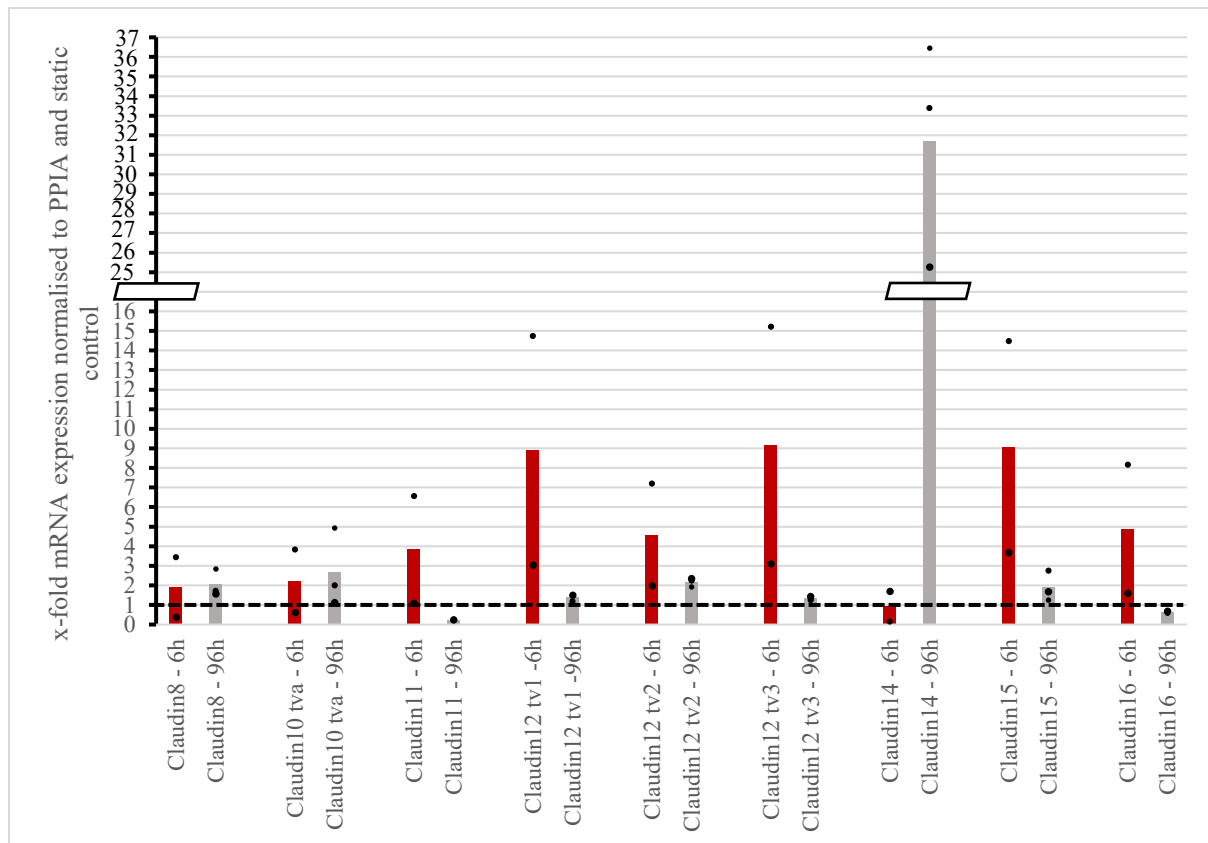
Figure 68: Bar graph 2 with trending mRNA expression level changes for 0.1 dyne/cm² after 96 hours (Red) 6 hours. (Gray) 96 hours. n=3: Claudin8, Claudin10 tva, Claudin11, Claudin12 tv1, Claudin12 tv2, Claudin12 tv3, Claudin14, Claudin15, Claudin16 – 96 hours; n=2: Claudin8, Claudin10 tva, Claudin11, Claudin12 tv1, Claudin12 tv2, Claudin12 tv3, Claudin14, Claudin15, Claudin16 – 6 hours.

Claudin8 was 1.92-fold upregulated after a 6-hour-exposure and 2.05-fold upregulated after a 96-hour-exposure to 0.1 dyne/cm² in comparison to the static control and PPIA. Therefore, Claudin8 did not show a significant difference in its mRNA expression from 6 to 96 hours of exposure to the final shear stress.

Claudin10 tva was 2.23-fold higher after 6 hours of final shear stress exposure and 2.70-fold higher after a 96-hour-exposure to 0.1 dyne/cm² in comparison to the static control and PPIA. Consequently, Claudin10 tva was slightly upregulated with an increased duration of exposure to the final shear stress.

Claudin11 was 3.84-fold higher after a 6-hour-exposure and 0.25-fold lower after a 96-hour-exposure to 0.1 dyne/cm² in comparison to the static control and PPIA. As a result, Claudin11 was significantly downregulated from 6 to 96 hours after final shear stress induction.

Claudin12 tv1 was 8.89-fold upregulated after a 6-hour-exposure and 1.41-fold upregulated after a 96-hour-exposure to 0.1 dyne/cm² in comparison to the static control and PPIA. Therefore, Claudin12 tv1 displayed a downregulation in its mRNA expression from 6 to 96 hours of exposure to the final shear stress.

Claudin12 tv3 showed a 9.17-fold upregulation after a 6-hour-exposure and a 1.33-fold upregulation after a 96-hour-exposure to 0.1 dyne/cm² in comparison to the static control and PPIA. As a result, Claudin12 tv3 presented a significant downregulation in its mRNA expression from 6 to 96 hours after final shear stress induction.

Claudin14 did not show a significant difference after a 6-hour-exposure, however, was 31.71-fold upregulated after a 96-hour-exposure to 0.1 dyne/cm² in comparison to the static control and PPIA. Therefore, Claudin14 was significantly upregulated with an increased duration of exposure to the final shear stress.

Claudin15 was 9.09-fold higher after a 6-hour-exposure and 1.91-fold higher after a 96-hour-exposure to 0.1 dyne/cm² in comparison to the static control and PPIA. Hence, there was a significant downregulation in Claudin15-expression with an increased duration of exposure to 0.1 dyne/cm².

Claudin16 was 4.89-fold upregulated 6 hours after final shear stress induction and 0.63-fold lower after a 96-hour-exposure to 0.1 dyne/cm² in comparison to the static control and PPIA. Therefore, a significant downregulation was noted for Claudin16 from 6 to 96 hours of exposure to 0.1 dyne/cm².
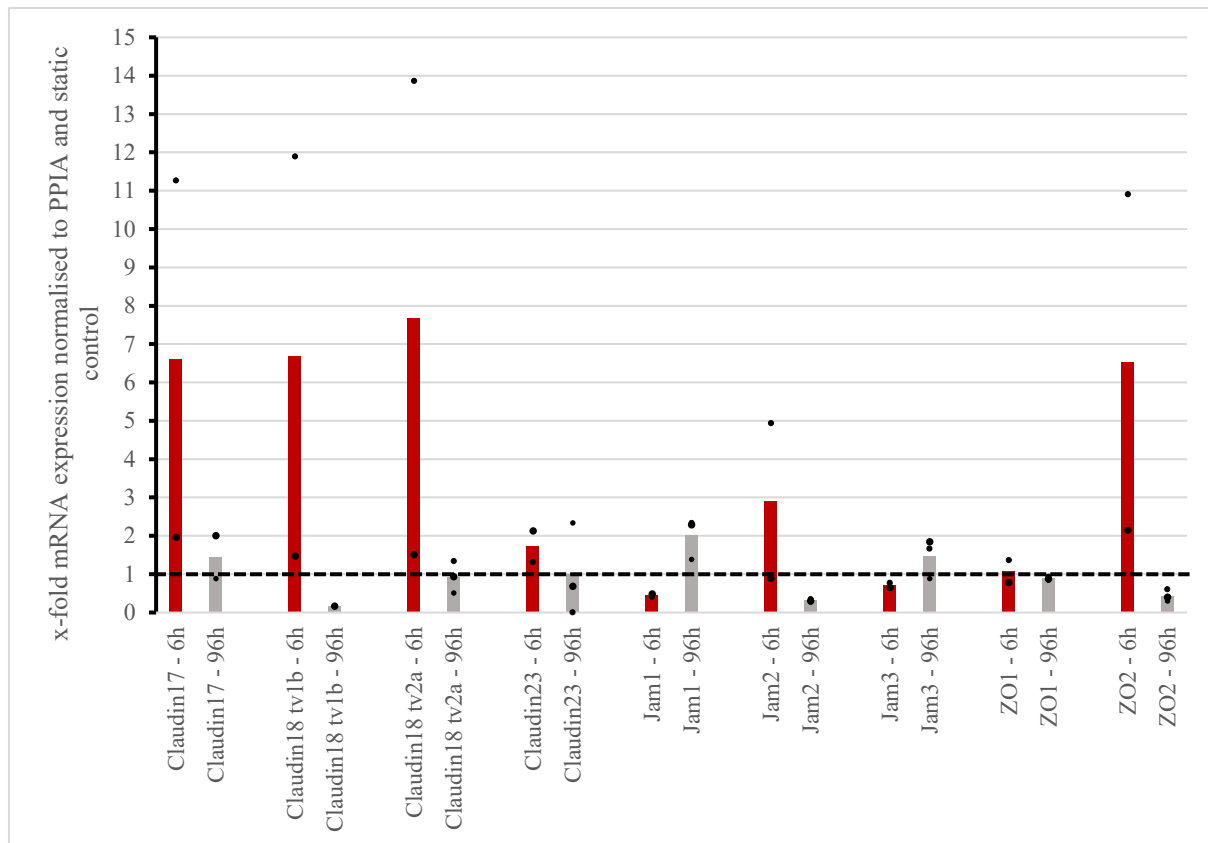
Figure 69: Bar graph 3 with trending mRNA expression level changes for 0.1 dyne/cm² after 96 hours
(Red) 6 hours. (Gray) 96 hours. n=3: Claudin18 tv1b, Claudin18 tv2a, Claudin23, Jam1, Jam2, Jam3, ZO1, ZO2
– 96 hours; n=2: Claudin17, Claudin18 tv1b, Claudin18 tv2a, Claudin23, Jam1, Jam2, Jam3, ZO1, ZO2 – 6 hours;
Claudin17 – 96 hours.

Claudin 17 was 6.62-fold upregulated after a 6-hour-exposure and 1.45-fold higher after a 96-hour-exposure to 0.1 dyne/cm² in comparison to the static control and PPIA. Consequently, there was a downregulation in Claudin17-expression with an increased duration of exposure to 0.1 dyne/cm².

Claudin18 tv1b was 6.68-fold higher after a 6-hour-exposure and 0.17-fold lower after a 96-hour-exposure to 0.1 dyne/cm² in comparison to the static control and PPIA. Hence, Claudin18 tv1b showed a significant downregulation in its mRNA expression from 6 to 96 hours of exposure to the final shear stress.

Claudin18 tv2a was 7.69-fold upregulated after 6 hours of exposure to the final shear stress and did not indicate a significant difference after a 96-hour-exposure to 0.1 dyne/cm² in comparison to the static control and PPIA. Therefore, Claudin18 tv2a was significantly downregulated from 6 to 96 hours of exposure to 0.1 dyne/cm².

Claudin23 was 1.72-fold higher after a 6-hour-exposure and did not present a significant variation after a 96-hour-exposure to 0.1 dyne/cm² in comparison to the static control and PPIA. As a result, Claudin23 was downregulated from 6 to 96 hours of exposure to the final shear stress.

120

Jam1 was 0.45-fold lower after a 6-hour-exposure and 2.01-fold higher after a 96-hour-exposure to 0.1 dyne/cm² in comparison to the static control and PPIA. Consequently, Jam1 showed an upregulation in its mRNA expression from 6 to 96 hours of exposure to the final shear stress.

Jam2 displayed a 2.92-fold upregulation 6 hours after final shear stress induction and a 0.32-fold decrease after a 96-hour-exposure to 0.1 dyne/cm² in comparison to the static control and PPIA. Hence, Jam2 showed a downregulation in its mRNA expression with an increased duration of exposure to 0.1 dyne/cm².

Jam3 was 0.72-fold downregulated after a 6-hour-exposure and 1.47-fold upregulated after a 96-hour-exposure to 0.1 dyne/cm² in comparison to the static control and PPIA. Hence, Jam3 was upregulated in its mRNA expression from 6 to 96 hours of exposure to the final shear stress.

ZO1 did not reveal a significant change in its mRNA expression 6 hours after final shear stress induction, however, presented a 0.89-fold decrease after a 96-hour-exposure to 0.1 dyne/cm² in comparison to the static control and PPIA. Consequently, ZO1 was slightly downregulated from 6 to 96 hours of exposure to 0.1 dyne/cm².

ZO2 was 6.53-fold higher 6 hours after final shear stress induction and 0.44-fold lower after a 96-hour-exposure to 0.1 dyne/cm² in comparison to the static control and PPIA. Therefore, ZO2 was significantly downregulated in its mRNA expression with an increased duration of exposure to the final shear stress.
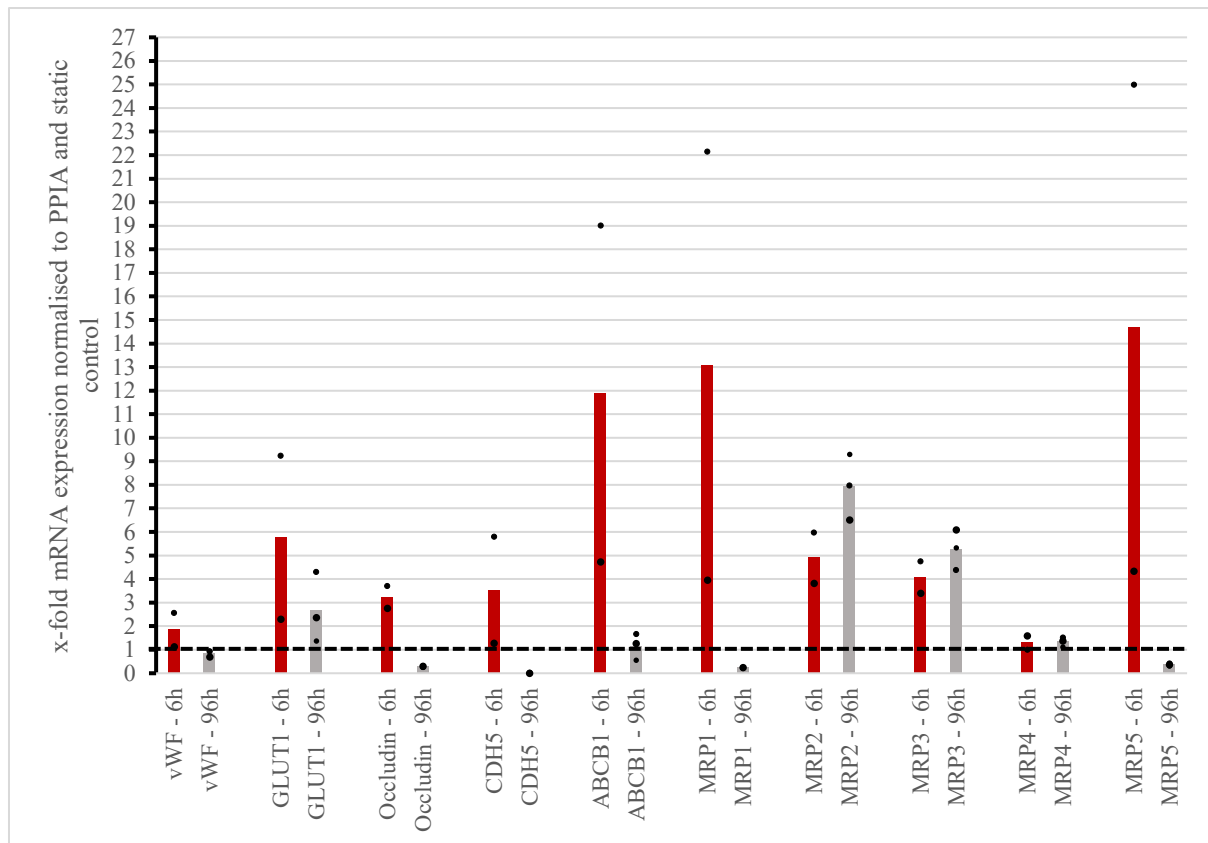
Figure 70: Bar graph 4 with trending mRNA expression level changes for 0.1 dyne/cm² after 96 hours (Red) 6 hours. (Gray) 96 hours. n=3: VWF, GLUT1, Occludin, CDH5, ABCB1m MRP1, MRP2, MRP3, MRP4, MRP5 – 96 hours; n=2: vWF, GLUT1, Occludin, CDH5, ABCB1, MRP1, MRP2, MRP3, MRP4, MRP5 – 6 hours.

vWF was 1.85-fold increased after a 6-hour-exposure and 0.86-fold decreased after a 96-hour-exposure to 0.1 dyne/cm² in comparison to the static control and PPIA. Hence, vWF was decreased in its mRNA expression with an increased duration of exposure to the final shear stress.

GLUT1 was 5.77-fold higher 6 hours after final shear stress induction and 2.69-fold higher after a 96-hour-exposure to 0.1 dyne/cm² in comparison to the static control and PPIA. Therefore, GLUT1 was downregulated from 6 to 96 hours of exposure to 0.1 dyne/cm².

Occludin displayed a 3.24-fold upregulation 6 hours after final shear stress exposure and a 0.31-fold downregulation after a 96-hour-exposure to 0.1 dyne/cm² in comparison to the static control and PPIA. Therefore, Occludin was significantly downregulated with an increased duration of exposure to 0.1 dyne/cm².

CDH5 was 3.54-fold higher after 6 hours of final shear stress exposure and 0.013-fold lower after a 96-hour-exposure to 0.1 dyne/cm² in comparison to the static control and PPIA. Consequently, CDH5 was significantly downregulated from 6 to 96 hours of exposure to 0.1 dyne/cm².

ABCB1 was 11.88-fold upregulated after a 6-hour-exposure and 1.17-fold upregulated after a 96-hour-exposure to 0.1 dyne/cm² in comparison to the static control and PPIA. As a result, ABCB1 was downregulated with an increased duration of exposure to 0.1 dyne/cm².

MRP1 was 13.06-fold increased after 6 hours and 0.24-fold lower after a 96-hour-exposure to 0.1 dyne/cm² in comparison to the static control and PPIA. Therefore, MRP1 was significantly downregulated with an increased period of exposure to the final shear stress.

MRP2 presented a 4.91-fold increase after a 6-hour-exposure and a 7.93-fold increase after a 96-hour-exposure to 0.1 dyne/cm² in comparison to the static control and PPIA. As a result, there was an upregulation in the mRNA expression of MRP2 with an increased duration of exposure to the final shear stress.

MRP3 was 4.08-fold higher after a 6-hour-exposure and 5.28-fold higher after a 96-hour-exposure to 0.1 dyne/cm² in comparison to the static control and PPIA. Hence, MRP3 was slightly upregulated with an increased period of exposure to the final shear stress.

MRP4 was 1.30-fold higher after a 6-hour-exposure and 1.34-fold higher after a 96-hour-exposure to 0.1 dyne/cm² in comparison to the static control and PPIA. As a result, MRP4 did not show a significant variation in its mRNA expression with an increased duration of exposure to 0.1 dyne/cm².

MRP5 presented a 14.67-fold upregulation after 6 hours and a 0.37-fold downregulation after a 96-hour-exposure to 0.1 dyne/cm² in comparison to the static control and PPIA. Therefore, MRP5 was significantly downregulated from 6 to 96 hours of exposure to the final shear stress.
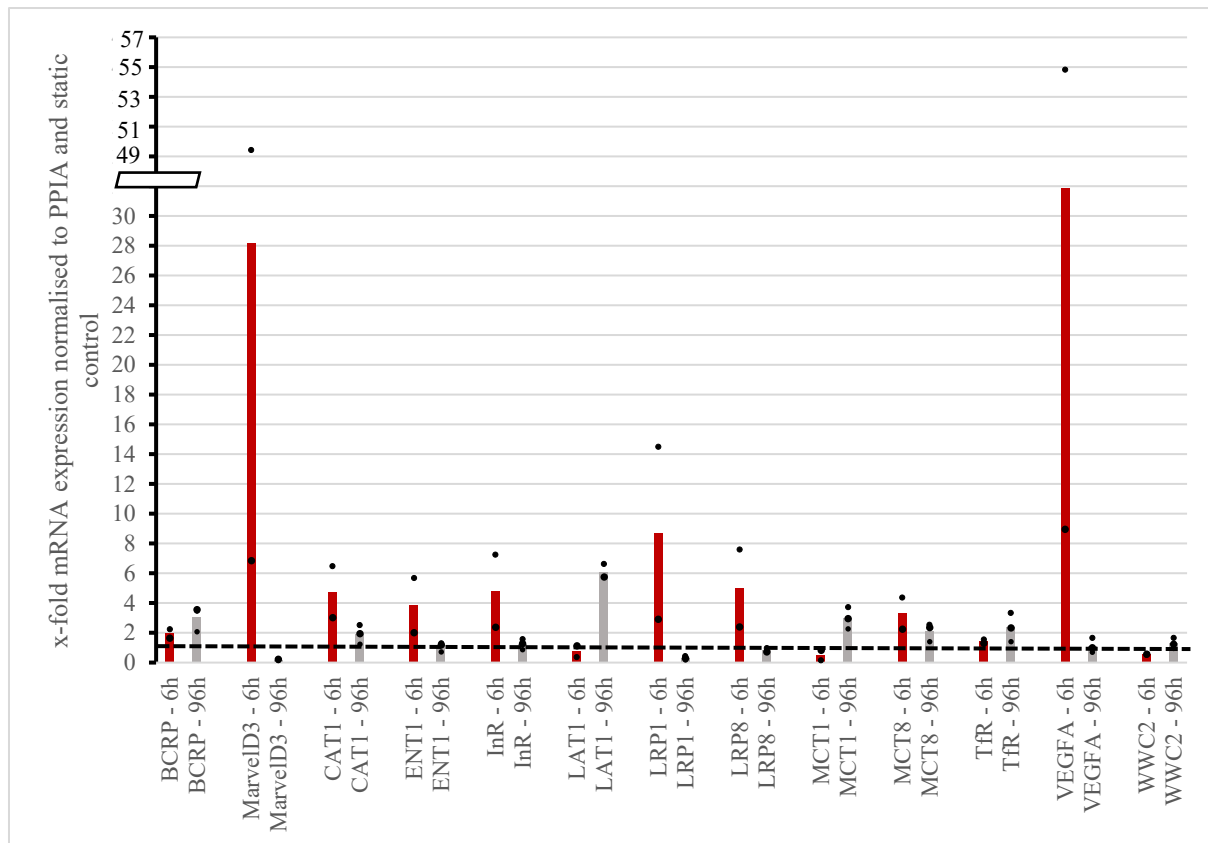
Figure 71: Bar graph 5 with trending mRNA expression level changes for 0.1 dyne/cm² after 96 hours
(Red) 6 hours. (Gray) 96 hours. n=3: BCRP, MARVELD3, CAT1, ENT1, InR, LAT1, LRP1, LRP8, MCT1,
MCT8, TfR, VEGFA, WWC2 – 96 hours; BCRP, MARVELD3, CAT1, ENT1, InR, LAT1, LRP1, LRP8, MCT1,
MCT8, TfR, VEGFA, WWC2 – 6 hours.

BCRP was 1.95-fold higher after a 6-hour-exposure and 3.06-fold higher after a 96-hour-exposure to 0.1 dyne/cm² compared to the static control and PPIA. Consequently, BCRP was upregulated from 6 to 96 hours of exposure to the final shear stress.

MarvelD3 was 28.15-fold increased and 0.20-fold decreased in relation to the static control and PPIA after a 6- and a 96-hour-exposure to 0.1 dyne/cm², respectively. Therefore, MarvelD3 was significantly decreased in its mRNA expression with an increased duration of exposure to 0.1 dyne/cm².

CAT1 showed a 4.76-fold upregulation after a 6-hour-exposure and a 1.91-fold upregulation after a 96-hour-exposure to 0.1 dyne/cm² in comparison to the static control and PPIA. Hence, CAT1 displayed a downregulation from 6 to 96 hours of exposure to 0.1 dyne/cm².

ENT1 was 3.87-fold higher after 6 hours and did not show a significant difference after a 96-hour-exposure to 0.1 dyne/cm² related to the static control and PPIA. As a result, ENT1 was decreased in its mRNA expression with an increased duration of exposure to 0.1 dyne/cm².

InR presented a 4.83-fold increase after a 6-hour-exposure and a 1.26-fold increase after a 96-hour-exposure to 0.1 dyne/cm² compared to the static control and PPIA. Thus, InR was downregulated from 6 to 96 hours of exposure to the final shear stress.

LAT1 was 0.76-fold lower 6 hours and 6.07-fold higher after a 96-hour-exposure to 0.1 dyne/cm² in comparison to the static control and PPIA. Therefore, LAT1 presented a significant upregulation from 6 to 96 hours of exposure to the final shear stress.

LRP1 was 8.72-fold increased after a 6-hour-exposure and 0.31-fold decreased after a 96-hour-exposure to 0.1 dyne/cm² in relation to the static control and PPIA. As a result, LRP1 was significantly decreased in its mRNA expression with an increased duration of exposure to 0.1 dyne/cm².

LRP8 was 5.01-fold upregulated after 6 hours and 0.84-fold downregulated after a 96-hour-exposure to 0.1 dyne/cm² compared to the static control and PPIA. Hence, LRP8 was significantly downregulated with an increased duration of exposure to 0.1 dyne/cm².

MCT1 was 0.50-fold decreased after a 6-hour-exposure and 3-fold increased after a 96-hour-exposure to 0.1 dyne/cm² in relation to the static control and PPIA. Thus, MCT1 showed an upregulation in its mRNA expression from 6 to 96 hours of exposure to the final shear stress.

MCT8 showed a 3.33-fold upregulation after 6 hours and a 2.11-fold upregulation after a 96-hour-exposure to 0.1 dyne/cm² in comparison to the static control and PPIA. Consequently, MCT8 was slightly downregulated with an increased duration of exposure to 0.1 dyne/cm².

TfR was 1.43-fold increased and 2.37-fold increased after 6 and 96 hours of exposure to 0.1 dyne/cm² in relation to the static control and PPIA, respectively. Therefore, TfR was slightly upregulated among the two points in time.

VEGFA was 31.91-fold higher after a 6-hour-exposure and 1.13-fold higher after a 96-hour-exposure to 0.1 dyne/cm² in comparison to the static control and PPIA. Thus, VEGFA was significantly downregulated in its mRNA expression from 6 to 96 hours of exposure to the final shear stress.

WWC2 was 0.56-fold lower after 6 hours and 1.30-fold higher after 96 hours of exposure to 0.1 dyne/cm² in comparison to the static control and PPIA. As a result, WWC2 was upregulated with an increased duration of exposure to 0.1 dyne/cm².
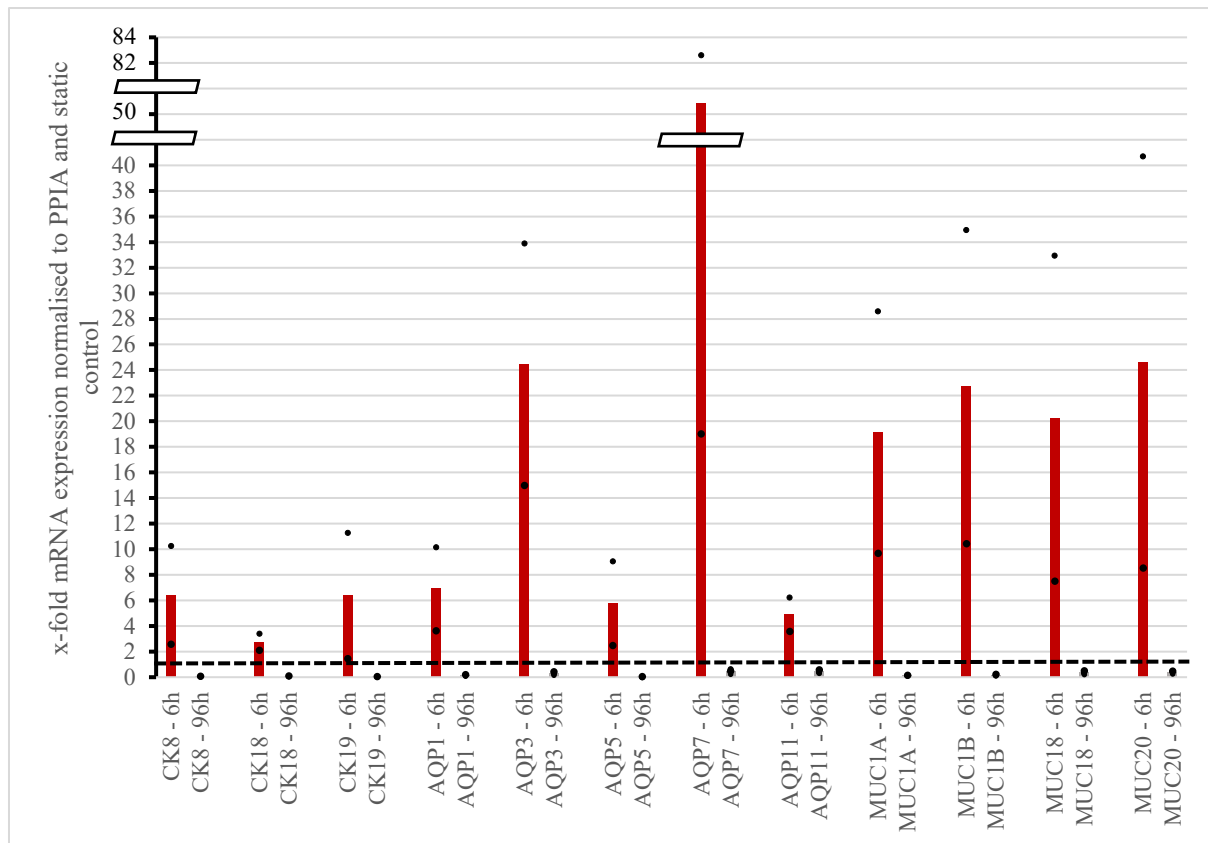
Figure 72: Bar graph 6 with trending mRNA expression level changes for 0.1 dyne/cm² after 96 hours (Red) 6 hours. (Gray) 96 hours. n=3: CK8, CK18, CK19, AQP3, AQP5, AQP7, AQP11, MUC1A, MUC1B, MUC18, MUC20 – 96 hours; n=2: CK8, CK18, CK19, AQP1, AQP3, AQP5, AQP7, AQP11, MUC1A, MUC1B, MUC18, MUC20 – 6 hours; AQP1 – 96 hours.

CK8 was 6.43-fold upregulated after a 6-hour-exposure and 0.08-fold downregulated after a 96-hour-exposure to 0.1 dyne/cm² in relation to the static control and PPIA. Hence, CK8 was significantly downregulated from 6 to 96 hours of exposure to the final shear stress.

CK18 was 2.76-fold higher and 0.091-fold lower after 6 hours and 96 hours of exposure to 0.1 dyne/cm² in comparison to the static control and PPIA, respectively. Thus, CK18 was also significantly downregulated with an increased duration of exposure to 0.1 dyne/cm².

CK19 showed a 6.39-fold upregulation after 6 hours and a 0.06-fold downregulation after 96 hours of exposure to 0.1 dyne/cm² compared to the static control and PPIA. Therefore, CK19 was significantly downregulated with a prolonged duration of exposure to 0.1 dyne/cm².

AQP1 was 6.91-fold increased and 0.15-fold decreased after the exposure to 0.1 dyne/cm² related to the static control and PPIA after 6 and 96 hours, respectively. Consequently, AQP1 was significantly decreased in its mRNA expression from a 6- to a 96-hour-exposure to final shear stress.

AQP3 was 24.45-fold higher and 0.31-fold lower after 6 hours and 96 hours of exposure to 0.1 dyne/cm² in comparison to the static control and PPIA, respectively. Thus, AQP3 was also

significantly downregulated in its mRNA expression with an increased duration of exposure to the final shear stress.

AQP5 was 5.78-fold upregulated after a 6-hour-exposure and 0.045-fold downregulated after a 96-hour-exposure to 0.1 dyne/cm² in relation to the static control and PPIA. Hence, AQP5 was also significantly downregulated from 6 to 96 hours of exposure to the final shear stress.

AQP7 showed a 50.82-fold upregulation after 6 hours and a 0.45-fold downregulation after 96 hours of exposure to 0.1 dyne/cm² compared to the static control and PPIA. Therefore, AQP7 was significantly downregulated with a prolonged duration of exposure to 0.1 dyne/cm².

AQP11 was 4.91-fold increased and 0.43-fold decreased after the exposure to 0.1 dyne/cm² related to the static control and PPIA after 6 and 96 hours, respectively. Consequently, AQP11 was significantly decreased in its mRNA expression from a 6- to a 96-hour-exposure to final shear stress.

MUC1A was 19.14-fold upregulated after a 6-hour-exposure and 0.14-fold downregulated after a 96-hour-exposure to 0.1 dyne/cm² in relation to the static control and PPIA. Hence, MUC1A was significantly downregulated from 6 to 96 hours of exposure to the final shear stress.

MUC1B showed a 22.7-fold upregulation after 6 hours and a 0.17-fold downregulation after 96 hours of exposure to 0.1 dyne/cm² compared to the static control and PPIA. Therefore, MUC1B was significantly downregulated with a prolonged duration of exposure to 0.1 dyne/cm².

MUC18 was 20.24-fold higher and 0.36-fold lower after 6 hours and 96 hours of exposure to 0.1 dyne/cm² in comparison to the static control and PPIA, respectively. Thus, MUC18 was also significantly downregulated with an increased duration of exposure to the final shear stress.

MUC20 was 24.63-fold upregulated after a 6-hour-exposure and 0.40-fold downregulated after a 96-hour-exposure to 0.1 dyne/cm² in relation to the static control and PPIA. Hence, MUC20 was also significantly downregulated from 6 to 96 hours of exposure to 0.1 dyne/cm².
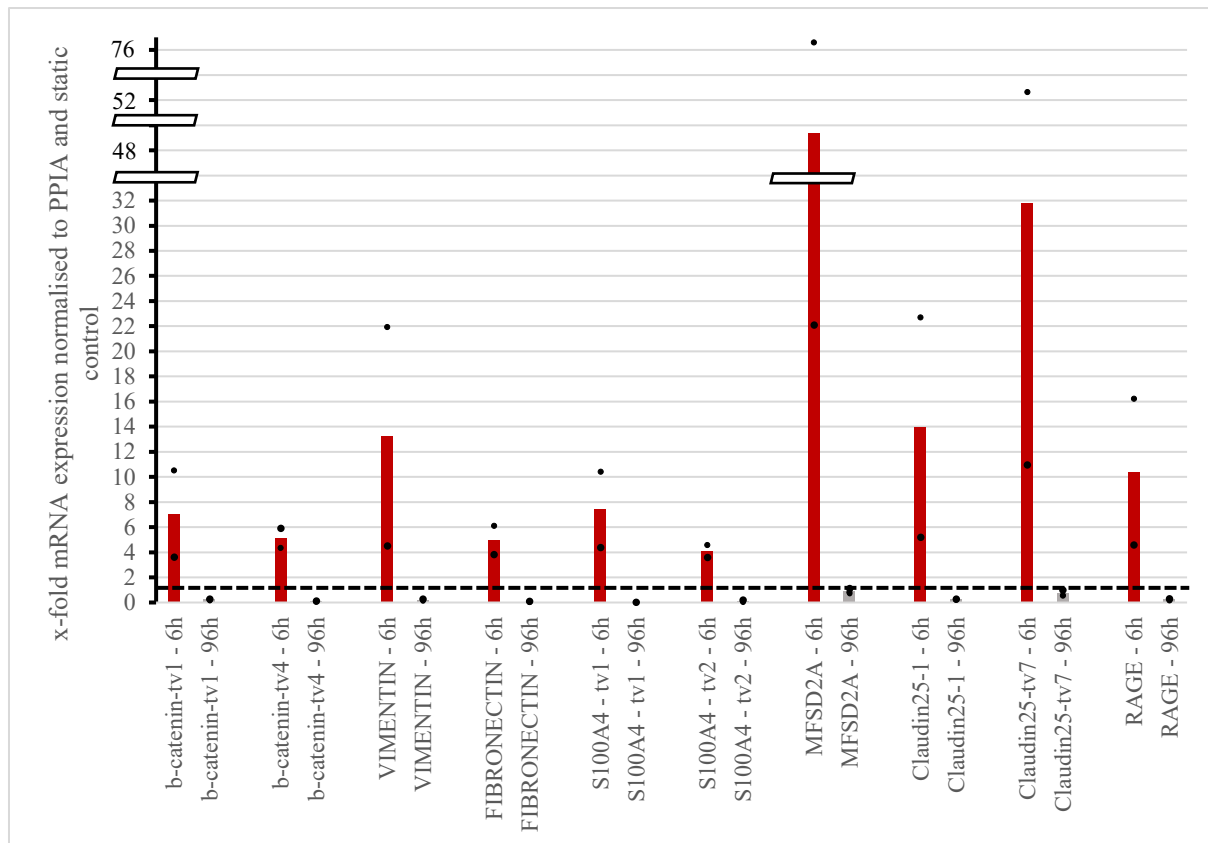
Figure 73: Bar graph 7 with trending mRNA expression level changes for 0.1 dyne/cm² after 96 hours (Red) 6 hours. (Gray) 96 hours. n=3: b catenin tv1, b-catenin tv4, VIMENTIN, FIBRONECTIN, S100A4 tv1, S100A4 tv2, MFSD2A, Claudin25 tv7, RAGE – 96 hours; n=2: b catenin tv1, b catenin tv4, VIMENTIN, FIBRONECTIN, S100A4 tv1, S100A4 tv2, MFSD2A, Claudin25 tv7, RAGE – 6 hours.

B catenin tv1 was 7.08-fold upregulated after a 6-hour-exposure and 0.25-fold downregulated after a 96-hour-exposure to 0.1 dyne/cm² in relation to the static control and PPIA. Hence, b catenin tv1 was significantly downregulated from 6 to 96 hours of exposure to the final shear stress.

B catenin tv4 was 5.15-fold higher and 0.13-fold lower after 6 hours and 96 hours of exposure to 0.1 dyne/cm² in comparison to the static control and PPIA, respectively. Thus, b catenin tv4 was significantly downregulated with an increased duration of exposure to the final shear stress.

VIMENTIN was 13.24-fold increased and 0.22-fold decreased after the exposure of 6 and 96 hours to 0.1 dyne/cm² related to the static control and PPIA, respectively. Consequently, VIMENTIN was significantly decreased in its mRNA expression from a 6- to a 96-hour-exposure to the final shear stress.

FIBRONECTIN was 4.98-fold upregulated after a 6-hour-exposure and 0.072-fold downregulated after a 96-hour-exposure to 0.1 dyne/cm² in relation to the static control and PPIA. Hence, FIBRONECTIN was significantly downregulated from 6 to 96 hours of exposure to the final shear stress.

S100A4 tv1 showed a 7.41-fold upregulation after 6 hours and a 0.026-fold downregulation after 96 hours of exposure to 0.1 dyne/cm² compared to the static control and PPIA. Therefore, S100A4 tv1 was significantly downregulated with a prolonged duration of exposure to 0.1 dyne/cm².

S100A4 tv2 was 4.1-fold increased and 0.12-fold decreased after 6 and 96 hours of exposure to 0.1 dyne/cm² related to the static control and PPIA, respectively. Consequently, S100A4 tv2 was significantly decreased in its mRNA expression from a 6- to a 96-hour-exposure to the final shear stress.

MFSD2A was 49.36-fold higher and 0.89-fold lower 6 hours and 96 hours after the exposure to 0.1 dyne/cm² in comparison to the static control and PPIA, respectively. Thus, MFSD2A was also significantly downregulated with an increased duration of exposure to the final shear stress.

Claudin25-1 was 13.95-fold upregulated after a 6-hour-exposure and 0.26-fold downregulated after a 96-hour-exposure to 0.1 dyne/cm² in relation to the static control and PPIA. Hence, Claudin25-1 was significantly downregulated from 6 to 96 hours of exposure to 0.1 dyne/cm².

Claudin25 tv7 showed a 31.82-fold upregulation after 6 hours and a 0.72-fold downregulation after 96 hours of exposure to 0.1 dyne/cm² compared to the static control and PPIA. Therefore, Claudin25 tv7 was significantly downregulated with a prolonged duration of exposure to 0.1 dyne/cm².

RAGE was 10.41-fold upregulated after a 6-hour-exposure and 0.24-fold downregulated after a 96-hour-exposure to 0.1 dyne/cm² in relation to the static control and PPIA. Hence, RAGE was significantly downregulated from 6 to 96 hours of exposure to the final shear stress.

Overall, most of the targets presented downregulations in their mRNA expressions from 6 to 96 hours of exposure to 0.1 dyne/cm².

4.5.4 mRNA expression level changes at 1 dyne/cm² at different points in time

The final shear stress of 1 dyne/cm² was measured 6, 24 and 48 hours after its exposure to the cells. The corresponding timeline is shown in Figure 74. The resulting up- and downregulations of the targets over time at 1 dyne/cm² are visualised in Figure 75 to Figure 83 .
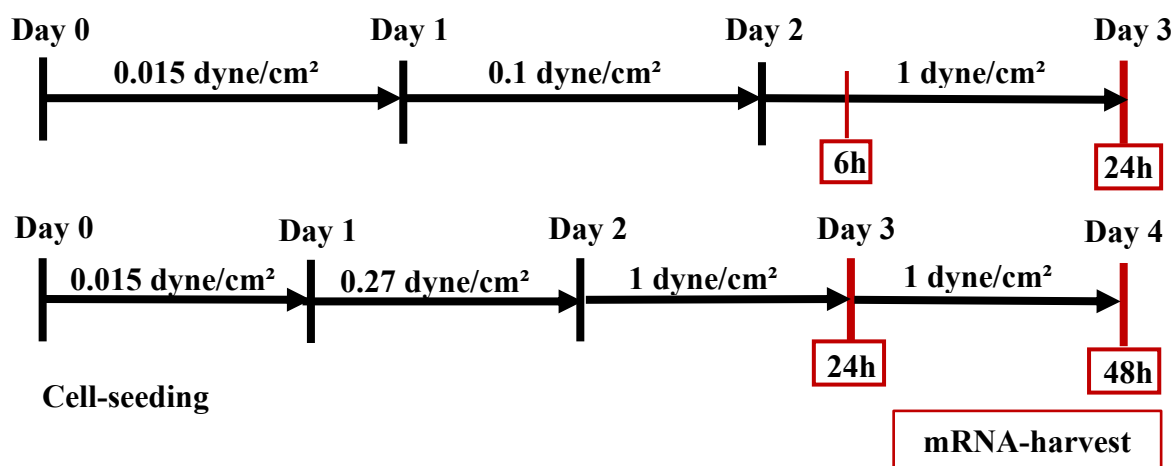
Figure 74: Experimental setup of mRNA-harvest for 1 dyne/cm² after 6, 24 and 48 hours
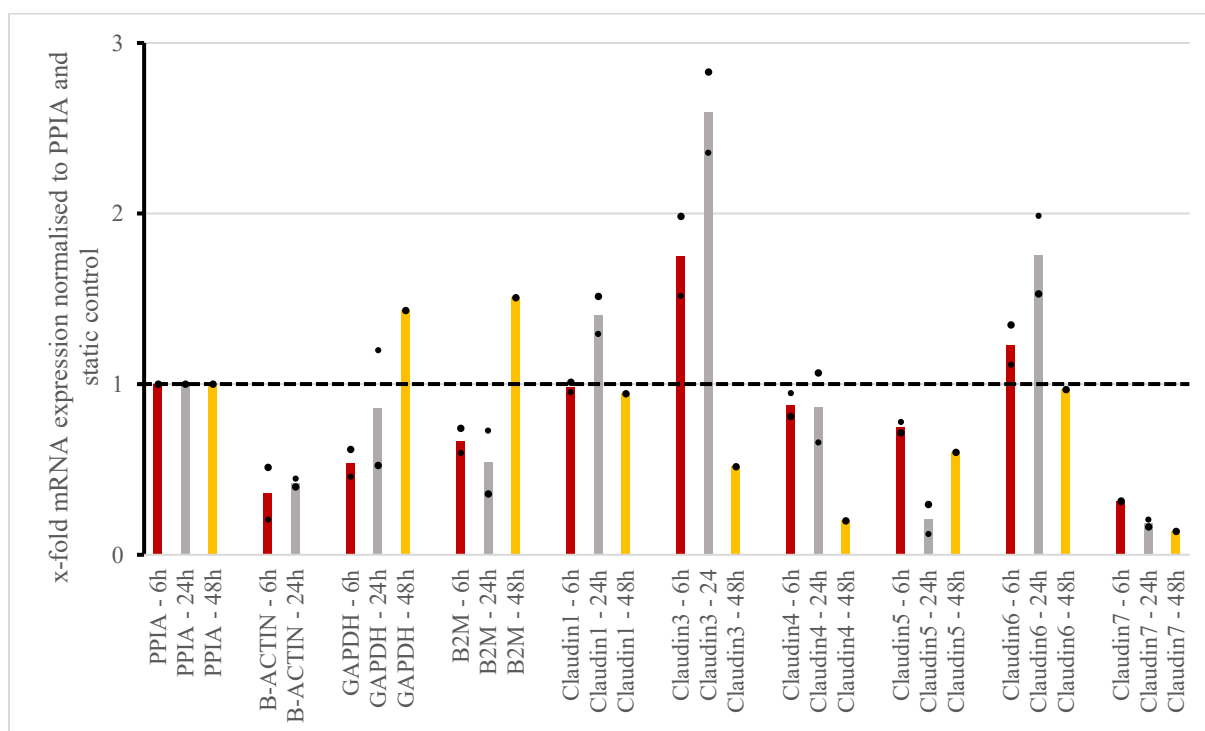
Figure 75: Bar graph 1 with trending mRNA level changes for 1 dyne/cm² after 6, 24 and 48 hours
(Red) 6 hours. (Gray) 24 hours. (Yellow) 48 hours. n=2: PPIA, B-ACTIN, GAPDH, B2M, Claudin1, Claudin3, Claudin4, Claudin5, Claudin6, Claudin7 – 6 hours; PPIA, B-ACTIN, GAPDH, B2M, Claudin1, Claudin3, Claudin4, Claudin5, Claudin6, Claudin7 – 24 hours; n=1: PPIA, GAPDH, B2M, Claudin1, Claudin3, Claudin4, Claudin5, Claudin6, Claudin7 – 48 hours.

B-ACTIN was 0.35-fold lower after 6 hours and 0.42-fold lower after 24 hours of exposure to 1 dyne/cm² in comparison to the static control and PPIA. Thus, there was no significant difference in the mRNA expression of B-ACTIN with a prolonged duration of exposure to 1 dyne/cm². The qPCR for 48 hours of the mRNA expression of B-ACTIN did not function.

GAPDH was 0.54-fold lower after 6 hours, 0.86-fold lower after 24 hours and 1.43-fold higher after 48 hours of exposure to 1 dyne/cm² related to the static control and PPIA. Hence, GAPDH showed a trend towards upregulation from 6 to 24 hours and from 24 to 48 hours of exposure to the final shear stress.

B2M presented a 0.67-fold decrease after a 6-hour-exposure, a 0.54-fold decrease after a 24-hour-exposure and a 1.51-fold increase after a 48-hour-exposure to 1 dyne/cm² compared to the static control and PPIA. As a result, there was no significant difference between a 6- and 24-hour-exposure and an increase in the mRNA expression of B2M from 24 to 48 hours of exposure to 1 dyne/cm².

Claudin1 did not show a significant variation after 6 hours, a 1.4-fold increase after 24 hours and again no significant difference after 48 hours of exposure to 1 dyne/cm² in comparison to the static control and PPIA. Consequently, there was an upregulation of Claudin1 from 6 to 24 hours and a downregulation from 24 to 48 hours of exposure to the final shear stress.

Claudin3 was 1.75-fold increased after a 6-hour-exposure, 2.59-fold increased after a 24-hour-exposure and 0.51-fold decreased after a 48-hour-exposure to 1 dyne/cm² related to the static control and PPIA. Thus, Claudin3 was upregulated from 6 to 24 hours and downregulated from 24 to 48 hours of exposure to the final shear stress.

Claudin4 was 0.87-fold lower after 6 hours, 0.86-fold lower after 24 hours and 0.2-fold lower after 48 hours of exposure to 1 dyne/cm² compared to the static control and PPIA. Hence, Claudin4 did not show a significant variation between the first two points of cell lysis, however, Claudin4 revealed a downregulation in its mRNA expression between the second and the third point of cell lysis.

Claudin5 displayed a 0.75-fold downregulation after a 6-hour-exposure, a 0.21-fold downregulation after a 24-hour-exposure and a 0.60-fold downregulation after a 48-hour-exposure to 1 dyne/cm² in relation to the static control and PPIA. Thus, Claudin5 was downregulated from 6 to 24 hours and upregulated from 24 to 48 hours of exposure to the final shear stress.

Claudin6 showed a 1.23-fold increase after 6 hours, a 1.76-fold increase after 24 hours and no significant difference after 48 hours of exposure to 1 dyne/cm² in comparison to the static

control and PPIA. Consequently, there was an upregulation of Claudin6 from 6 to 24 hours and a downregulation from 24 to 48 hours of exposure to the final shear stress.

Claudin7 was 0.31-fold lower after 6 hours, 0.19-fold lower after 24 hours and 0.14-fold lower after 48 hours of exposure to 1 dyne/cm² compared to the static control and PPIA. Hence, Claudin7 did not show a significant variation in its mRNA expression among the different points in time after the exposure to 1 dyne/cm².
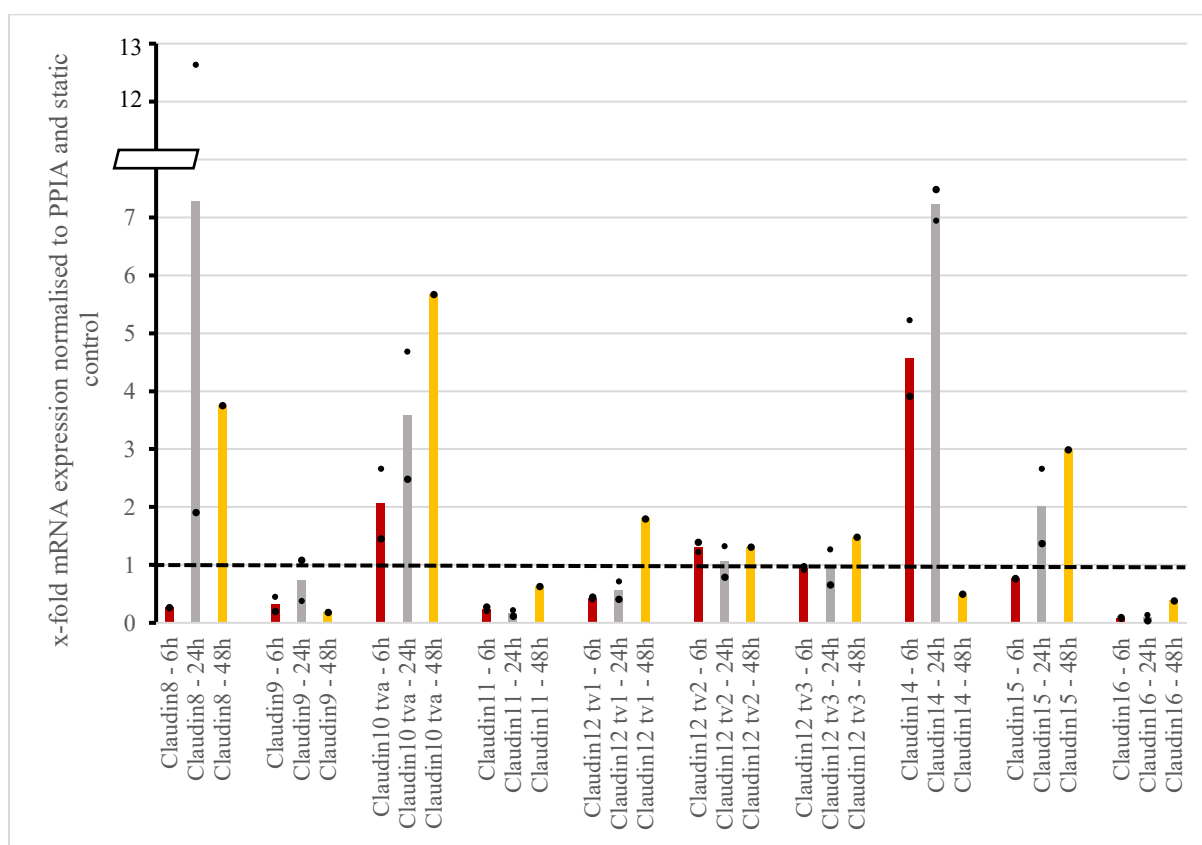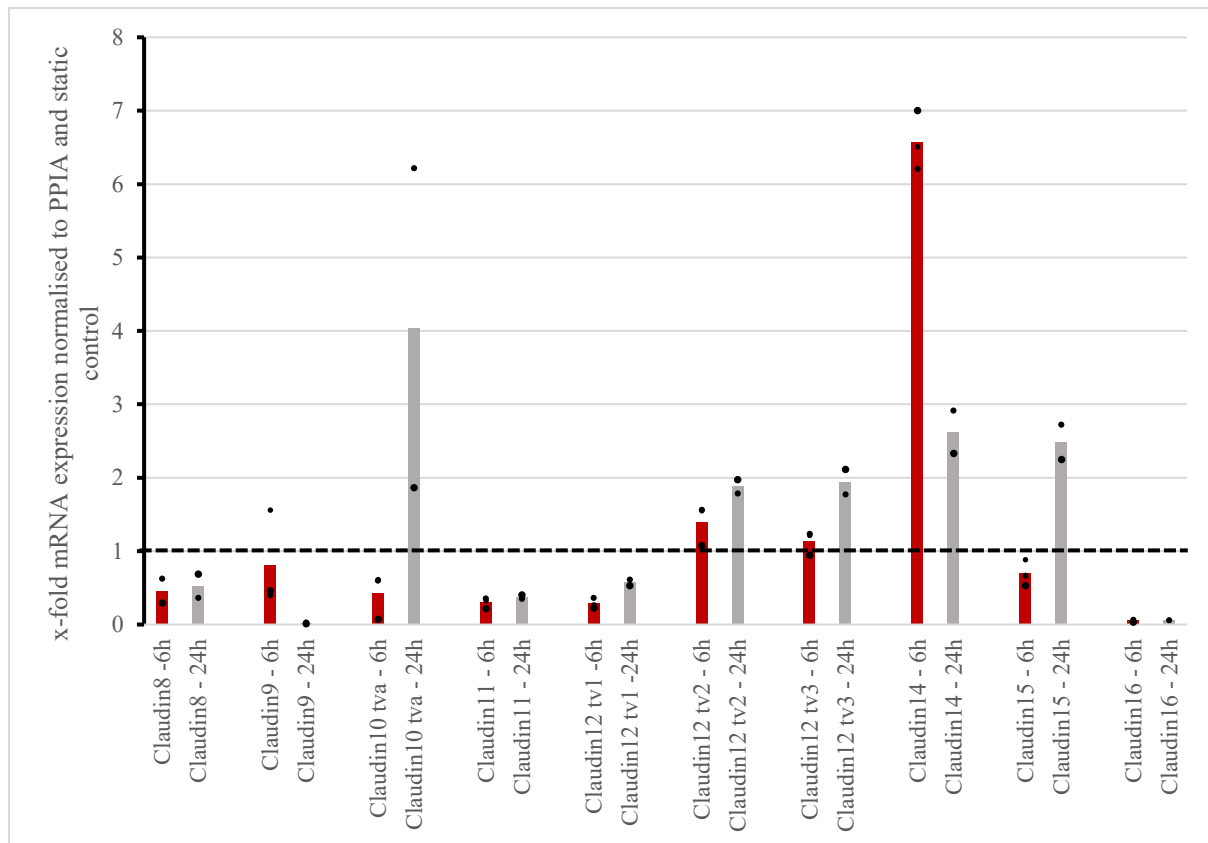

Figure 76: Bar graph 2 with trending mRNA level changes for 1 dyne/cm² after 6, 24 and 48 hours
(Red) 6 hours. (Gray) 24 hours. (Yellow) 48 hours. n=2: Claudin9, Claudin10 tva, Claudin11, Claudin12 tv1, Claudin12 tv2, Claudin12 tv3, Claudin14, Claudin15, Claudin16 – 6 hours; Claudin8, Claudin9, Claudin10 tva, Claudin11, Claudin12 tv1, Claudin12 tv2, Claudin12 tv3, Claudin14, Claudin15, Claudin16 – 24 hours; n=1: Claudin8, Claudin9, Claudin10 tva, Claudin11, Claudin12 tv1, Claudin12 tv2, Claudin12 tv3, Claudin14, Claudin15, Claudin16 – 48 hours; Claudin8 – 6 hours.

Claudin8 was 0.27-fold decreased after a 6-hour-exposure, 7.27-fold increased after a 24-hour-exposure and 3.76-fold increased after a 48-hour-exposure to 1 dyne/cm² related to the static control and PPIA. Thus, there was an upregulation of Claudin8 from 6 to 24 hours and a downregulation from 24 to 48 hours of exposure to 1 dyne/cm².

Claudin9 presented a 0.33-fold decrease after a 6-hour-exposure, a 0.73-fold decrease after a 24-hour exposure and a 0.19-fold decrease after a 48-hour-exposure to 1 dyne/cm² compared to the static control and PPIA. As a result, there was an upregulation from a 6- to a 24-hour-exposure and a downregulation of Claudin9 from 24 to 48 hours of exposure to 1 dyne/cm².

Claudin10 tva was 2.06-fold higher after 6 hours, 3.6-fold higher after 24 hours and 5.68-fold higher after 48 hours of exposure to 1 dyne/cm² related to the static control and PPIA. Hence, Claudin10 tva was upregulated from 6 to 24 hours and from 24 to 48 hours of exposure to the final shear stress.

Claudin11 was 0.24-fold lower after 6 hours, 0.17-fold lower after 24 hours and 0.63-fold lower after 48 hours of exposure to 1 dyne/cm² compared to the static control and PPIA. Hence, Claudin11 did not show a significant variation between the first two points of cell lysis, however, revealed a downregulation in its mRNA expression between the second and the third point of cell lysis.

Claudin12 tv1 displayed a 0.42-fold downregulation after a 6-hour-exposure, a 0.56-fold downregulation after a 24-hour-exposure and a 1.8-fold upregulation after a 48-hour-exposure to 1 dyne/cm² in relation to the static control and PPIA. Thus, Claudin12 tv1 did not indicate a significant variation in its mRNA expression from 6 to 24 hours, however, was upregulated from 24 to 48 hours of exposure to the final shear stress.

Claudin12 tv2 displayed a 1.31-fold upregulation after a 6-hour-exposure, no significant variation after a 24-hour-exposure and again a 1.31-fold downregulation after a 48-hour-exposure to 1 dyne/cm² in relation to the static control and PPIA. Thus, Claudin12 tv2 did not show a significant trend between the different durations of exposure to 1 dyne/cm².

Claudin12 tv3 did not show a significant change in its mRNA expression after 6 and 24 hours, however, a 1.48-fold increase after 48 hours of exposure to 1 dyne/cm² related to the static control and PPIA. Thus, there was no significant difference between 6 and 24 hours of exposure to the final shear stress, nonetheless, Claudin12 tv3 was upregulated from 24 to 48 hours of exposure to 1 dyne/cm².

Claudin14 was 4.57-fold increased after a 6-hour-exposure, 7.22-fold increased after a 24-hour-exposure and 0.5-fold decreased after a 48-hour-exposure to 1 dyne/cm² related to the static control and PPIA. Thus, there was an upregulation of Claudin14 from 6 to 24 hours and a downregulation from 24 to 48 hours of exposure to 1 dyne/cm².

Claudin15 was 0.76-fold lower after 6 hours, 2.02-fold higher after 24 hours and 3-fold higher after 48 hours of exposure to 1 dyne/cm² related to the static control and PPIA. Hence, Claudin15 showed a trend towards upregulation from 6 to 24 hours and from 24 to 48 hours of exposure to the final shear stress.

Claudin16 was 0.083-fold lower after 6 hours, 0.087-fold lower after 24 hours and 0.38-fold lower after 48 hours of exposure to 1 dyne/cm² compared to the static control and PPIA. Hence, Claudin16 did not show a significant variation between the first two points of cell lysis,

however, revealed an upregulation in its mRNA expression between the second and the third point of cell lysis.
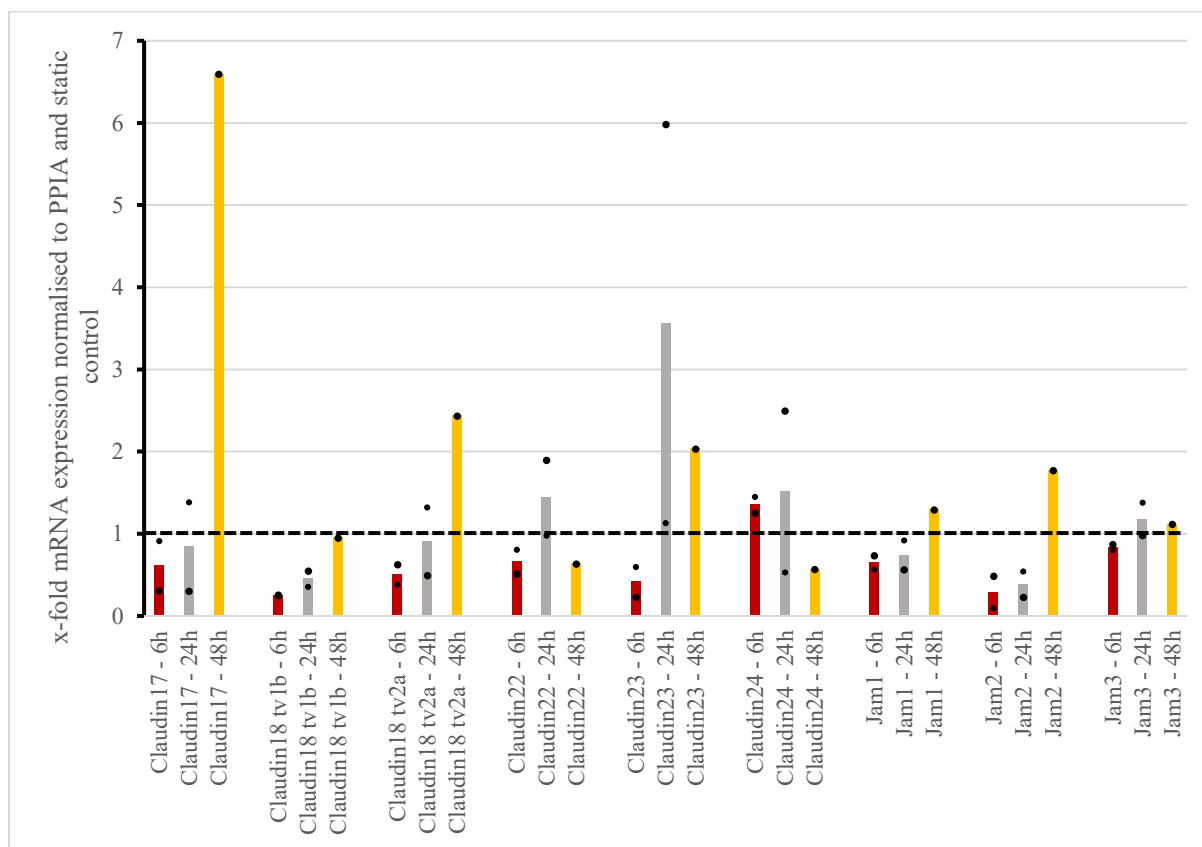
Figure 77: Bar graph 3 with trending mRNA level changes for 1 dyne/cm² after 6, 24 and 48 hours
(Red) 6 hours. (Gray) 24 hours. (Yellow) 48 hours. n=2: Claudin17, Claudin18 tv1b, Claudin18 tv2a, Claudin22, Claudin23, Claudin24, Jam1, Jam2, Jam3 – 6 and 24 hours; n=1: Claudin17, Claudin18 tv1b, Claudin18 tv2a, Claudin22, Claudin23, Claudin24, Jam1, Jam2, Jam3 – 48 hours.

Claudin17 was 0.61-fold lower after 6 hours, 0.84-fold lower after 24 hours and 6.59-fold higher after 48 hours of exposure to 1 dyne/cm² related to the static control and PPIA. Hence, Claudin17 did not show a significant trend in its mRNA expression from 6 to 24 hours, however, displayed an upregulation from 24 to 48 hours of exposure to the final shear stress.

Claudin18 tv1b revealed a 0.25-fold decrease after 6 hours, a 0.45-fold decrease after 24 hours and no significant change in its mRNA expression after 48 hours of exposure to 1 dyne/cm² in comparison to the static control and PPIA. Hence, Claudin18 tv1b did not show a significant trend from 6 to 24 hours, however, displayed an upregulation from 24 to 48 hours of exposure to 1 dyne/cm².

Claudin18 tv2a was 0.5-fold lower after 6 hours, did not indicate a significant variation after 24 hours and was 2.43-fold higher after 48 hours of exposure to 1 dyne/cm² in relation to the static control and PPIA. Hence, Claudin18 tv2a showed a trend towards upregulation in its mRNA expression from 6 to 24 hours and from 24 to 48 hours of exposure to the final shear stress.

134

Claudin22 was 0.66-fold decreased after a 6-hour-exposure, 1.43-fold increased after a 24-hour-exposure and 0.63-fold decreased after a 48-hour-exposure to 1 dyne/cm² related to the static control and PPIA. Thus, there was an upregulation in Claudin22-expression from 6 to 24 hours and a downregulation from 24 to 48 hours of exposure to 1 dyne/cm².

Claudin23 presented a 0.41-fold decrease after a 6-hour-exposure, a 3.56-fold increase after a 24-hour exposure and a 2.03-fold increase after a 48-hour-exposure to 1 dyne/cm² compared to the static control and PPIA. As a result, there was an upregulation between a 6- and 24-hour-exposure and a downregulation of Claudin23 from 24 to 48 hours of exposure to 1 dyne/cm².

Claudin24 showed a 1.35-fold upregulation in its mRNA expression after 6 hours, a 1.51-fold upregulation after 24 hours and a 0.6-fold downregulation after 48 hours of exposure to 1 dyne/cm² related to the static control and PPIA. Thus, there was no significant difference between 6 and 24 hours, nonetheless, a downregulation occurred between 24 and 48 hours of exposure to 1 dyne/cm².

Jam1 displayed a 0.65-fold downregulation after a 6-hour-exposure, a 0.74-fold downregulation after a 24-hour-exposure and a 1.29-fold upregulation after a 48-hour-exposure to 1 dyne/cm² in relation to the static control and PPIA. Thus, Jam1 did not indicate a significant variation in its mRNA expression from 6 to 24 hours, however, was upregulated from 24 to 48 hours of exposure to 1 dyne/cm².

Jam2 was 0.29-fold lower after 6 hours, 0.39-fold lower after 24 hours and 1.77-fold higher after 48 hours of exposure to 1 dyne/cm² related to the static control and PPIA. Consequently, there was no significant difference in Jam2-expression between 6 and 24 hours, nonetheless, an upregulation of Jam2 occurred between 24 and 48 hours of exposure to 1 dyne/cm².

Jam3 was 0.84-fold decreased after a 6-hour-exposure, 1.18-fold increased after a 24-hour-exposure and 1.12-fold increased after a 48-hour-exposure to 1 dyne/cm² compared to the static control and PPIA. Accordingly, there was a slight upregulation of Jam3 from 6 to 24 hours and no further significant variation from 24 to 48 hours of exposure to 1 dyne/cm².
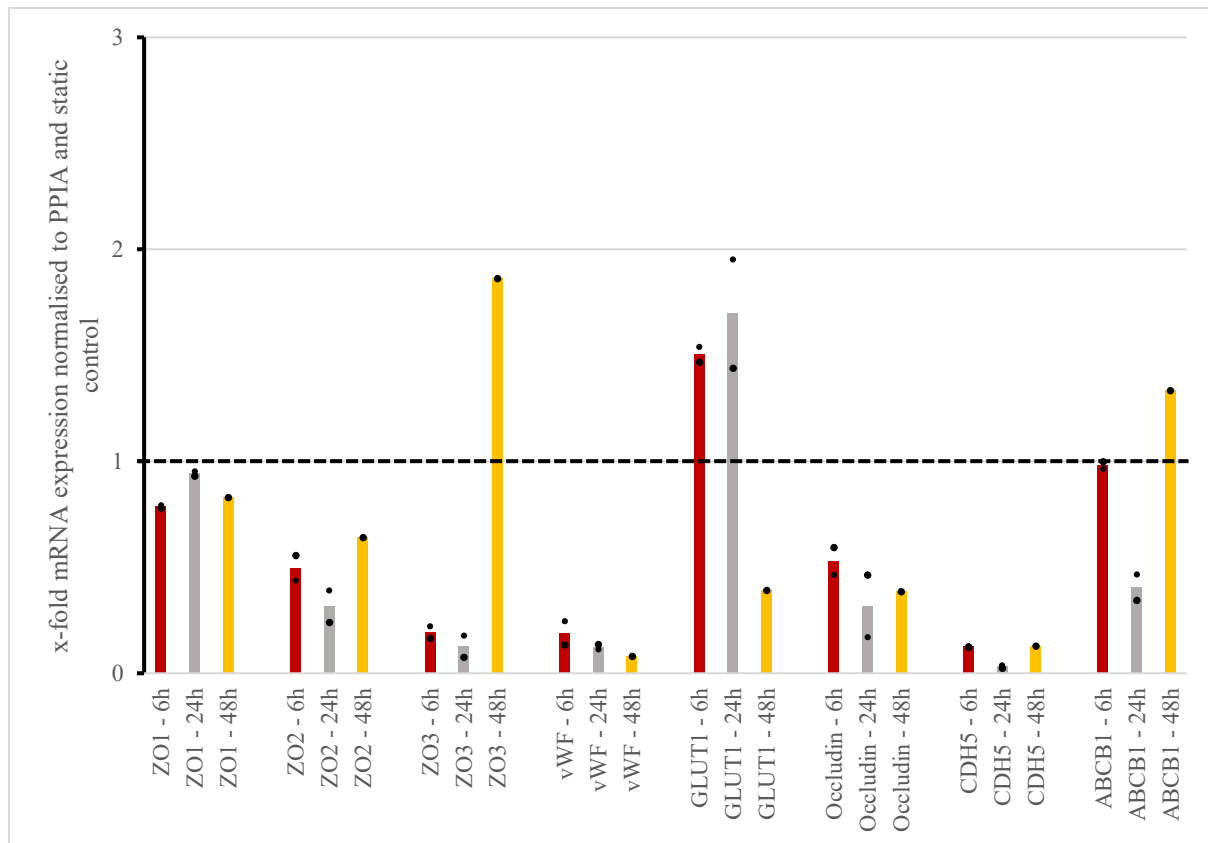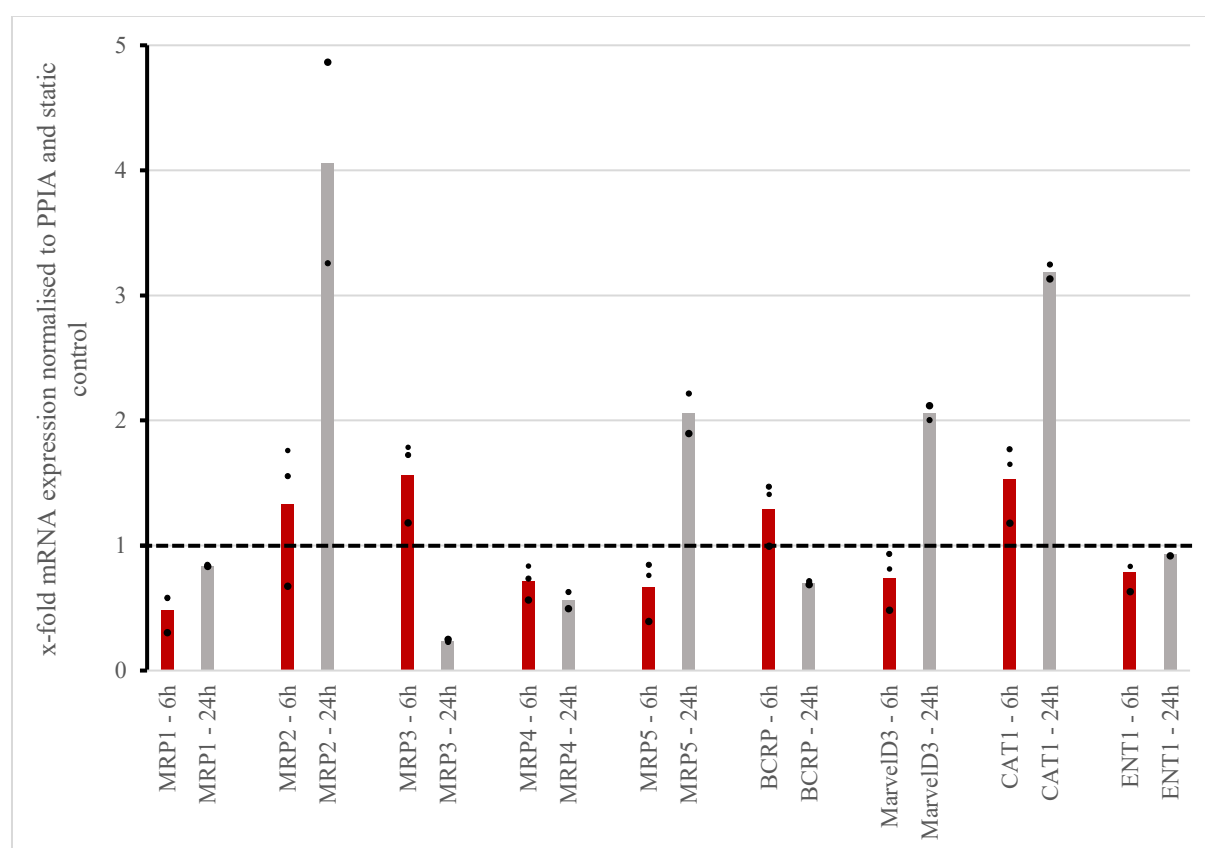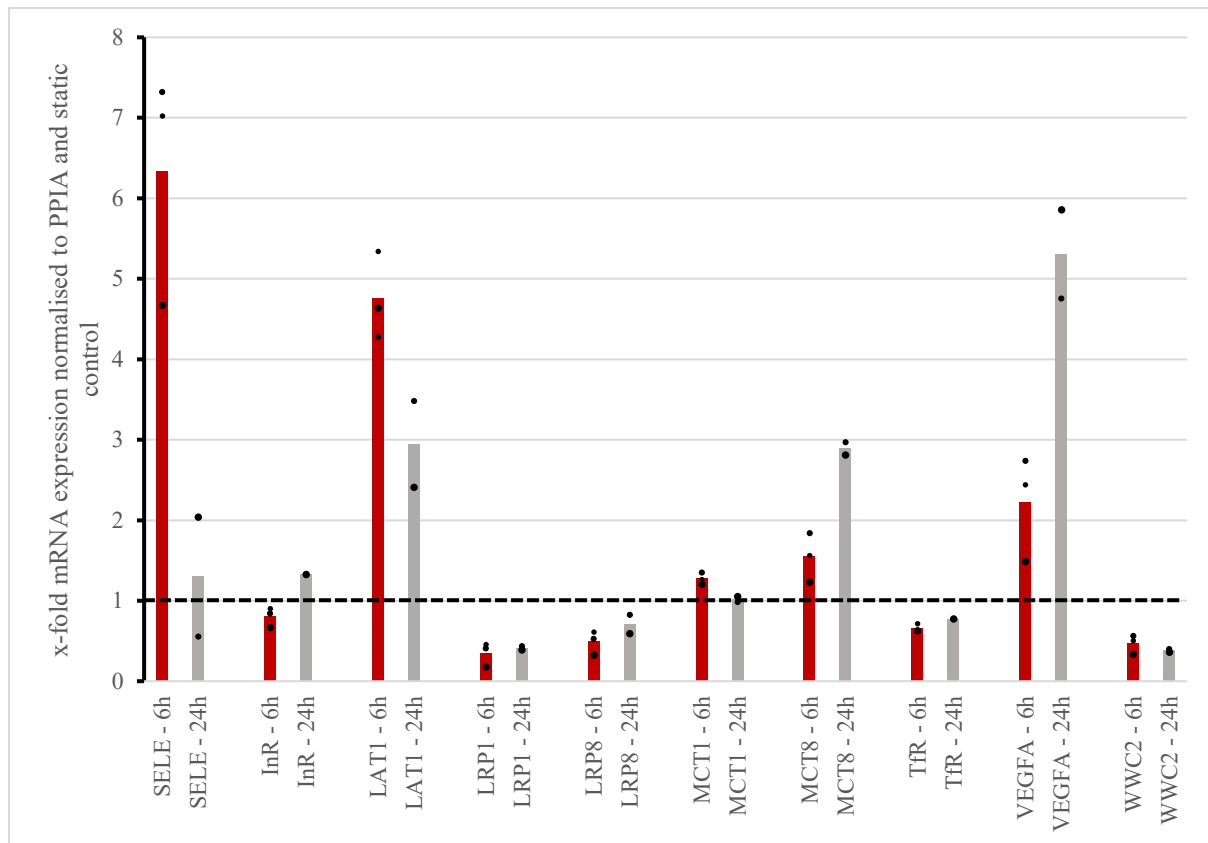
Figure 78: Bar graph 4 with trending mRNA level changes for 1 dyne/cm² after 6, 24 and 48 hours
(Red) 6 hours. (Gray) 24 hours. (Yellow) 48 hours. n=2: ZO1, ZO2, ZO3, vWF, GLUT1, Occludin, CDH5, ABCB1 – 6 and 24 hours; n=1: ZO1, ZO2, ZO3, vWF, GLUT1, Occludin, CDH5, ABCB1 – 48 hours.

ZO1 revealed a 0.79-fold decrease after 6 hours, no significant variation in its mRNA expression after 24 hours and a 0.83-fold decrease after 48 hours of exposure to 1 dyne/cm² in comparison to the static control and PPIA. Hence, ZO1 did not show a significant trend from 6 to 24 hours as well as from 24 to 48 hours of exposure to 1 dyne/cm².

ZO2 was 0.5-fold lower after 6 hours, 0.32-fold lower after 24 hours and 0.64-fold lower after 48 hours of exposure to 1 dyne/cm² in relation to the static control and PPIA. Hence, ZO2 did not reveal a significant variation in its mRNA expression from 6 to 24 hours, however, showed a slight upregulation from 24 to 48 hours of exposure to the final shear stress.

ZO3 was 0.19-fold decreased after a 6-hour-exposure, 0.13-fold decreased after a 24-hour-exposure and 1.86-fold increased after a 48-hour-exposure to 1 dyne/cm² related to the static control and PPIA. Thus, there was no significant difference in ZO3-expression from 6 to 24 hours and there was an upregulation from 24 to 48 hours of exposure to 1 dyne/cm².

vWF presented a 0.19-fold decrease after a 6-hour-exposure, a 0.12-fold decrease after a 24-hour exposure and a 0.08-fold decrease after a 48-hour-exposure to 1 dyne/cm² compared to the static control and PPIA. As a result, there was no significant variation in vWF-expression from 6 to 24 hours and from 24 to 48 hours of exposure to 1 dyne/cm².

GLUT1 showed a 1.5-fold upregulation in its mRNA expression after 6 hours, a 1.7-fold upregulation after 24 hours and a 0.39-fold downregulation after 48 hours of exposure to 1 dyne/cm² related to the static control and PPIA. Thus, there was no significant difference in the mRNA expression of GLUT1 between 6 and 24 hours, nonetheless, there was a downregulation from 24 to 48 hours of exposure to 1 dyne/cm².

Occludin displayed a 0.53-fold downregulation after a 6-hour-exposure, a 0.32-fold downregulation after a 24-hour-exposure and a 0.39-fold downregulation after a 48-hour-exposure to 1 dyne/cm² in relation to the static control and PPIA. Thus, Occludin did not indicate a significant variation in its mRNA expression from 6 to 24 hours as well as from 24 to 48 hours of exposure to the final shear stress.

CDH5 revealed a 0.13-fold decrease after 6 hours, a 0.032-fold decrease after 24 hours and a 0.13-fold decrease after 48 hours of exposure to 1 dyne/cm² in comparison to the static control and PPIA. As a result, there was a downregulation in CDH5-expression from 6 to 24 hours and an upregulation from 24 to 48 hours of exposure to 1 dyne/cm².

ABCB1 did not show a significant change in its mRNA expression after 6 hours, however, ABCB1 was 0.41-fold lower after 24 hours and 1.33-fold higher after 48 hours of exposure to 1 dyne/cm² in relation to the static control and PPIA. Hence, ABCB1-expression was decreased from 6 to 24 hours and increased from 24 to 48 hours of exposure to 1 dyne/cm².
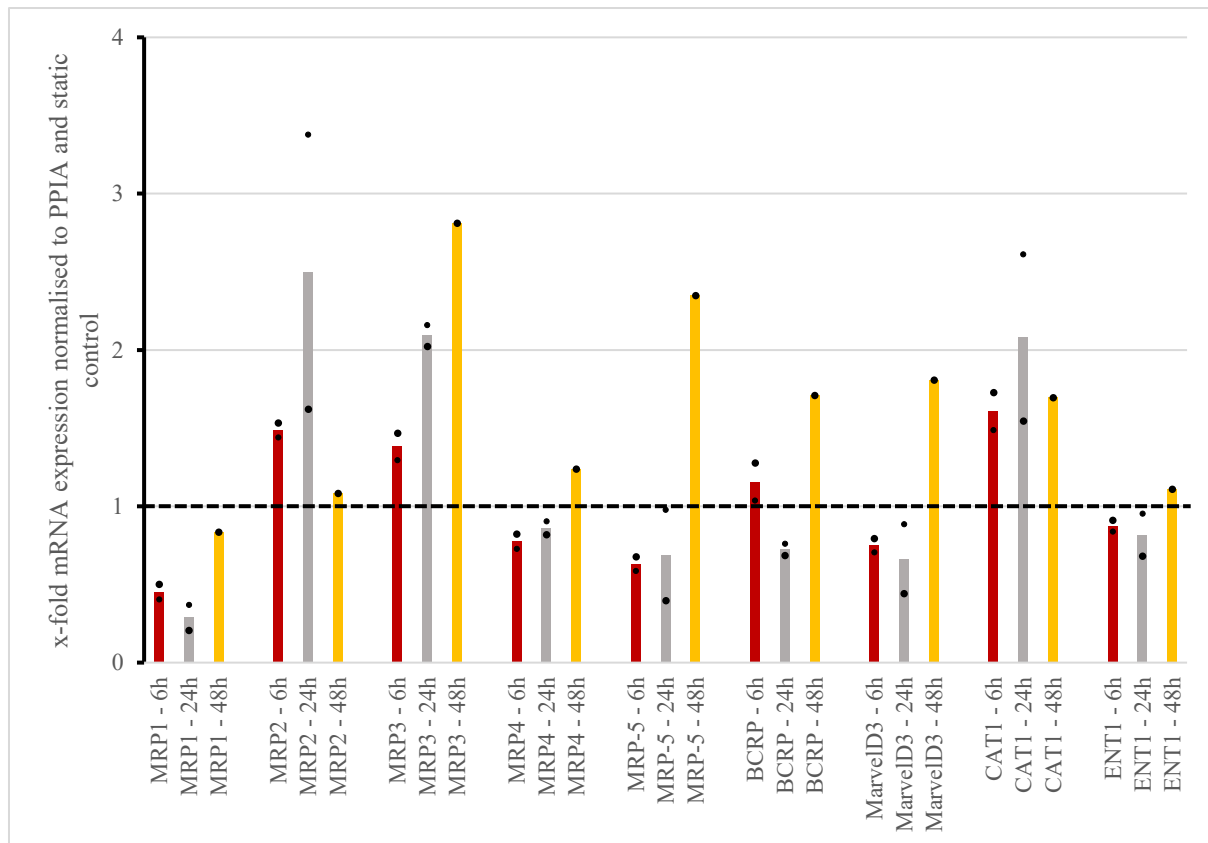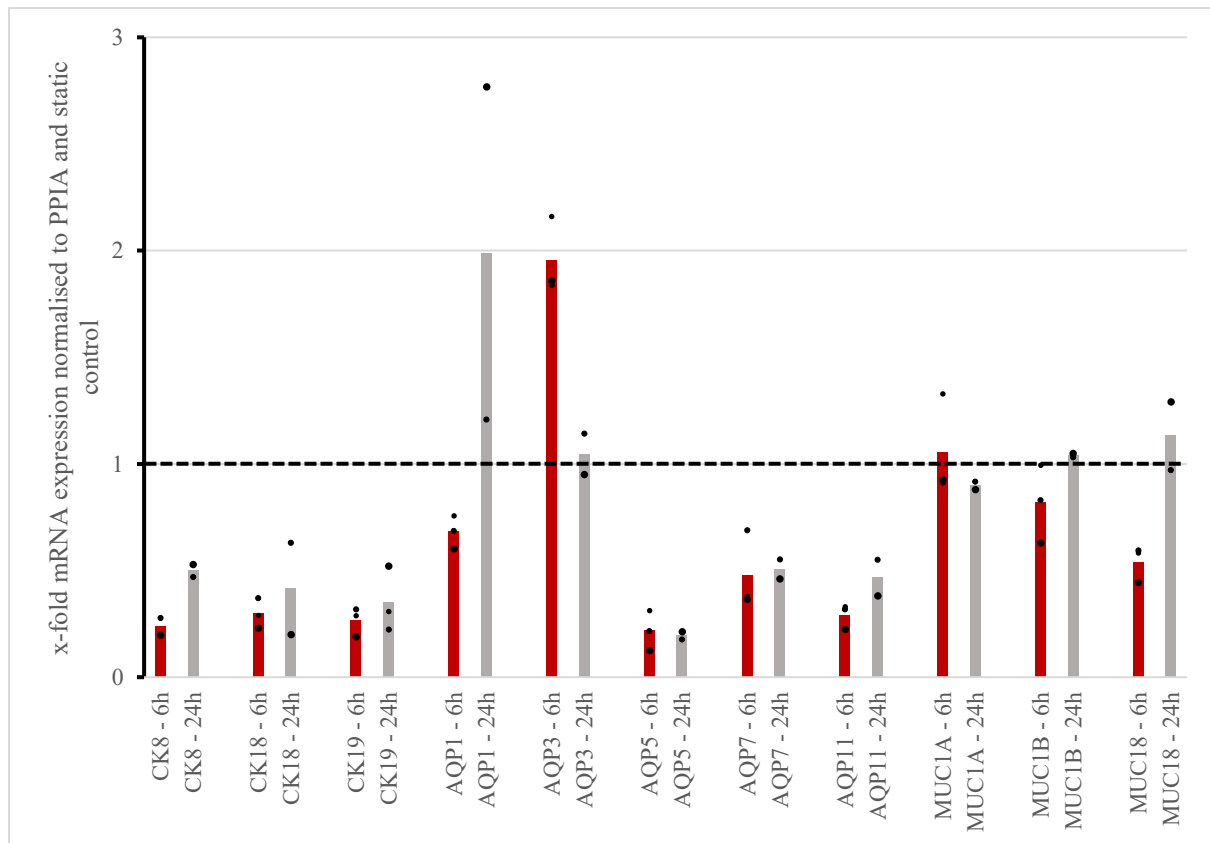
Figure 79: Bar graph 5 with trending mRNA level changes for 1 dyne/cm² after 6, 24 and 48 hours
(Red) 6 hours. (Gray) 24 hours. (Yellow) 48 hours. n=2: MRP1, MRP2, MRP3, MRP4, MRP5, BCRP,
MarvelD3, CAT1, ENT1 – 6 and 24 hours; n=1: MRP1, MRP2, MRP3, MRP4, MRP5, BCRP, MarvelD3,
CAT1, ENT1 – 48 hours.

MRP1 was 0.45-fold lower after 6 hours, 0.29-fold lower after 24 hours and 0.84-fold lower
after 48 hours of exposure to 1 dyne/cm² related to the static control and PPIA. Hence, MRP1
did not show a significant trend from 6 to 24 hours, however, displayed an upregulation in its
mRNA expression from 24 to 48 hours of exposure to the final shear stress.

MRP2 revealed a 1.49-fold increase after 6 hours, a 2.5-fold increase after 24 hours and no
significant change in its mRNA expression after 48 hours of exposure to 1 dyne/cm² in
comparison to the static control and PPIA. Hence, MRP2 was upregulated from 6 to 24 hours
and displayed a downregulation from 24 to 48 hours of exposure to 1 dyne/cm².

MRP3 was 1.38-fold higher after 6 hours, 2.09-fold higher after 24 hours and 2.81-fold higher
after 48 hours of exposure to 1 dyne/cm² in relation to the static control and PPIA. Hence,
MRP3 showed a trend towards upregulation in its mRNA expression from 6 to 24 hours and
from 24 to 48 hours of exposure to the final shear stress.

MRP4 was 0.78-fold decreased after a 6-hour-exposure, 0.86-fold decreased after a 24-hour-
exposure and 1.24-fold increased after a 48-hour-exposure to 1 dyne/cm² related to the static
control and PPIA. Thus, there was no significant difference in MRP4-expression from 6 to
24 hours, nonetheless, there was an upregulation from 24 to 48 hours of exposure to 1 dyne/cm².

MRP5 presented a 0.63-fold decrease after a 6-hour-exposure, a 0.69-fold decrease after a 24-hour exposure and a 2.35-fold increase after a 48-hour-exposure to 1 dyne/cm² compared to the static control and PPIA. As a result, there was no significant variation in MRP5-expression between a 6- and a 24-hour-exposure, however, there was an upregulation from 24 to 48 hours of exposure to 1 dyne/cm².

BCRP displayed a 1.16-fold upregulation after a 6-hour-exposure, a 0.72-fold downregulation after a 24-hour-exposure and a 1.71-fold upregulation after a 48-hour-exposure to 1 dyne/cm² in relation to the static control and PPIA. Thus, BCRP revealed a downregulation in its mRNA expression from 6 to 24 hours, however, was upregulated from 24 to 48 hours of exposure to 1 dyne/cm².

MarvelD3 was 0.75-fold lower after 6 hours, 0.66-fold lower after 24 hours and 1.81-fold higher after 48 hours of exposure to 1 dyne/cm² related to the static control and PPIA. Consequently, there was no significant change in MarvelD3-expression between 6 and 24 hours, nonetheless, an upregulation occurred from 24 to 48 hours of exposure to 1 dyne/cm².

CAT1 was 1.61-fold increased after a 6-hour-exposure, 2.08-fold increased after a 24-hour-exposure and 1.7-fold increased after a 48-hour-exposure to 1 dyne/cm² compared to the static control and PPIA. Accordingly, there was an upregulation of CAT1 from 6 to 24 hours and a downregulation from 24 to 48 hours of exposure to 1 dyne/cm².

ENT1 was 0.87-fold lower after 6 hours, 0.82-fold lower after 24 hours and 1.11-fold higher after 48 hours of exposure to 1 dyne/cm² in comparison to the static control and PPIA. Therefore, ENT1 did not reveal a significant change in its mRNA expression from 6 to 24 hours, however, there was a slight upregulation from 24 to 48 hours of exposure to the final shear stress.
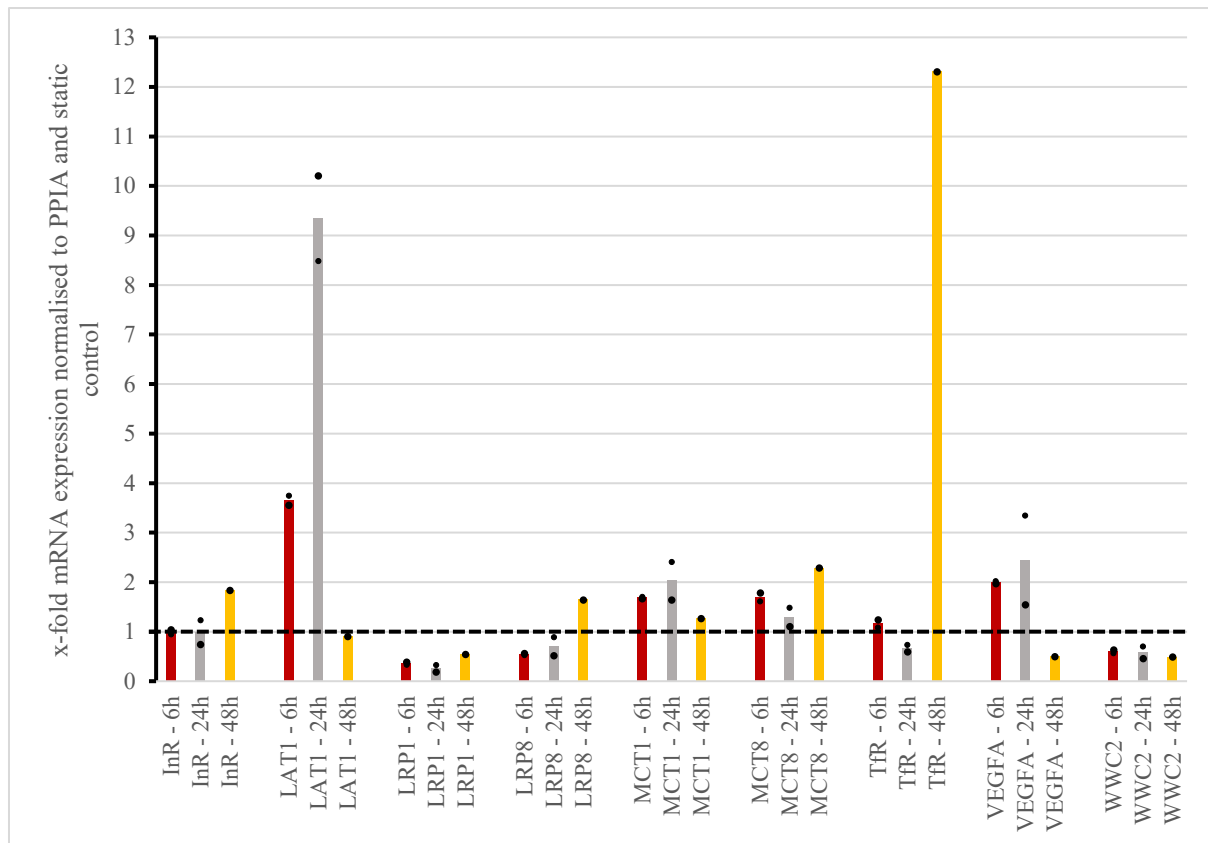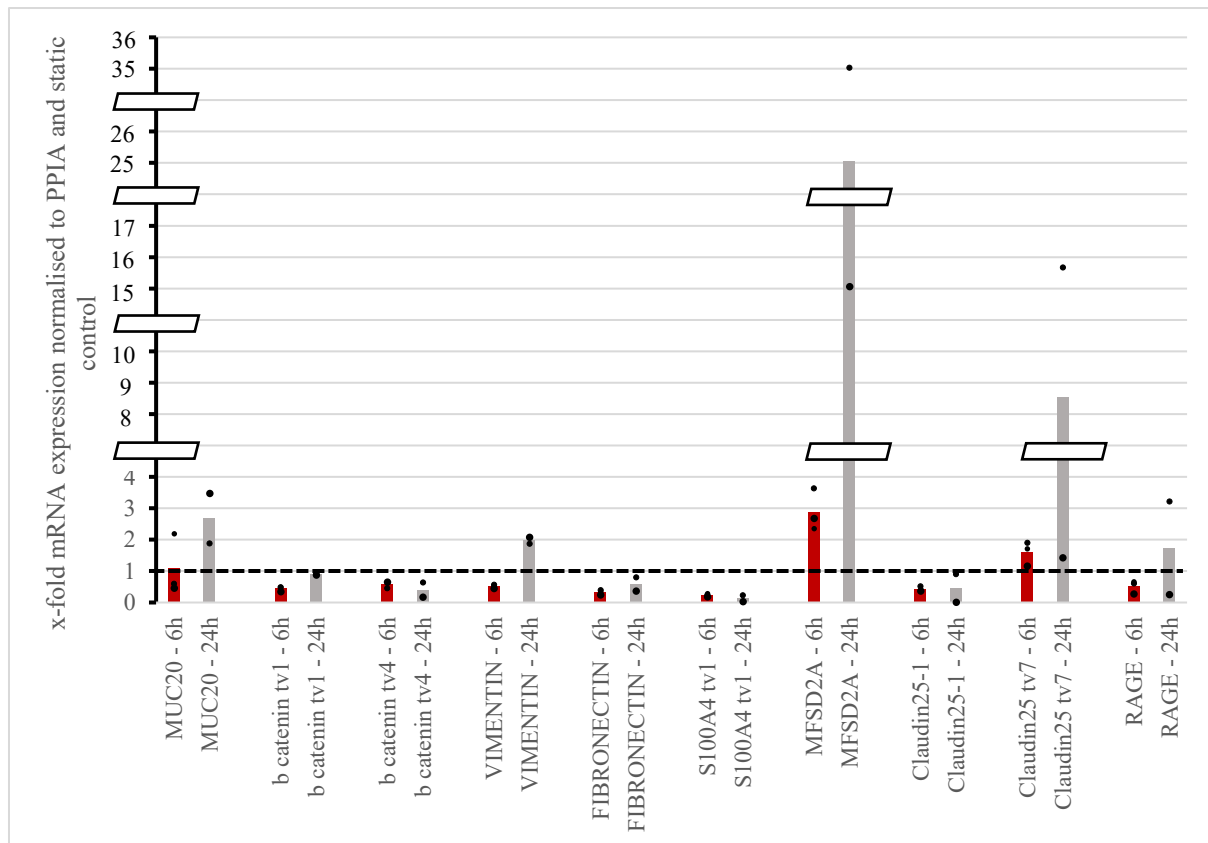
Figure 80: Bar graph 6 with trending mRNA level changes for 1 dyne/cm² after 6, 24 and 48 hours
(Red) 6 hours. (Gray) 24 hours. (Yellow) 48 hours. n=2: InR, LAT1, LRP1, LRP8, MCT1, MCT8, TfR, VEGFA, WWC2 – 6 and 24 hours; n=1: InR, LAT1, LRP1, LRP8, MCT1, MCT8, TfR, VEGFA, WWC2 – 48 hours.

InR did not reveal significant differences in its mRNA expression after 6 and 24 hours, however, showed a 1.84-fold increase after 48 hours of exposure to 1 dyne/cm² in comparison to the static control and PPIA. Hence, InR did not show a significant trend between 6 and 24 hours, nonetheless, an upregulation occurred in its mRNA expression from 24 to 48 hours of exposure to 1 dyne/cm².

LAT1 was 3.65-fold higher after 6 hours, 9.35-fold higher after 24 hours and 0.91-fold lower after 48 hours of exposure to 1 dyne/cm² in relation to the static control and PPIA. Hence, LAT1 was upregulated from 6 to 24 hours and significantly downregulated from 24 to 48 hours of exposure to the final shear stress.

LRP1 was 0.36-fold decreased after a 6-hour-exposure, 0.26-fold decreased after a 24-hour-exposure and 0.54-fold decreased after a 48-hour-exposure to 1 dyne/cm² related to the static control and PPIA. Thus, there was no significant difference in LRP1-expression between 6 and 24 hours, but there was a slight upregulation from 24 to 48 hours of exposure to 1 dyne/cm².

LRP8 presented a 0.54-fold decrease after a 6-hour-exposure, a 0.70-fold decrease after a 24-hour exposure and a 1.65-fold increase after a 48-hour-exposure to 1 dyne/cm² compared to the static control and PPIA. As a result, there was no significant variation in LRP8-expression

140

between a 6- and a 24-hour-exposure, however, there was an upregulation in the mRNA expression of LRP8 from 24 to 48 hours of exposure to 1 dyne/cm².

MCT1 showed a 1.69-fold upregulation in its mRNA expression after 6 hours, a 2.03-fold upregulation after 24 hours and a 1.27-fold upregulation after 48 hours of exposure to 1 dyne/cm² related to the static control and PPIA. Thus, there was a slight upregulation of MCT1 between 6 and 24 hours and a downregulation from 24 to 48 hours of exposure to 1 dyne/cm².

MCT8 displayed a 1.7-fold upregulation after a 6-hour-exposure, a 1.3-fold upregulation after a 24-hour-exposure and a 2.29-fold upregulation after a 48-hour-exposure to 1 dyne/cm² in relation to the static control and PPIA. Thus, MCT8 showed a downregulation in its mRNA expression from 6 to 24 hours and an upregulation from 24 to 48 hours of exposure to 1 dyne/cm².

TfR revealed a 1.16-fold increase after 6 hours, a 0.67-fold decrease after 24 hours and a 12.31-fold increase after 48 hours of exposure to 1 dyne/cm² in comparison to the static control and PPIA. Hence, TfR was downregulated from 6 to 24 hours and upregulated from 24 to 48 hours of exposure to 1 dyne/cm².

VEGFA was 2-fold higher after 6 hours, 2.45-fold higher after 24 hours and 0.5-fold lower after 48 hours of exposure to 1 dyne/cm² in relation to the static control and PPIA. Accordingly, VEGFA-expression was increased from 6 to 24 hours and decreased from 24 to 48 hours of exposure to 1 dyne/cm².

WWC2 was 0.6-fold decreased after a 6-hour-exposure, 0.58-fold decreased after a 24-hour-exposure and 0.49-fold decreased after a 48-hour-exposure to 1 dyne/cm² compared to the static control and PPIA. Thus, there was no significant trend in WWC2-expression between 6 and 24 hours and between 24 and 48 hours of exposure to 1 dyne/cm².
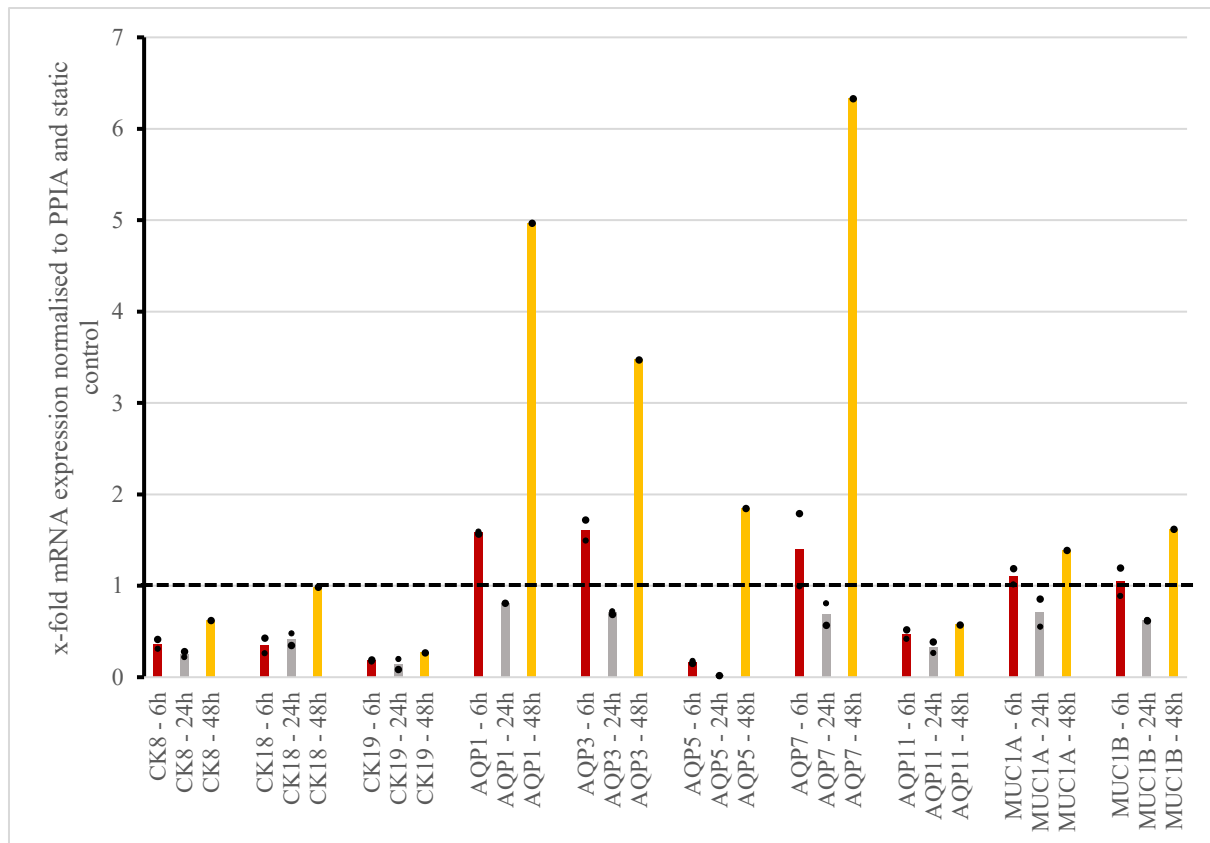
Figure 81: Bar graph 7 with trending mRNA level changes for 1 dyne/cm² after 6, 24 and 48 hours
(Red) 6 hours. (Gray) 24 hours. (Yellow) 48 hours. n=2: CK8, CK18, CK19, AQP1, AQP3, AQP5, AQP7, AQP11, MUC1A, MUC1B – 6 hours; CK8, CK18, CK19, AQP3, AQP5, AQP7, AQP11, MUC1A, MUC1B – 24 hours; n=1: CK8, CK18, CK19, AQP1, AQP3, AQP5, AQP7, AQP11, MUC1A, MUC1B – 48 hours; AQP1 – 24 hours.

CK8 was 0.36-fold decreased after a 6-hour-exposure, 0.25-fold decreased after a 24-hour-exposure and 0.62-fold decreased after a 48-hour-exposure to 1 dyne/cm² related to the static control and PPIA. Thus, there was no significant trend in CK8-expression between 6 and 24 hours and a slight upregulation from 24 to 48 hours of exposure to 1 dyne/cm².

CK18 displayed a 0.35-fold decrease after a 6-hour-exposure, a 0.42-fold decrease after a 24-hour-exposure and no significant change after a 48-hour-exposure to 1 dyne/cm² compared to the static control and PPIA. As a result, there was no significant difference between a 6- and a 24-hour-exposure and an upregulation of CK18 from 24 to 48 hours of exposure to 1 dyne/cm².

CK19 was 0.18-fold lower after 6 hours, 0.14-fold lower after 24 hours and 0.27-fold lower after 48 hours of exposure to 1 dyne/cm² related to the static control and PPIA. Hence, CK19 did not show significant changes in its mRNA expression between 6 and 24 hours and between 24 and 48 hours of exposure to the final shear stress.

AQP1 was 1.58-fold higher after 6 hours, 0.81-fold lower after 24 hours and 4.97-fold higher after 48 hours of exposure to 1 dyne/cm² compared to the static control and PPIA. Hence, AQP1 was downregulated from 6 to 24 hours, however, revealed an upregulation in its mRNA expression between the second and the third point of cell lysis.

142

AQP3 displayed a 1.61-fold upregulation after a 6-hour-exposure, a 0.71-fold downregulation after a 24-hour-exposure and a 3.47-fold upregulation after a 48-hour-exposure to 1 dyne/cm² in relation to the static control and PPIA. Thus, AQP3 was downregulated from 6 to 24 hours and upregulated from 24 to 48 hours of exposure to the final shear stress.

AQP5 displayed a 0.17-fold downregulation after a 6-hour-exposure, a 0.017-fold downregulation after a 24-hour-exposure and a 1.85-fold upregulation after a 48-hour-exposure to 1 dyne/cm² in relation to the static control and PPIA. Thus, AQP5 was downregulated from 6 to 24 hours and upregulated from 24 to 48 hours of exposure to 1 dyne/cm².

AQP7 was 1.39-fold higher after 6 hours, 0.69-fold lower after 24 hours and 6.33-fold higher after 48 hours of exposure to 1 dyne/cm² related to the static control and PPIA. Thus, there was a downregulation of AQP7 from 6 to 24 hours and a significant upregulation from 24 to 48 hours of exposure to 1 dyne/cm².

AQP11 was 0.47-fold decreased after a 6-hour-exposure, 0.33-fold decreased after a 24-hour-exposure and 0.58-fold decreased after a 48-hour-exposure to 1 dyne/cm² related to the static control and PPIA. Thus, there was no significant trend in the mRNA expression of AQP11 from 6 to 24 hours and from 24 to 48 hours of exposure to 1 dyne/cm².

MUC1A did not reveal a significant variation in its mRNA expression after 6 hours, however, MUC1A was 0.71-fold lower after 24 hours and 1.39-fold higher after 48 hours of exposure to 1 dyne/cm² related to the static control and PPIA. Hence, MUC1A was downregulated from 6 to 24 hours and upregulated from 24 to 48 hours of exposure to the final shear stress.

MUC1B did not change significantly in its mRNA expression after 6 hours, however, MUC1B was 0.62-fold lower after 24 hours and 1.62-fold higher after 48 hours of exposure to 1 dyne/cm² compared to the static control and PPIA. Hence, MUC1B was downregulated between the first two points of cell lysis and revealed an upregulation in its mRNA expression from the second to the third point of cell lysis.
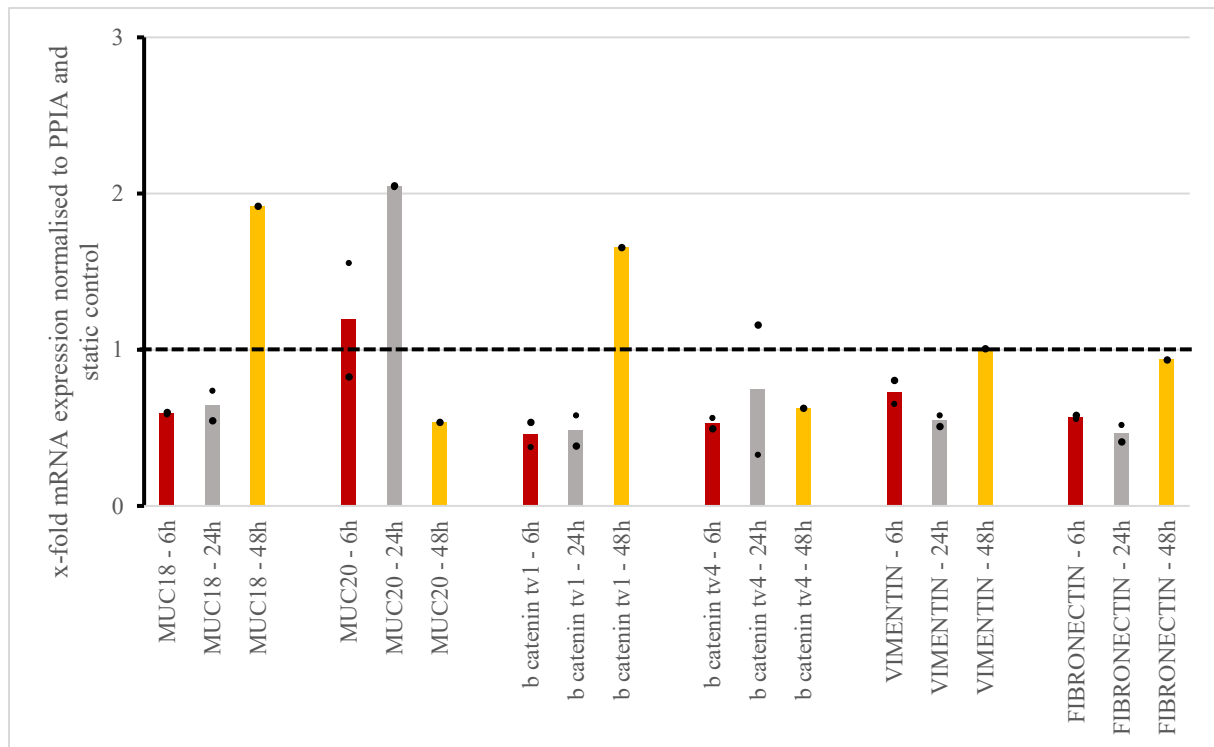
Figure 82: Bar graph 8 with trending mRNA level changes for 1 dyne/cm² after 6, 24 and 48 hours
(Red) 6 hours. (Gray) 24 hours. (Yellow) 48 hours. n=2: MUC18, MUC20, b-catenin tv1, b-catenin tv4, VIMENTIN, FIBRONECTIN – 6 and 24 hours; n=1: MUC18, MUC20, b catenin tv1, b catenin tv4, VIMENTIN, FIBRONECTIN – 48 hours.

MUC18 was 0.59-fold lower after 6 hours, 0.64-fold lower after 24 hours and 1.92-fold higher after 48 hours of exposure to 1 dyne/cm² in relation to the static control and PPIA. Hence, MUC18 was not significantly changed in its mRNA expression from 6 to 24 hours, however, was upregulated from 24 to 48 hours of exposure to the final shear stress.

MUC20 was 1.19-fold increased after a 6-hour-exposure, 2.05-fold increased after a 24-hour-exposure and 0.54-fold decreased after a 48-hour-exposure to 1 dyne/cm² related to the static control and PPIA. Thus, there was an upregulation of MUC20 from 6 to 24 hours and a downregulation from 24 to 48 hours of exposure to 1 dyne/cm².

B catenin tv1 displayed a 0.46-fold decrease after a 6-hour-exposure, a 0.48-fold decrease after a 24-hour-exposure and a 1.66-fold increase after a 48-hour-exposure to 1 dyne/cm² compared to the static control and PPIA. As a result, there was no significant variation in b catenin tv1-expression between a 6- and a 24-hour-exposure and there was an upregulation from 24 to 48 hours of exposure to 1 dyne/cm².

B catenin tv4 showed a 0.53-fold downregulation after 6 hours, a 0.74-fold downregulation after 24 hours and a 0.63-fold downregulation after 48 hours of exposure to 1 dyne/cm² related to the static control and PPIA. Thus, there was no significant difference between 6 and 24 hours as well as between 24 and 48 hours of exposure to the final shear stress.

VIMENTIN displayed a 0.73-fold downregulation after a 6-hour-exposure, a 0.55-fold downregulation after a 24-hour-exposure and no significant change in its mRNA expression after a 48-hour-exposure to 1 dyne/cm² in relation to the static control and PPIA. Thus, VIMENTIN did not show a significant variation in its mRNA expression from 6 to 24 hours, however, was upregulated from 24 to 48 hours of exposure to 1 dyne/cm².

FIBRONECTIN was 0.57-fold lower after 6 hours, 0.46-fold lower after 24 hours and did not reveal a significant variation in its mRNA expression after 48 hours of exposure to 1 dyne/cm² related to the static control and PPIA. Consequently, there was no significant difference in FIBRONECTIN-expression between 6 and 24 hours, nonetheless, a slight upregulation occurred between 24 and 48 hours of exposure to 1 dyne/cm².
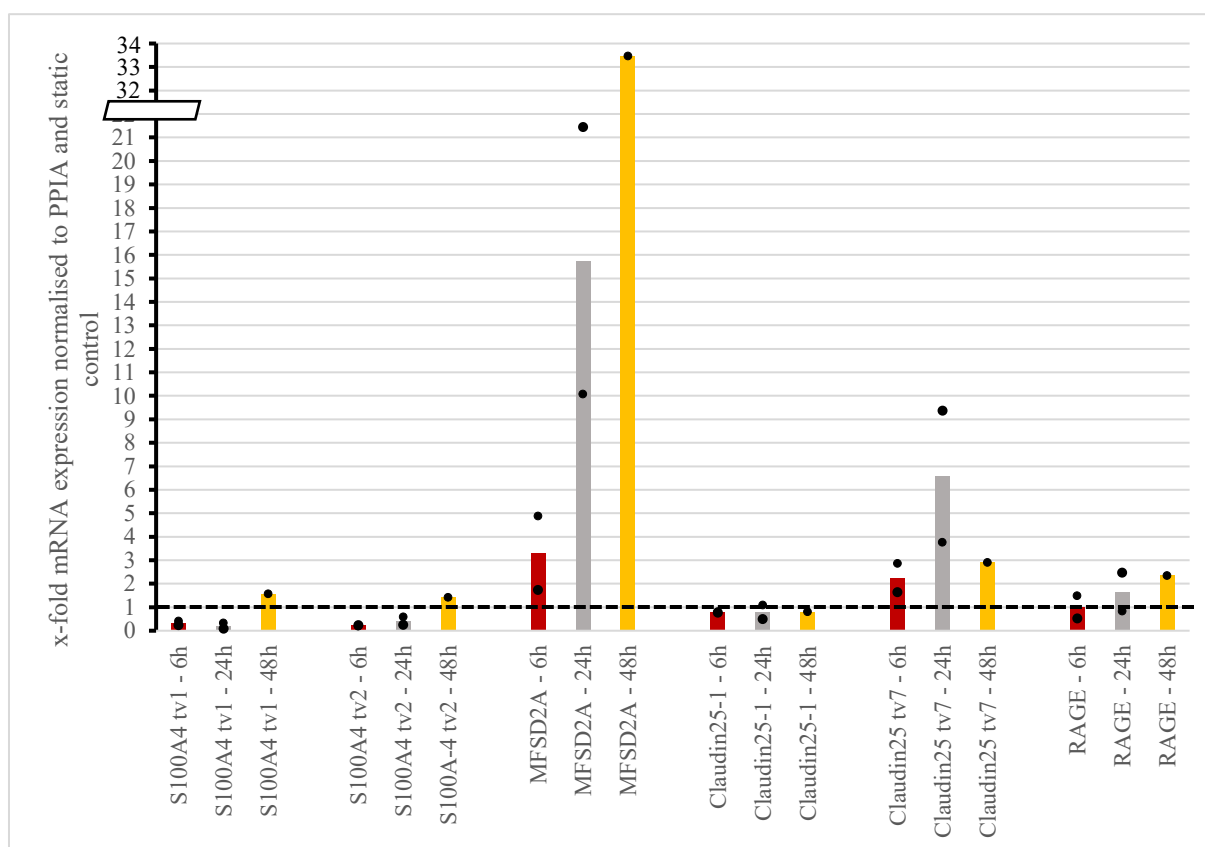
Figure 83: Bar graph 9 with trending mRNA level changes for 1 dyne/cm² after 6, 24 and 48 hours
(Red) 6 hours. (Gray) 24 hours. (Yellow) 48 hours. n=2: S100A4 tv1, S100A4 tv2, MFSD2A, Claudin25-1, Claudin25 tv7, RAGE – 6 and 24 hours; n=1: S100A4 tv1, S100A4 tv2, MFSD2A, Claudin25-1, Claudin25 tv7, RAGE – 48 hours.

S100A4 tv1 was 0.32-fold decreased after a 6-hour-exposure, 0.21-fold decreased after a 24-hour-exposure and 1.56-fold increased after a 48-hour-exposure to 1 dyne/cm² related to the static control and PPIA. Thus, there was no significant difference in S100A4 tv1-expression between 6 and 24 hours, but there was an upregulation from 24 to 48 hours of exposure to 1 dyne/cm².

S100A4 tv2 presented a 0.21-fold decrease after a 6-hour-exposure, a 0.41-fold decrease after a 24-hour-exposure and a 1.41-fold increase after a 48-hour-exposure to 1 dyne/cm² compared to the static control and PPIA. As a result, there was no significant change in the mRNA expression of S100A4 tv2 between a 6- and a 24-hour-exposure, but there was an upregulation of S100A4 tv2 from 24 to 48 hours of exposure to 1 dyne/cm².

MFSD2A was 3.3-fold higher after 6 hours, 15.75-fold higher after 24 hours and 33.46-fold higher after 48 hours of exposure to 1 dyne/cm² related to the static control and PPIA. Hence, MFSD2A showed a trend towards upregulation from 6 to 24 hours and from 24 to 48 hours of exposure to the final shear stress.

Claudin25-1 was 0.78-fold lower after 6 hours, 0.79-fold lower after 24 hours and 0.80-fold lower after 48 hours of exposure to 1 dyne/cm² compared to the static control and PPIA. Hence, Claudin25-1 did not show a significant trend from 6 to 24 hours and from 24 to 48 hours of exposure to 1 dyne/cm².

Claudin25 tv7 displayed a 2.25-fold upregulation after a 6-hour-exposure, a 6.56-fold upregulation after a 24-hour-exposure and a 2.9-fold upregulation after a 48-hour-exposure to 1 dyne/cm² in relation to the static control and PPIA. Thus, Claudin25 tv7 revealed an upregulation from 6 to 24 hours and was downregulated from 24 to 48 hours of exposure to the final shear stress.

RAGE did not display a significant change in its mRNA expression after a 6-hour-exposure, however, RAGE showed a 1.65-fold increase after a 24-hour-exposure and a 2.35-fold increase after a 48-hour-exposure to 1 dyne/cm² in relation to the static control and PPIA. Thus, RAGE was upregulated with the prolonged durations of exposure to 1 dyne/cm².

4.5.5   mRNA expression level changes at 3 dyne/cm² at different points in time

Lysates of the final shear stress of 3 dyne/cm² were obtained at two different points (at 6 and 24 hours) after the conclusive exposure. The associated timeline is illustrated in Figure 84, corresponding to experiment no. 21 (3.8.14.2). Moreover, the up- and downregulations of the targets over time at 3 dyne/cm² are visualised in Figure 85 to Figure 92.
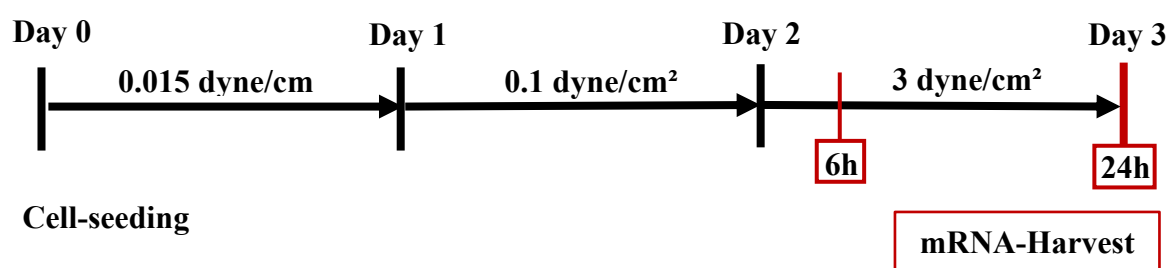
Figure 84: Experimental setup of mRNA-harvest for 3 dyne/cm² after 6 and 24 hours
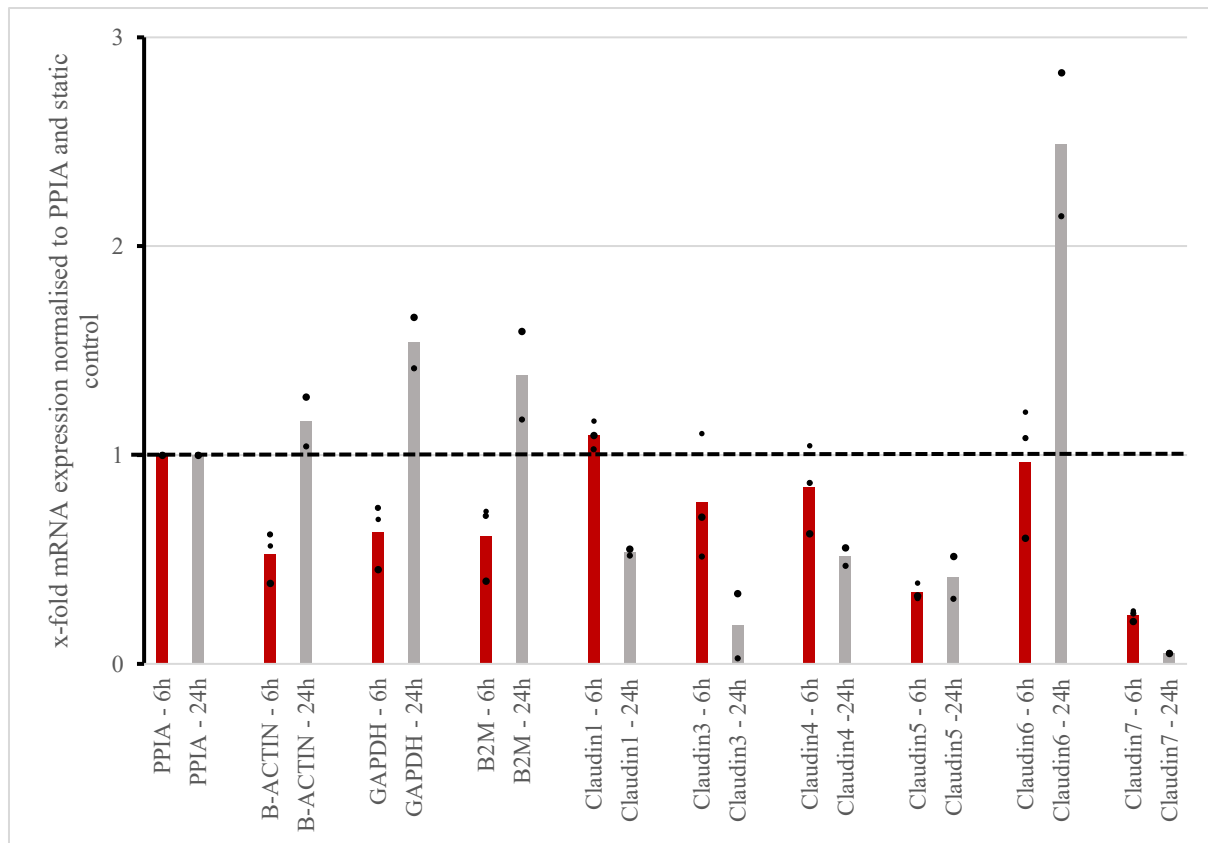
Figure 85: Bar graph 1 with trending mRNA expression level changes for 3 dyne/cm² after 6 and 24 hours (Red) 6 hours. (Gray) 24 hours. n=3: PPIA, B-ACTIN, GAPDH, B2M, Claudin1, Claudin3, Claudin4, Claudin5, Claudin6, Claudin7 – 6 hours; n=2: : PPIA, B-ACTIN, GAPDH, B2M, Claudin1, Claudin3, Claudin4, Claudin5, Claudin6, Claudin7 – 24 hours.

B-ACTIN was 0.52-fold lower after a 6-hour-exposure and 1.16-fold higher after a 24-hour-exposure to 3 dyne/cm² compared to the static control and PPIA. Hence, B-ACTIN was upregulated from 6 to 24 hours of exposure to the final shear stress.

GAPDH presented a 0.63-fold downregulation after a 6-hour-exposure and a 1.54-fold upregulation after a 24-hour-exposure to 3 dyne/cm² in comparison to the static control and PPIA. Therefore, GAPDH was upregulated with a prolonged duration of exposure to 3 dyne/cm².

B2M was 0.61-fold lower after a 6-hour-exposure and 1.38-fold higher after a 24-hour-exposure to 3 dyne/cm² related to the static control and PPIA. As a result, B2M was upregulated with an increased duration of exposure to the final shear stress.

Claudin1 did not show a significant difference in its mRNA expression after a 6-hour-exposure, however, displayed a 0.53-fold downregulation after a 24-hour-exposure to 3 dyne/cm² in comparison to the static control and PPIA. Consequently, there was a downregulation in the mRNA expression of Claudin1 from 6 to 24 hours of exposure to the final shear stress.

Claudin3 was 0.77-fold lower after a 6-hour-exposure and 0.18-fold lower after a 24-hour-exposure to 3 dyne/cm² compared to the static control and PPIA. Therefore, Claudin3 was downregulated from a 6- to a 24-hour-exposure to 3 dyne/cm².

Claudin4 was 0.85-fold lower after a 6-hour-exposure and 0.51-fold lower after a 24-hour-exposure to 3 dyne/cm² in comparison to the static control and PPIA. Thus, Claudin4 showed a downregulation in its mRNA expression from a 6- to a 24-hour-exposure to the final shear stress.

Claudin5 was 0.34-fold downregulated after a 6-hour-exposure and 0.41-fold downregulated after a 24-hour-exposure to 3 dyne/cm² in relation to the static control and PPIA. Therefore, Claudin5 did not show a significant difference in its mRNA expression with an increased final shear stress duration.

Claudin6 did not show a significant change in its mRNA expression after 6 hours and was 2.49-fold increased after 24 hours of exposure to 3 dyne/cm² compared to the static control and PPIA. Hence, Claudin6 was upregulated from 6 to 24 hours of exposure to 3 dyne/cm².

Claudin7 was 0.23-fold lower after a 6-hour-exposure and 0.052-fold lower after a 24-hour-exposure to 3 dyne/cm² related to the static control and PPIA. As a result, Claudin7 revealed a downregulation in its mRNA expression with an increased duration of exposure to the final shear stress.

Figure 86: Bar graph 2 with trending mRNA expression level changes for 3 dyne/cm² after 6 and 24 hours (Red) 6 hours. (Gray) 24 hours. n=3: Claudin9, Claudin10 tva, Claudin11, Claudin12 tv1, Claudin12 tv2, Claudin12 tv3, Claudin14, Claudin15, Claudin16 – 6 hours; n=2: Claudin8, Claudin9, Claudin10 tva, Claudin11, Claudin12 tv1, Claudin12 tv2, Claudin12 tv3, Claudin14, Claudin15, Claudin16 – 24 hours; Claudin8 – 6 hours.

Claudin8 was 0.46-fold downregulated after a 6-hour-exposure and 0.57-fold downregulated after a 24-hour-exposure to 3 dyne/cm² in comparison to the static control and PPIA. Consequently, there was no significant difference in Claudin8-expression with an increased duration of exposure to 3 dyne/cm².

Claudin9 was 0.81-fold lower after a 6-hour-exposure and 0.023-fold lower after a 24-hour-exposure to 3 dyne/cm² in comparison to the static control and PPIA. Thus, Claudin 9 showed a significant downregulation from 6 to 24 hours of exposure to the final shear stress.

Claudin10 tva was 0.43-fold downregulated after 6 hours and 4.04-fold upregulated after a 24-hour-exposure to 3 dyne/cm² in comparison to the static control and PPIA. Therefore, Claudin10 tva was significantly upregulated from 6 to 24 hours of exposure to 3 dyne/cm².

Claudin11 was 0.3-fold lower after a 6-hour-exposure and 0.39-fold lower after a 24-hour-exposure to 3 dyne/cm² in comparison to the static control and PPIA. As a result, Claudin11 did not reveal a significant difference in its mRNA expression from 6 to 24 hours of exposure to the final shear stress.

Claudin12 tv1 was 0.29-fold lower after a 6-hour-exposure and 0.57-fold lower after a 24-hour-exposure to 3 dyne/cm² in relation to the static control and PPIA. Consequently, Claudin12 tv1

did not show a significant difference in its mRNA expression from 6 to 24 hours of exposure to the final shear stress.

Claudin12 tv2 displayed a 1.4-fold upregulation 6 hours after final shear stress exposure and a 1.88-fold upregulation after a 24-hour-exposure to 3 dyne/cm² compared to the static control and PPIA. Hence, Claudin12 tv2 showed an upregulation in its mRNA expression with an increased duration of exposure to 3 dyne/cm².

Claudin12 tv3 was 1.13-fold upregulated after a 6-hour-exposure and 1.94-fold upregulated after a 24-hour-exposure to 3 dyne/cm² in relation to the static control and PPIA. Hence, Claudin12 tv3 was upregulated from 6 to 24 hours of exposure to 3 dyne/cm².

Claudin14 was 6.58-fold higher 6 hours after final shear stress induction and 2.63-fold higher after a 24-hour-exposure to 3 dyne/cm² in comparison to the static control and PPIA. Consequently, Claudin14 was downregulated from 6 to 24 hours of exposure to the final shear stress.

Claudin15 was 0.7-fold downregulated 6 hours after final shear stress induction and 2.5-fold upregulated after a 24-hour-exposure to 3 dyne/cm² compared to the static control and PPIA. Therefore, Claudin15 was upregulated with an increased duration of exposure to 3 dyne/cm².

Claudin16 was 0.057-fold lower after 6 hours and 0.056-fold lower after 24 hours of exposure to 3 dyne/cm² related to the static control an PPIA. Hence, Claudin16 did not reveal a significant variation in its mRNA expression from 6 to 24 hours of exposure to the final shear stress.
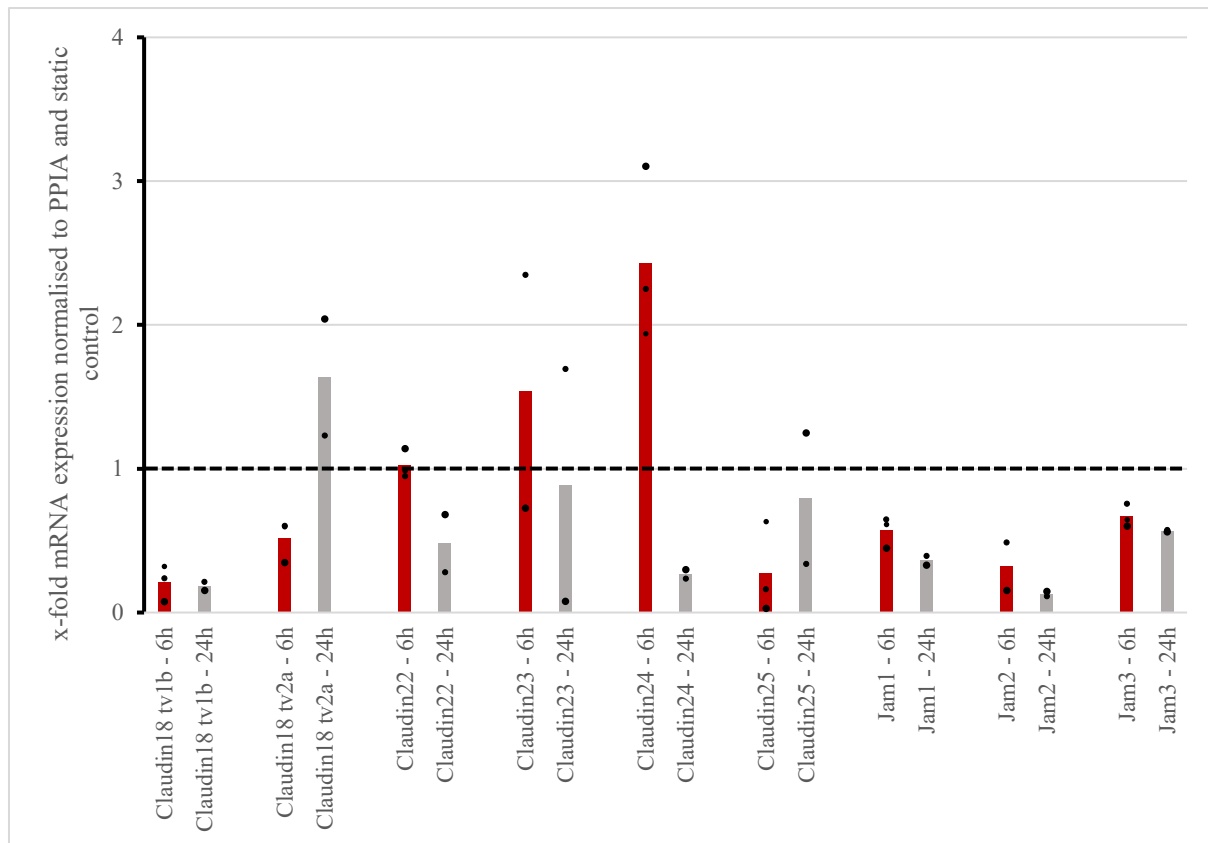
Figure 87: Bar graph 3 with trending mRNA expression level changes for 3 dyne/cm² after 6 and 24 hours (Red) 6 hours. (Gray) 24 hours. n=3: Claudin18 tv1b, Claudin18 tv2a, Claudin22, Claudin24, Claudin25, Jam1, Jam3 – 6 hours; n=2: Claudin18 tv1b, Claudin18 tv2a, Claudin22, Claudin23, Claudin24, Claudin25, Jam1, Jam2, Jam3 – 24 hours; Claudin23, Jam2 – 6 hours.

Claudin18 tv1b was 0.21-fold downregulated after a 6-hour-exposure and 0.19-fold downregulated after a 24-hour-exposure to 3 dyne/cm² in relation to the static control and PPIA. Hence, Claudin18 tv1b did not show a significant difference in its mRNA expression from 6 to 24 hours of exposure to 3 dyne/cm².

Claudin18 tv2a was 0.52-fold lower after a 6-hour-exposure and 1.63-fold higher after a 24-hour-exposure to 3 dyne/cm² in comparison to the static control and PPIA. Thus, Claudin18 tv2a was upregulated with an increased duration of exposure to the final shear stress.

Claudin22 did not present a significant change in its mRNA expression after 6 hours and showed a 0.48-fold downregulation after 24 hours of exposure to 3 dyne/cm² compared to the static control and PPIA. Therefore, Claudin22 was downregulated with a prolonged duration of exposure to 3 dyne/cm².

Claudin23 was 1.54-fold increased and 0.89-fold decreased after the exposure to 3 dyne/cm² related to the static control and PPIA after 6 and 24 hours, respectively. Consequently, Claudin23 was decreased from a 6- to a 24-hour-exposure to the final shear stress.

Claudin24 was 2.43-fold higher and 0.27-fold lower 6 and 24 hours, respectively, after the exposure to 3 dyne/cm² in comparison to the static control and PPIA. Thus, Claudin24 was also significantly downregulated with an increased duration of exposure to the final shear stress.

Claudin25 was 0.28-fold downregulated after a 6-hour-exposure and 0.79-fold downregulated after a 24-hour-exposure to 3 dyne/cm² in relation to the static control and PPIA. Hence, Claudin25-expression was slightly increased from 6 to 24 hours of exposure to the final shear stress.

Jam1 showed a 0.57-fold downregulation after 6 hours and a 0.36-fold downregulation after 24 hours of exposure to 3 dyne/cm² compared to the static control and PPIA. Therefore, Jam1 did not show a significant trend in its mRNA expression with a prolonged duration of exposure to 3 dyne/cm².

Jam2 was 0.32-fold decreased and 0.13-fold decreased after the exposure to 3 dyne/cm² related to the static control and PPIA after 6 and 24 hours, respectively. Consequently, Jam2 did not show a significant variation in its mRNA expression from a 6- to a 24-hour-exposure to the final shear stress.

Jam3 was 0.67-fold downregulated after a 6-hour-exposure and 0.57-fold downregulated after a 24-hour-exposure to 3 dyne/cm² in relation to the static control and PPIA. Hence, Jam3 was not significantly changed in its mRNA expression from 6 to 24 hours of exposure to the final shear stress.
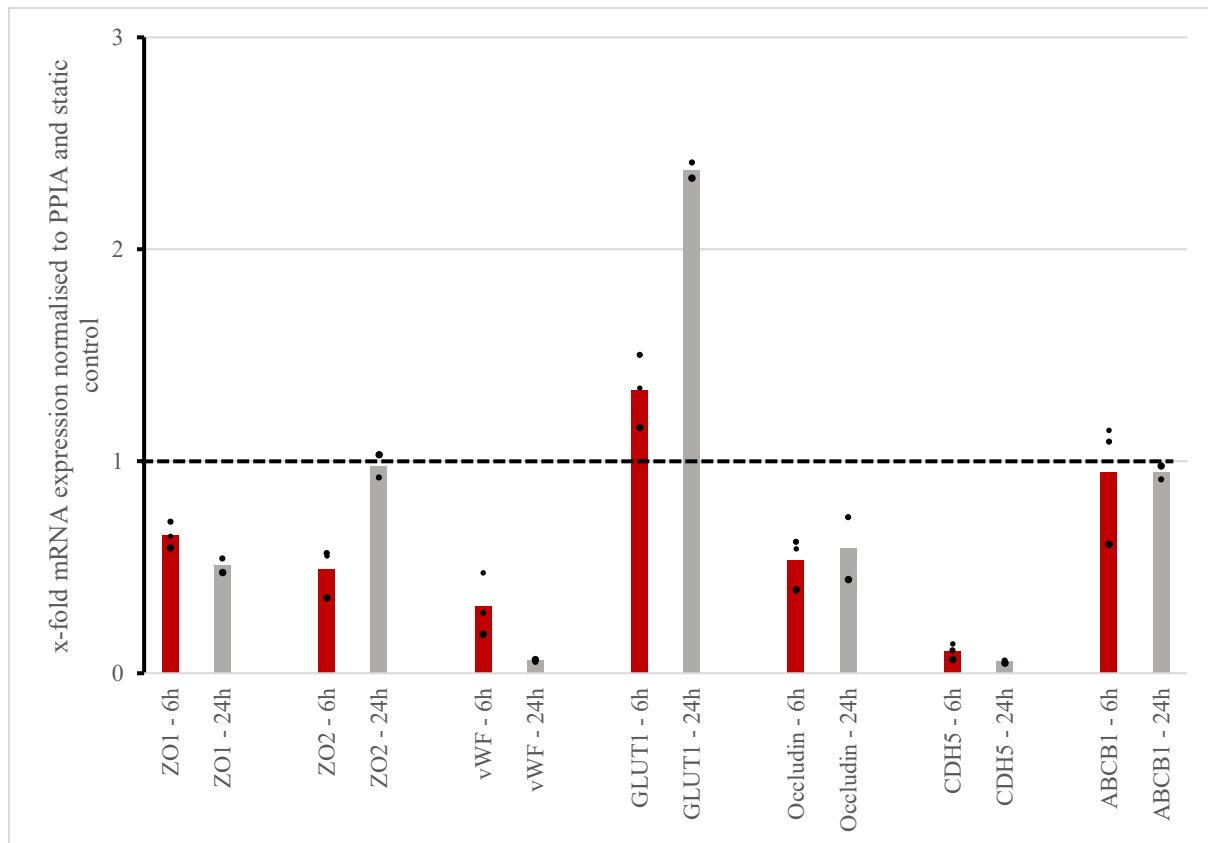
Figure 88: Bar graph 4 with trending mRNA expression level changes for 3 dyne/cm² after 6 and 24 hours
(Red) 6 hours. (Gray) 24 hours. n=3: ZO1, ZO2, vWF, GLUT1, Occludin, CDH5, ABCB1 – 6 hours; n=2: ZO1,
ZO2, vWF, GLUT1, Occludin, CDH5, ABCB1 – 24 hours.

ZO1 was 0.65-fold lower after a 6-hour-exposure and 0.51-fold lower after a 24-hour-exposure
to 3 dyne/cm² compared to the static control and PPIA. Hence, ZO1 was not significantly
changed in its mRNA expression from 6 to 24 hours of exposure to the final shear stress.

ZO2 presented a 0.49-fold downregulation after a 6-hour-exposure and did not show a
significant difference in its mRNA expression after a 24-hour-exposure to 3 dyne/cm² in
comparison to the static control and PPIA. Therefore, ZO2 was slightly upregulated with a
prolonged duration of exposure to 3 dyne/cm².

vWF was 0.31-fold lower after a 6-hour-exposure and 0.06-fold lower after a 24-hour-exposure
to 3 dyne/cm² related to the static control and PPIA. As a result, vWF was downregulated with
an increased duration of exposure to the final shear stress.

GLUT1 was 1.34-fold higher after a 6-hour-exposure and 2.37-fold higher after a 24-hour-
exposure to 3 dyne/cm² compared to the static control and PPIA. Therefore, GLUT1 was
upregulated from a 6- to a 24-hour-exposure to 3 dyne/cm².

Occludin was 0.53-fold downregulated after a 6-hour-exposure and 0.59-fold downregulated
after a 24-hour-exposure to 3 dyne/cm² in relation to the static control and PPIA. Therefore,

Occludin did not show a significant difference in its mRNA expression with an increased final shear stress duration.

CDH5 was 0.1-fold lower after a 6-hour-exposure and 0.055-fold lower after a 24-hour-exposure to 3 dyne/cm² in comparison to the static control and PPIA. Thus, CDH5 showed a downregulation in its mRNA expression from a 6- to a 24-hour-exposure to the final shear stress.

ABCB1 did not show a significant difference in its mRNA expression after 6 and 24 hours of exposure to 3 dyne/cm² compared to the static control and PPIA. Hence, ABCB1-expression did also not change from 6 to 24 hours of exposure to 3 dyne/cm².

Figure 89: Bar graph 5 with trending mRNA expression level changes for 3 dyne/cm² after 6 and 24 hours (Red) 6 hours. (Gray) 24 hours. n=3: MRP1, MRP2, MRP3, MRP4, MRP5, BCRP, MarvelD3, CAT1, ENT1 – 6 hours; n=2: MRP1, MRP2, MRP3, MRP4, MRP5, BCRP, MarvelD3, CAT1, ENT1 – 24 hours.

MRP1 was 0.49-fold downregulated after a 6-hour-exposure and 0.84-fold downregulated after a 24-hour-exposure to 3 dyne/cm² compared to the static control and PPIA. Consequently, there was a slight upregulation in MRP1-expression with an increased duration of exposure to 3 dyne/cm².

MRP2 was 1.33-fold higher after a 6-hour-exposure and 4.06-fold higher after a 24-hour-exposure to 3 dyne/cm² in comparison to the static control and PPIA. Thus, MRP2 showed a

significant upregulation in the mRNA expression from 6 to 24 hours of exposure to the final shear stress.

MRP3 was 1.56-fold upregulated after 6 hours and 0.24-fold downregulated after a 24-hour-exposure to 3 dyne/cm² in comparison to the static control and PPIA. Therefore, MRP3 was downregulated from 6 to 24 hours of exposure to 3 dyne/cm².

MRP4 was 0.71-fold lower after a 6-hour-exposure and 0.56-fold lower after a 24-hour-exposure to 3 dyne/cm² related to the static control and PPIA. As a result, MRP4 did not reveal a significant difference in its mRNA expression from 6 to 24 hours of exposure to the final shear stress.

MRP5 was 0.67-fold decreased after a 6-hour-exposure and 2.06-fold increased after a 24-hour-exposure to 3 dyne/cm² in relation to the static control and PPIA. Consequently, MRP5 showed an upregulation in its mRNA expression from 6 to 24 hours of exposure to the final shear stress.

BCRP displayed a 1.29-fold upregulation 6 hours after final shear stress exposure and a 0.70-fold downregulation after a 24-hour-exposure to 3 dyne/cm² compared to the static control and PPIA. Hence, BCRP showed a downregulation in its mRNA expression with an increased duration of exposure to the final shear stress.

MarvelD3 was 0.74-fold downregulated after a 6-hour-exposure and 2.06-fold upregulated after a 24-hour-exposure to 3 dyne/cm² in relation to the static control and PPIA. Hence, MarvelD3 was upregulated from 6 to 24 hours of exposure to 3 dyne/cm².

CAT1 was 1.53-fold higher 6 hours after final shear stress induction and 3.19-fold higher after a 24-hour-exposure to 3 dyne/cm² compared to the static control and PPIA. Consequently, there was an increase in the mRNA expression of CAT1 from 6 to 24 hours of exposure to the final shear stress.

ENT1 was 0.79-fold downregulated 6 hours after final shear stress induction and did not reveal a significant change in its mRNA expression after a 24-hour-exposure to 3 dyne/cm² compared to the static control and PPIA. Thus, there was no significant variation in the mRNA expression of ENT1 with an increased duration of exposure to 3 dyne/cm².

Figure 90: Bar graph 6 with trending mRNA expression level changes for 3 dyne/cm² after 6 and 24 hours (Red) 6 hours. (Gray) 24 hours. n=3: SELE, InR, LAT1, LRP1, LRP8, MCT1, MCT8, TfR, VEGFA, WWC2 – 6 hours; n=2: SELE, InR, LAT1, LRP1, LRP8, MCT1, MCT8, TfR, VEGFA, WWC2 – 24 hours.

SELE was 6.34-fold higher after a 6-hour-exposure and 1.3-fold higher after a 24-hour-exposure to 3 dyne/cm² in relation to the static control and PPIA. Hence, SELE showed a decrease in its mRNA expression from 6 to 24 hours of exposure to 3 dyne/cm².

InR was 0.81-fold lower after a 6-hour-exposure and 1.32-fold higher after a 24-hour-exposure to 3 dyne/cm² in comparison to the static control and PPIA. Thus, InR was upregulated with an increased duration of exposure to the final shear stress.

LAT1 was 4.75-fold upregulated after 6 hours and 2.95-fold upregulated after 24 hours of exposure to 3 dyne/cm² compared to the static control and PPIA. Therefore, LAT1 was downregulated with a prolonged duration of exposure to 3 dyne/cm².

LRP1 was 0.35-fold decreased and 0.41-fold decreased after the exposure to 3 dyne/cm² related to the static control and PPIA after 6 and 24 hours, respectively. Thus, there was no significant change in the mRNA expression of LRP1 from 6 to 24 hours of exposure to the final shear stress.

LRP8 revealed a 0.49-fold downregulation after 6 hours and a 0.71-fold downregulation after 24 hours of exposure to 3 dyne/cm² in comparison to the static control and PPIA. Hence, there

156

was no significant change in LRP8-expression with an increased duration of exposure to the final shear stress.

MCT1 was 1.27-fold upregulated after a 6-hour-exposure and was not significantly changed in its mRNA expression after a 24-hour-exposure to 3 dyne/cm² in relation to the static control and PPIA. Hence, MCT1-expression was slightly decreased from 6 to 24 hours of exposure to the final shear stress.

MCT8 showed a 1.55-fold upregulation after 6 hours and a 2.89-upregulation after 24 hours of exposure to 3 dyne/cm² compared to the static control and PPIA. Therefore, MCT8 was upregulated with a prolonged duration of exposure to 3 dyne/cm².

TfR was 0.66-fold decreased and 0.77-fold decreased after the exposure to 3 dyne/cm² related to the static control and PPIA after 6 and 24 hours, respectively. Consequently, TfR did not present a significant variation in its mRNA expression from a 6- to a 24-hour-exposure to the final shear stress.

VEGFA was 2.22-fold upregulated after a 6-hour-exposure and 5.31-fold upregulated after a 24-hour-exposure to 3 dyne/cm² in relation to the static control and PPIA. Hence, VEGFA was increased in its mRNA expression from 6 to 24 hours of exposure to the final shear stress.

WWC2 was 0.47-fold lower after 6 hours and 0.38-fold lower after 24 hours of exposure to 3 dyne/cm² in comparison to PPIA and the static control. Thus, there was no significant change in WWC2-expression with a prolonged duration of exposure to 3 dyne/cm².

Figure 91: Bar graph 7 with trending mRNA expression level changes for 3 dyne/cm² after 6 and 24 hours (Red) 6 hours. (Gray) 24 hours. n=3: CK18, CK19, AQP1, AQP3, AQP5, AQP7, AQP11, MUC1A, MUC1B, MUC18 – 6 hours; n=2: CK8, CK18, CK19, AQP1, AQP3, AQP5, AQP7, AQP11, MUC1A, MUC1B, MUC18 – 24 hours; CK8 – 6 hours.

CK8 was 0.24-fold lower after a 6-hour-exposure and 0.50-fold lower after a 24-hour-exposure to 3 dyne/cm² compared to the static control and PPIA. Hence, CK8 did not show a significant change in its mRNA expression from a 6- to a 24-hour-exposure to the final shear stress.

CK18 revealed a 0.3-fold downregulation after a 6-hour-exposure and a 0.42-fold downregulation after a 24-hour-exposure to 3 dyne/cm² in comparison to the static control and PPIA. Thus, there was no significant variation in CK18-expression with a prolonged duration of exposure to 3 dyne/cm².

CK19 was 0.27-fold lower after a 6-hour-exposure and 0.35-fold lower after a 24-hour-exposure to 3 dyne/cm² related to the static control and PPIA. As a result, CK19 was not significantly altered in its mRNA expression with an increased duration of exposure to the final shear stress.

AQP1 was 0.68-fold decreased in its mRNA expression after a 6-hour-exposure and 1.99-fold increased after a 24-hour-exposure to 3 dyne/cm² in comparison to the static control and PPIA. Consequently, there was an upregulation of AQP1 from 6 to 24 hours of exposure to the final shear stress.

AQP3 was 1.95-fold higher after a 6-hour-exposure and did not present a significant change in its mRNA expression after a 24-hour-exposure to 3 dyne/cm² compared to the static control and PPIA. Therefore, AQP3 was downregulated from a 6- to a 24-hour-exposure to 3 dyne/cm².

AQP5 was 0.21-fold downregulated after a 6-hour-exposure and 0.20-fold downregulated after a 24-hour-exposure to 3 dyne/cm² in comparison to the static control and PPIA. Thus, AQP5 did not show a significant change in its mRNA expression from a 6- to a 24-hour-exposure to the final shear stress.

AQP7 was 0.48-fold decreased after a 6-hour-exposure to the final shear stress and 0.51-fold decreased after a 24-hour-exposure to 3 dyne/cm² in relation to the static control and PPIA. Therefore, AQP7 did not show a significant difference in its mRNA expression with an increased final shear stress duration.

There was no significant change in MUC1A-expression after 6 and 24 hours of exposure to 3 dyne/cm² compared to the static control and PPIA. Hence, there was also no significant variation in the mRNA expression of MUC1A between 6 and 24 hours of exposure to 3 dyne/cm².

MUC1B was 0.82-fold lower after a 6-hour-exposure and did not display a significant difference in its mRNA expression after a 24-hour-exposure to 3 dyne/cm² related to the static control and PPIA. As a result, MUC1B also did not show a significant trend with an increased duration of exposure to the final shear stress.

MUC18 was 0.54-fold decreased after 6 hours and 1.13-fold increased after 24 hours of exposure to 3 dyne/cm² in comparison to PPIA and the static control. Consequently, there was an upregulation of MUC18 from 6 to 24 hours of exposure to 3 dyne/cm².

Figure 92: Bar graph 8 with trending mRNA expression level changes for 3 dyne/cm² after 6 and 24 hours (Red) 6 hours. (Gray) 24 hours. n=3: MUC20, b catenin tv1, b catenin tv4, VIMENTIN, FIBRONECTIN, S100A4 tv1, MFSD2A, Claudin25-1, Claudin25 tv7, RAGE – 6 hours; n=2: MUC20, b catenin tv1, b catenin tv4, VIMENTIN, FIBRONECTIN, S100A4 tv1, MFSD2A, Claudin25-1, Claudin25 tv7, RAGE – 24 hours.

There was no significant variation in MUC20-expression after a 6-hour-exposure and a 2.68-fold increase after a 24-hour-exposure to 3 dyne/cm² compared to the static control and PPIA. Hence, MUC20 was upregulated from 6 to 24 hours of exposure to the final shear stress.

B catenin tv1 presented a 0.44-fold downregulation after a 6-hour-exposure and did not show a significant difference after a 24-hour-exposure to 3 dyne/cm² in comparison to the static control and PPIA. Therefore, b catenin tv1 was slightly upregulated with a prolonged duration of exposure to 3 dyne/cm².

B catenin tv4 was 0.58-fold lower after a 6-hour-exposure and 0.41-fold lower after a 24-hour-exposure to 3 dyne/cm² related to the static control and PPIA. As a result, b catenin tv4 was not significantly changed in its mRNA expression with an increased duration of exposure to the final shear stress.

VIMENTIN was 0.52-fold decreased after a 6-hour-exposure and 1.98-fold increased after a 24-hour-exposure to 3 dyne/cm² in comparison to the static control and PPIA. Consequently, there was an upregulation in the mRNA expression of VIMENTIN from 6 to 24 hours of exposure to the final shear stress.

FIBRONECTIN was 0.33-fold lower after a 6-hour-exposure and 0.59-fold lower after a 24-hour-exposure to 3 dyne/cm² compared to the static control and PPIA. Therefore, FIBRONECTIN was not significantly altered in its mRNA expression from a 6- to a 24-hour-exposure to 3 dyne/cm².

S100A4 tv1 was 0.24-fold downregulated after a 6-hour-exposure and 0.14-fold downregulated after a 24-hour-exposure to 3 dyne/cm² in relation to the static control and PPIA. Therefore, S100A4 tv1 did not show a significant difference in its mRNA expression with an increased final shear stress duration.

MDSF2A was 2.9-fold higher after a 6-hour-exposure and 25.05-fold higher after a 24-hour-exposure to 3 dyne/cm² in comparison to the static control and PPIA. Thus, MFSD2A showed a significant upregulation in its mRNA expression from a 6- to a 24-hour-exposure to the final shear stress.

Claudin25-1 revealed a 0.44-fold downregulation after 6 hours and a 0.46-fold downregulation after 24 hours of exposure to 3 dyne/cm² compared to the static control and PPIA. Hence, Claudin25-1 did not present a significant difference in its mRNA expression between 6 and 24 hours of exposure to 3 dyne/cm².

Claudin25 tv7 was 1.6-fold increased and 8.55-fold increased after a 6- and a 24-hour-exposure to 3 dyne/cm² in relation to PPIA and the static control, respectively. Therefore, Claudin25 tv7 was significantly increased in its mRNA expression with a prolonged duration of exposure to the final shear stress.

RAGE was 0.52-fold lower after 6 hours and 1.74-fold higher after 24 hours of exposure to 3 dyne/cm² compared to PPIA and the static control. As a result, there was an upregulation of RAGE from 6 to 24 hours of exposure to 3 dyne/cm².

4.5.6 mRNA expression level changes at static control conditions at different points in time

The well experiments served as static control as setup without flow (0 dyne/cm²). These values were compared to the flow experiments and normalised to 1, displayed as the dotted line in the sections 4.5.1 to 4.5.5. In the following, the potency values of the static controls were utilised for a comparison within the static control group over time. The cell-lysates for subsequent qPCR were obtained at the same points of lysis as the flow experiments, which were taken after 6 hours of exposure on day 2 and 24 hours of exposure on day 3 in the last set of experiments (3.8.14). In addition, the cell-lysates of experiment no. 7 (3.8.4) were included, which were taken after 96 hours of final shear stress exposure in the flow setup. The up- and downregulations of the targets related to the ΔCt values of PPIA, set to 1 at each time point, are visualised in Figure 94 to Figure 101 and the timeline of cell lysis is summarised in Figure 93.
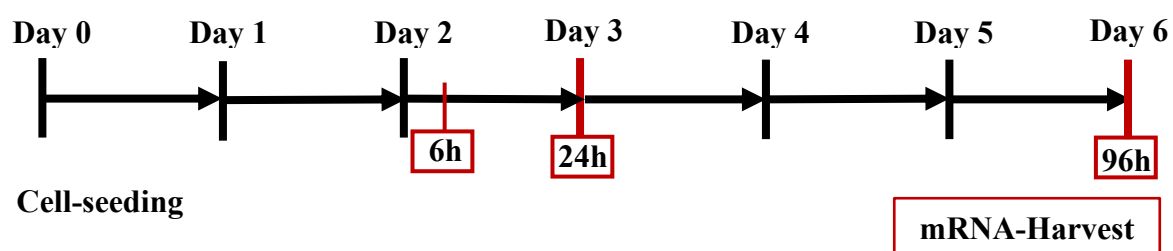
Figure 93: Experimental setup of mRNA-harvest for 0 dyne/cm² after 6 (day 2), 24 (day 3) and 96 hours (day 6)
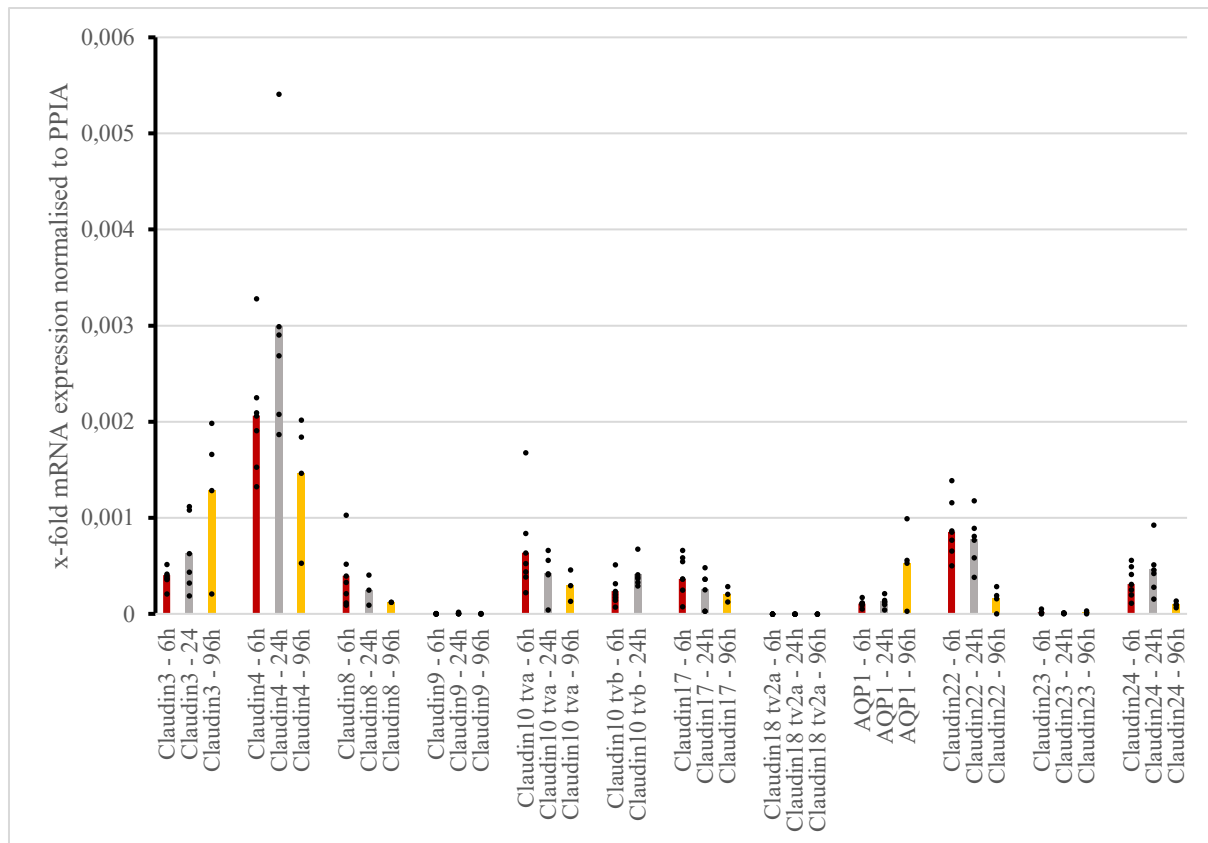
Figure 94: Bar graph 1 with trending mRNA expression level changes for 0 dyne/cm² after 6 (day 2), 24 (day 3) and 96 hours (day 6). (Red) 6 hours. (Gray) 24 hours. (Yellow) 96 hours. n=7: Claudin3, Claudin4, Claudin8, Claudin9, Claudin10 tva, Claudin17, Claudin18 tv2a, AQP1, Claudin22, Claudin24 – 6 hours; n=6: Claudin10 tva – 6 hours; n=5: Claudin3, Claudin4, Claudin9, Claudin10 tvb, Claudin17, Claudin18 tv2a, Claudin22, Claudin23, Claudin24 – 24 hours; Claudin23 – 6 hours; n=4: Claudin10 tva, AQP1 – 24 hours; n=3: Claudin3, Claudin9, Claudin18 tv2a, AQP1, Claudin22, Claudin24 – 96 hours; n=2: Claudin8 – 24 hours; Claudin10 tva, Claudin17, Claudin23 – 96 hours; n=1: Claudin8 – 96 hours

Claudin3 was 0.0004-fold lower after 6 hours, 0.00063-fold lower after 24 hours and 0.0013-fold lower after 96 hours in static conditions related PPIA. Hence, Claudin3 did not show a significant trend from 6 to 24 hours, however, displayed an upregulation from 24 to 96 hours.

Claudin4 was 0.0021-fold lower after 6 hours, 0.003-fold lower after 24 hours and 0.0015-fold lower after 96 hours in static conditions in comparison to PPIA. Hence, Claudin4 did not show a significant trend in its mRNA expression among the different points of cell lysis.

Claudin8 was 0.0004-fold lower after 6 hours, 0.00025-fold lower after 24 hours and 0.00012-fold lower after 96 hours in static conditions in relation to PPIA. Hence, Claudin8 did not present a significant trend in its mRNA expression between 6 and 24 hours and between 24 and 48 hours.

Claudin9 was 0.000003-fold lower after 6 hours, 0.000073-fold lower after 24 hours and 0.0000037-fold lower after 96 hours in static conditions related to PPIA. Thus, there was no significant difference in Claudin9-expression between 6 and 24 hours and between 24 and 96 hours.

Claudin10 tva was 0.00064-fold lower after 6 hours, 0.00042-fold lower after 24 hours and 0.0003-fold lower after 96 hours in the well experiments compared to PPIA. As a result, there was no variation in Claudin10 tva-expression between 6 and 24 hours as well as between 24 and 96 hours.

Claudin10 tvb was 0.00024-fold lower after 6 hours and 0.00041-fold lower after 24 hours in the well experiments in relation to PPIA. The qPCR of the 96-hour-values did not function for Claudin10 tvb. There was no difference in the mRNA expression of Claudin10 tvb between 6 and 24 hours.

Claudin17 was 0.00036-fold lower after 6 hours, 0.00025-fold lower after 24 hours and 0.00021-fold lower after 96 hours in the well experiments compared to PPIA. Thus, there was no significant change in Claudin17-expression in the well experiments among the different experiment durations.

Claudin18 tv2a was 4.425E-298-fold lower after 6 hours, 3.72E-298-fold lower after 24 hours and 4.45E-298-fold lower after 96 hours in the well experiments in comparison to PPIA. Consequently, there was no significant difference in Claudin18 tv2a-expression between 6 and 24 hours and between 24 and 96 hours in static conditions.

AQP1 was 0.00011-fold lower after 6 hours, 0.00013-fold lower after 24 hours and 0.00053-fold lower after 96 hours in static conditions compared to PPIA. Accordingly, there was no significant change in the mRNA expression of AQP1 between 6 and 24 hours and there was a slight upregulation from 24 to 96 hours in the well experiments.

Claudin22 was 0.00085-fold lower after 6 hours, 0.00077-fold lower after 24 hours and 0.00016-fold lower after 96 hours in static conditions compared to PPIA. Therefore, Claudin22-expression did not significantly change from 6 to 24 hours and was downregulated from 24 to 96 hours.

Claudin23 was 0.000017-fold lower after 6 hours, 0.0000099-fold lower after 24 hours and 0.000018-fold lower after 96 hours in the well experiments related to PPIA. Hence, Claudin23 did not show a significant trend in its mRNA expression between 6 and 24 hours as well as between 24 and 96 hours.

Claudin24 was 0.00031-fold lower after 6 hours, 0.00046-fold lower after 24 hours and 0.000098-fold lower after 96 hours in static conditions in comparison to PPIA. Hence, Claudin24-expression was not significantly changed from 6 to 24 hours and was downregulated from 24 to 96 hours.
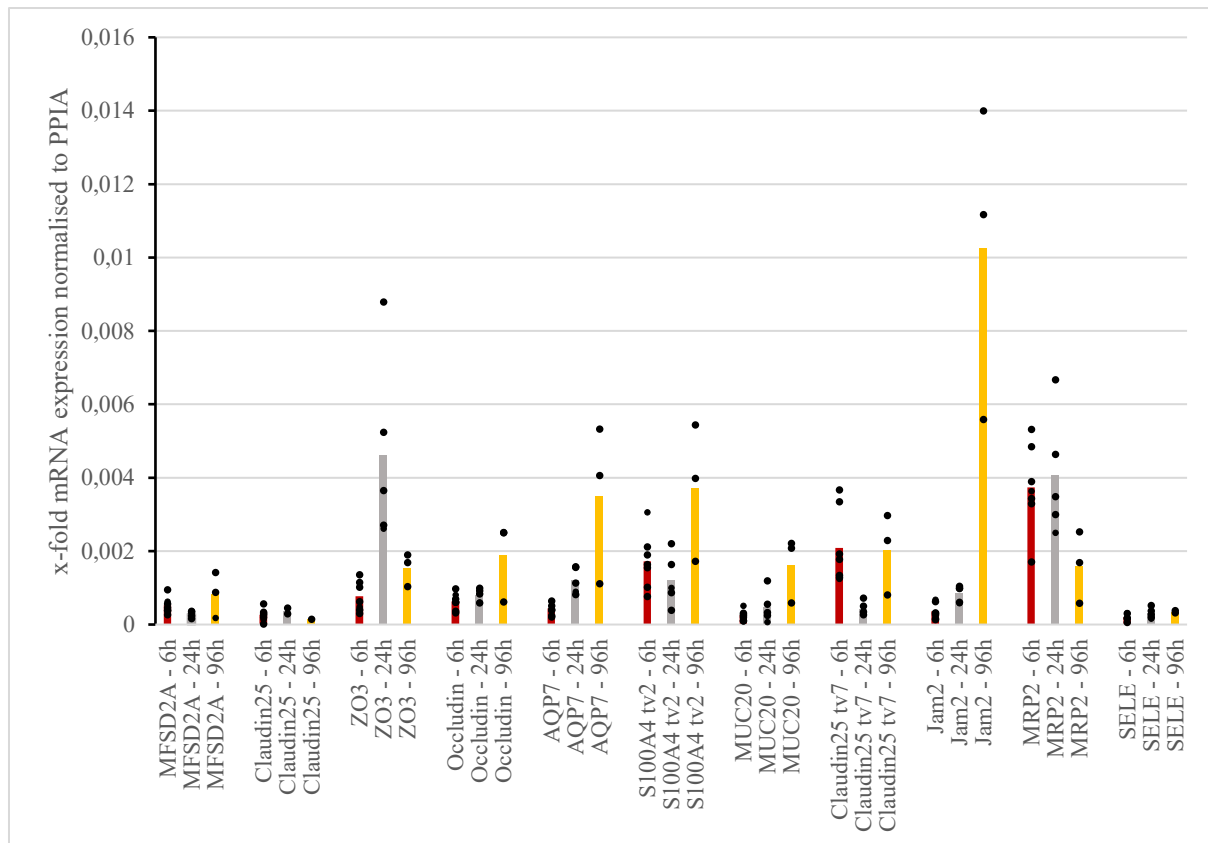
Figure 95: Bar graph 2 with trending mRNA expression level changes for 0 dyne/cm² after 6 (day 2), 24 (day 3) and 96 hours (day 6). (Red) 6 hours. (Gray) 24 hours. (Yellow) 96 hours. n=7: MFSD2A, Claudin25, ZO3, Occludin, AQP7, S100A4 tv2, MUC20, Claudin25 tv7, Jam2, MRP2 – 6 hours; n=5: MFSD2A, ZO3, Occludin, AQP7, MUC20, Claudin25 tv7, Jam2 MRP2, SELE – 24 hours; SELE – 6 hours; n=3: MFSD2A, ZO3, Occludin, AQP7, S100A4 tv2, MUC20, Claudin25 tv7, Jam2, MRP2 – 96 hours; n=2: Claudin25 – 24 hours, SELE – 96 hours; n=1: Claudin25 – 96 hours.

MFSD2A was 0.00052-fold lower after 6 hours, 0.00029-fold lower after 24 hours and 0.00083-fold lower after 96 hours in the well experiments related to PPIA. Hence, MFSD2A did not present a significant trend between 6 and 24 hours and was increased in its mRNA expression from 24 to 96 hours in the well experiments.

Claudin25 was 0.00027-fold lower after 6 hours, 0.00038-fold lower after 24 hours and 0.00015-fold lower after 96 hours in static conditions related to PPIA. Thus, there was no significant difference in Claudin25-expression between 6 and 24 hours and between 24 and 96 hours.

ZO3 was 0.00077-fold lower after 6 hours, 0.0046-fold lower after 24 hours and 0.0015-fold lower after 96 hours in the well experiments compared to PPIA. As a result, there was an upregulation in ZO3-expression from 6 to 24 hours and a downregulation from 24 to 96 hours.

Occludin was 0.00063-fold lower in its mRNA expression after 6 hours, 0.00079-fold lower after 24 hours and 0.0019-fold lower in the well experiments in relation to PPIA. Thus, there

was no significant difference in Occludin-expression between 6 and 24 hours and there was a slight upregulation from 24 to 96 hours.

AQP7 was 0.00044-fold lower after 6 hours, 0.0012-fold lower after 24 hours and 0.0035-fold lower after 96 hours in static conditions compared to PPIA. Thus, there was an upregulation in AQP7-expression from 6 to 24 hours and no further significant trend from 24 to 96 hours in the well experiments.

S100A4 tv2 was 0.0017-fold lower after 6 hours, 0.0012-fold lower after 24 hours and 0.0037-fold lower after 96 hours in the well experiments in comparison to PPIA. Consequently, there was no significant difference in S100A4 tv2-expression between 6 and 24 hours and a slight upregulation from 24 to 96 hours.

MUC20 was 0.00025-fold lower after 6 hours, 0.00049-fold lower after 24 hours and 0.0016-fold lower after 96 hours in static conditions compared to PPIA. Thus, there was no significant change in the mRNA expression of MUC20 between 6 and 24 hours and a slight upregulation from 24 to 96 hours in the well experiments.

Claudin25 tv7 was 0.0021-fold lower after 6 hours, 0.00043-fold lower after 24 hours and 0.002-fold lower after 96 hours in static conditions compared to PPIA. Therefore, Claudin25 tv7-expression was downregulated from 6 to 24 hours and was upregulated from 24 to 96 hours.

Jam2 was 0.00036-fold lower after 6 hours, 0.00085-fold lower after 24 hours and 0.01-fold lower after 96 hours in the well experiments in comparison to PPIA. Hence, Jam2 displayed upregulations in its mRNA expression from 6 to 24 hours and from 24 to 96 hours in static conditions.

MRP2 was 0.0037-fold lower after 6 hours, 0.0041-fold lower after 24 hours and 0.0016-fold lower after 96 hours in static conditions in comparison to PPIA. Hence, MRP2-expression was not significantly changed between 6 and 24 hours and between 24 and 96 hours.

SELE was 0.00021-fold lower after 6 hours, 0.00031-fold lower after 24 hours and 0.00035-fold lower after 96 hours in the well experiments related to PPIA. Hence, SELE did not present a significant trend in its mRNA expression between 6 and 24 hours and between 24 and 96 hours.
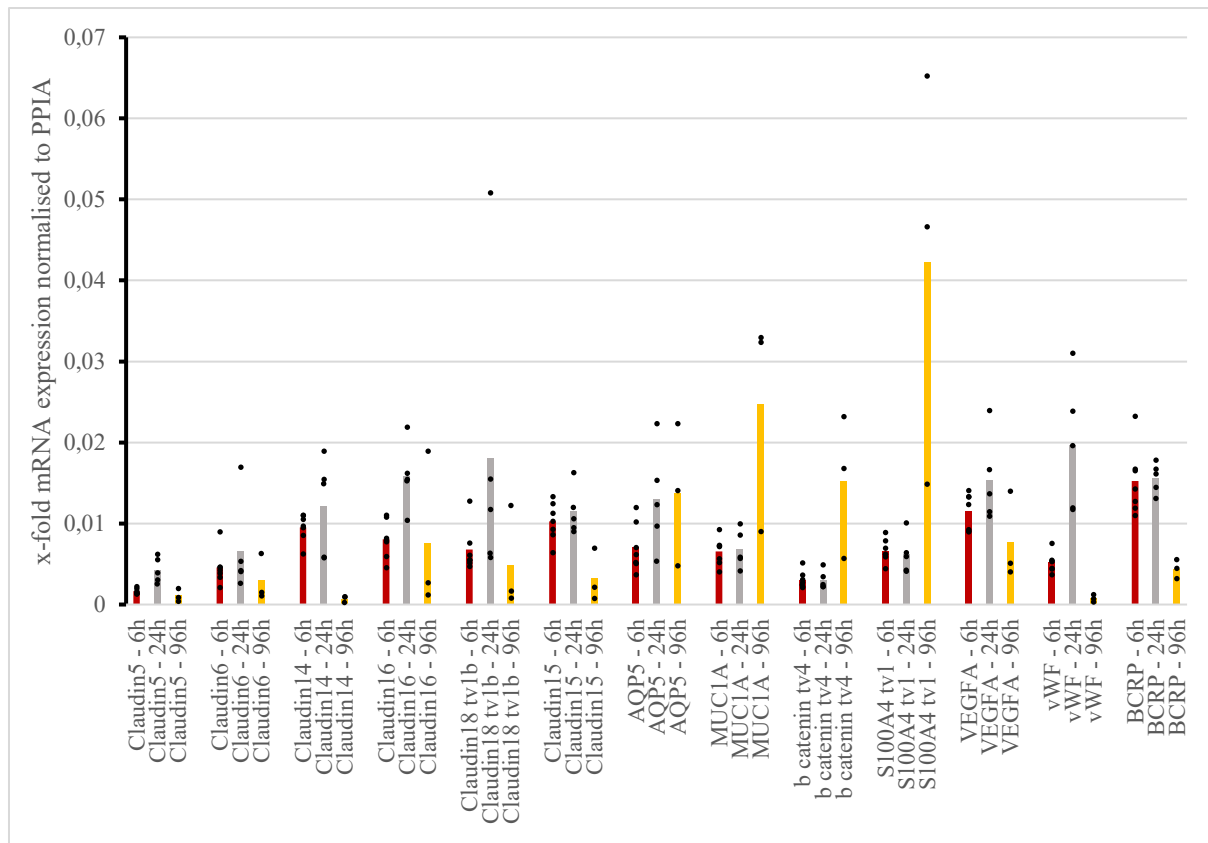
Figure 96: Bar graph 3 with trending mRNA expression level changes for 0 dyne/cm² after 6 (day 2), 24 (day 3) and 96 hours (day 6). (Red) 6 hours. (Gray) 24 hours. (Yellow) 96 hours. n=7: Claudin5, Claudin6, Claudin14, Claudin18 tv1b, Claudin15, AQP5, MUC1A, b catenin tv4, S100A4 tv1, VEGFA, vWF, BCRP – 6 hours; n=5: Claudin5, Claudin6, Claudin14, Claudin18 tv1b, Claudin15, AQP5, MUC1A, b catenin tv4, S100A4 tv1, VEGFA, vWF, BCRP – 24 hours; n=3: Claudin5, Claudin6, Claudin14, Claudin18 tv1b, Claudin15, AQP5, MUC1A, b catenin tv4, S100A4 tv1, VEGFA, vWF, BCRP – 96 hours.

Claudin5 was 0.0016-fold lower after 6 hours, 0.0043-fold lower after 24 hours and 0.0011-fold lower after 96 hours in the well experiments related to PPIA. Hence, Claudin5 was slightly upregulated from 6 to 24 hours and downregulated from 24 to 96 hours in the well experiments. Claudin6 was 0.0046-fold lower after 6 hours, 0.0067-fold lower after 24 hours and 0.0067-fold lower after 96 hours in static conditions related to PPIA. Thus, there was no significant difference in Claudin6-expression between 6 and 24 hours and between 24 and 96 hours. Claudin14 was 0.0095-fold lower after 6 hours, 0.012-fold lower after 24 hours and 0.00074-fold lower after 96 hours in the well experiments compared to PPIA. As a result, there was no significant trend in Claudin14-expression between 6 and 24 hours and a downregulation from 24 to 96 hours. Claudin16 was 0.0081-fold lower after 6 hours, 0.016-fold lower after 24 hours and 0.0076-fold lower after 96 hours in the well experiments in relation to PPIA. Thus, there was a slight upregulation of Claudin16 from 6 to 24 hours and a slight downregulation from 24 to 96 hours.

Claudin18 tv1b was 0.0068-fold lower after 6 hours, 0.018-fold lower after 24 hours and 0.0049-fold lower after 96 hours in static conditions compared to PPIA. Thus, there was an upregulation in Claudin18 tv1b-expression from 6 to 24 hours and a downregulation from 24 to 96 hours.

Claudin15 was 0.01-fold lower after 6 hours, 0.011-fold lower after 24 hours and 0.0033-fold lower after 96 hours in static conditions in comparison to PPIA. Consequently, there was no significant difference in Claudin15-expression between 6 and 24 hours and there was a downregulation of Claudin15 from 24 to 96 hours.

AQP5 was 0.0071-fold lower after 6 hours, 0.013-fold lower after 24 hours and 0.014-fold lower after 96 hours in static conditions compared to PPIA. Thus, there was a trend towards upregulation in AQP5-expression from 6 to 24 hours and no significant change between 24 and 96 hours.

MUC1A was 0.0066-fold lower after 6 hours, 0.0069-fold lower after 24 hours and 0.025-fold lower after 96 hours in the well experiments compared to PPIA. Therefore, MUC1A-expression was not significantly changed between 6 and 24 hours and was slightly upregulated from 24 to 96 hours.

B catenin tv4 was 0.0031-fold lower after 6 and 24 hours and 0.015-fold lower after 96 hours in the well experiments in comparison to PPIA. Hence, b catenin tv4 did not show a difference in its mRNA expression between 6 and 24 hours, however, b catenin tv4-expression was upregulated from 24 to 96 hours.

S100A4 tv1 was 0.0067-fold lower after 6 hours, 0.0062-fold lower after 24 hours and 0.042-fold lower after 96 hours in static conditions in comparison to PPIA. Hence, S100A4 tv1-expression was not significantly changed between 6 and 24 hours, nonetheless, S100A4 tv1 was upregulated from 24 to 96 hours in the well experiments.

VEGFA was 0.011-fold lower after 6 hours, 0.015-fold lower after 24 hours and 0.0077-fold lower after 96 hours in the well experiments related to PPIA. Hence, VEGFA did not display a significant trend in its mRNA expression between 6 and 24 hours, however, VEGFA was downregulated from 24 to 96 hours.

vWF was 0.0052-fold lower after 6 hours, 0.02-fold lower after 24 hours and 0.0008-fold lower after 96 hours in static conditions compared to PPIA. Accordingly, vWF-expression was upregulated from 6 to 24 hours and significantly downregulated from 24 to 96 hours in the well experiments.

BCRP was 0.015-fold lower after 6 hours, 0.016-fold lower after 24 hours and 0.0044-fold lower after 96 hours in static conditions in comparison to PPIA. Thus, BCRP did not show a significant difference between 6 and 24 hours and was downregulated from 24 to 96 hours.
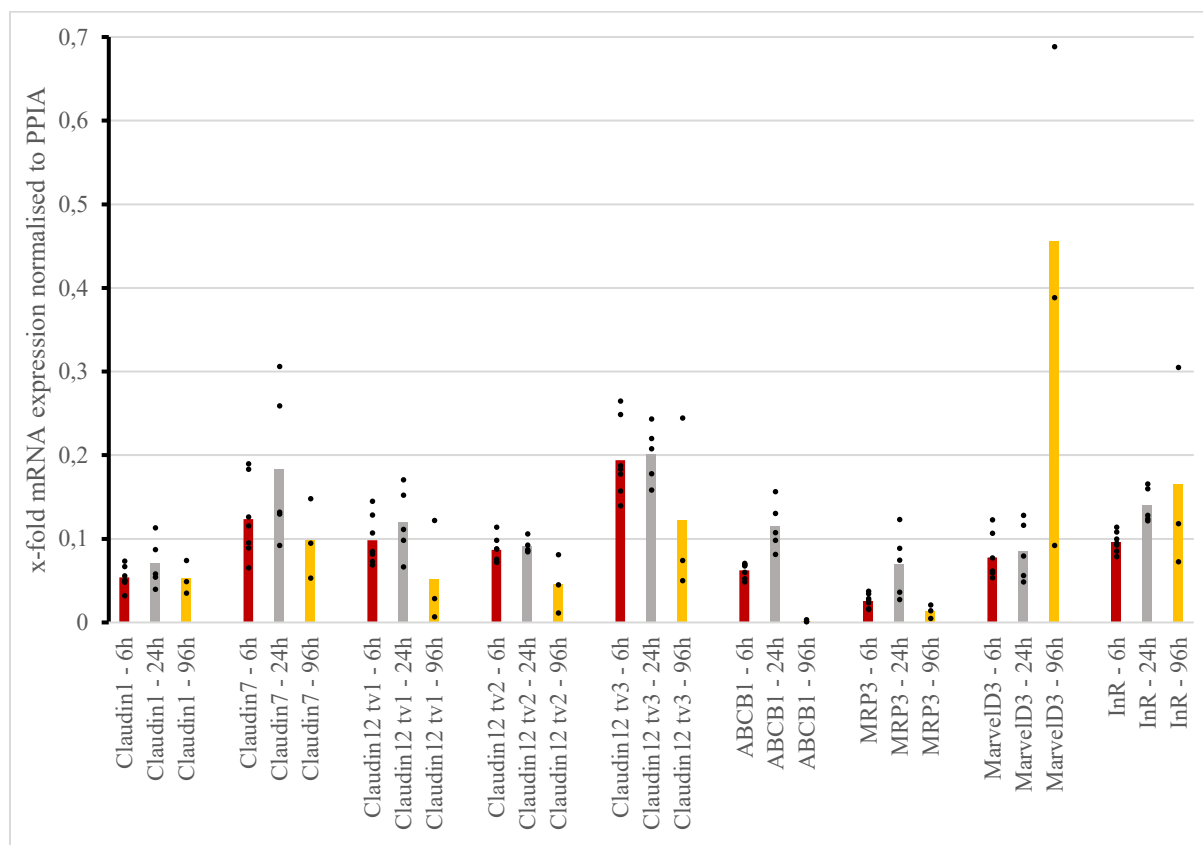
Figure 97: Bar graph 4 with trending mRNA expression level changes for 0 dyne/cm² after 6 (day 2), 24 (day 3) and 96 hours (day 6). (Red) 6 hours. (Gray) 24 hours. (Yellow) 96 hours. n=7: Claudin1, Claudin7, Claudin12 tv1, Claudin12 tv2, Claudin12 tv3, ABCB1, MRP3, MarvelD3, InR – 6 hours; n=5: Claudin1, Claudin7, Claudin12 tv1, Claudin12 tv2, Claudin12 tv3, ABCB1, MRP3, MarvelD3, InR – 24 hours; n=3: Claudin1, Claudin7, Claudin12 tv1, Claudin12 tv2, Claudin12 tv3, ABCB1, MRP3, MarvelD3, InR – 96 hours.

Claudin1 was 0.054-fold lower after 6 hours, 0.07-fold lower after 24 hours and 0.053-fold lower after 96 hours in the well experiments compared to PPIA. As a result, there was no significant trend in Claudin1-expression between 6 and 24 hours and between 24 and 96 hours. Claudin7 was 0.12-fold lower after 6 hours, 0.18-fold lower after 24 hours and 0.098-fold lower after 96 hours in static conditions in relation to PPIA. Thus, there was no significant trend in Claudin7-expression between 6 and 24 hours as well as between 24 and 96 hours.

Claudin12 tv1 was 0.098-fold lower after 6 hours, 0.12-fold lower after 24 hours and 0.052-fold lower after 96 hours in static conditions compared to PPIA. Thus, there was no significant trend in Claudin12 tv1-expression between 6 and 24 hours and there was a downregulation from 24 to 96 hours.

Claudin12 tv2 was 0.087-fold lower after 6 hours, 0.091-fold lower after 24 hours and 0.046-fold lower after 96 hours in static conditions in comparison to PPIA. Consequently, there was no significant difference in Claudin12 tv2-expression between 6 and 24 hours and a slight downregulation from 24 to 96 hours in the corresponding well experiments.

Claudin12 tv3 was 0.19-fold lower after 6 hours, 0.2-fold lower after 24 hours and 0.12-fold lower after 96 hours in static conditions compared to PPIA. Thus, there was no significant trend in Claudin12 tv3-expression from 6 to 24 hours and from 24 to 96 hours in the well experiments.

ABCB1 was 0.062-fold lower after 6 hours, 0.11-fold lower after 24 hours and 0.0018-fold lower after 96 hours in the well experiments compared to PPIA. Therefore, ABCB1-expression was slightly increased from 6 to 24 hours and decreased from 24 to 96 hours.

MRP3 was 0.026-fold lower after 6 hours, 0.07-fold lower after 24 hours and 0.013-fold lower after 96 hours in the well experiments in comparison to PPIA. Hence, MRP3 displayed an upregulation from 6 to 24 hours and a downregulation from 24 to 96 hours.

MarvelD3 was 0.077-fold lower after 6 hours, 0.086-fold lower after 24 hours and 0.46-fold lower after 96 hours in the well experiments related to PPIA. Hence, MarvelD3 did not show a significant trend in its mRNA expression between 6 and 24 hours and was upregulated from 24 to 96 hours.

InR was 0.096-fold lower after 6 hours, 0.14-fold lower after 24 hours and 0.17-fold lower after 96 hours in static conditions compared to PPIA. Accordingly, InR-expression did not significantly change among the different points in time of cell lysis.
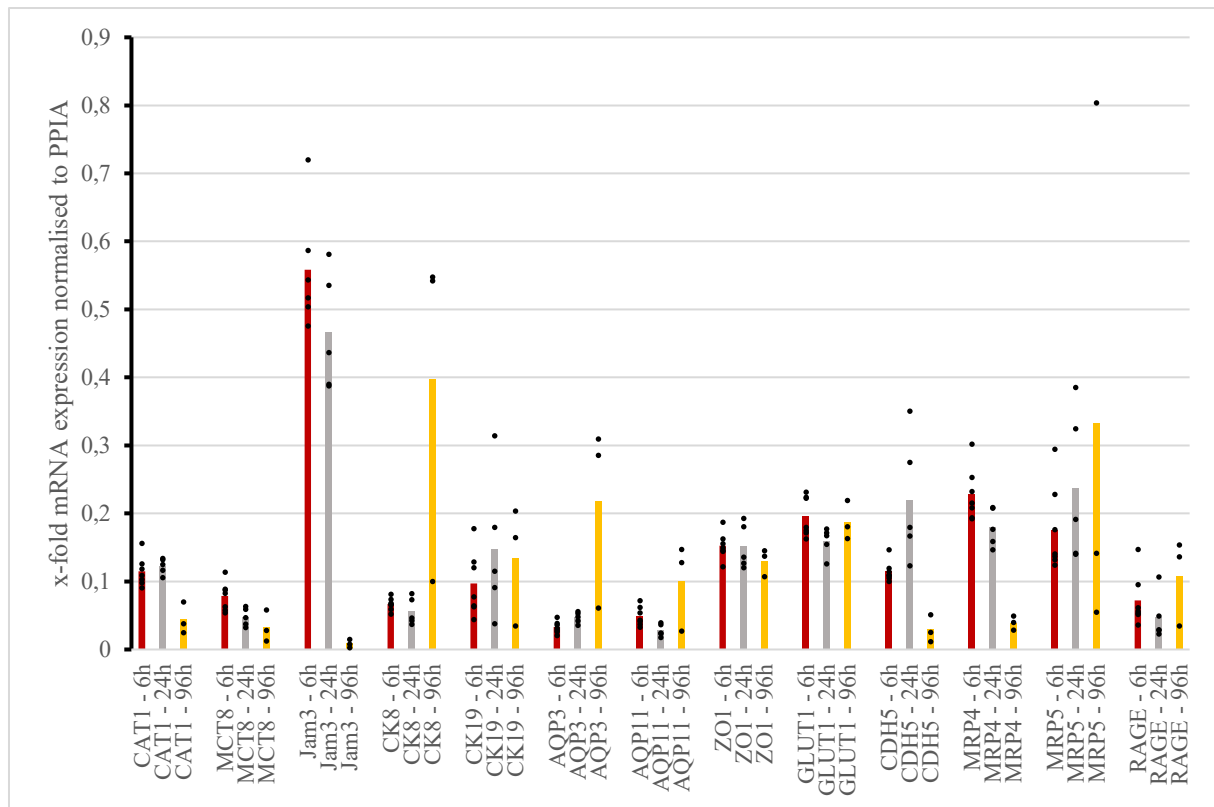
Figure 98: Bar graph 5 with trending mRNA expression level changes for 0 dyne/cm² after 6 (day 2), 24 (day 3) and 96 hours (day 6). (Red) 6 hours. (Gray) 24 hours. (Yellow) 96 hours. n=7: CAT1, MCT8, Jam3, CK8, CK19, AQP3, AQP11, ZO1, GLUT1, CDH5, MRP4, MRP5, RAGE – 6 hours; n=5: CAT1, MCT8, Jam3, CK8, CK19, AQP3, AQP11, ZO1, GLUT1, CDH5, MRP4, MRP5, RAGE – 24 hours; n=3: CAT1, MCT8, Jam3, CK8, CK19, AQP3, AQP11, ZO1, GLUT1, CDH5, MRP4, MRP5, RAGE – 96 hours.

CAT1 was 0.11-fold lower after 6 hours, 0.13-fold lower after 24 hours and 0.044-fold lower after 96 hours in static conditions compared to PPIA. Hence, CAT1 did not show a significant difference between 6 and 24 hours and was downregulated from 24 to 96 hours in the well experiments.

MCT8 was 0.078-fold lower after 6 hours, 0.048-fold lower after 24 hours and 0.033-fold lower after 96 hours in static conditions related to PPIA. Accordingly, there was a slight downregulation of MCT8 from 6 to 24 hours and no further significant difference in the mRNA expression of MCT8 between 24 and 96 hours.

Jam3 was 0.56-fold lower after 6 hours, 0.47-fold lower after 24 hours and 0.0088-fold lower after 96 hours in the well experiments compared to PPIA. As a result, there was no significant trend in Jam3-expression between 6 and 24 hours and a significant downregulation from 24 to 96 hours.

CK8 was 0.067-fold lower after 6 hours, 0.057-fold lower after 24 hours and 0.4-fold lower after 96 hours in the well experiments in relation to PPIA. Thus, there was no significant change in CK8-expression between 6 and 24 hours and there was an upregulation from 24 to 96 hours.

CK19 was 0.097-fold lower after 6 hours, 0.15-fold lower after 24 hours and 0.13-fold lower after 96 hours in static conditions compared to PPIA. Thus, there was no significant trend in CK19-expression among the different points in time of cell lysis.

AQP3 was 0.033-fold lower after 6 hours, 0.047-fold lower after 24 hours and 0.22-fold lower after 96 hours in the well experiments in comparison to PPIA. Consequently, there was no significant difference in AQP3-expression between 6 and 24 hours and there was an upregulation from 24 to 96 hours in the corresponding well experiments.

AQP11 was 0.049-fold lower after 6 hours, 0.029-fold lower after 24 hours and 0.1-fold lower after 96 hours in static conditions compared to PPIA. Thus, there was no significant trend in AQP11-expression between 6 and 24 hours and an upregulation from 24 to 96 hours.

ZO1 was 0.15-fold lower after 6 and 24 hours as well as 0.13-fold lower after 96 hours in the well experiments compared to PPIA. Therefore, ZO1-expression was not significantly changed among the three points in time of cell lysis.

GLUT1 was 0.2-fold lower after 6 hours, 0.16-fold lower after 24 hours and 0.19-fold lower after 96 hours in static conditions in comparison to PPIA. Hence, GLUT1 did not show a significant difference in its mRNA expression between 6 and 24 hours as well as between 24 and 96 hours.

CDH5 was 0.12-fold lower after 6 hours, 0.22-fold lower after 24 hours and 0.03-fold lower after 96 hours in static conditions in comparison to PPIA. Hence, CDH5-expression was not significantly changed between 6 and 24 hours, nonetheless, CDH5 was downregulated from 24 to 96 hours in the well experiments.

MRP4 was 0.23-fold lower after 6 hours, 0.18-fold lower after 24 hours and 0.04-fold lower after 96 hours in the well experiments related to PPIA. Hence, MRP4 did not show a significant trend in its mRNA expression between 6 and 24 hours and was downregulated from 24 to 96 hours.

MRP5 was 0.18-fold lower after 6 hours, 0.24-fold lower after 24 hours and 0.33-fold lower after 96 hours in static conditions compared to PPIA. Accordingly, MRP5-expression did not show a significant variation among the three points in time of cell lysis.

RAGE was 0.07-fold lower after 6 hours, 0.05-fold lower after 24 hours and 0.11-fold lower after 96 hours in the well experiments in comparison to PPIA. Thus, RAGE did not show a significant difference between 6 and 24 hours, however, was upregulated from 24 to 96 hours.
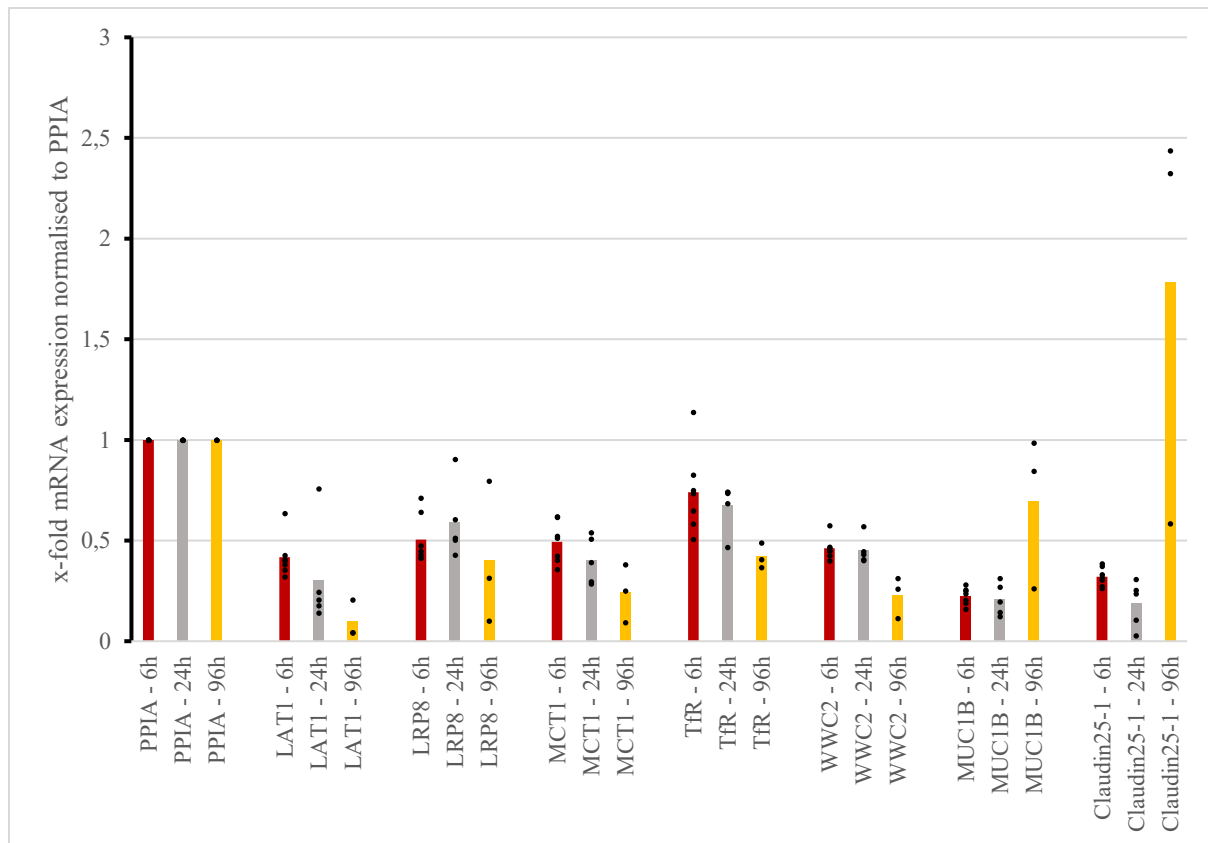
Figure 99: Bar graph 6 with trending mRNA expression level changes for 0 dyne/cm² after 6 (day 2), 24 (day 3) and 96 hours (day 6). (Red) 6 hours. (Gray) 24 hours. (Yellow) 96 hours. n=7: PPIA, LAT1, LRP8, MCT1, TfR, WWC2, MUC1B, Claudin25-1 – 6 hours; n=5: : PPIA, LAT1, LRP8, MCT1, TfR, WWC2, MUC1B, Claudin25-1 – 24 hours; n=3: PPIA, LAT1, LRP8, MCT1, TfR, WWC2, MUC1B, Claudin25-1 – 96 hours.

LAT1 was 0.42-fold lower after 6 hours, 0.31-fold lower after 24 hours and 0.1-fold lower after 96 hours in the well experiments compared to PPIA. As a result, there was no significant trend in LAT1-expression between 6 and 24 hours as well as between 24 and 96 hours.

LRP8 was 0.5-fold lower after 6 hours, 0.6-fold lower after 24 hours and 0.4-fold lower after 96 hours in static conditions in relation to PPIA. Thus, there was no significant trend in LRP8-expression between 6 and 24 hours as well as between 24 and 96 hours.

MCT1 was 0.49-fold lower after 6 hours, 0.40-fold lower after 24 hours and 0.24-fold lower after 96 hours in the static conditions compared to PPIA. Accordingly, there was no significant trend in MCT1-expression between 6 and 24 hours as well as between 24 and 96 hours.

TfR was 0.74-fold lower after 6 hours, 0.67-fold lower after 24 hours and 0.42-fold lower after 96 hours in static conditions in comparison to PPIA. Consequently, there was no significant difference in TfR-expression between 6 and 24 hours, however, there was a slight downregulation from 24 to 96 hours in the well experiments.

WWC2 was 0.46-fold lower after 6 hours, 0.45-fold lower after 24 hours and 0.23-fold lower after 96 hours in static conditions compared to PPIA. Accordingly, there was no significant trend in WWC2-expression between 6 and 24 hours as well as between 24 and 96 hours.

MUC1B was 0.23-fold lower after 6 hours, 0.21-fold lower after 24 hours and 0.7-fold lower after 96 hours in the well experiments compared to PPIA. Therefore, MUC1B-expression did not show a significant change between 6 and 24 hours, however, increased from 24 to 96 hours. Claudin25-1 was 0.32-fold lower after 6 hours, 0.19-fold lower after 24 hours and 1.78-fold higher after 96 hours in the well experiments in comparison to PPIA. Hence, Claudin25-1 did not display a significant difference in its mRNA expression between 6 and 24 hours, however, showed an upregulation from 24 to 96 hours.
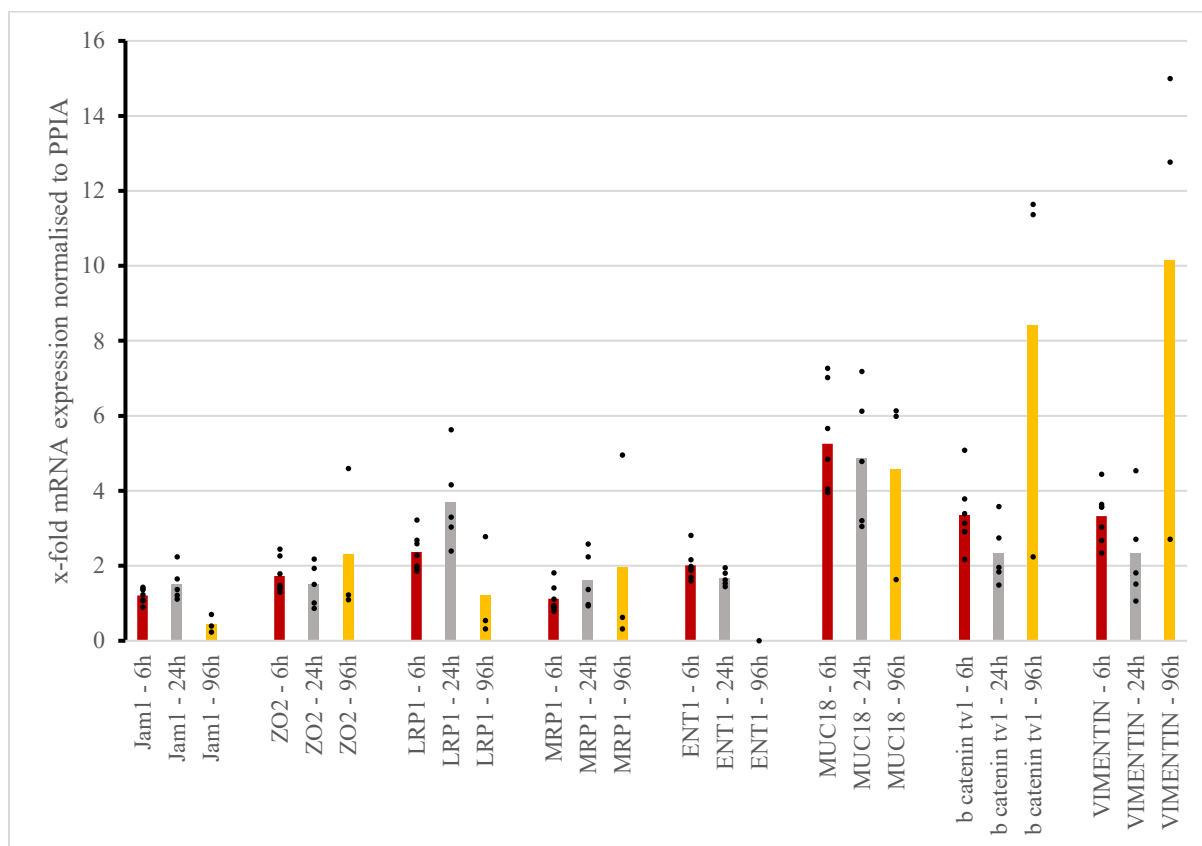
Figure 100: Bar graph 7 with trending mRNA expression level changes for 0 dyne/cm² after 6 (day 2), 24 (day 3) and 96 hours (day 6). (Red) 6 hours. (Gray) 24 hours. (Yellow) 96 hours. n=7: Jam1, ZO2, LRP1, MRP1, ENT1, MUC18, b-catenin tv1, VIMENTIN – 6 hours; n=5: Jam1, ZO2, LRP1, MRP1, ENT1, MUC18, b catenin tv1, VIMENTIN – 24 hours; n=3: Jam1, ZO2, LRP1, MRP1, MUC18, b catenin tv1, VIMENTIN – 96 hours; ENT1 – 96 hours.

Jam1 was 1.21-fold higher after 6 hours, 1.52-fold higher after 24 hours and 0.44-fold lower after 96 hours in the well experiments related to PPIA. Hence, Jam1 was slightly upregulated from 6 to 24 hours and was downregulated from 24 to 96 hours in the well experiments.

ZO2 was 1.73-fold higher after 6 hours, 1.5-fold higher after 24 hours and 2.31-fold higher after 96 hours in static conditions related to PPIA. Thus, there was no significant difference in ZO2-expression between 6 and 24 hours, however, there was an upregulation from 24 to 96 hours.

LRP1 was 2.37-fold higher after 6 hours, 3.7-fold higher after 24 hours and 1.21-fold higher after 96 hours in the well experiments compared to PPIA. As a result, there was an upregulation in LRP1-expression from 6 to 24 hours and a downregulation from 24 to 96 hours.

MRP1 was 1.12-fold higher after 6 hours, 1.62-fold higher after 24 hours and 1.97-fold higher after 96 hours in the well experiments in relation to PPIA. Thus, there was a trend towards upregulation in MRP1-expression from 6 to 24 hours and from 24 to 96 hours.

ENT1 was 2-fold higher after 6 hours, 1.67-fold higher after 24 hours and 0.000035-fold lower after 96 hours in static conditions compared to PPIA. Thus, there was a trend towards downregulation in ENT1-expression from 6 to 24 hours and from 24 to 96 hours.

MUC18 was 5.25-fold higher after 6 hours, 4.87-fold higher after 24 hours and 4.58-fold higher after 96 hours in the well experiments in comparison to PPIA. Consequently, there was a continuous downregulation in the mRNA expression of MUC18 from 6 to 24 hours and from 24 to 96 hours in the well experiments.

B catenin tv1 was 3.34-fold higher after 6 hours, 2.32-fold higher after 24 hours and 8.42-fold higher after 96 hours in static conditions compared to PPIA. Thus, there was a downregulation of b catenin tv1 from 6 to 24 hours and an upregulation from 24 to 96 hours in the well experiments.

VIMENTIN was 3.33-fold higher after 6 hours, 2.33-fold higher after 24 hours and 10.16-fold higher after 96 hours in static conditions compared to PPIA. Therefore, VIMENTIN was downregulated from 6 to 24 hours and upregulated from 24 to 96 hours.
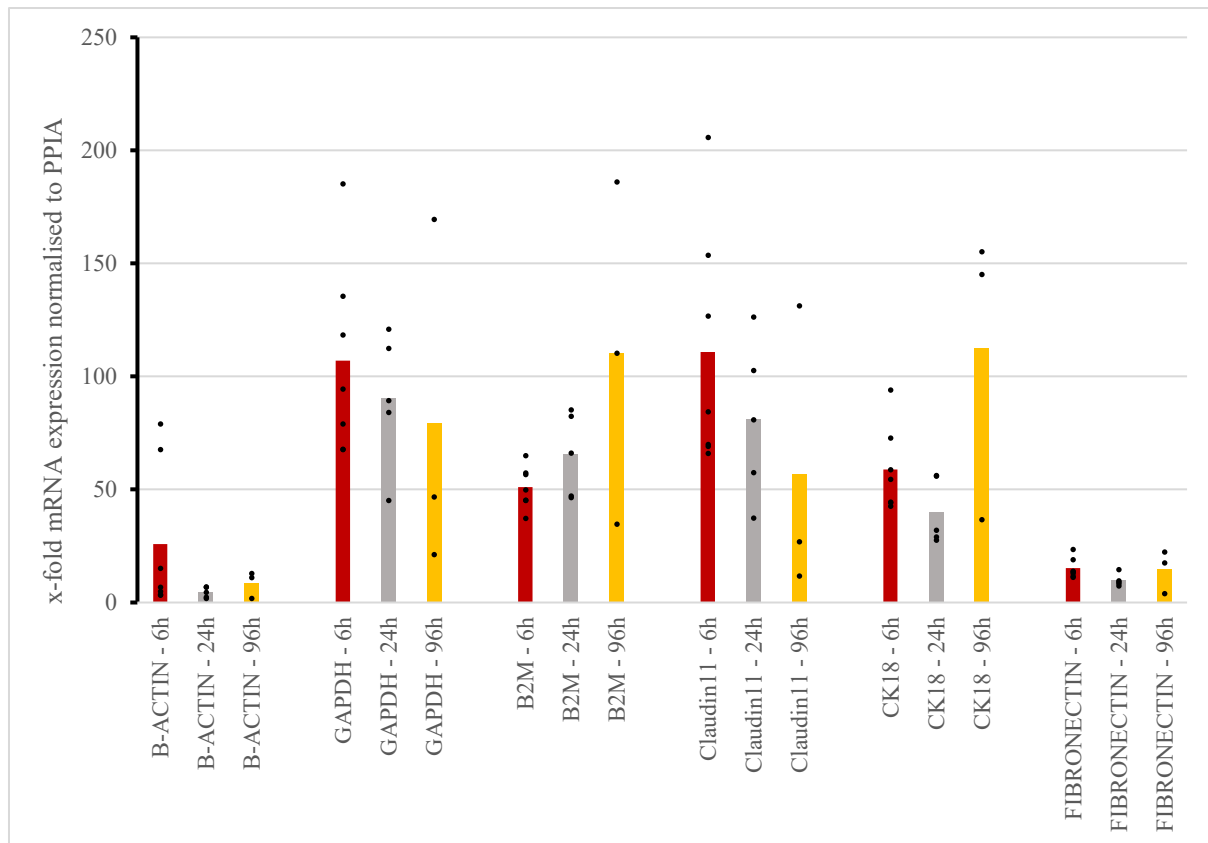
Figure 101: Bar graph 8 with trending mRNA expression level changes for 0 dyne/cm² after 6 (day 2), 24 (day 3) and 96 hours (day 6). (Red) 6 hours. (Gray) 24 hours. (Yellow) 96 hours. n=7: B-ACTIN, GAPDH, B2M, Claudin11, CK18, FIBRONECTIN – 6 hours; n=5: B-ACTIN, GAPDH, B2M, Claudin11, CK18, FIBRONECTIN – 24 hours; n=3: B-ACTIN, GAPDH, B2M, Claudin11, CK18, FIBRONECTIN – 96 hours.

B-ACTIN was 25.84-fold higher after 6 hours, 4.6-fold higher after 24 hours and 8.63-fold higher after 96 hours in static conditions in comparison to PPIA. Hence, B-ACTIN was downregulated from 6 to 24 hours and upregulated from 24 to 96 hours.

GAPDH was 107-fold higher after 6 hours, 90.48-fold higher after 24 hours and 79.2-fold higher after 96 hours in static conditions in relation to PPIA. Hence, GAPDH was continuously downregulated from 6 to 24 hours and from 24 to 96 hours.

B2M was 51.02-fold higher after 6 hours, 65.57-fold higher after 24 hours and 110.38-fold higher after 96 hours in static conditions related to PPIA. Thus, there was a continuous upregulation in B2M-expression from 6 to 24 hours and from 24 and 96 hours.

Claudin11 was 110.9-fold higher after 6 hours, 81.05-fold higher after 24 hours and 56.72-fold higher after 96 hours in the well experiments compared to PPIA. As a result, there was a trend towards downregulation in Claudin11-expression from 6 to 24 hours and from 24 to 96 hours.

CK18 was 58.82-fold higher after 6 hours, 40.22-fold higher after 24 hours and 112.4-fold higher after 96 hours in the well experiments in relation to PPIA. Therefore, CK18 did not show a significant difference between 6 and 24 hours, however, was upregulated from 24 to 96 hours.

FIBRONECTIN was 15.16-fold higher after 6 hours, 9.89-fold higher after 24 hours and 14.73-fold higher after 96 hours in the well experiments compared to PPIA. Thus, there was no significant change in FIBRONECTIN-expression in the well experiments among the different experiment durations.

Overall, most of the targets did not show a significant trend from 6 to 24 hours. However, there was either an up- or downregulation in the mRNA expression of these targets from 24 to 96 hours.

4.5.7 Overview of regulations of mRNA expressions for the BBB relevant targets compared to the static control and PPIA

The regulations of mRNA expressions in comparison to the static control and PPIA of the targets relevant to the BBB are summarised in Table 36. Thus, the arrows indicate the up- and downregulations in comparison to the corresponding static control. It is to be stated that the qPCR of some shear stress or time values did not function for each target, because their mRNA expression was too low. This is visualised through the sign /. The setups are according to the timelines of cell lysis, illustrated in 4.5.1 to 4.5.6.

Table 36: Overview showing the up- and downregulations of mRNA expressions of the targets relevant to the BBB in comparison to the static control.

Target	6 hours 0.1→1→3 [dyne/cm²]	24 hours 1→3 [dyne/cm²]	0.1 dyne/cm² 6→96 [hours]	1 dyne/cm² 6→24→48 [hours]	3 dyne/cm² 6→24 [hours]	Static control 6→2→96 [hours]
B-ACTIN	/↓↓	↓↑	//	↓↓/	↓↑	↑↑↑
GAPDH	↑↓↓	↓↑	↑↔	↓↓↑	↓↑	↑↑↑
B2M	↑↓↓	↓↑	↑↓	///	↓↑	↑↑↑
Claudin1	↔ ↔ ↔	↑↓	↑↑	↔↑↔	↔↓	↓↓↓
Claudin3	↓↑↓	↓↓	↔↑	↑↑↓	↓↓	↓↓↓
Claudin4	↔ ↔ ↔	↓↓	↔↑	↓↓↓	↓↓	↓↓↓
Claudin5	↑↓↓	↓↓	↑↔	↓↓↓	↓↓	↓↓↓
Claudin6	↑↔↔	↑↑	↑↑	↑↑↔	↔↑	↓↓↓
Claudin7	↓↓↓	↓↓	↓↓	↓↓↓	↓↓	↓↓↓
Claudin8	↑↓↓	↑↑	↑↑	↓↑↑	↓↓	↓↓↓

177

Claudin9	/↓↓	↓↓	//	↓↓↓	↓↓	↓↓↓
Claudin10 tva	↑↑↓	↑↑	↑↑	↑↑↑	↓↑	↓↓↓
Claudin10 tvb	↑↓↓	//	//	///	//	↓↓/
Claudin11	↑↓↓	↓↓	↑↓	↓↓↓	↓↓	↑↑↑
Claudin12 tv1	↑↓↓	↓↓	↑↑	↓↓↑	↓↓	↓↓↓
Claudin12 tv2	↑↑↑	↔↑	↑↑	↑↔↑	↑↑	↓↓↓
Claudin12 tv3	↑↔↑	↔↑	↑↑	↔↔↑	↑↑	↓↓↓
Claudin14	↔↑↑	↑↑	↔↑	↑↑↓	↑↑	↓↓↓
Claudin15	↑↓↓	↑↑	↑↑	↓↑↑	↓↑	↓↓↓
Claudin16	↑↓↓	↓↓	↑↓	↓↓↓	↓↓	↓↓↓
Claudin17	↑↓/	↓↑	↑↑	↓↓↑	//	↓↓↓
Claudin18 tv1b	↑↓↓	↓↓	↑↓	↓↓↔	↓↓	↓↓↓
Claudin18 tv2a	↑↓↓	↔↑	↑↔	↓↔↑	↓↑	↓↓↓
Claudin22	/↓↔	↑↓	//	↓↑↓	↔↓	↓↓↓
Claudin23	↑↓/	↑↓	↑↔	↓↑↑	↑↓	↓↓↓
Claudin24	/↑↑	↑↓	//	↑↑↓	↑↓	↓↓↓
Claudin25	/↑↓	//	//	///	↓↓	↓↓↓
Jam1	↓↓↓	↓↓	↓↑	↓↓↑	↓↓	↑↑↓
Jam2	↑↓/	↓↓	↑↓	↓↓↑	↓↓	↓↓↓
Jam3	↓↓↓	↑↓	↓↑	↓↑↑	↓↓	↓↓↓
ZO1	↔↓↓	↔↓	↔↓	↓↔↓	↓↓	↓↓↓
ZO2	↑↓↓	↔↑	↑↓	↓↓↓	↓↔	↑↑↑
ZO3	/↓↓	//	//	↓↓↑	↓↓	↓↓↓
vWF	↑↓↓	↓↓	↑↓	↓↓↓	↓↓	↓↓↓
GLUT1	↑↑↑	↑↑	↑↑	↑↑↓	↑↑	↓↓↓
Occludin	↑↓↓	↓↓	↑↓	↓↓↓	↓↓	↓↓↓
CDH5	↑↓↓	↓↓	↑↓	↓↓↓	↓↓	↓↓↓
ABCB1	↑↔↔	↓↔	↑↑	↔↓↑	↔↔	↓↓↓

MRP1	↑↓↓	↓↓	↑↓	↓↓↓	↓↓	↑↑↑
MRP2	↑↑↑	↑↑	↑↑	↑↑↔	↑↑	↓↓↓
MRP3	↑↑↑	↑↓	↑↑	↑↑↑	↑↓	↓↓↓
MRP4	↑↓↓	↓↓	↑↑	↓↓↑	↓↓	↓↓↓
MRP5	↑↓↓	↓↑	↑↓	↓↓↑	↓↑	↓↓↓
BCRP	↑↑↑	↓↓	↑↑	↑↓↑	↑↓	↓↓↓
MarvelD3	↑↑↓	↓↑	↑↓	↓↓↑	↓↑	↓↓↓
CAT1	↑↑↑	↑↑	↑↑	↑↑↑	↑↑	↓↓↓
ENT1	↑↑↓	↓↔	↑↔	↓↓↑	↓↔	↓↑↑
SELE	/↑↑	//	//	///	↑↑	↓↓↓
InR	↑↔↓	↓↑	↑↑	↔↔↑	↓↑	↓↓↓
LAT1	↓↑↑	↑↑	↓↑	↑↑↔	↑↑	↓↓↓
LRP1	↑↓↓	↓↓	↑↓	↓↓↓	↓↓	↑↑↑
LRP8	↑↓↓	↓↓	↑↓	↓↓↑	↓↓	↓↓↓
MCT1	↓↑↑	↑↔	↓↑	↑↑↑	↑↔	↓↓↓
MCT8	↑↑↑	↑↑	↑↑	↑↑↑	↑↑	↓↓↓
TfR	↑↑↓	↓↓	↑↑	↑↑↓	↓↓	↓↓↓
VEGFA	↑↑↑	↑↑	↑↑	↑↑↓	↑↑	↓↓↓
WWC2	↓↓↓	↓↓	↓↑	↓↓↓	↓↓	↓↓↓
CK8	↑↓↓	↓↓	↑↓	↓↓↓	↓↓	↓↓↓
CK18	↑↓↓	↓↓	↑↓	↓↓↔	↓↓	↑↑↑
CK19	↑↓↓	↓↓	↑↓	↓↓↓	↓↓	↓↓↓
AQP1	↑↑↓	//	↑↓	↑↓↑	↓↑	↓↓↓
AQP3	↑↑↑	↓↔	↑↓	↑↓↑	↑↔	↓↓↓
AQP5	↑↓↓	↓↓	↑↓	↓↓↑	↓↓	↓↓↓
AQP7	↑↑↓	↓↓	↑↓	↑↑↓	↓↓	↓↓↓
AQP11	↑↓↓	↓↓	↑↓	↓↓↓	↓↓	↓↓↓
MUC1A	↑↔↔	↓↔	↑↓	↔↓↑	↔↔	↓↓↓

Target	6 hours 0.1→1→3 [dyne/cm²]	24 hours 1→3 [dyne/cm²]	0.1 dyne/cm² 6→96 [hours]	1 dyne/cm² 6→24→48 [hours]	3 dyne/cm² 6→24 [hours]	Static control 6→24→96 [hours]
MUC1B	↑↔↓	↓↔	↑↓	↔↓↑	↓↔	↓↓↓
MUC18	↑↓↓	↓↑	↑↓	↓↓↑	↓↑	↑↑↑
MUC20	↑↑↔	↑↑	↑↓	↑↑↓	↔↑	↓↓↓
b catenin tv1	↑↓↓	↓↔	↑↓	↓↓↑	↓↔	↑↑↑
b catenin tv4	↑↓↓	↓↓	↑↓	↓↓↓	↓↓	↓↓↓
VIMENTIN	↑↓↓	↓↑	↑↓	↓↓↔	↓↑	↑↑↑
FIBRONECTIN	↑↓↓	↓↓	↑↓	↓↓↔	↓↓	↑↑↑
S100A4 tv1	↑↓↓	↓↓	↑↓	↓↓↑	↓↓	↓↓↓
S100A4 tv2	↑↓↓	//	↑↓	↓↓↑	//	↓↓↓
MFSD2A	↑↑↑	↑↑	↑↓	↑↑↑	↑↑	↓↓↓
Claudin25-1	↑↓↓	↓↓	↑↓	↓↓↓	↓↓	↓↓↑
Claudin25 tv7	↑↑↑	↑↑	↑↓	↑↑↑	↑↑	↓↓↓
RAGE	↑↔↓	↑↑	↑↓	↔↑↑	↓↑	↓↓↓

4.5.8 Overview of regulations of mRNA expressions for the BBB relevant targets among the shear stresses or points in time

The shear- and time dependent regulations of mRNA expressions of the targets relevant to the BBB are summarised in Table 37. Thus, the arrows indicate the up- and downregulations as a comparison between one shear stress to another and from one point in time to the next one. It is to be stated that the qPCR of some shear stress or time values did not function for each target, because their mRNA expression was too low. This is visualised through the sign **/.** The setups are according to the timelines of cell lysis, illustrated in 4.5.1 to 4.5.6.

Table 37: Overview showing the up- and downregulations of mRNA expressions of the targets relevant to the BBB dependent to flow and time.

Target	6 hours 0.1→1→3 [dyne/cm²]	24 hours 1→3 [dyne/cm²]	0.1 dyne/cm² 6→96 [hours]	1 dyne/cm² 6→24→48 [hours]	3 dyne/cm² 6→24 [hours]	Static control 6→24→96 [hours]
B-ACTIN	/↑	↑	/	↔/	↑	↓↑
GAPDH	↓↔	↑	↓	↔↑	↑	↓↓
B2M	↓↔	↑	↓	↔↑	↑	↑↑
Claudin1	↔↔	↓	↑	↑↓	↓	↔↔

	1	2	3	4	5	6
Claudin3	↑↓	↓	/	↑↓	↓	↔↑
Claudin4	↔↔	↓	↔	↔↓	↔	↔↔
Claudin5	↓↓	↔	↓	↓↑	↔	↑↓
Claudin6	↓↔	↑	↓	↑↓	↑	↔↓
Claudin7	↔↔	↓	↑	↔↔	↓	↔↔
Claudin8	↓↔	↓	↔	↑↓	↔	↔↔
Claudin9	/↑	↓	/	↔↓	↓	↔↔
Claudin10 tva	↔↓	↑	↑	↑↑	↑	↔↔
Claudin10 tvb	↓↔	/	/	//	/	↔/
Claudin11	↓↔	↔	↓	↔↑	↔	↓↓
Claudin12 tv1	↓↔	↑	↓	↔↑	↔	↔↓
Claudin12 tv2	↓↔	↑	↓	↔↔	↑	↔↓
Claudin12 tv3	↓↔	↑	↓	↔↑	↓	↔↓
Claudin14	↑↑	↓	↑	↑↓	↓	↔↓
Claudin15	↓↔	↑	↓	↑↑	↑	↔↓
Claudin16	↓↔	↔	↓	↔↑	↔	↑↓
Claudin17	↓/	↑	↓	↔↑	/	↔↔
Claudin18 tv1b	↓↔	↔	↓	↔↑	↔	↑↓
Claudin18 tv2a	↓↔	↑	↓	↑↑	↑	↔↔
Claudin22	/↑	↓	↓	↑↓	↓	↔↓
Claudin23	↓/	↓	/	↑↓	↓	↔↔
Claudin24	/↑	↓	/	↔↓	↓	↔↓
Claudin25	/↓	/	/	//	↑	↔↔
Jam1	↔↔	↓	↑	↔↑	↔	↑↓
Jam2	↓/	↓	↓	↔↑	↔	↑↑
Jam3	↔↔	↓	↑	↑↔	↔	↔↓
ZO1	↓↔	↓	↔	↔↔	↔	↔↔
ZO2	↓↔	↑	↓	↔↑	↑	↔↑
ZO3	/↔	/	/	↔↑	/	↑↓
vWF	↓↔	↔	↓	↔↔	↓	↑↓
GLUT1	↓↔	↑	↓	↔↓	↑	↔↔
Occludin	↓↔	↑	↓	↔↔	↑	↔↑
CDH5	↓↔	↔	↓	↓↑	↔	↑↓
ABCB1	↓↔	↑	↓	↔↑	↔	↑↓
MRP1	↓↔	↑	↓	↔↑	↑	↑↑
MRP2	↓↔	↑	↑	↑↓	↑	↔↔

	Col1	Col2	Col3	Col4	Col5	Col6
MRP3	↓ ↔	↓	↑	↑ ↑	↓	↑ ↓
MRP4	↓ ↔	↓	↔	↔ ↔	↔	↔ ↓
MRP5	↓ ↔	↑	↓	↔ ↑	↑	↔ ↑
BCRP	↓ ↔	↔	↑	↓ ↓	↓	↔ ↓
MarvelD3	↓ ↔	↑	↓	↔ ↑	↑	↔ ↑
CAT1	↓ ↔	↑	↓	↑ ↓	↑	↔ ↓
ENT1	↓ ↔	↔	↓	↔ ↑	↔	↓ ↓
SELE	/ ↑	/	/	//	↓	↔ ↔
InR	↓ ↔	↑	↓	↔ ↑	↑	↔ ↔
LAT1	↑ ↑	↓	↑	↑ ↓	↓	↔ ↔
LRP1	↓ ↔	↔	↓	↔ ↑	↔	↑ ↓
LRP8	↓ ↔	↔	↓	↔ ↑	↔	↔ ↔
MCT1	↑ ↓	↓	↑	↑ ↓	↓	↔ ↔
MCT8	↓ ↔	↑	↓	↑ ↑	↑	↓ ↔
TfR	↓ ↓	↔	↑	↓ ↑	↔	↔ ↓
VEGFA	↓ ↔	↑	↓	↑ ↓	↑	↔ ↓
WWC2	↔ ↔	↔	↑	↔ ↔	↔	↔ ↔
CK8	↓ ↔	↔	↓	↔ ↑	↔	↔ ↑
CK18	↓ ↔	↔	↓	↔ ↑	↔	↓ ↑
CK19	↓ ↔	↔	↓	↔ ↔	↔	↔ ↔
AQP1	↓ ↓	/	↓	↓ ↑	↑	↔ ↑
AQP3	↓ ↑	↑	↓	↓ ↑	↓	↔ ↑
AQP5	↓ ↔	↑	↓	↓ ↑	↔	↑ ↔
AQP7	↓ ↓	↔	↓	↓ ↑	↔	↑ ↔
AQP11	↓ ↔	↔	↓	↔ ↔	↔	↔ ↑
MUC1A	↓ ↔	↔	↓	↓ ↑	↔	↔ ↑
MUC1B	↓ ↔	↑	↓	↓ ↑	↔	↔ ↑
MUC18	↓ ↔	↑	↓	↔ ↑	↑	↓ ↓
MUC20	↓ ↔	↑	↓	↑ ↓	↑	↔ ↑
b catenin tv1	↓ ↔	↑	↓	↔ ↑	↑	↓ ↑
b catenin tv4	↓ ↔	↓	↓	↔ ↔	↔	↔ ↑
VIMENTIN	↓ ↔	↑	↓	↔ ↑	↑	↓ ↑
FIBRONECTIN	↓ ↔	↔	↓	↔ ↑	↔	↔ ↔
S100A4 tv1	↓ ↔	↔	↓	↔ ↑	↔	↔ ↑
S100A4 tv2	↓ ↔	/	↓	↔ ↑	/	↔ ↑
MFSD2A	↓ ↓	↑	↓	↑ ↑	↑	↔ ↑
Claudin25-1	↓ ↓	↓	↓	↔ ↔	↔	↔ ↑
Claudin25 tv7	↓ ↓	↑	↓	↑ ↓	↑	↓ ↑
RAGE	↓ ↓	↔	↓	↑ ↑	↑	↔ ↑

5 Discussion

The BBB is a crucial barrier to prevent harmful substances from entering the brain. However, it is also an obstacle for various substances to reach the brain, that have potential in the cure of different diseases such as Morbus Parkinson or dementia (e.g. Morbus Alzheimer). An important parameter, that potentially alters the functionality of the BBB is the blood flow and the consequential shear stress, preferably in the physiological range, which is 10 to 20 dyne/cm² in brain capillaries according to Ferreira (2019). Wang *et al.* (2020) even suggested a higher range of shear stress of 10 to 70 dyne/cm² in the arterial circulation and 2.8 to 95.5 dyne/cm² in the capillary circulation. Hence, the physiological flow characteristics in capillaries were partly met by the induced flow in the current study. Recent studies emphasised the importance of the introduction of flow in *in vitro* models with the BBB adapting to varying flow conditions.

Contributing to that, Rochfort and Cummins (2015) even demonstrated that disrupting the barrier of human brain microvascular endothelial cells (HBMECs) by tumour necrosis factor-alpha (TNF-alpha) and interleukin-6 (IL-6) could be antagonised by the implementation of physiological shear stress of 8 dyne/cm² according to Wang *et al.* (2020). Moreover, Cucullo *et al.* (2011) showed that capillary-like shear stress of 6.2 dyne/cm² altered the expression of genes related to TJs and adhesion molecules for instance. The cytoskeletal protein levels were also upregulated as a morphological response of the endothelium to the flow and structural support for the TJ complexes. The current study applied shear stress values of up to 7.5 dyne/cm². Thus, similar effects could have been expected.

Furthermore, Ferreira (2019) stressed the importance of utilising shear stress in a BBB model to increase the contact area between the cells in order to create a robust BBB. Hence, our study focussed on applying shear stress onto the cells, which appeared to be a key parameter in recent *in vitro* studies. However, the suggested shear stress range by Ferreira (2019) of 10 to 20 dyne/cm² in brain capillaries was not reached in this work. In order to achieve the aimed range of shear stress, it was important to understand that the surface of the chip is a key-parameter.

Walter *et al.* (2016) tried to achieve sufficient surface properties for the cells to adhere by using a porous PDMS-membrane from it4ip. In addition, they also applied a phase without flow prior to the flow-experiment for cultivation purposes. However, they only applied low shear stress conditions of 0.15 dyne/cm² throughout their studies, which was lower than the suggested physiological range. Similarly, Sellgren, Hawkins, and Grego (2015) also used a porous membrane and a 2 mg/mL collagen hydrogel as an interface between a co-culture of ACs (in the hydrogel) and BCECs with an applied shear stress of 5 dyne/cm². A similar approach was conducted by Booth and Kim (2012), who seeded cells on porous membranes coated with

10 µg/mL fibronectin. Another method to extent the duration of the hCMEC/D3 cells' adherence on the microfluidic device, was to use a static culture for 3 days first and then expose the cells to flow (Griep *et al.*, 2012). Moreover, a surface modification could be conducted. This could be performed by introducing the cross-linker glutaraldehyde, which can be used to immobilise the coating solution on PDMS in combination with APTES as proposed by Kuddannaya *et al.* (2013).

Several studies employed the afore mentioned nanoporous membranes also to introduce co-cultures in their experiments. Booth and Kim (2012) stressed the importance of utilising a co-culture composed of endothelial cells and ACs for developing an *in vivo*-like BBB model. Moreover, Wang *et al.* (2020) pointed out that a monolayer culture leads to an inadequate barrier, as the interactions with other cells are important for the barrier properties. In this regard, Wang *et al.* (2016) showed an increased expression of the P-gp efflux pump with an increased number of days in cell culture in bi- and triculture models of BCECs and PCs alone or together with ACs. Janzer and Raff (1987) already presented evidence that ACs directly influence the phenotype of endothelial cells of non-nervous system origin. In the current study a monoculture of BCECs was used with the application of the growth factor hbFGF and the introduction of shear stress to develop the *in vivo* phenotype. In future studies, a second compartment could be arranged to enable the use of a co-culture as technically already accomplished by Booth and Kim (2012).

DeStefano *et al.* (2018) suggested on the contrary, that the use of a co-culture is not essential for tight junction formation when using hiPSC-derived BMECs. This was also supported by the current study, even without using hiPSCs, as VE-Cadherin was successfully stained after the flow induction. In addition, the qPCR-analysis indicated the presence of various tight junction proteins. Nonetheless, DeStefano *et al.* (2017) also pointed out, that TEER-measurements were increased in the presence of ACs and pericytes, with important functions for barrier integrity. Hence, the importance of the use of co-cultures is still debated. In this regard, the advantages of a second cell line and the additional technical effort must be carefully balanced. The introduction of a second cell line necessitates a second compartment, which is not required for every research question as our study demonstrated. In addition, it could be an interesting research proposal whether the relevant targets of the BBB show different adaptations to flow in the presence of ACs or pericytes. Contributing to that Neuhaus (2020) suggested the research question if other cells than endothelial cells, used in cell culture models, also show independent tube formation in hydrogels or react to stimuli, as VEGF for instance, with increased migration or barrier collapse.

A major disadvantage of microfluidic models is the small growth surface area to lyse cells for molecular analysis, e.g. qPCR as conducted in the current study, stated Neuhaus (2020). This important parameter contradicts the application of physiological shear stress, as both of these parameters are dependent on the width of the channels of the microfluidic device. For sufficient molecular analysis a channel growth area of 1 cm² was aimed in our study and an according channel width had to be designed to achieve this goal. As the wider the channel, the lower the flow and hence the shear stress, higher flow rates had to be applied to compensate this. This issue presented one of the major disadvantages when combining a microfluidic model with subsequent molecular analysis. The application of microfluidic models in terms of drug transport studies remains another issue due to small sample volumes according to Neuhaus (2020). A solution to this problem in future studies might be the application of millifluidic models. Anyhow, these models are not as suitable for high-throughput applications and require more growth medium and a higher number of cells.

In section 4.4 the live/dead ratios of the relevant experiments were calculated. Looking at the final set of experiments (experiment no. 20 to experiment no.23), it was noticeable that experiment no. 20 at a flow rate of 130 µL/min (1 dyne/cm²) showed the highest live/dead-ratio with 29.42:1 when comparing the chip-experiments amongst each other. In contrast, experiments no. 22 with 3.36:1 (7.5 dyne/cm², 985 µL/min) and 23 (0.1 dyne/cm², 13 µL/min) with 3.7:1 revealed low live/dead-ratios in the chip-experiments and experiment no. 21 (3 dyne/cm², 390 µL/min) with 11.55:1 lied in between. A possible explanation for this phenomenon could be, that a shear stress of 0.1 dyne/cm² (13 µL/min) induced cells to overgrow and additionally did not provide sufficient flow for dead cells to be flushed away in comparison to the higher flow rates. At a final shear stress of 7.5 dyne/cm² (985 µL/min), also looking at the microfluidic image (Figure 43), a less dense cell layer and consequently fewer live cells were apparent. The same observation accounted for a final shear stress of 3 dyne/cm² (390 µL/min).

The images that form the basis for the estimation of the live/dead-ratios, were taken 24 hours and in the case of experiment no. 17, 48 hours after final shear stress induction. For future experiments it would be important to take live/dead images after 6 hours of final shear stress induction as the cells in each experiment showed a comparable dense cell layer at this point (4.3.1 to 4.3.12). Moreover, looking at the live/dead-ratios of experiments no. 17 (2.5 dyne/cm², 330 µL/min, 48 hours) with 3.88:1 and no. 21 (3 dyne/cm², 390 µL/min, 24 hours) with 11.55:1, which had similar final shear stresses but applied over a different time period, it became apparent that experiment no. 17 with an increased final shear stress period showed a

lower live/dead ratio. This indicated that the ratio of live cells decreased at a similar final shear stress after additional 24 hours.

Considering the live/dead ratios of the well experiments, variations became apparent, even though the well experiments were seeded with the same cell number under equal conditions. A possible explanation could be the different passage numbers of hCMEC/D3 or the subjective selection of the counted image sections by view. Moreover, generally higher live/dead-ratios in the static well experiments were detected. This could be due to the reason, that a higher quantity of cells was flushed away in the flow experiments with an overall less dense cell carpet in comparison to the well experiments. Another reason could be that the conditions in the well experiments for cell division were in favour of the hCMEC/D3 cells compared to the conditions in the flow experiments.

The regulation of the expression levels of mRNA target genes due to flow and time were analysed in our study by means of qPCR. The tight junction proteins Claudin5 and ZO1 both showed a decrease in mRNA expression levels compared to the static control throughout the current study.

Brown *et al.* (2019) also used hCMEC/D3 cells in their work. They subjected them to a shear stress of 2.73 dyne/cm² over a period of 24 hours. As a result, they found an upregulation of ZO1 and Claudin5 after the application of hemodynamic-like shear stress. However, Brown *et al.* (2019) made this observation by means of immunochemistry staining of the relevant tight junction proteins which could differ to the mRNA level at the same time point. Garcia-polite *et al.* (2017) similarly subjected their HBMECs to higher shear stress of 10 to 20 dyne/cm² and found an upregulation in protein expression levels of ZO1 and Occludin. However, when exposed to high shear stress of 40 dyne/cm² and pulsatile flow profiles, they interestingly observed a downregulation of protein-expression levels. In the current study, decreasing mRNA expression levels of ZO1 were noted. Nonetheless, when discussing protein- and mRNA expression levels, it is important to keep in mind, that mRNA levels might differ in comparison to protein levels. This is due to adaption processes as the cells might have already produced an excess of proteins.

Colgan *et al.* (2020) subjected their bovine brain microvascular endothelial cells (BBMvEC) to pulsatile flow at a shear stress of 10 dyne/cm² over a period of 24 hours. They detected increases in mRNA expression levels of Occludin and ZO1. Occludin was found to be downregulated in comparison to the static control throughout our study. Contributing to that, De Stefano *et al.* (2017) found that ZO1 expression was statistically lower at 4 dyne/cm² compared to static

conditions. However, they detected no statistical difference between 4 and 12 dyne/cm² in ZO1 expression levels. In this case again protein expression levels were investigated.

Another target of the BBB was the carrier protein von Willebrand factor (vWF). According to Peyvandi, Garagiola, & Baronciani (2011), vWF has an important role for primary haemostasis where it is involved in platelet adhesion of the damaged vascular subendothelium. Galbusera *et al.* (1997) found a higher cumulative of vWF production in human umbilical cord vascular endothelial cells (HUVECs) exposed to 2, 8 and 12 dyne/cm² in comparison to static cultures, however, no statistical significance was observed at 2 dyne/cm². In addition, they did not detect a statistical difference when exposing the HUVECs to shear stress of 12 dyne/cm² over a period of 6 hours compared to static cultures. However, they found an increase in vWF cumulative production when exposing the HUVECs over a period of 15 hours to 12 dyne/cm². Nonetheless, they also noted that HUVECs exposed to laminar flow did not have an impact on mRNA expression. The qPCR analysis of our study even showed a decrease in mRNA expression levels in comparison to the static control. In addition, Bortot *et al.* (2019) linked high cleavage of vWF to a turbulent flow situation as present in aortic stenosis for instance. In the current study a physiological laminar flow situation was modelled. Hence, it could be speculated, that also the type of flow has an impact on vWF. As Bortot *et al.* (2019) found a higher cleavage rate of vWF in a turbulent flow situation, that causes dysfunctional vWF, it could further be speculated that the endothelial cells react with an increase of mRNA expression as a compensation mechanism towards the dysfunctional vWF. In contrast to that, when subjected to physiological and laminar flow, as conducted in our study, it could be assumed that the vWF levels remain constant or might even be downregulated. Moreover, Gogia and Neelamegham (2015) stated that vWF has an important role in keeping healthy haemostasis in the vasculature where high shear conditions are encountered. They further found that multimeric vWF is structurally changed by high shear stress and structural changes in globular A1, A2 and A3 occur. Hence, shear stress and the flow situation seem to have an influence on vWF function. In addition, it can be assumed that mRNA- and protein-levels might also be subject to the predominant fluid situation in the vessels.

Another interesting target investigated by qPCR in the current study was the adherens-junction protein VE-Cadherin. Sulistyowati, Permatasari and Widobo (2017) subjected their endothelial cells to a shear stress of 10 dyne/cm² for 5, 8, 12 and 15 minutes and a glucose-treatment 7 days prior to the treatment with shear stress. After the induction of shear stress, they found the detachment of endothelial cells from the base, which they associated to the function of VE-Cadherin. In our study, also declining levels of VE-Cadherin were detected with increased shear

stress (Figure 52) and over time (Figure 61) in comparison to the static control. Therefore, it could be assumed that shear stress alters VE-Cadherin function and hence caused cells to detach from the surface.

VEGFA is an important growth factor inducing angiogenesis. It could be assumed that induced angiogenesis results in decreased barrier tightness. This is supported by Rahimi (2017), who associated blood vessel leakiness with tumour-induced angiogenesis and tumour-associated blood vessels, which get hyperpermeable. VEGFA levels will rise when angiogenesis is induced. In our study VEGFA-expression levels were upregulated from 1 to 3 dyne/cm² after a 24-hour-exposure and from 6 to 24 hours exposed to 3 dyne/cm². In addition, VEGFA-expression was almost constantly higher compared to the corresponding static control. According to Wragg *et al.* (2014) high and low shear stress, and hence two opposites, both activated angiogenesis. They speculated that endothelial cells sense these variations from normal conditions and induce angiogenesis as a response. Moreover, they found that different subtypes of VEGF showed different adaptations due to shear. Thus, VEGFA was upregulated due to flow, whereas VEGFB seemed to be upregulated in static conditions (Müller-Esterl, 2004).

According to Green (2020) CAT1 is involved in the transport of L-arginine into the BCECs, where nitric oxide (NO) is produced in a reaction cascade and eventually released into the vascular smooth muscles cells, where it leads to the dilatation of the muscle cells' vessels. Green (2020) further stated that a loss of normal CAT1 function could be associated with atherosclerosis, which leads to cardiovascular diseases (CVD). Thus, the transporter CAT1 also functions as a disease marker for CVD. CAT1 was upregulated in comparison to the static control throughout our study (Table 36) and was also upregulated with increasing shear stress from 1 to 3 dyne/cm² after 24 hours of exposure (Table 37). It could be assumed, that hCMEC/D3 reacted to the application of flow and the resulting shear stress with an increased CAT1-activity. This could be due to their physiological tasks, as they sought to dilate the blood vessel. This was also supported by Green (2020), who showed that shear stress increased L-arginine transport in HUVEC's at 15 and 20 dyne/cm² in comparison to the static control of 0 dyne/cm² in combination with urea, that even inhibits CAT1-acitivity. In addition, shear stress increased CAT1-expression in her study, 6 hours after the induction of the application of shear stress for 12 minutes. This coincides with the results of our study, which also showed an upregulation of CAT1 in response to shear stress.

Discussing the most common sources of error is important for the current study, as the entire process of manufacturing the microfluidic device took multiple sensitive steps until the seeding

of the cells and therefore errors were likely to occur, affecting the experiments. Thus, there were flaws emergent from the technical microfluidics side arising before the start, however, altering the actual experiment (3.4.1). Additionally, the flow-setup with the cells was equally error-prone. In the following, the most common sources of errors are explained in greater detail. The plasma-chamber is a device that was used to create silanol groups on the PDMS and hydroxyl groups on the microscopic slides, hence forming hydrogen bonds and a tight connection between these two layers. The first important step towards the seal among these components was the preparation of clean object slides. Therefore, the latter were rinsed in isopropanol and a vacuum gun subsequently removed the dust, which prevented the successful glass-plasma bonding. Additionally, the glass plate inside the plasma chamber had to be maintained dust-free.

The second parameter affecting the successful binding was the gas-composition inside the chamber. In our study, oxygen was utilised for this purpose. This was important, as the gas components affect the type of chemical links, created on the surfaces of glass and PDMS. Oil from the vacuum pump was often a pollutant worsening this development (https://www.elveflow.com/microfluidic-tutorials/soft-lithography-reviews-and-tutorials/how-to-get-the-best-process/soft-lithography-glass-pdms-bonding/, accessed April 6, 2020).

Thirdly, the process duration was a key factor when bonding PDMS to glass. In the current study, the time was set to 2 minutes. An insufficient time span prohibited the plasma-cleaner from functionalising the whole surface area. In contrast, applying the plasma for too long could have rendered the surface dysfunctional. In addition, the attachment of PDMS to the upper- and lower microscopic slides was conducted immediately after the treatment in the plasma-cleaner. This was important, to enable the use of the complete activated surface for efficient bonding and the development of a tight seal between the components.

After assembling the PDMS with the upper- and lower microscopic slides, air bubbles were squeezed out between the layers by hand. When applying insufficient hand pressure, air bubbles remained and the chip got leaky. On the other hand, when using excessive force, the chip could break or the channels were deformed.

If any of these steps in the process of plasma bonding and the attachment of the components were conducted incorrectly, the microfluidic device was leaky with air bubble formation (Figure 104) or medium leaking out of the system (https://www.elveflow.com/microfluidic-tutorials/soft-lithography-reviews-and-tutorials/how-to-get-the-best-process/soft-lithography-glass-pdms-bonding/, accessed April 6, 2020).

The sensitivity of the cells towards the surface of the channel was an important issue emerging in our study. After fabricating the microfluidic device, the baking was the last important step, before seeding the cells. This phase was crucial for the epoxy glue to dry and form a tight connection to the microfluidic device as well as the functioning of APTES (3.4.1.5).

The step of chip baking was performed at 70°C for 2-, 24- and 48-hour intervals respectively in different experiments throughout the current study. Though, when conducted for 24 or 48 hours, the cells did not adhere to the surface of the microfluidic device in the subsequent experiments (Figure 102A, B). This was likely due to the fact, that extensive baking caused the removal of hydroxyl groups on the surface, "drying" the chip, which made it more hydrophobic. Consequently, the coating proteins, fibronectin/collagen IV, did not bind to the surface sufficiently and the adhesion of the cells was reduced accordingly. When baking the microfluidic device at 70 °C for 48 hours, the cells remained in their rounded shape and did not adhere to the surface at all (Figure 102A). This effect was less visible when baking for 24 hours, as the cells attached to the surface, but moved closer together to form aggregates. This behaviour was a strong indicator that the surface did not fit the cells. This phenomenon did not appear after baking was done for 2 hours. In that case, cells formed their usually known morphology (Figure 102C).

However, a reduced time of baking meant in turn that the epoxy adhesive would not fully dry, possibly causing a leaking device.

Another enhancement of the chip surface would be the introduction of glutaraldehyde as a cross-linker between APTES and the coating solution. According to Kuddannaya *et al*. (2013), this modification showed efficiency in immobilising proteins and might improve the adhesion of the cells. This adjustment was not conducted in our study (Kuddannaya *et al.*, 2013).

48 h of baking　　　**24 h of baking**　　　**2 h of baking**

Adhesion of cells 2 h after seeding
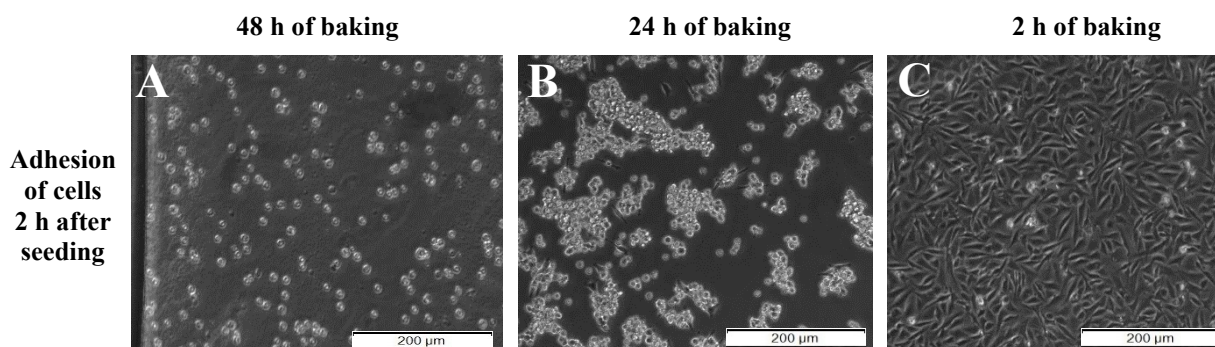
Figure 102: Brightfield microscopic images of the adhesion of the cells 2 hours after the seeding
(A) 48 hours of baking (Experiment no.3). (B) 24 hours of baking (Experiment no.4). (C) 2 hours of baking (Experiment no.8). Images were taken with a 10x objective.

Another issue during the current study was the stability of the coating solution collagen IV/ fibronectin. This mixture was used repeatedly, being sterile filtered after each use. Though, following the fourth usage, the cells did no longer attach properly to the surface (Figure 103A-C). Consequently, 2 hours after the cell seeding, more unattached cells were visible when reusing the coating solution than applying a freshly prepared one (Figure 103B, E). After 24 hours at a flow rate of 2 µL/min, the cells on the freshly prepared coating solution adhered and formed a thorough cell layer (Figure 103D-F). In contrast, the cells on the more than four times reused coating solution were completely washed out from the microfluidic device (Figure 103C). The main reason for this phenomenon was the consumption of proteins due to the repeated coating procedure, eventually resulting in a reduced concentration of proteins in the coating solution. In addition, the amount of proteins could also be reduced in the process of sterile filtration or proteins denatured throughout their storage. Thus, the coating solution should not be used more than four times to provide a functionalised surface for the adhesion of the cells.

Seeding	2 h after seeding	0.015 dyne/cm² (2 µL/min), 24 h
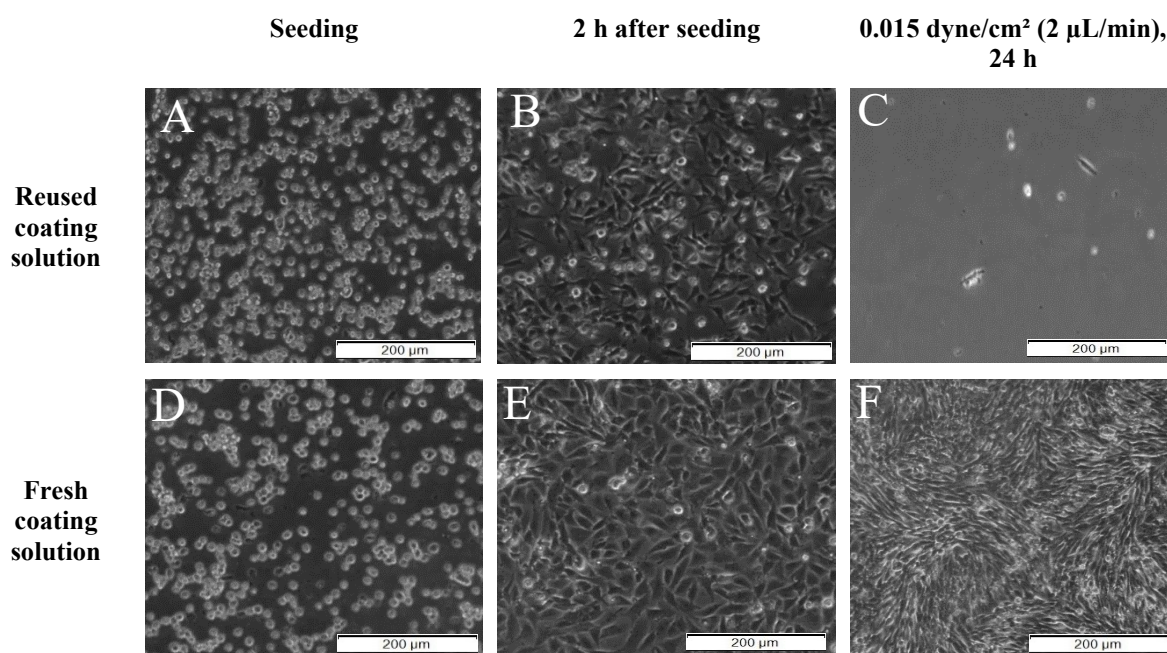
Figure 103: Brightfield microscopic images of the adhesion of hCMEC/D3 cells
(A-C) Reused coating solution > four times (Experiment no.19). (D-F) Fresh coating solution (Experiment no.20). (A, D) Seeding. (B, E) 2 hours after seeding. (C, F) 0.015 dyne/cm² (2 µl/min), 24 hours. Images were taken with a 10x objective.

The last important step towards a fully functioning microfluidic device was the attachment of the ports to connect the tubes to the chip (3.4.1.6). The ports functioned as a connection between the tubes of the medium stock and the cells within the channels of the chip. Therefore, a strong connection between the upper microscopic slide and the ports was vital.

This was accomplished by using epoxy adhesive, whose components were mixed immediately before usage until a "gum-like" structure was produced. Afterwards, its consistency changed and the glue no longer dried. This resulted in the epoxy adhesive being permeable to the medium, which was consequently leaking out of the microfluidic device. Also, air could be sucked inside the channels, which caused the appearance of air bubbles detaching the cells. Moreover, the epoxy resin was solidified by incubating the chips for 15 minutes until the first portion of the epoxy underneath each channel was dry and for 2 hours until the second portion around each channel was dry at 37 °C, respectively. If this duration was shortened, the glue again did not solidify.

The appearance of air bubbles within the channels of the microfluidic device caused significant damage to cells in our study. Two different types of air bubbles were to be differentiated. On the one hand, there were large blebs, which took up the complete diameter of the channel and detached the cells from the surface (Figure 104red). Furthermore, when air bubbles were trapped inside a channel during the coating procedure, collagen IV/fibronectin did not bind in these areas. Thus, the surface was not fully functionalised for the cells to adhere.

Once the air bubbles were inside the channel, they were hardly removable. One action to eliminate them was the upward placement of the chips in the incubator, which induced the bubbles to pass the channel faster (Figure 16/1).

Beyond that, temperature variations were another factor contributing to air bubble formation. Hence, the chip was placed within a 37 °C incubator throughout the majority of experiments, whereas the connecting tubes and pumps were placed outside of it. Consequently, gas dissolved in the medium was possibly released due to these temperature variations. This could be prevented by placing the entire system inside a 37 °C incubator (https://www.chemyx.com/support/knowledge-base/applications/chemyx-syringe-pumps-nanofibers-bone-tissue-engineering-2/, accessed April 7, 2020).

Moreover, the connection of the tubes with the fittings was critical to prevent air from entering (https://www.chemyx.com/support/knowledge-base/applications/chemyx-syringe-pumps-nanofibers-bone-tissue-engineering-2/). Thus, it was crucial to ensure that the fittings were not leaking and to check their tightness in advance. This was automatically done by rinsing the system prior to connecting the microfluidic device and checking for leaked EBM-2 medium (https://www.elveflow.com/microfluidic-tutorials/microfluidic-reviews-and-tutorials/air-bubbles-and-microfluidics/, accessed April 6, 2020).

Another reason for the appearance of air bubbles was the first filling of the channels with the medium. It is possible that some air bubbles maintained in the device after filling. This was prevented by flushing the entire system with EBM-2 prior to the experiment. Before the system was filled with medium, ethanol and PBS were introduced into the chip. This was conducted to disinfect and rinse the setup before the cells were seeded (3.4.1.7). During this process, air bubbles could also have emerged due to the replacement of the different fluids (https://www.elveflow.com/microfluidic-tutorials/microfluidic-reviews-and-tutorials/air-bubbles-and-microfluidics/, accessed April 6, 2020).

Finally, the flow rate affected the formation of air bubbles. Accordingly, the higher the flow rate the more likely air bubbles were to leave the microfluidic device. Consequently, when designing the experimental setup, it was crucial to reach an adequate flow rate early in the course of the experiments to minimise the risk of the development of air bubbles (https://www.chemyx.com/support/knowledge-base/applications/chemyx-syringe-pumps-nanofibers-bone-tissue-engineering-2/, accessed April 7, 2020; https://www.elveflow.com/microfluidic-tutorials/microfluidic-reviews-and-tutorials/air-bubbles-and-microfluidics/, accessed April 7, 2020).

When working in cell culture, it is vital to operate in a sterile environment under a laminar airflow to avoid contamination with bacteria, yeast or fungi. However, due to the laboratory facilities at the University of Technology, Vienna, it was not possible to arrange the actual flow experiments in such a working environment. Thus, the setting was assembled in a non-sterile atmosphere after the cell seeding. Consequently, the experimental arrangement was more vulnerable to possible sources of contamination. This could not be fully prevented by the treatment of the surfaces, the incubator and the connections between the tubes with 70 % ethanol.

Possible infection may have altered the cell's behaviour and possibly the mRNA expression patterns. In future studies, the experimental setup should occur under sterile conditions. However, infections were not visible in the course of the current study.
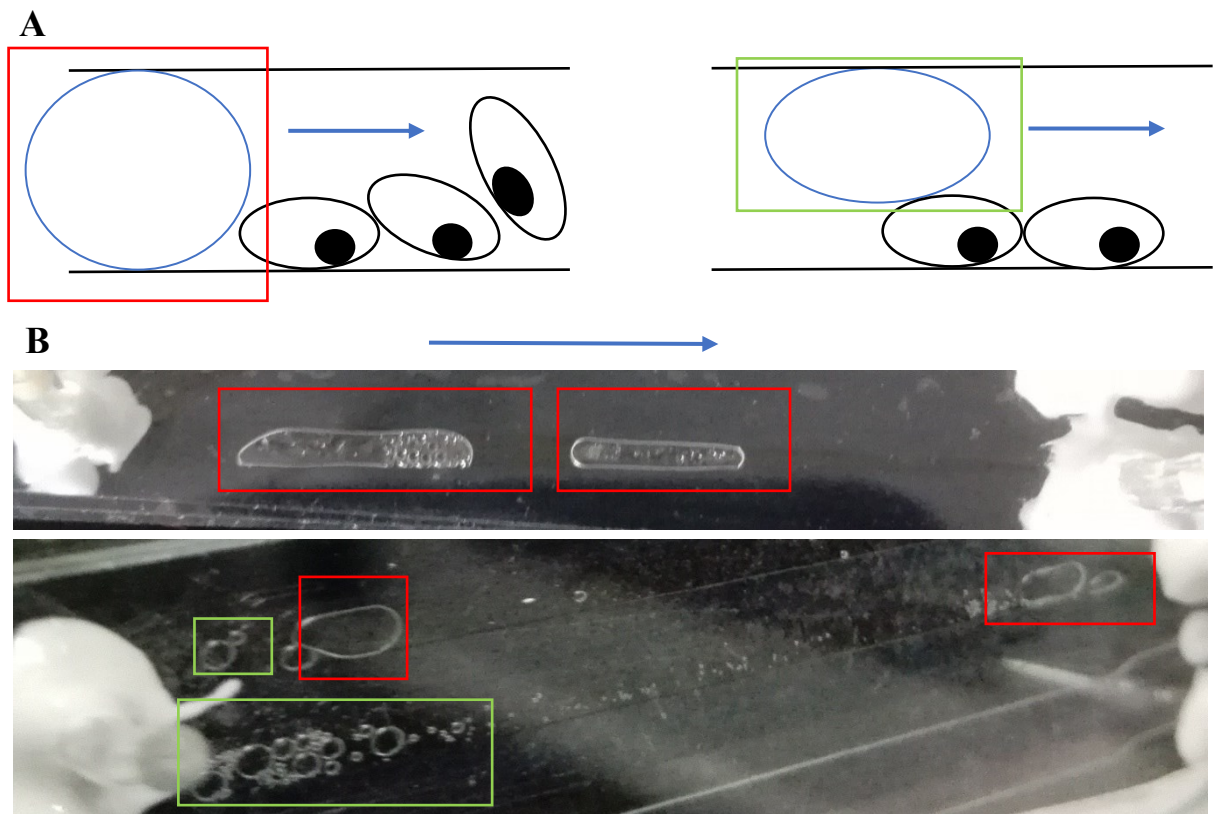
Figure 104: Images of air bubble formation in the channels of the microfluidic device
(Red) Air bubbles taking up the complete diameter of the channel. (Green) Air bubbles floating on top of the cells.
(A) Side view of the channel. (B) Top view of the channel.

6 Conclusion

The development of a microfluidic setup for hCMEC/D3 was an approach to simulate the BBB under flow conditions and to study the influence of different shear stresses on the expression of various barrier markers. For this purpose, a 3-day-setup was developed with a 6- and 24-hour final shear stress exposure.

The current study showed that the final influence of shear stress extending 6 hours was not feasible above 3 dyne/cm². The brightfield microscopic images revealed the detachment of hCMEC/D3 cells above both parameters applied. Flow conditions also detached the cells in setups with overall periods extending 3 days. Consequently, in future studies, 6-hour exposures should be conducted for shear stresses ranging from 0.1 to 7.5 dyne/cm² to detect flow dependency. Additionally, shear stresses below, presumably, 3 dyne/cm² should be compared to observe time dependency. Immunostainings of VE-Cadherin, f-actin and further structural proteins should be conducted for all final shear stresses to visualise their impact.

During the establishment of this setup, it became apparent that the steps in the process of manufacturing the microfluidic device, for instance the plasma bonding, were error-prone with a leaking chip as result. Besides, it emerged that the cells were sensitive towards the surface of the chip. Hence, baking the microfluidic device longer than 2 hours, deteriorated the cells' adherence to the surface.

Nonetheless, the current study also demonstrated that flow conditions and the resulting shear stress influence the mRNA expression levels of 96 targets including transporters and tight junction proteins. For example, CAT1 and VEGFA were upregulated accordingly and the targets ZO1, vWF and VE-Cadherin were downregulated in comparison to the static control.

The accomplished basic work of our study with successfully establishing a microfluidic setup for hCMEC/D3, combined with the stated perspectives, could provide the basis for future research on the impact of flow and shear stress on BBB properties.

7 Index of abbreviations

μ	velocity
ABC	ATP-binding cassette transporter
AC	Astrocyte
AIT	Austrian Institute of Technology
AJ	Adherent junction
AMT	Adsorptive-mediated transport
APTES	3- Aminopropyltriethoxysilane
AQP	Aquaporine
B2M	Beta-2 Microglobulin
b-actin	Beta-actin
BBB	Blood Brain Barrier
BBMcEC	Bovine brain microvascular endothelial cells
BCEC	Brain capillary endothelial cell
BCRP	Breast cancer resistance protein
BHS	Blut-Hirn-Schranke
BM	Basal membrane
BSA-V	Bovine serum albumin-Fraction V
CAT	Cationic aminoacid transporter
CDH	Cadherin
cDNA	Complementary DNA
CK	Creatine kinase
Cldn	Claudin
CMT	Carrier-mediated transport

CNS	Central nervous system
Ct	Threshold cycle
CVD	Cardiovascular disease
DAPI	4',6-diaminidino-2-phenylindole
d/cm²	dyne/cm²
DNA	Desoxyribonucleic acid
E cadherin	Epithelial cadherin
EBM-2	Endothelial cell growth basal medium-2
ENT	Equilibrative nucleoside transporter
EtOH	ethanol
Ex/em	Excitation/emission
FBS	Fetal bovine serum
GAPDH	Glyceraldehyde 3-phosphate dehydrogenase
Glut	Glucose transporter
ht	height
h	hour
hbFGF	Human basic fibroblast growth factor
HBMEC	Human brain microvascular endothelial cells
hCMEC/D3	Human capillary microvascular endothelial cells
hiPSC	Human-induced pluripotent stem cells
HEPES	4-(2-hydroxyethyl)-1-piperazineethanesulfonic acid
HSPG	Hepatan sulphate proteoglycan
HUVECs	Human umbilical cord vascular endothelial cells
IL-6	Interleukin-6

InR	Insulin-like receptor
Jam	Junctional adhesion molecules
LAT	L-type amino acid transporter
LRP	Lipoprotein receptor-related protein
MCT	Monocarboxylate transporter
Mfsd2a	Major facilitator superfamily domain-conatining protein 2
mRNA	Messenger RNA
MRP	Multidrug resistance-associated protein
MUC	Mucin
NO	Nitric oxide
Occ	Overexpressed in colorectal carcinoma
PBS	Phosphate buffered saline
PC	Pericyte
PDMS	Polydimethylsiloxane foil
PECAM	Platelet endothelial cell adhesion molecule
PEEK	Polyetheretherketone
Pen/Strep	Penicillin/streptomycin
PFA	Paraformaldehyde
Pgp	P-Glycoprotein
PPIA	Peptidylpropyl isomerase A
Q	Flow rate
qPCR	Real time quantitative PCR
RAGE	Receptor for advanced glycosylation end product
rcf	Relative Centrifugal Force

Rf-level	Radio-frequency-level
RLT	RNeasy Lysis Buffer
RMT	Receptor-mediated transport
RNA	Ribonucleic acid
RPE	RNeasy Purification Buffer
rpm	Rounds per minute
RW1	RNeasy Washing Buffer
RT	Room temperature
S100A4	Calcium binding protein A4
SELE	Selectin
SLC	Solute carrier
τ	Shear stress
TEER	Transendothelial electrical resistance
TNF	Tumor necrosis factor
TfR	Transferrin receptor
TJ	Tight junction
VE-Cadherin	Vascular endothelial cadherin
VEGF	Vascular endothelial growth factor
vWF	Von Willebrand factor
w	Width
W	Watt
WWC2	WW and C2 domain containing 2
ZO	Zonula occludens

8   References

Abbott, N. J., Patabendige, A. A. K., Dolman, D. E. M., Yusof, S. R., & Begley, D. J. (2010). Structure and function of the blood-brain barrier. *Neurobiology of Disease*, *37*(1), 13–25. https://doi.org/10.1016/j.nbd.2009.07.030

AutoCAD software available at https://www.autodesk.com/products/autocad/overview, September 27, 2019. (n.d.). Retrieved September 27, 2019, from https://www.autodesk.com/products/autocad/overview

Autodesk CFD software available at https://www.autodesk.com/products/cfd/overview, April 11, 2020. (n.d.). Retrieved April 11, 2020, from https://www.autodesk.com/products/cfd/overview

Ballermann, B. J., Dardik, A., Eng, E., & Liu, A. (1998). Shear stress and the endothelium. *Kidney International, Supplement*, *54*(67), 100–108. https://doi.org/10.1046/j.1523-1755.1998.06720.x

Booth, R., & Kim, H. (2012). *Lab on a Chip Miniaturisation for che m istry , physics , biology , m aterials science and bioengineering*. *12*(10). https://doi.org/10.1039/c2lc40094d

Bortot, M., Ashworth, K., Sharifi, A., Walker, F., Crawford, N. C., Neeves, K. B., … Di Paola, J. (2019). Turbulent Flow Promotes Cleavage of VWF (von Willebrand Factor) by ADAMTS13 (A Disintegrin and Metalloproteinase With a Thrombospondin Type-1 Motif, Member 13). *Arteriosclerosis, Thrombosis, and Vascular Biology*, *39*(9), 1831–1842. https://doi.org/10.1161/ATVBAHA.119.312814

Brown, T. D., Nowak, M., Bayles, A. V, Prabhakarpandian, B., Karande, P., Lahann, J., … Mitragotri, S. (2019). *RESEARCH REPORT A microfluidic model of human brain (μ HuB) for assessment of blood brain barrier*. (December 2018), 1–13. https://doi.org/10.1002/btm2.10126

Colgan, O. C., Ferguson, G., Collins, N. T., Murphy, R. P., Meade, G., Cahill, P. A., … Meade, G. (2020). *Regulation of bovine brain microvascular endothelial tight junction assembly and barrier function by laminar shear stress*. 3190–3197. https://doi.org/10.1152/ajpheart.01177.2006.

Cucullo, L., Hossain, M., Puvenna, V., Marchi, N., & Janigro, D. (2011). The role of shear stress in Blood-Brain Barrier endothelial physiology. *BMC Neuroscience*, *12*(1), 40. https://doi.org/10.1186/1471-2202-12-40

Daneman, R. (2012). The blood-brain barrier in health and disease. *Annals of Neurology*, *72*(5), 648–672. https://doi.org/10.1002/ana.23648

Daneman, R., & Prat, A. (2015). The Blood-Brain Barrier. *Developmental Medicine & Child Neurology*, *3*(5), 510–514. https://doi.org/10.1111/j.1469-8749.1961.tb10410.x

Destefano, J. G., Jamieson, J. J., Linville, R. M., & Searson, P. C. (2018). Benchmarking in vitro tissue - engineered blood – brain barrier models. *Fluids and Barriers of the CNS*, (December). https://doi.org/10.1186/s12987-018-0117-2

Destefano, J. G., Xu, Z. S., Williams, A. J., Yimam, N., & Searson, P. C. (2017). Effect of shear stress on iPSC - derived human brain microvascular endothelial cells (dhBMECs). *Fluids and Barriers of the CNS*, 1–15. https://doi.org/10.1186/s12987-017-0068-z

Ferreira, L. (2019). What human blood-brain barrier models can tell us about BBB function and drug discovery? *Expert Opinion on Drug Discovery*, *14*(11), 1113–1123. https://doi.org/10.1080/17460441.2019.1646722

Fischer. (2012). Wirkort Gehirn. *DAZ*, 1–11.

Fischer, P. D. D. *DAZ 2012, Nr. 8, S. 62: Wirkort Gehirn*. Retrieved from https://www.deutsche-apotheker-zeitung.de/daz-az/2012/daz-8-2012/wirkort-gehirn

Galbusera, B. M., Zoja, C., Donadelli, R., Paris, S., Morigi, M., Benigni, A., … Remuzzi, A. (1997). Vascular Endothelium. *BLOOD*, *90*(4), 1558–1564. https://doi.org/10.1182/blood.V90.4.1558

Garcia-polite, F., Martorell, J., Rey-puech, P. Del, Melgar-lesmes, P., Brien, C. C. O., Roquer, J., … Balcells, M. (2017). *Pulsatility and high shear stress deteriorate barrier phenotype in brain microvascular endothelium*. https://doi.org/10.1177/0271678X16672482

Gogia, S., & Neelamegham, S. (2015). *Role of fluid shear stress in regulating VWF structure, function and related blood disorders*. *52*, 319–335. https://doi.org/10.3233/BIR-15061

Green, S. B. (2020). *THE EFFECT OF SHEAR STRESS AND UREA ON ENDOTHELIAL CATIONIC AMINO ACID TRANSPORTER-1 AND ENDOTHELIAL NITRIC OXIDE SYNTHASE by Sophie B . Green A dissertation submitted to the Faculty of the University of Delaware in partial fulfillment of the requirements*.

Griep, L., Wolbers, F., Wagenaar, B. De, & Braak, P. (2012). *BBB ON CHIP : microfluidic platform to mechanically and biochemically modulate blood-brain barrier function*. (May 2014). https://doi.org/10.1007/s10544-012-9699-7

https://biologydictionary.net/cytoskeleton/, accessed October 2, 2019

https://www.abcam.com/protocols/phalloidin-staining-protocol, accessed October 02, 2019.

https://www.chemyx.com/support/knowledge-base/applications/chemyx-syringe-pumps-nanofibers-bone-tissue-engineering-2/. Retrieved April 7, 2020

https://www.elveflow.com/microfluidic-tutorials/microfluidic-reviews-and-tutorials/air-

bubbles-and-microfluidics/, accessed April 07, 2020

https://www.elveflow.com/microfluidic-tutorials/microfluidic-reviews-and-
tutorials/microfluidic-fittings-and-tubing-resources/the-basics-of-microfluidic-tubing-
sleeves/, accessed September 27, 2019

https://www.elveflow.com/microfluidic-tutorials/soft-lithography-reviews-and-tutorials/how-
to-get-the-best-process/soft-lithography-glass-pdms-bonding/. Retrieved April 6, 2020

https://www.genomics-online.com/resources/16/5049/housekeeping-genes/, April 04, 2020.

https://www.mpibpc.mpg.de/151749/Desinfizierende_Wirkung_von_Alkohol, accessed
September 30, 2019

https://www.ncbi.nlm.nih.gov/pubmed/26621373, accessed October 02, 2019

https://www.omega.com/en-us/resources/flow-meters, accessed September 28. 2019

https://www.sciencedirect.com/topics/agricultural-and-biological-sciences/phalloidin,
accessed October 2, 2019

Ibidi, cells in focus (Vol. 1). (2016).

Image of APTES available at https://www.carlroth.com/de/de/Life-Science/Histologie-
Mikroskopie/Reagenzien/Standardreagenzien/3-Aminopropyltriethoxysilan-
%28APTES%29/p/000000000001ade600030023_de, accessed September 27, 2019.

Janzer, R. C., & Raff, M. C. (1987). Astrocytes induce blood-brain barrier properties in
endothelial cells. *NeuroReport*. https://doi.org/10.1097/00001756-199904260-00035

Kiessling, H., Schulz, I., Haltner, E., Fricker, G., Stelzle, M., & Schütte, J. (2015).
Mikrofluidisches 3D-Zellkulturmodell der Blut-Hirn-Schranke. *BioSpektrum*, *21*(2),
175–178. https://doi.org/10.1007/s12268-015-0558-y

Kuddannaya, S., Chuah, Y. J., Lee, M. H. A., Menon, N. V., Kang, Y., & Zhang, Y. (2013).
Surface chemical modification of poly(dimethylsiloxane) for the enhanced adhesion and
proliferation of mesenchymal stem cells. *ACS Applied Materials and Interfaces*, *5*(19),
9777–9784. https://doi.org/10.1021/am402903e

Lara Winckler, Florian Fisch, Valérie Labonté, H. Z. (2012). Die Entdeckung der
Schnelligkeit Gelebte Mikrofluidik Erst durch die gezielte Anwendung erhalte.
Laborjournal, *3*, 40–49.

McMillan, A. (2017). Shear stress in microfluidic devices. Retrieved May 9, 2020, from
https://darwin-microfluidics.com/blogs/reviews/shear-stress-in-microfluidic-devices

Molecular-Probes. (2005). LIVE/DEAD Viability/Cytotoxicity Kit for mammalian cells.
Product Information. Retrieved January 29, 2021, from
https://tools.thermofisher.com/content/sfs/manuals/mp03224.pdf

Müller-Esterl, W. (2004). *Biochemie - Eine Einführung für Mediziner und Naturwissenschaftler* (1. Auflage).

Neuhaus, W. (2020). In Vitro Models of the Blod-Brain Barrier. *In Vitro*, 258–282.

Neuhaus, W., Lauer, R., Oelzant, S., Fringeli, U. P., Ecker, G. F., & Noe, C. R. (2006). A novel flow based hollow-fiber blood-brain barrier in vitro model with immortalised cell line PBMEC/C1-2. *Journal of Biotechnology*, *125*(1), 127–141. https://doi.org/10.1016/j.jbiotec.2006.02.019

Pankov, R., & Yamada, K. M. (2002). Fibronectin at a glance. *Journal of Cell Science*, *115*(20), 3861–3863. https://doi.org/10.1242/jcs.00059

Paszkowiak JJ, D. A. Arterial wall shear stress: observations from the bench to the bedside. Retrieved May 9, 2020, from https://www.ncbi.nlm.nih.gov/pubmed/12577139

Peyvandi, F., Garagiola, I., & Baronciani, L. (2011). *Role of von Willebrand factor in the haemostasis*. 3–8. https://doi.org/10.2450/2011.002S

Phalloidin structure available at https://www.abcam.com/phalloidin-f-actin-depolymerization-inhibitor-ab143533.html, accessed October 2, 2019

Picture of glass-lab-dish with cover available at: https://www.walmart.com/ip/Kinto-Schale-Glass-Lab-Dish-with-Cover-10-1-oz/340837587, accessed November 19, 2019

Place, S. (2008). Plasma Bonding. *Encyclopedia of Microfluidics and Nanofluidics*, 1673–1673. https://doi.org/10.1007/978-0-387-48998-8_1249

PPIAhttps://www.uniprot.org/uniprot/P62937, accessed April 4, 2020

Principle of Live-Dead-Stain available at https://slideplayer.com/slide/4088630/, October 02, 2019

Qiagen. (2005). AllPrep DNA / RNA Mini Handbook For simultaneous purification of genomic. *Biosystems*, (November).

Rahimi, N. (2017). Defenders and challengers of endothelial barrier function. *Frontiers in Immunology*, *8*(DEC), 1–10. https://doi.org/10.3389/fimmu.2017.01847

Ramme, A. P., Koenig, L., Hasenberg, T., Schwenk, C., Magauer, C., Faust, D., … Dehne, E. M. (2019). Autologous induced pluripotent stem cell-derived four-organ-chip. *Future Science OA*, *5*(8). https://doi.org/10.2144/fsoa-2019-0065

Rochfort, K. D., & Cummins, P. M. (2015). The blood-brain barrier endothelium: A target for pro-inflammatory cytokines. *Biochemical Society Transactions*, *43*(October), 702–706. https://doi.org/10.1042/BST20140319

Roland CutStudio Software available at https://www.rolanddg.de/produkte/software/roland-cutstudio, accessed September 25, 2019

Saunders, N. R., Liddelow, S. A., & Dziegielewska, K. M. (2012). Barrier mechanisms in the developing brain. *Frontiers in Pharmacology*, *3 MAR*(March), 1–18. https://doi.org/10.3389/fphar.2012.00046

Sellgren, K. L., Hawkins, B. T., & Grego, S. (2015). An optically transparent membrane supports shear stress studies in a three-dimensional microfluidic neurovascular unit model. *Biomicrofluidics*, *9*(6), 1–4. https://doi.org/10.1063/1.4935594

Shuler, L., & Hickman, J. J. (2016). *systems* (Vol. 20). https://doi.org/10.1177/2211068214561025.TEER

Siegenthaler, J. A., Sohet, F., & Daneman, R. (2013). "Sealing off the CNS": Cellular and molecular regulation of blood-brain barriergenesis. *Current Opinion in Neurobiology*, *23*(6), 1057–1064. https://doi.org/10.1016/j.conb.2013.06.006

Skafte-Poedersen, P., Hemmingsen, M., Sabourin, D., Blaga, F. S., Bruus, & Dufva, M. (2011). A self- contained, programmable microfluidic cell culture system with real-time microscopy access. *Biomedical Microdevices*.

Spreyer, P. (2008). *Etablierung einer Multiplex real-time PCR zur Detektion und Differenzierung der equiden Herpesviren 1 und 4*.

Sulistyowati, E., Permatasari, N., & Widobo, M. A. (2017). Combined effects of shear stress and glucose on the morphology , actin fi laments , and VE-cadherin of endothelial cells in vitro. *IJC Heart & Vasculature*, *15*, 31–35. https://doi.org/10.1016/j.ijcha.2017.03.004

Sweeney, M. D., Sagare, A. P., & Zlokovic, B. V. (2018). Blood-brain barrier breakdown in Alzheimer disease and other neurodegenerative disorders. *Nature Reviews Neurology*, *14*(3), 133–150. https://doi.org/10.1038/nrneurol.2017.188

Vestweber, D. (2008). VE-cadherin: The major endothelial adhesion molecule controlling cellular junctions and blood vessel formation. *Arteriosclerosis, Thrombosis, and Vascular Biology*, *28*(2), 223–232. https://doi.org/10.1161/ATVBAHA.107.158014

Vinyl Cutter, picture available at https://www.signmakingandsupplies.co.uk/roland-camm-1-gs-24-vinyl-plotter-cutter-19689-p.asp, accessed September 25, 2019

Walter, F. R., Valkai, S., Kincses, A., Petneházi, A., Czeller, T., Veszelka, S., … Dér, A. (2016). A versatile lab-on-a-chip tool for modeling biological barriers. *Sensors and Actuators, B: Chemical*, *222*, 1209–1219. https://doi.org/10.1016/j.snb.2015.07.110

Wang, J. D., Khafagy, E.-S., Khanafer, K., Takayama, S., & El Sayed, M. E. H. (2016). *Organization of Endothelial Cells, Pericytes, and Astrocytes into a 3D Micro fl uidic in Vitro Model of the Blood − Brain Barrier*. https://doi.org/10.1021/acs.molpharmaceut.5b00805

Wang, X., Xu, B., Xiang, M., Yang, X., Liu, Y., Liu, X., & Shen, Y. (2020). Advances on fluid shear stress regulating blood-brain barrier. *Microvascular Research*, *128*(March 2019), 103930. https://doi.org/10.1016/j.mvr.2019.103930

Watson Marlow Schlauchpumpen für Forschund und Labor.

Weksler, B., Romero, I. A., & Couraud, P. O. (2013). The hCMEC/D3 cell line as a model of the human blood brain barrier. *Fluids and Barriers of the CNS*, *10*(1), 1. https://doi.org/10.1186/2045-8118-10-16

Wragg, J. W., Durant, S., McGettrick, H. M., Sample, K. M., Stuart Egginton, & Bicknell, R. (2014). *Shear stress regulated gene expression and angiogenesis in vascular endothelium*.

9 List of tables

10 List of figures

I made every effort to find the owners of the used images and figures to get their permission for the image rights and for using these. However, in the case of a potential copyright infringement, ask for notice.